Computational Intelligence and Neuroscience

Multidimensional Cognitive Information-Driven Fuzzy Intelligent Computing and Decision Making

Lead Guest Editor: Zaoli Yang
Guest Editors: Yuchen Li and Salman Ahmad

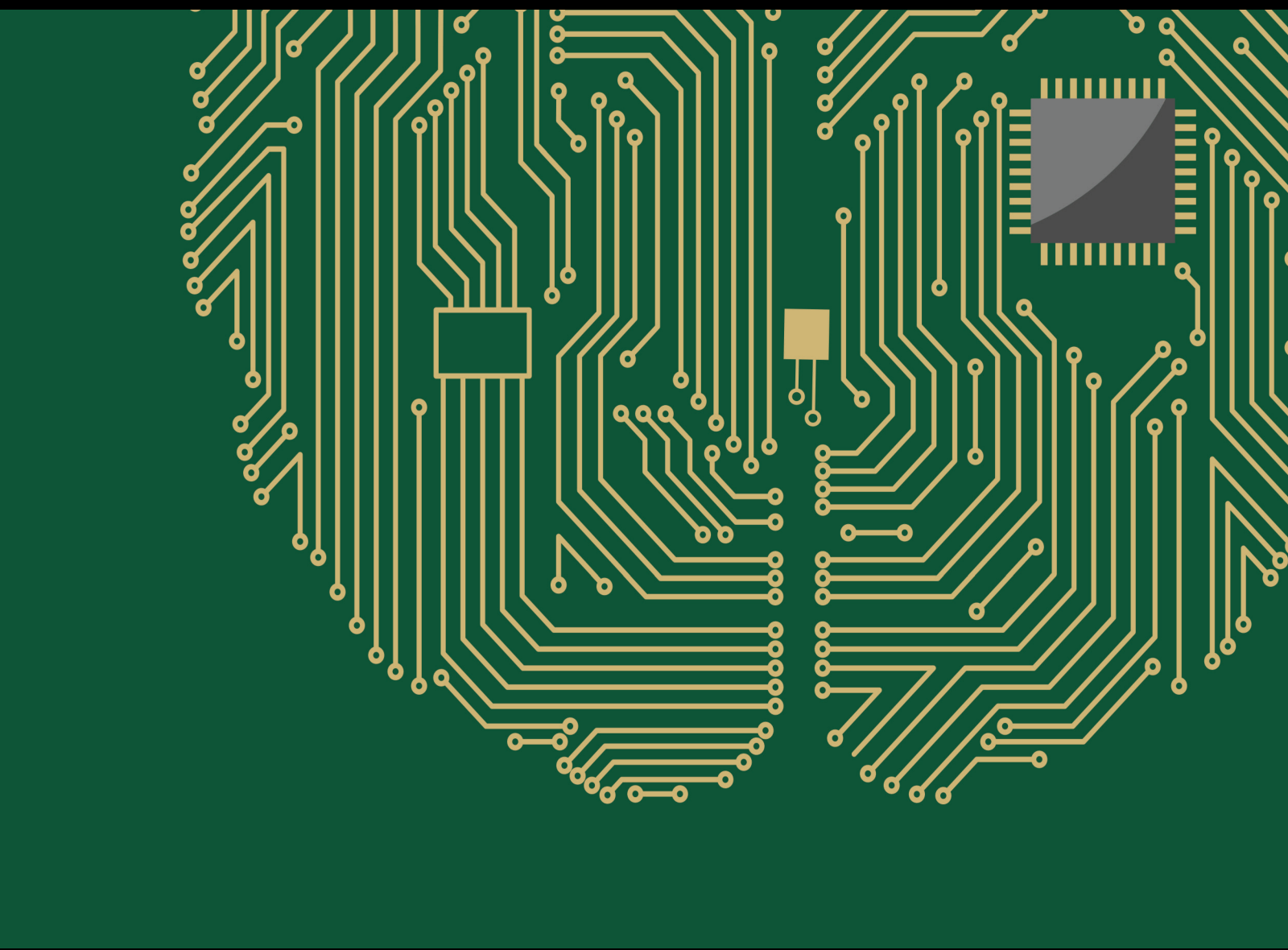

Multidimensional Cognitive Information-Driven Fuzzy Intelligent Computing and Decision Making

Computational Intelligence and Neuroscience

Multidimensional Cognitive Information-Driven Fuzzy Intelligent Computing and Decision Making

Lead Guest Editor: Zaoli Yang
Guest Editors: Yuchen Li and Salman Ahmad

Contents

Retracted: A Lightweight Semantic Segmentation Algorithm Based on Deep Convolutional Neural Networks
Computational Intelligence and Neuroscience
Retraction (1 page), Article ID 9790234, Volume 2023 (2023)

Retracted: Research on Four-Dimensional Innovative Intelligent Education Platform Based on Cloud Edge-End Architecture
Computational Intelligence and Neuroscience
Retraction (1 page), Article ID 9836398, Volume 2023 (2023)

[Retracted] Research on Four-Dimensional Innovative Intelligent Education Platform Based on Cloud Edge-End Architecture
Buyu Wang, Jingwei Qi, Xiaoping An, Jiangyin Fu, Yuan Wang, Na Liu, and Meian Li
Research Article (11 pages), Article ID 2263033, Volume 2023 (2023)

An Image Classification Method Based on Adaptive Attention Mechanism and Feature Extraction Network
Juanjuan Luo and Defa Hu
Research Article (11 pages), Article ID 4305594, Volume 2023 (2023)

High-Discrimination Comparison Algorithm for the Comprehensive Evaluation of Innovation Ability in Colleges and Universities under Uncertain Information
Ming Fu, Lifang Wang, Xueneng Cao, Bingyun Zheng, Xianxian Zhou, and Shishu Yin
Research Article (14 pages), Article ID 7842651, Volume 2022 (2022)

Research on Domain-Specific Knowledge Graph Based on the RoBERTa-wwm-ext Pretraining Model
Xingli Liu, Wei Zhao, and Haiqun Ma
Research Article (11 pages), Article ID 8656013, Volume 2022 (2022)

A Generative Image Inpainting Model Based on Edge and Feature Self-Arrangement Constraints
Fan Yao and Yanli Chu
Research Article (12 pages), Article ID 5904043, Volume 2022 (2022)

Learning of Short Video Text Description of Nursing Teaching Based on Transformer
Xuenan Cao
Research Article (9 pages), Article ID 6989374, Volume 2022 (2022)

Analysis and Construction of the User Characteristic Model in the Adaptive Learning System for Personalized Learning
Xuekong Zhao, Shirong Long, and Defa Hu
Research Article (14 pages), Article ID 5503153, Volume 2022 (2022)

Research on Decision-Making of Hybrid Dominant Closed-Loop Supply Chain considering Different Logistics Modes
Wanxian Wu and Lin Miao
Research Article (12 pages), Article ID 9889292, Volume 2022 (2022)

Forecasting Slope Displacement of the Agricultural Mountainous Area Based on the ACO-SVM Model
Juan Chen, Yiliang Wei, and Xiaohui Ma
Research Article (10 pages), Article ID 2519035, Volume 2022 (2022)

Optimal Control of False Information Clarification System under Major Emergencies Based on Differential Game Theory
Bowen Li, Hua Li, Qiubai Sun, and Rongjian Lv
Research Article (19 pages), Article ID 7291735, Volume 2022 (2022)

A Fine-Grained Image Classification and Detection Method Based on Convolutional Neural Network Fused with Attention Mechanism
Yue Zhang
Research Article (10 pages), Article ID 2974960, Volume 2022 (2022)

A Closed-Loop Method for Multiperiod Intelligent Information Processing with Cost Constraints under the Fuzzy Environment
Ming Fu, Lifang Wang, Xueneng Cao, Bingyun Zheng, Xianxian Zhou, and Shishu Yin
Research Article (19 pages), Article ID 3871129, Volume 2022 (2022)

[Retracted] A Lightweight Semantic Segmentation Algorithm Based on Deep Convolutional Neural Networks
Chengzhi Yang and Hongjun Guo
Research Article (9 pages), Article ID 5339664, Volume 2022 (2022)

Hindawi
Computational Intelligence and Neuroscience
Volume 2023, Article ID 9790234, 1 page
https://doi.org/10.1155/2023/9790234

Retraction

Retracted: A Lightweight Semantic Segmentation Algorithm Based on Deep Convolutional Neural Networks

Computational Intelligence and Neuroscience

Received 10 October 2023; Accepted 10 October 2023; Published 11 October 2023

This article has been retracted by Hindawi following an investigation undertaken by the publisher [1]. This investigation has uncovered evidence of one or more of the following indicators of systematic manipulation of the publication process:

(1) Discrepancies in scope
(2) Discrepancies in the description of the research reported
(3) Discrepancies between the availability of data and the research described
(4) Inappropriate citations
(5) Incoherent, meaningless and/or irrelevant content included in the article
(6) Peer-review manipulation

The presence of these indicators undermines our confidence in the integrity of the article's content and we cannot, therefore, vouch for its reliability. Please note that this notice is intended solely to alert readers that the content of this article is unreliable. We have not investigated whether authors were aware of or involved in the systematic manipulation of the publication process.

Wiley and Hindawi regrets that the usual quality checks did not identify these issues before publication and have since put additional measures in place to safeguard research integrity.

We wish to credit our own Research Integrity and Research Publishing teams and anonymous and named external researchers and research integrity experts for contributing to this investigation.

The corresponding author, as the representative of all authors, has been given the opportunity to register their agreement or disagreement to this retraction. We have kept a record of any response received.

References

[1] C. Yang and H. Guo, "A Lightweight Semantic Segmentation Algorithm Based on Deep Convolutional Neural Networks," *Computational Intelligence and Neuroscience*, vol. 2022, Article ID 5339664, 9 pages, 2022.

Hindawi
Computational Intelligence and Neuroscience
Volume 2023, Article ID 9836398, 1 page
https://doi.org/10.1155/2023/9836398

Retraction

Retracted: Research on Four-Dimensional Innovative Intelligent Education Platform Based on Cloud Edge-End Architecture

Computational Intelligence and Neuroscience

Received 1 August 2023; Accepted 1 August 2023; Published 2 August 2023

This article has been retracted by Hindawi following an investigation undertaken by the publisher [1]. This investigation has uncovered evidence of one or more of the following indicators of systematic manipulation of the publication process:

(1) Discrepancies in scope
(2) Discrepancies in the description of the research reported
(3) Discrepancies between the availability of data and the research described
(4) Inappropriate citations
(5) Incoherent, meaningless and/or irrelevant content included in the article
(6) Peer-review manipulation

The presence of these indicators undermines our confidence in the integrity of the article's content and we cannot, therefore, vouch for its reliability. Please note that this notice is intended solely to alert readers that the content of this article is unreliable. We have not investigated whether authors were aware of or involved in the systematic manipulation of the publication process.

Wiley and Hindawi regrets that the usual quality checks did not identify these issues before publication and have since put additional measures in place to safeguard research integrity.

We wish to credit our own Research Integrity and Research Publishing teams and anonymous and named external researchers and research integrity experts for contributing to this investigation.

The corresponding author, as the representative of all authors, has been given the opportunity to register their agreement or disagreement to this retraction. We have kept a record of any response received.

References

[1] B. Wang, J. Qi, X. An et al., "Research on Four-Dimensional Innovative Intelligent Education Platform Based on Cloud Edge-End Architecture," *Computational Intelligence and Neuroscience*, vol. 2023, Article ID 2263033, 11 pages, 2023.

Hindawi
Computational Intelligence and Neuroscience
Volume 2023, Article ID 9836398, 1 page
https://doi.org/10.1155/2023/9836398

Retraction

Retracted: Research on Four-Dimensional Innovative Intelligent Education Platform Based on Cloud Edge-End Architecture

Computational Intelligence and Neuroscience

Received 1 August 2023; Accepted 1 August 2023; Published 2 August 2023

This article has been retracted by Hindawi following an investigation undertaken by the publisher [1]. This investigation has uncovered evidence of one or more of the following indicators of systematic manipulation of the publication process:

(1) Discrepancies in scope
(2) Discrepancies in the description of the research reported
(3) Discrepancies between the availability of data and the research described
(4) Inappropriate citations
(5) Incoherent, meaningless and/or irrelevant content included in the article
(6) Peer-review manipulation

The presence of these indicators undermines our confidence in the integrity of the article's content and we cannot, therefore, vouch for its reliability. Please note that this notice is intended solely to alert readers that the content of this article is unreliable. We have not investigated whether authors were aware of or involved in the systematic manipulation of the publication process.

Wiley and Hindawi regrets that the usual quality checks did not identify these issues before publication and have since put additional measures in place to safeguard research integrity.

We wish to credit our own Research Integrity and Research Publishing teams and anonymous and named external researchers and research integrity experts for contributing to this investigation.

The corresponding author, as the representative of all authors, has been given the opportunity to register their agreement or disagreement to this retraction. We have kept a record of any response received.

References

[1] B. Wang, J. Qi, X. An et al., "Research on Four-Dimensional Innovative Intelligent Education Platform Based on Cloud Edge-End Architecture," *Computational Intelligence and Neuroscience*, vol. 2023, Article ID 2263033, 11 pages, 2023.

Hindawi
Computational Intelligence and Neuroscience
Volume 2023, Article ID 2263033, 11 pages
https://doi.org/10.1155/2023/2263033

Research Article

Research on Four-Dimensional Innovative Intelligent Education Platform Based on Cloud Edge-End Architecture

Buyu Wang,[1,2] **Jingwei Qi**,[2,3] **Xiaoping An**,[2,3] **Jiangyin Fu**,[4] **Yuan Wang**,[2,3] **Na Liu**,[2,3] **and Meian Li**[1,2]

[1]*College of Computer and Information Engineering, Inner Mongolia Agricultural University, Hohhot 010018, Inner Mongolia, China*
[2]*Key Laboratory of Smart Animal Husbandry, Universities of Inner Mongolia Automomous Region, Hohhot 010018, Inner Mongolia, China*
[3]*College of Animal Science, Inner Mongolia Agricultural University, Hohhot 010018, Inner Mongolia, China*
[4]*Department of Electrical and Computer Engineering, Tandon School of Engineering, New York University, New York, NY 11201, USA*

Correspondence should be addressed to Jingwei Qi; qijingwei@imau.edu.cn

Received 26 August 2022; Accepted 10 October 2022; Published 1 March 2023

Academic Editor: Zaoli Yang

In order to solve the problem of backward talent training mode in agriculture-related colleges and universities, this paper proposed a scheme to build a smart teaching platform by using cloud architecture, combining virtualization and twinning technology. The intelligent teaching platform is developed using the 5G converged network architecture and cloud edge system architecture. The intelligent teaching platform has realized such teaching modes as real scene teaching, combination of virtual and real teaching, immersive teaching, multi-teacher collaborative teaching and live interactive teaching. The smart teaching platform has established a new model of digital education, with the functions of teaching, teaching research, teaching management and teaching evaluation, and provides smart teaching cloud services for teachers and students of agriculture-related colleges and universities as well as external tutors. The research of multi-dimensional evaluation system solves the precise management of teaching process. The teaching effect has been significantly improved, and the management cost has been reduced, which meets the goal of training new agricultural talents in agricultural and forestry colleges.

1. Introduction

How to cultivate applied talents required by the development of global agriculture 4.0, how to achieve accurate evaluation of education quality, and then realize the implementation of new agricultural science construction, are the core issues of intelligent education research in animal husbandry discipline.

Cai et al. [1] do to wisdom education curriculum design of exploratory research, puts forward adopting the micro-course or animation display before the class, for students in the class group autonomous teaching and carry out online teaching practice after class in the method of combining effectively promote the students' autonomous learning ability and innovation ability, which laid a foundation for further enhance the level of talent training. Tai et al. [2] pointed out that the reconstruction of smart teaching environment is the deep integration of information technology and education and teaching, which is a higher form of education informatization. He studied the construction of smart teaching environment and proposed the environment construction standard of "interconnection, accurate service and data support". Gu and Zhang [3] pointed out that wisdom space by classroom teaching equipment management, teaching management, students' attendance management and remote interactive teaching management software and hardware space composition, and the wisdom of teaching space modeling were studied, based on the

cloud-side together the wisdom of the education system, solved the "full content and full time domain, the whole process, all terminal, the whole audience" teaching management needs, Fill the gap in the industry. Xu et al. [4] conducted in-depth research on the intelligent teaching system based on artificial intelligence (AI) and computer technology, and found that the application of the intelligent system not only helped students improve their learning efficiency by 9.8%, but also was favored by 56.8% of teachers and students. Gao's [5] research for conducting scientific and objective of education quality evaluation conducted in-depth research, use of big data and artificial intelligence technology to build a quantitative evaluation index system of university teachers' teaching quality and quantitative methods of research and the realization method of intelligent as well as the construction of university teachers' teaching quality quantitative evaluation system of research and implementation method, The authors explores the technical way to find the effectiveness of measurable factors in the evaluation of teaching quality, and the results have important practical significance for scientific evaluation of teaching quality. Zeng's [6] research has applied virtual reality (VR) technology to the intelligent multimedia remote teaching system, and used VR technology to complete the reasonable allocation of multimedia teaching resources and effectively improve the quality of multimedia teaching. Intelligent multimedia distance teaching system can effectively reduce the transmission energy and signal to noise ratio of teaching resource data, which has certain practical value.

The training of compound applied talents in colleges and universities mainly includes skill type and applied research type. The skilled, represented by higher vocational colleges, have conducted extensive research and exploration on the skilled intelligent education. The most representative is Yu's [7] proposal of how to better cultivate the intelligent teaching model of global industry 4.0 talents under the background of 5G, which connects the four educational links of "teaching, learning, evaluation and capital". The exponential intelligent teaching mode should be implemented from the aspects of teaching methods, learning forms, evaluation systems and teaching resources. However, there are also some problems such as low enthusiasm of teachers to carry out smart teaching, single smart teaching model and serious fragmentation of resources. For undergraduate education, intelligent education focuses on the application of the cultivation of research talents, Yuan and Li [8] from policy management perspective, put forward the "management, professorial teaching, environment, resources, training objectives," five elements of M-PERT model, for the building of the model and its effectiveness done in-depth research, verified the value of intelligent education. Intelligent education in colleges and universities not only covers environmental construction, software and hardware support, but also analyzes the application potential and technical application level of intelligent objects in combination with educational theory and practice, and constructs practical application scenarios for different application objects, in application fields, and implementation paths for more application fields. Promote the cloud, intelligent, virtual, two-way evaluation of education services, solve the openness, diversity, collaboration, fairness and sustainability of education, build an intelligent teaching platform, and realize the revolutionary reform of education [9–14].

To sum up, a lot of research work has been done on the use of Internet of Things technology and artificial intelligence technology to carry out intelligent education, and a series of research results have been obtained from teaching activities, teaching management, curriculums construction to teaching evaluation. However, there are two problems: first, all the research focuses on the field of engineering education, and there is no relevant research on the wisdom education of animal husbandry. Secondly, all the studies did not propose how to build a unified cloud platform to carry out intelligent education in the whole process of education. Aiming at the goal of talent training in animal husbandry in agricultural universities in the future, the intelligent education platform composed of 5G converged network [15, 16], intelligent teaching data center, intelligent teaching resource sharing and intelligent teaching cloud service system is researched and constructed by using advanced intelligent technologies such as Internet of Things, cloud computing, big data, artificial intelligence and virtual reality. A linkage closed-loop talent training mode with four dimensions(teaching, teaching research, teaching management and teaching evaluation) of mutual empowerment has been constructed, put forward the four dimensions(multimedia teaching, the teaching of actual scenario and combination of virtual and real teaching and wisdom breeding double team teaching) of teaching mode, solve the problem of the new agricultural livestock disciplines personnel training, The intelligent teaching cloud platform including teaching, teaching research, teaching management and teaching evaluation has been established.

The contribution of this paper mainly has four aspects. Firstly, the architecture and functional architecture of intelligent teaching cloud platform based on cloud edge and end collaboration are proposed. Secondly, the integrated network architecture based on 5G is proposed to reconstruct the teaching space management, which provides support for the development of intelligent teaching management and accurate teaching evaluation. Third, new teaching resources for animal husbandry have been established, including real scene resources of livestock farms, virtual reality resources and smart breeding digital resources. Fourth, the cloud service system of teaching, teaching research, teaching management and teaching evaluation is studied, which makes exploration and research for the establishment of a universal cloud platform of intelligent education for animal husbandry discipline.

2. Intelligent Education Platform Architecture

The architecture of the intelligent education platform adopts cloud edge architecture, and the application architecture adopts multi-level application architecture with security and standards as two wings, as shown in Figure 1. The standard wing mainly includes teaching standards, resource standards, terminal access standards, breeding business

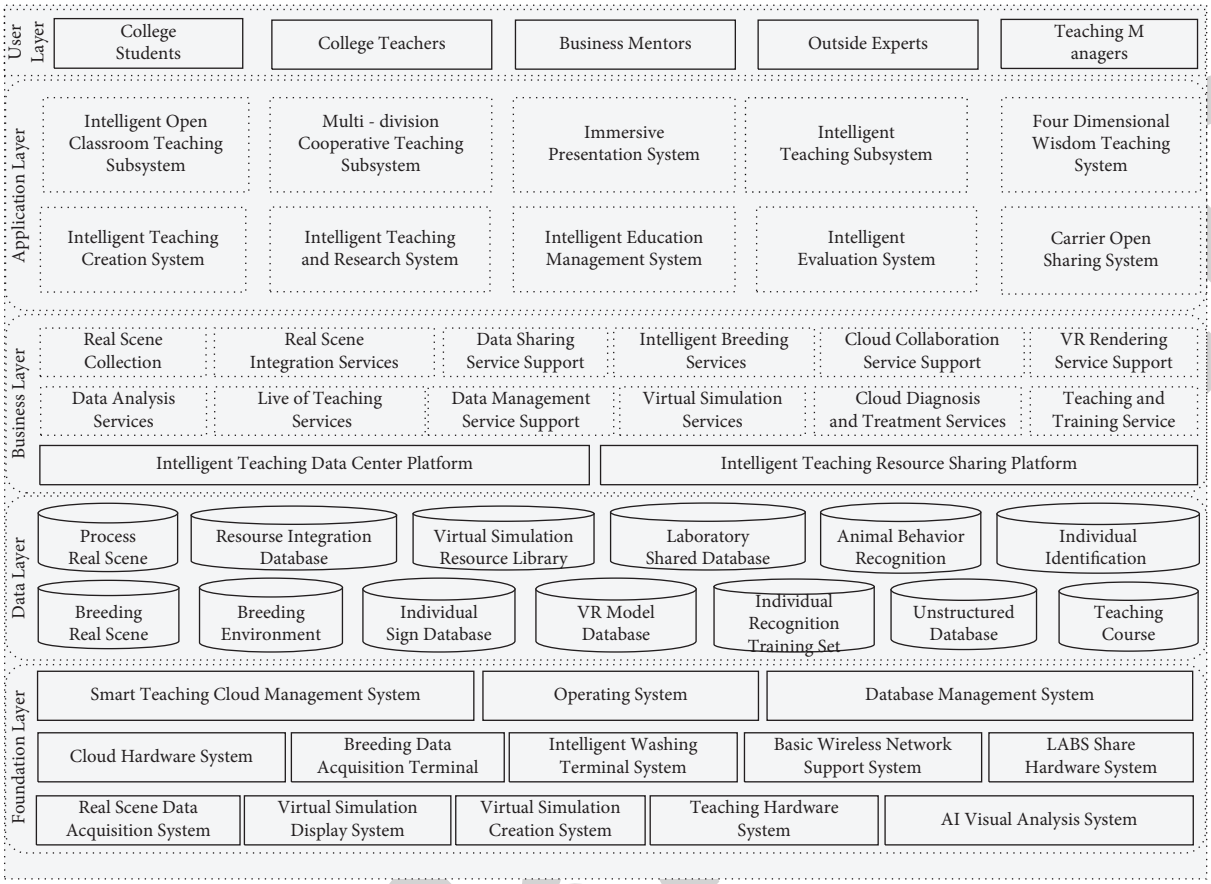

Figure 1: Overall framework diagram of intelligent education platform.

standards and livestock data standards. The safety wing mainly includes biological safety, production safety and food safety. The multi-layer application consists of the basic software and hardware platform layer, data resource layer, education service support layer, intelligent education application system layer, and user layer. The basic platform layer is the system hardware and software platform needed to support the system operation. The data resource layer contains all the underlying databases of the platform. Business support layer is the middleware necessary to support system operation. The application system layer embodies the function of intelligent teaching cloud service, which consists of teaching, teaching research, teaching management and teaching evaluation. The platform provides intelligent education services for teachers and students of agricultural and forestry universities, off-campus tutors, teaching administrators and platform operation and maintenance personnel.

As can be seen from Figure 1, the cloud platform is a five-layer application architecture with security and standards as its two wings. The five layers include foundation layer, data layer, business layer, application layer and user layer. The foundation layer consists of system software, system hardware and data acquisition and rendering system. The system software includes three sets of Smart Teaching Cloud Management System, Operating System and Database Management System. The system hardware includes Cloud Hardware System, Breeding Data Acquisition Terminal, Intelligent Washing Terminal System, and Basic Wireless Network Support System and LABS Share Hardware System five sets of hardware systems. The data acquisition and rendering system consists of Real Scene Data acquisition System, Virtual Simulation Display System, and Virtual Simulation Creation System, Teaching Hardware System and AI Visual Analysis System five sets of hardware and software integrated data acquisition and rendering systems. The hardware system provides hardware computing, storage and network services, the system software provides node operating system, cloud management system and database level system management functions, and the data collection and rendering system provides services for platform data collection, processing, rendering and display. The data layer consists of Breeding Real Scene, Breeding Environment, Individual Sign Database, VR Model Database, and Individual Recognition Training Set, Animal behavior recognition, Individual Identification and other 13 structured and unstructured databases. The business layer consists of the Intelligent Teaching Data Center Platform and the Intelligent Teaching Resource Sharing Platform. The teaching business support layer provides data distribution and sharing services for the data layer and application layer. The application layer consists of Intelligent Teaching Creation System, Intelligent Teaching and Research System, and Intelligent Education Management System, Intelligent

Evaluation System, Carrier Open Sharing System, Intelligent Open Classroom Teaching Subsystem, Multi-Division Cooperative Teaching Subsystem, Immersive Presentation System, Intelligent Teaching Subsystem, Four Dimensional Wisdom Teaching System is composed of 10 systems, providing users with a full range of intelligent teaching services from teaching, teaching research, teaching management to teaching evaluation. The user layer consists of college students, college teachers, outside experts, business mentors, and teaching managers, and provides services for the above five types of users.

Aiming at the privacy and security protection of multi-terminal data in cloud edge architecture, in-depth research is carried out from three aspects: formal verification of security, analysis of attack mechanism and construction of defense strategy. The data processing model of data layer is verified by security formalization, and the complex data processing model which is difficult to explain is transformed into a clearer form of logical constraints. Interpretable adversarial attack generation mechanism analysis method and high-dimensional feature space geometry analysis, decision transfer pathway detection, feature information attribution and visualization techniques are used to analyze the attack generation mechanism to ensure data security.

3. Network Architecture of Intelligent Education Platform

The network architecture of the intelligent teaching platform adopts the cloud side-end collaborative network architecture, and the edge and access mobile network adopt 5G converged network [17]. The backbone network mainly consists of the server corresponding to the platform, network and communication system, storage and backup system, network security system, data forwarding system and edge fusion network system. The converged network architecture is shown in Figure 2.

As can be seen from FIG. 2, the 5G converged network is composed of the Internet of Things acquisition terminal network, edge computing network, data center network and network security system. It provides the cloud platform with the fusion network architecture of cloud edge and end cooperation, ensures the network is stable and reliable, and the commercial privacy of data collection is effectively protected. The farm consists of poultry farms (laying hens, etc.) and livestock farms (horses, cattle, sheep, pigs, etc.). The network of IOT collection terminals in breeding farms is composed of four dimensions: Environment Sensor (5 Para), Cameras, individual signs, and handheld Terminals. The edge network uses 5G mobile standby network and WIFI wireless coverage working network to achieve full coverage, with bandwidth ranging from 20 Mbps to 100 Mbps. The data center network consists of Big Data Research, Business Cloud Services, Smart Education Data Center, and Smart Education Resource Sharing Center consists of four service data centers, which provide network support for data management, scientific research, data sharing and cloud services. The internal core exchange loan is 10 Gbps. It provides security systems ranging from firewall, fortress machine and online behavior management. The commercial data is calculated on the edge server, and the desensitized data is stored in the cloud data center, which ensures the commercial privacy security of the farm data.

The cloud edge-end architecture is an integrated 5G fusion network with low delay, high speed and large capacity from cloud (intelligent teaching data center), edge (edge computing network and edge computing node of school-enterprise cooperation base) to end (sensing terminal, 5G handheld terminal, 5G mobile terminal and various VR/AR terminals). Implement equipment, network infrastructure at the level of unity can be run through the cloud platform promotion goal, completely solve high network latency, low bandwidth, network, the problem of abort, frequently for subsequent development from the teaching, research, teaching research to the evaluation of low latency and high bandwidth, high availability, regulation of 5 g converged network service support.

4. Research of Intelligent Teaching Data Center System

The intelligent teaching data center system provides computing, storage, data services and basic business support for the intelligent teaching platform. It is composed of cloud pipe system, cloud real big data management, data processing, data integration and asset management subsystems. Build a 5G fusion network based on 5G technology and cloud side-end architecture, collect four-dimensional cloud panoramic data, establish real data assets, achieve the construction of four-dimensional real scene to simulation panorama of environment (5 Parameters are temperature, humidity, carbon dioxide, ammonia, hydrogen sulfide), scene, process and physical signs, and realize the collection, fusion, storage and asset services of four-dimensional real scene/panoramic data. The system adopts a three-layer architecture to carry the business, namely, the cloud layer, the basic cloud platform and the cloud service. Among them, the cloud layer mainly includes the data sensing end, acquisition terminal, edge computing terminal, data forwarding node, 5G terminal and standby 5G network to complete data collection and primary filtering functions. The basic cloud platform mainly includes cloud storage, cloud computing, and 5G cloud switching. Cloud services mainly include cloud teaching, cloud teaching research, cloud teaching management and cloud teaching evaluation services.

Wisdom teaching data center system, provide for industry application in the field of teaching immersive anytime and anywhere in the wisdom of open classroom (cloud online courses, more open, collaboration in interactive teaching in classroom and wisdom open class), live interactive teaching (panoramic live interactive teaching, the four-dimensional live interactive teaching, wisdom, open class) and the actual situation combined with teaching practice. The system architecture of intelligent teaching data center is shown in Figure 3.

As can be seen from Figure 3, the architecture of Intelligent Teaching Data Center System is a typical cloud edge architecture, consisting of three layers: Edge of Cloud

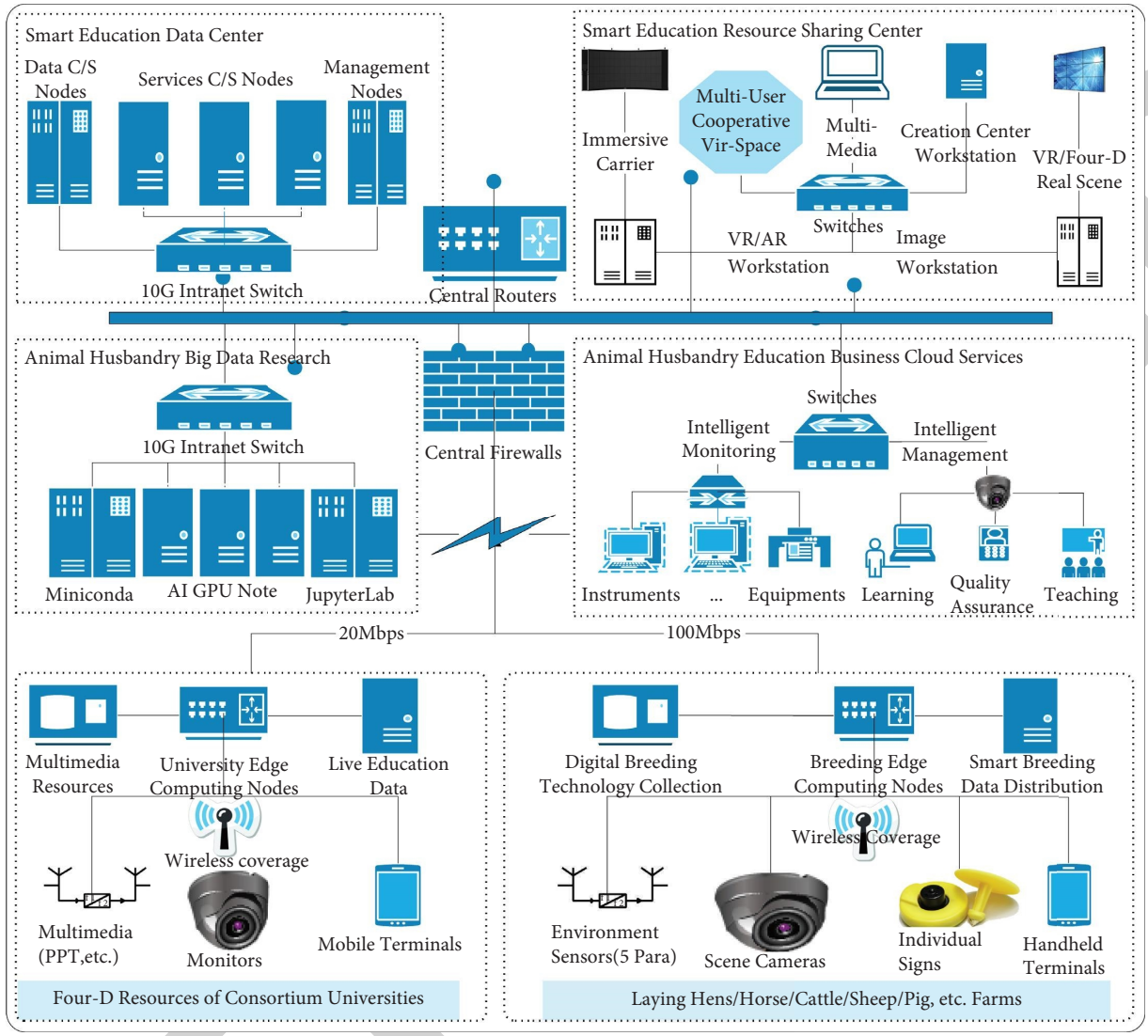

Figure 2: 5G converged network architecture diagram.

Terminal, Cloud Platform and Cloud Service. Edge of Cloud Terminal mainly completes the collection of real environment data, scene data, process data and individual physical signs data. The Cloud Platform mainly completes the computation, storage, fusion and sharing tasks of structured, semi-structured and unstructured data. The Cloud Service provides teaching, teaching research, Teaching management, and teaching evaluation services for users.

In order to solve the problem of real-time and anywhere immersive teaching in the practice base, real scene collection, construction of immersive virtual simulation resources and cloud distribution to the data center, to provide support for the development of real scene/panoramic online teaching. Through digital twinning technology, the production process twinning of the practice base is built into teaching resources to provide real production process support for intelligent teaching. The collection of the environment of the practice base and the real scene of the individual physical signs of the practice object realizes the overall digital materialization learning from the group to the individual. Based on the cloud-side 5G fusion network, real-time collection and fusion of the 4d real scene of the practice base are realized to generate real-time data assets, providing basic real-time panoramic data support for further realizing real-time control of production process, real-time access of teaching process and real-time analysis of scientific research process.

5. Research of Intelligent Teaching Resource Sharing System

The intelligent teaching and training resource sharing platform, relying on the cloud animal husbandry resource sharing platform and using 5G edge network, can meet the needs of users to access the platform anytime and anywhere to obtain shared resources, and provide the resource support required for the "5G + Cloud animal husbandry" intelligent teaching and training platform. The platform consists of data resource sharing system, teaching resource sharing system, platform resource sharing system and carrier resource

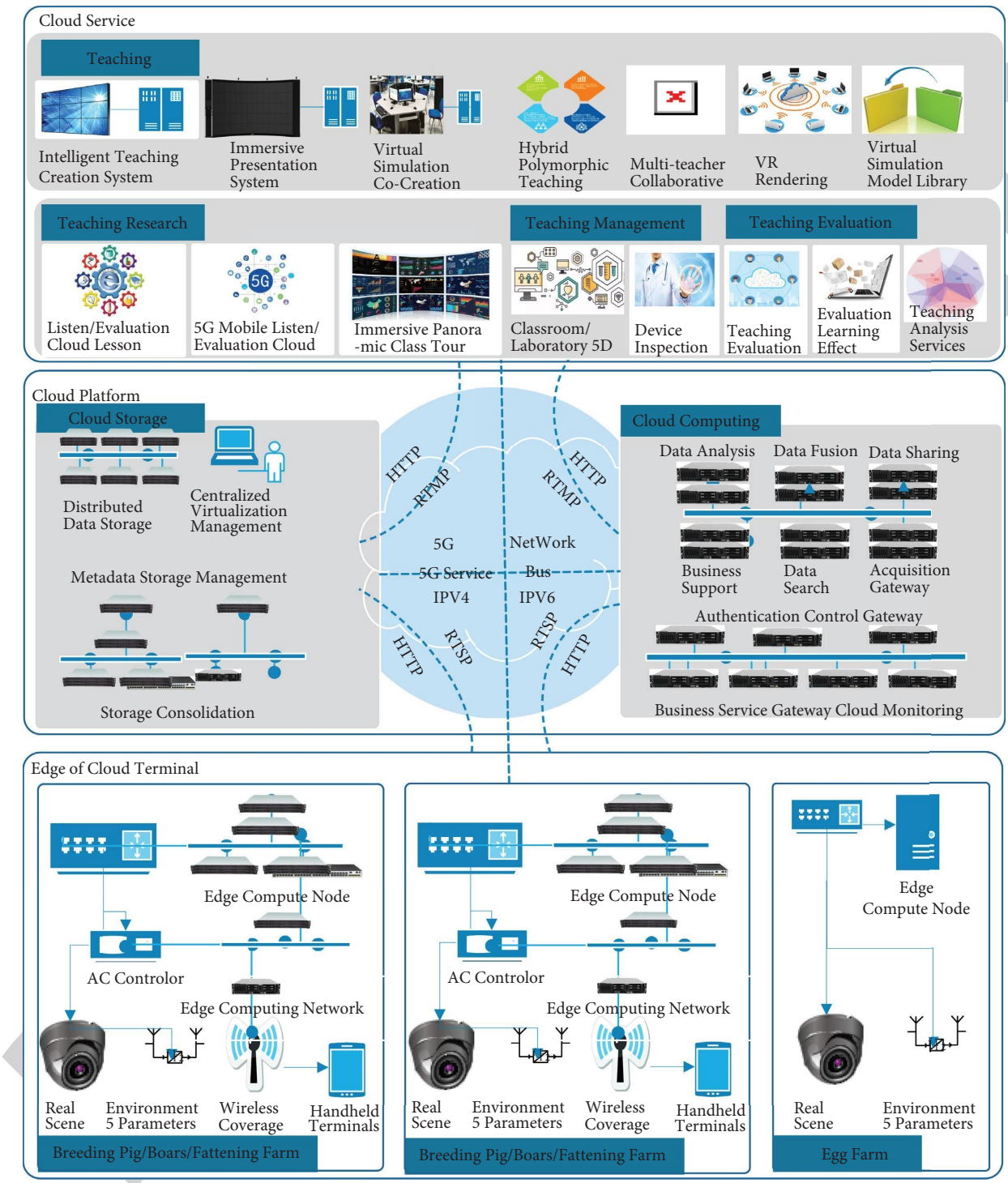

Figure 3: Intelligent education data center system cloud edge-end architecture diagram.

sharing system., respectively, to provide users with data from the assets (wisdom breeding four-dimensional imaging data, breeding the four-dimensional imaging fusion breeding four-dimensional imaging teaching material data resources, virtual simulation model, individual animals recognition training set data, animal contour recognition training set data, animal behavior recognition intensive track training set data), teaching resources, animal husbandry and teaching resources, Virtual simulation of teaching resources and teaching resources, combining false and true collaboration in twin teaching resources, teaching resources, digital teaching resources of the VR/AR), the platform resources (intelligence cultivation platform resource sharing systems, visualization analysis of environmental data sharing system, the big development suite sharing system, animal behavior analysis system, cloud recognition system, cloud, cloud

collaboration system diagnosis and treatment, live teaching system Training system), carrier resources (intelligent teaching virtual simulation creation carrier resources, intelligent teaching digital twin creation carrier resources, intelligent teaching collaborative creation carrier resources, intelligent teaching immersive display carrier resources, AI visual analysis carrier resources, cloud desktop carrier resources).

As can be seen from Figure 4, the Intelligent Teaching Resource Sharing System provides four types of sharing services: data Resource Sharing, Teaching Resource Sharing, platform Resource Sharing, and carrier Resource Sharing. Data resource sharing provides multi-tenant sharing, API data sharing, and swap space sharing. Teaching resource sharing mainly consists of real scene material sharing, virtual reality teaching resource sharing and animal husbandry course resource sharing. Platform resource sharing mainly includes big data analysis platform and visual big data analysis platform for animal husbandry professional users. Carrier resource sharing is composed of virtual simulation carrier resource sharing, digital twin carrier resource sharing, remote collaboration carrier resource sharing, virtual and real carrier resource sharing, cloud desktop carrier resource sharing. Through the sharing mechanism of the above four kinds of resources, the all-round sharing of teaching resources is realized and the sharing support for the intelligent education cloud platform is provided.

The system provides different recommender services for different users. The system can record users' multi-dimensional cognitive information [18], such as resource discipline, quantity, frequency, comments, likes, forwarding, expressions, to provide support for users to make complex sharing decisions and recommendations in the big data environment. In view of user preference fuzzy probability [19], a Bernoulli matrix decomposition recommendation algorithm based on intuitionistic fuzzy set is used to recommend shared resources for target users [20]. Three-layer Agent is designed to implement intelligent resource sharing recommendation. Agent 1: With the help of the relevant theoretical knowledge of intuitive fuzzy set, the user preference rating matrix is transformed into membership matrix, non-membership matrix and hesitation matrix; Agent 2: Use Bernoulli matrix decomposition model to fit 0–1 matrix in parallel to get the best set of potential feature vectors; Agent 3: The inner product of the feature vector of the matrix is divided and sorted proportionally to determine the intuitionistic fuzzy number favored by the target user. According to the comparison rules of intuitionistic fuzzy number, the intuitionistic fuzzy number set of the resources applied by the user is resorted, and the top one is selected as the recommended application resources.

6. Research of Intelligent Education Cloud Service System

Relying on the intelligent teaching data center and resource sharing center system, the construction of intelligent teaching cloud service system serves the construction of first-class specialty, promotes intelligent education and realizes the subversive revolution of teaching. Through the combination of virtual simulation and real scene panorama, traditional classroom, smart classroom, innovative practice and smart teaching are combined to open up new teaching approaches and realize new teaching forms. The intelligent teaching cloud service system is composed of four systems: intelligent teaching subsystem, intelligent teaching and research subsystem, intelligent teaching tube system and intelligent teaching evaluation subsystem. It provides users with real-scene teaching, virtual simulation teaching, immersive role-playing practice teaching, live interactive teaching and panoramic interactive live teaching. Carried out from the open classroom wisdom (cloud online courses, more open classroom, multi-dimensional holographic wisdom and open teaching, open hole 3 d class), teaching and research of cloud (cloud evaluation, immersive panorama online tour lecture), cloud taught tube (5 d open classroom/laboratory, equipment intelligent inspection) to the intelligent evaluation (teaching process evaluation, study effect evaluation) of disruptive innovation.

6.1. Research of Intelligent Teaching Subsystem. The intelligent teaching subsystem mainly carries out four-dimensional teaching composed of four dimensions: traditional multimedia, real scene panorama, virtual simulation and industry intelligent production. Based on cloud architecture of fusion network, the design of the open classroom, four-dimensional bricks, many live together and trainers, and other functions module, give full play to the 5 g low latency, high rate and large capacity, the characteristics of the integrated use of based on artificial intelligence, big data, cloud computing, Internet of things, virtual simulation, such as information technology, around the "teaching and research, tubes, review" and other key areas of teaching link, It provides convenient online teaching and training services for students, teachers, enterprise mentors, outside experts, education management personnel and technical personnel, improves network delay and lag, improves communication and interaction experience of teaching and training users, promotes balanced development of education resources and promotes education equity. The four-dimensional virtual and real combined teaching scenario is shown in Figure 5.

6.2. Design of Intelligent Teaching and Research Subsystem. The intelligent teaching and research subsystem consists of cloud listening and class evaluation and immersive online panoramic class tour function modules. Cloud listening and evaluating classes supports access to all classes anytime and anywhere, and real-time access to the listening and evaluating system for teachers' real-time picture acquisition, blackboard tracking and monitoring, student interaction and teachers' audio and video images under open classes, so as to carry out the listening and evaluating work for courses from a multi-dimensional and all-round perspective. Immersive online panoramic tour. To carry out online panoramic immersive tour, two modes are provided, one is automatic mode and the other is artificial mode. Automatic mode: including early warning mode and recommendation

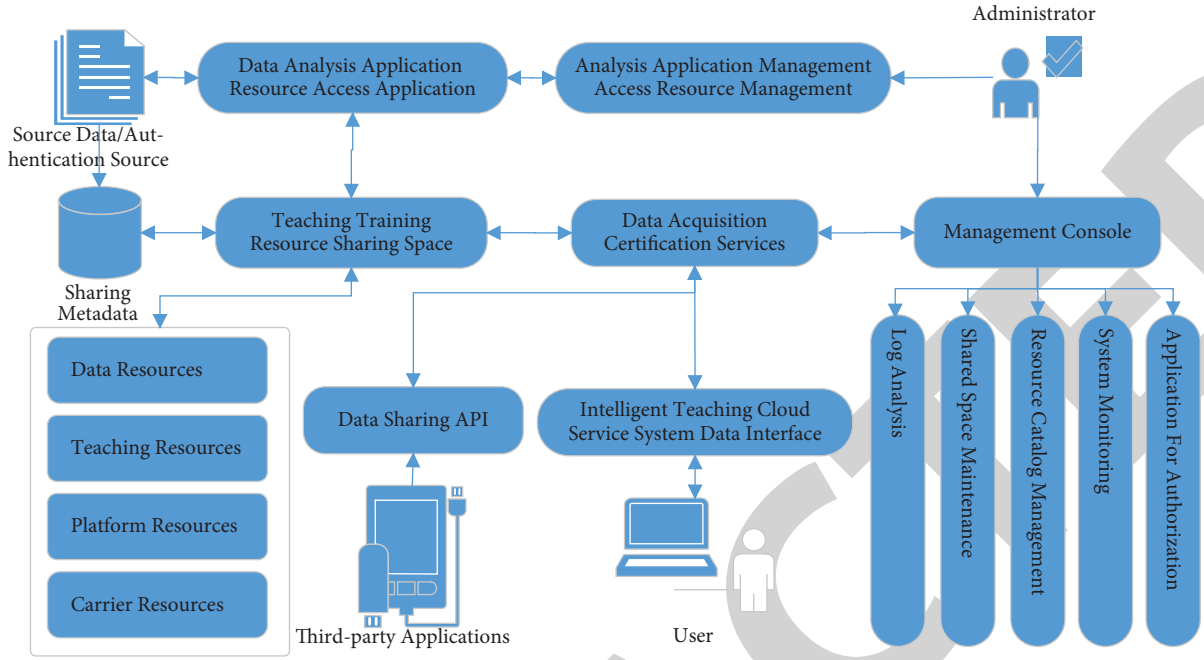

Figure 4: Architecture diagram of intelligent teaching resource sharing system.

Figure 5: Four-dimensional virtual and real combined teaching scenario.

mode, through the AI algorithm of the system, combined with all kinds of teaching and management information to automatically analyze the class, the patrol staff can warn the problem class and recommend the quality class, the patrol staff can carry out targeted work, save a lot of manpower and material resources, improve the efficiency of the tour; Manual mode: Immersive panoramic tour is provided for the tour staff, which can fully realize the change of management concept from "blocking" to "estrangement" for the courses they are interested in, improve teaching level, standardize teaching behavior, and improve the quality of teaching and research. The smart teaching and research is shown in Figure 6.

6.3. Intelligent Teaching Management System Research. Intelligent teaching pipe system consists of five-dimensional open management of classroom and laboratory and equipment AI inspection function. Five-dimensional open management of classroom and laboratory, to create an open experimental carrier system with five dimensions of time, space, object, process and content, to realize unattended and automatic operation of carrier and equipment management, and to facilitate the promotion and operation of smart teaching and training platform. Intelligent device inspection provides automatic online inspection function for the central server, edge server and all kinds of terminal equipment (5G terminal, network terminal, breeding farm production terminal, etc.) of the intelligent teaching management platform, provides real-time warning and provides certain degree of self-operation and maintenance services.

6.4. Intelligent Teaching Evaluation System Research. The intelligent evaluation subsystem carries out the teaching process evaluation and learning effect evaluation from the two dimensions of teachers and students, realizing the targeted online evaluation from the learning situation before, during and after class. The evaluation of smart is shown in Figure 7. The system supports a variety of evaluation systems, intelligent evaluation, real-time viewing of scores and effect analysis. Teaching process evaluation refers to the evaluation of the links or behaviors that affect the learning results of teachers in the process of teaching or interactive teaching. The assessment of teaching and learning effect, learning effect evaluation on learners learning after the completion of the final product testing or evaluation as overall rating of learners to participate in learning tasks, a full range of data, found that the participation of teaching and learning behavior model, the thinking process of digging their own to complete the task, real-time found problems in the process of problem solving, And then we can make immediate and accurate evaluation and intervention means through diversified and diverse forms. To evaluate the learning effect, students are evaluated comprehensively from

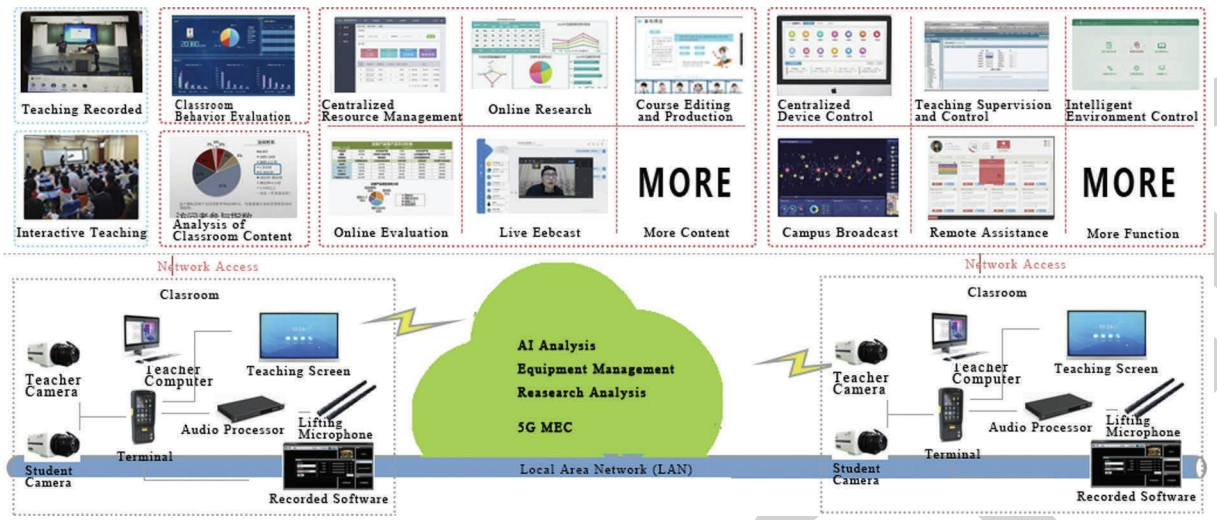

Figure 6: Smart teaching and research.

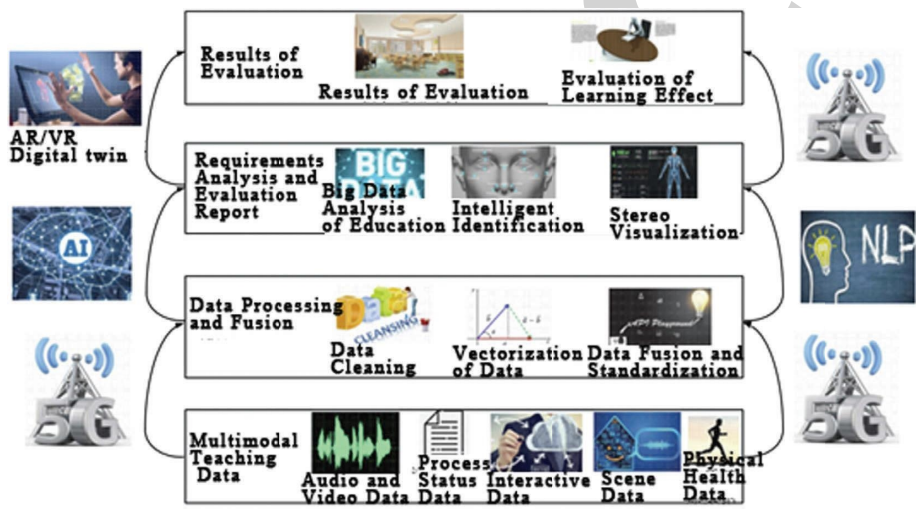

Figure 7: Evaluation of smart.

the whole learning process, three-dimensional and multi-dimensional data concerns to diversified interactive forms, and guidance and intervention after evaluation are provided for them.

The intelligent teaching evaluation system is studied, which focuses on the two dimensions of teaching process and learning effect, obtains multi-dimensional teaching evaluation data from the intelligent teaching subsystem, establishes the intelligent teaching evaluation engine, and realizes real-time automatic evaluation feedback. The data of teaching content, teaching means, course explanation, teaching attitude, learning state, learning duration, learning concentration, homework, experiment and examination are obtained from the intelligent teaching subsystem. Data such as gender and professional title are divided into classification data, and data such as scores are divided into numerical data. The teaching content, teaching methods and other data were scored according to the degree of satisfaction and then converted into numerical data. The k-Centers clustering algorithm proposed by Gao Feng was used to analyze the teaching characteristics of animal husbandry, find out the commonness and differences, and provide useful guidance for teaching improvement in real time.

The intelligent teaching evaluation system is studied, which focuses on the two dimensions of teaching process and learning effect, obtains multi-dimensional teaching evaluation data from the intelligent teaching subsystem, establishes the intelligent teaching evaluation engine, and realizes real-time automatic evaluation feedback. The data of teaching content, teaching means, course explanation, teaching attitude, learning state, learning duration, learning concentration, homework, experiment and examination are obtained from the intelligent teaching subsystem. Data such as gender and professional title are divided into classification data, and data such as scores are divided into numerical data. The teaching content, teaching methods and other data were scored according to the degree of satisfaction and then converted into numerical data. The detailed data planning is

Table 1: Teaching evaluation data set planning.

Dimension/Attribute	Type	Feature description
Teaching content, teaching methods, course explanation, teaching attitude, learning status, learning duration, learning concentration, homework, experiments to exams	Numeric	A 5-point scale is used. Note: The effect category is scored on a 5-point scale; numerical grades such as excellent, good, medium, pass and fail will be graded
Subject of the teacher	Can be classified	A total of 15 categories: Philosophy, economics, law, education, literature, history, science, engineering, agriculture, medicine, management, art, interdisciplinary, unknown
Professional title of teacher	Can be classified	There are four categories: Professor, associate professor, lecturer and assistant professor
Class student level	Can be classified	There are 2 categories: Undergraduate and graduate

shown in Table 1. The k-Centers clustering algorithm proposed by Gao's was used to analyze the teaching characteristics of animal husbandry, find out the commonness and differences, and provide useful guidance for teaching improvement in real-time [21].

K-centers algorithm (hard partition and fuzzy partition), minimize the objective function as shown in formula.

$$F(W,Z)=\sum_{l=1}^{k}\sum_{i=1}^{n}w_{li}^{\alpha}d(x_i,z_l). \tag{1}$$

The constraint conditions of fuzzy partition are shown in formula (2) and (3).

$$0\le w_{li}\le 1, 1\le l\le k, 1\le i\le n, \tag{2}$$

$$\sum_{l=1}^{k}w_{li}=1, 1\le i\le n, 0\le\sum_{i=1}^{n}w_{li}\le n, 1\le l\le k. \tag{3}$$

The constraint conditions of hard partition are shown in formula.

$$\min\{d(X_i,Z_l)\}\le\theta, 1\le l\le k, \tag{4}$$

where, $\alpha\ge 1$ represents fuzziness, when $\alpha=1$ is hard partition algorithm, and when $\alpha\rangle$ When 1, it is fuzzy partition algorithm.

The k-Centers algorithm process is described as follows:

(1) Select the initial clustering center $Z^{(1)}$ and the judgment ξ whether to terminate the iteration;

(2) According to the initial clustering center $Z^{(1)}$, the membership matrix $F(W,Z^{(1)})$ is obtained by minimizing $W^{(1)}$. For $t=1$;

(3) Minimize $F(W^{(t)},Z)$ to obtain a new clustering center $Z^{(t+1)}$. If $|F(W^{(t)},Z^{(t+1)})-F(W^{(t)},Z^{(t)})|\langle\xi$ is satisfied, stop.

(4) Minimize $F(W,Z^{(t+1)})$ to get a new membership matrix $W^{(t+1)}$. Stop, if $|X-Y|\langle\xi$ is satisfied, Where $X=F(W^{(t+1)},Z^{(t+1)})$, $Y=F(W^{(t)},Z^{(t+1)})$; Otherwise, let $t=(t+1)$ and return (3).

The complexity of the algorithm is O(n), and the computational complexity is approximately linear with the size of the data set, so that a large amount of data can be processed quickly and effectively [18], which meets the needs of real-time evaluation.

7. Conclusions

In view of the many challenges faced by agricultural and forestry colleges and universities in teaching, the intelligent teaching platform has been deeply studied, and the system architecture, application architecture and fusion network architecture have been proposed. Firstly, an in-depth study was carried out from the aspects of "openness, diversity, collaboration, equity and sustainability" of education, and it was proposed that online and offline teaching and double-teacher collaborative teaching should be carried out without being limited by time, space and safety prevention and control. Secondly, the teaching model of four dimensions from multimedia, real scene, virtual simulation to intelligent cultivation is studied. Thirdly, a smart teaching platform consisting of smart teaching, smart teaching research and smart evaluation is designed. The platform has been in operation for five years in relevant agricultural and forestry universities, which shows that the platform is reasonably designed, the sharing mechanism is complete, the cloud service is reliable, and it has the conditions for promotion and application in agricultural and forestry universities. However, the number of teaching resources related to real scene, virtual simulation and intelligent cultivation of the platform is limited, which is difficult to meet the teaching needs of all disciplines, and the corresponding new teaching resources are studied for different disciplines.

Data Availability

The data are available in the paper.

Conflicts of Interest

The authors declare that they have no conflicts of interest.

Acknowledgments

This work was supported by 2022 Basic Scientific Research Funding Project of Colleges and Universities—Improvement of Young Teachers' Scientific Research ability—Research on Key Technologies of Multi-dimensional Real Data Intelligent Analysis of Pasture (RZ2200001860), Inner Mongolia Autonomous Region Science and Technology Project 2022—Research and Application Demonstration of Key Technologies of Multi-dimensional Real data Acquisition and Intelligent Analysis and Processing in

Hindawi
Computational Intelligence and Neuroscience
Volume 2023, Article ID 4305594, 11 pages
https://doi.org/10.1155/2023/4305594

Research Article

An Image Classification Method Based on Adaptive Attention Mechanism and Feature Extraction Network

Juanjuan Luo[1] **and Defa Hu**[2]

[1]*Hunan International Economics University, Changsha 410205, Hunan, China*
[2]*Hunan University of Technology and Business, Changsha 410205, Hunan, China*

Correspondence should be addressed to Defa Hu; davenhu@hutb.edu.cn

Received 28 August 2022; Accepted 12 October 2022; Published 17 February 2023

Academic Editor: Zaoli Yang

The convolution neural network (CNN) not only has high fault tolerance but also has high computing capacity. The image classification performance of CNN has an important relationship with its network depth. The network depth is deeper, and the fitting ability of CNN is stronger. However, a further increase in the depth of CNN will not improve the accuracy of the network but will produce higher training errors, which will reduce the image classification performance of CNN. In order to solve the above problems, this paper proposes a feature extraction network, AA-ResNet with an adaptive attention mechanism. The residual module of the adaptive attention mechanism is embedded for image classification. It consists of a feature extraction network guided by the pattern, a generator trained in advance, and a complementary network. The feature extraction network guided by the pattern is used to extract different levels of features to describe different aspects of an image. The design of the model effectively uses the image information of the whole level and the local level, and the feature representation ability is enhanced. The whole model is trained as a loss function, which is about a multitask problem and has a specially designed classification, which helps to reduce overfitting and make the model focus on easily confused categories. The experimental results show that the method in this paper performs well in image classification for the relatively simple Cifar-10 dataset, the moderately difficult Caltech-101 dataset, and the Caltech-256 dataset with large differences in object size and location. The fitting speed and accuracy are high.

1. Introduction

Image classification is an image processing technology that extracts effective features from the most original image data and then achieves the goal of distinction of different categories of objects in the image. Now, image classification is one of the most important research hotspots in the field of computer vision. To realize image classification with traditional methods, it must be realized in two stages. First, the unstructured data of the original image data must be converted into structured data used to represent features. Then, the structured feature data must be input into a trainable classifier. Finally, the classification results can be obtained [1, 2]. However, the traditional image classification methods have some shortcomings in that the accuracy of image classification depends on the effectiveness of feature extraction to a large extent [3]. Sometimes, there are some features without discrimination in the image that may have a great negative impact on the classification results. However, the method based on CNN does not need complicated feature extraction and can directly integrate the feature analysis of image data into the CNN model. Only by adjusting the weight and offset of the network model, the effective distinction of image features can be quickly realized [4, 5].

In traditional methods, image classification often needs to work in stages. The first step is feature learning and then feature coding. There are also spatial constraints, of course, the classifier is indispensable, and the process is complex [6, 7]. This traditional method may be effective for some simple image classification tasks, but if the traditional classification method is applied to the actual complex scenes,

the results may not be too optimistic. Therefore, researchers began to try using convolutional neural networks to solve the task of image classification, using nonhuman operation methods to extract features from images and analyze the sample data in some aspects, to achieve the purpose of classifying specific targets into a certain label in a known mixed category [8]. However, when using CNN model for image classification, the image classification performance of CNN has a very important relationship with the depth of the network model. The network depth is deeper, and the fitting ability of the CNN is stronger. However, with the increasing depth of the network model, the classification accuracy of the model is not improved, the gradient disappears, and the network model produces higher errors [9, 10]. In view of the above problems, the ResNet model can solve the problem of performance degradation of the model under deep conditions to a certain extent [11]. Recent research shows that the performance of convolutional neural networks can be improved using cross-layer connections. The typical residual network (ResNet) uses this idea to achieve a very good image recognition effect through the identity mapping method. However, in the residual module, the layout of cross-layer connecting lines does not reach the optimal setting, resulting in the redundancy of information and waste of layers [12, 13].

The image classification performance of CNN has an important relationship with its network depth. The network depth is deeper, and the fitting ability of CNN is stronger. However, a further increase in the depth of the CNN will not improve the accuracy of the network but will produce higher training errors, which will reduce the image classification performance of the CNN. In order to solve the above problems, this paper proposes a feature extraction network, AA-ResNet, with an adaptive attention mechanism. The residual module of the adaptive attention mechanism is embedded for image classification.

2. Related Work

In recent years, with the advent of the big data era and the development of computer hardware conditions, people have started a more comprehensive and in-depth study of deep learning. Through a large number of theories and experiments, it is proved that the convolutional neural network in deep learning plays an irreplaceable role in the field of image classification. It can obtain image features through a large number of sample training, and the designed classifier is closely related to the extracted features [14]. Compared with traditional classification algorithms, convolutional neural networks can automatically learn the features of image data, and people do not need to spend a lot of experience manually extracting image features. This has a significant effect on image classification tasks with large sample sizes and small differences between categories [15].

The extremely deep convolutional neural network will not only cause the gradient disappearance but also increase the risk of network overfitting, which will affect the accuracy of image classification of the network model. The initial research method is mainly to solve the problem of network gradient disappearance by initializing the network model and conducting hierarchical training. At present, deep convolution neural networks mostly use the activation function ReLU to alleviate the problem of gradient disappearance. Compared with the sigmoid function, the ReLU function is more effective in alleviating the gradient disappearance [16]. The direct supervision method can be used to train the deep CNN model, but in the process of training the deep CNN model, once some inputs of the activation function ReLU enter the hard saturation region, the corresponding weights cannot be updated quickly [17]. The appearance of the neuron death phenomenon will make CNN difficult to converge. Therefore, many new activation functions have been proposed one after another, for example, the PReLU function introduces additional parameters to improve its performance. Another example is the ELU (exponential linear unit) function, which combines the Sigmoid and ReLU functions. Because of its left side saturation, the gradient disappearance problem of the network model can be greatly alleviated [18, 19]. Another example is the PELU (parametric exponential linear unit) function, which is to add parameters to the ELU function and controls the performance of the activation function by training the network model and updating the parameters of the network model in time to better control the offset drift and gradient disappearance during the training of the network [20, 21].

The depth of the CNN is further increased, but the accuracy of the model is not improved. On the contrary, the phenomenon of the gradient disappearing occurs, which results in a higher error. For the above problems, the ResNet model is better than an ordinary convolutional neural network in terms of convergence and classification performance [22]. The main innovation of the ResNet model is to introduce a residual structure into the network, which can quickly transfer the results of the previous layer to the next layer network. When the network model is further deepened, the error will not continue to increase, which makes the ResNet model have more layers and more accurate accuracy [23, 24]. With the increasing depth of the network model, the accuracy of the network model is gradually far from that of the ordinary network model. Obviously, this solves the problem of degradation of the image classification performance of the network model under the condition of depth to a certain extent [25].

3. Feature Extraction Network Based on Selective Attention Mechanism

3.1. Detailed Steps of Residual Block. The detailed steps of selecting the residual block based on the attention mechanism can be summarized as follows:

Step 1. For the intermediate feature map in the neural network layer $X_0 \in R^{H\times W\times C}$, to reduce the parameters and calculation amount, it is sent to the convolution kernel with a size of 1×1 to obtain the feature map $X_1 \in R^{H\times W\times C_1}$, where $H \times W$ represents the spatial dimension of the corresponding feature map C and C_1 representing the channel dimension of the corresponding feature map;

Step 2. Group convolution is used to perform a channel-based grouping operation on the feature map X_1 to obtain a plurality of subfeature maps with the same dimension, $X_1 = \{x_1 \cdots, \text{grop}\}$, $x_i \in R^{H\times W\times C_1/\text{group}}$, where group represents the number of subfeature maps, $i = \{1, \cdots, \text{group}\}$, and x_i represents the i th sub feature map;

Step 3. The specific operations of the spatial group enhanced attention transformation adopted for each subfeature map x_i are as follows:

(1) For all the obtained subfeature maps $x_i \in R^{m\times c}$, the global average pooling operation $F_{gp}(\bullet)$ based on space is performed to obtain the global semantic vector $g \in R^{1\times c}$ of the subfeature map x_i, where $m = H \times W$ represents the spatial dimension of the subfeature map and $c = C_1/\text{group}$ represents the channel dimension of the subfeature map;

(2) Use the global semantic vector of the subfeature map x_i and multiply it with each subfeature map point to obtain the importance coefficient $c_i \in R^{m\times 1}$ corresponding to each subfeature map;

(3) Each importance coefficient c_i is normalized in the spatial dimension to obtain c_i';

(4) Scale and translate each of the standardized importance coefficients c_i' to obtain a_i;

(5) The newly generated importance coefficient a_i generates a spatial enhanced feature map x_i' for each subfeature map through a Sigmoid function $\sigma(\bullet)$ combined with subfeature maps x_i corresponding a_i;

(6) The binding step (5) was formulated as the spatial enhancer feature map x_i', resulting in the feature maps $X_i' = \{x_i' \cdots, \text{group}'\}$, $x_i' \in R^{H\times W\times C_1/\text{group}'}$, where group' represents the number of spatial enhancer feature maps and $i = \{1, \cdots, \text{group}'\}$, and x_i' represent the ith post enhancer feature map;

(7) Feed X_i' into the convolutional layer in which the convolution kernel was 1×1 and perform ascending dimension manipulation, obtaining the feature map $X_0' \in R^{H\times W\times C}$ which has the same dimension of X_0, where $H \times W$ representing the spatial dimension of the feature map X_0' and C representing the channel dimension of the feature map X_0';

(8) Formulation of step (7) as an intermediate feature map X_0 combined with the newly derived feature map X_0', thus they yield the output feature map $\widehat{X}_0 \in R^{H\times W\times C}$ for this spatially grouped attention module, where $H \times W$ represents the spatial dimension of feature Fig. $\widehat{X}_0$ and C represents the channel dimension of the feature map $\widehat{X}_0$;

Intermediate feature maps obtain an enhanced attentional feature map when they go through the residual blocks of the middle layers of the network from the above steps. The feature maps were augmented to different degrees by stacked residual blocks. Similarly, with the aid of groupwise convolution, the width of the network is boosted, further enhancing the semantic information of the feature maps. The classification accuracy of the network model can be greatly improved by the network model [26, 27]. Therefore, this paper chose the ResNet101 residual network model as the benchmark model, and in the next step, attentional mechanisms will be incorporated into the ResNet101 model to further improve the classification accuracy.

3.2. Residual Module Improvement. The residual network can deepen the network without reducing the efficiency of the model, and its schematic is shown in Figure 1.

A neural network with the input of x and the output of $\alpha^{[l]}$. Adding new two layers to the end, the output becomes $\alpha^{[l+2]}$. These two layers that are newly added are turned into residual blocks. The network is activated using the ReLU activation function, and none of the activation values is less than 0. The value of $\alpha^{[l+2]}$ can be represented by (1):

$$\alpha^{[l+2]} = f\left(z^{[l+2]} + z^{[l]}\right). \tag{1}$$

Of these, f was the activation function; $z^{[l+2]}$ was the unactivated network output for the layer $l + 2$; $\alpha^{[l]}$ was the identity mapping of layers 11 to 22. From (1), it is guaranteed that $\alpha^{[l]}$ is the same dimension as $z^{[l+2]}$ to be computable. (1) can also be unfolded, as shown in (2):

$$\alpha^{[l+2]} = f\left(\omega^{[l+2]}\alpha^{[l+2]} + b^{[l+2]}\alpha^{[l]}\right). \tag{2}$$

Even if $\omega^{[l+2]}$ tends to 0, $b^{[l+2]}$ is equal to 0, $\alpha^{[l+2]} = f(\alpha^{[l]})$, since the entire network uses ReLU activation, $\alpha^{[l+2]} = \alpha^{[l]}$. That is, the jump connection can make it easy for the network to learn $\alpha^{[l+2]} = \alpha^{[l]}$. That is to say, even if the entire network adds two layers, the learning efficiency of the network will not decrease.

It is easy to learn the identity function of the network. Even if there are two more layers, $\alpha^{[l]}$ can be assigned to $\alpha^{[l+2]}$ through identity mapping. That is, the network performance will not be affected, and the network efficiency can be improved. In practice, $\omega^{[l+2]}$ will not be 0. That is, new information can be learned through the residual block. Networks are better than just learning identity functions. The ordinary network without residual block is difficult to learn the identity connection, and it will not be better than before. Therefore, creating residual blocks is advantageous to improve network efficiency. The parameters of the network model can be greatly reduced. Its principle is to reduce the dimension first and then increase the dimension by using the convolution kernel of size. In order to better extract the features of the image, the attention mechanism module is integrated into the original residual unit to form a new residual structure. The specific integration position is shown in Figure 2.

Although the attention mechanism will add some computational overhead, it is very beneficial to improve the classification accuracy of the network model. Figure 2 shows a feature map with an input of $64 \times 56 \times 56$, and the calculation process of the attention weight of each channel is generated through the residual unit. The feature map with the input of x and the size of $64 \times 56 \times 56$ will first pass through three two-dimensional convolutions. These two-

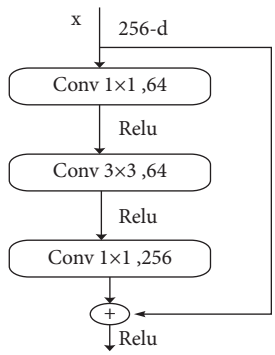

Figure 1: Network model for adding residual blocks.

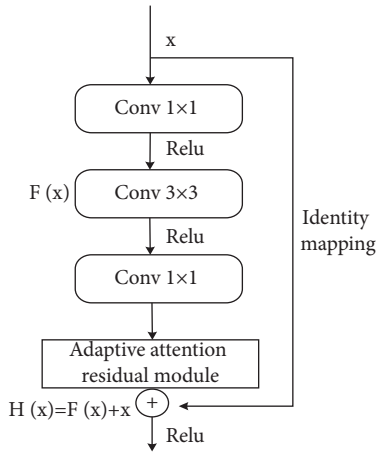

Figure 2: Residual unit integrated into attention mechanism.

dimensional convolution layers play a role in reducing the number of parameters. The first two convolution layers are activated by the ReLU function. The left side shows the relevant parameters of the step size, convolution kernel size, and filling value. After three convolutions and two activation operations, the output feature map size is $256 \times 56 \times 56$.

Secondly, when entering the attention mechanism module, the feature map output in the previous step will first undergo adaptive global average pooling to obtain an output feature map with a size of $256 \times 1 \times 1$; after removing one dimension and exchanging the positions of the remaining two dimensions, one-dimensional convolution is performed. In this step, the convolution kernel size is 3, the step size and filling are 1, and the feature map size is 1×256. By exchanging and expanding the dimensions of the feature map by one dimension, then Sigmoid activation is performed to obtain 256 weight values representing the weights of each dimension. The 256 weight values are multiplied by the initial feature information to obtain a new output feature map whose size is $256 \times 56 \times 56$. The above is the process of inputting x and obtaining $F(x)$.

Then, identity mapping is performed. In order to ensure that the feature map with input 11 and the feature map with output 22, feature maps have the same dimension and can be added, the dimension of x must be increased first, as shown on the right side in Figure 2, so that the channel dimension becomes 256. The output $H(x) = F(x) + x$ of the residual unit can be obtained.

4. Experimental Comparison and Analysis

4.1. The Setting of Model Parameters. When training the AA-ResNet model in this paper, the hyperparameters that need to be set mainly include the size of batch training, the size of the learning rate, the selection of classification number, and the weight decay rate. The size of batch training determines the descending direction of the AA-ResNet model. When the dataset is large enough, the size of batch training should be appropriately reduced to greatly reduce the calculation amount. If the data amount is small and there is noise data, the batch training should be set to a large value to reduce the interference of noise data. When batch training reaches a certain value, the AA-ResNet model is optimal in terms of training time and convergence accuracy.

The magnitude of weight update is closely related to the learning rate, so it is very beneficial to set the learning rate in an appropriate range to reduce the gradient of the AA-ResNet model to the optimal value. If the learning rate is set too large, the weight of the AA-ResNet model will exceed the optimal value and then swing back and forth at the end with a small error. However, if the learning rate is set too small, the optimization of the AA-ResNet model will require a lot of time, and even the model may not converge. The initial learning rate of the AA-ResNet model in this paper is set to 0.1. However, with the increase in the number of iterations of the model, it is gradually adjusted to 1/10000, to improve the accuracy of the AA-ResNet model while obtaining a faster training speed. In the training process, overfitting often occurs. The greater the weight of the AA-ResNet model, the greater the risk of overfitting. In order to reduce the risk of overfitting, a penalty term is added to the error function. The weight decay rate is the main parameter for calculating the regularization of L_2. The main function of the weight decay rate is to adjust the influence of the complexity of the AA-ResNet model on the loss function. The regularization of L_2 can obtain parameters with small values to reduce the risk of model overfitting.

4.2. Model Evaluation Index. In this paper, the evaluation indicators of the model include training time, train acc, test acc, loss value parameters, drawing confusion matrix, accuracy, and loss value change line graph, where train acc refers to the proportion of the number of correctly predicted samples in the training set to the total number of samples in the training set. In semantic segmentation, it refers to the proportion of correctly predicted pixels in the training set to the total number of pixels. Test acc refers to the proportion of the number of correctly predicted samples in the test set to the total number of samples in the test set. In segmentation, it refers to the proportion of correctly predicted pixels in the test set to the total number of pixels. The loss value reflects the degree to which the predicted value of the model is different from the real value. Calculate the cross entropy loss function of the loss value. For sample i, construct a vector $y^{(i)} \in R^q$ so that the $y^{(i)}$ element (discrete value of the category of sample i) is 1 and the rest is 0 to represent the real label; $\hat{y}^{(i)}$ denotes a probability distribution predicted by the model; Θ denotes model parameters. Training time

refers to the average time of training an epoch for the training set.

$$H\left(y^{(i)}, \hat{y}^{(i)}\right) = -\sum_{j=1}^{q} y^{(i)} \log \hat{y}^{(i)}, \tag{3}$$

$$l(\Theta) = \frac{1}{n} \sum_{i=0}^{n} H\left(y^{(i)}, \hat{y}^{(i)}\right). \tag{4}$$

4.3. Data Set. The image classification data used in this experiment include the Cifar-10, Caltech-101, and Caltech-256 data sets. Cifar-10 is a data set containing 60000 images, of which 50000 are training images and the other 10000 are test images. Each photo is a $32 * 32$ pixel color photo. All photos belong to 10 different categories, namely airplane, automobile, bird, cat, deer, dog, frog, horse, ship, and truck. In this experiment, 50000 training images are used to construct the dataset, and 5000 images are used in each class. According to the ratio of 8 : 2, 40000 images are constructed as the training set, and the other 10000 images are constructed as the test set. Caltech-101 is a data set containing 9144 images. The image is a color image, most of which have a separation rate of $300 * 300$ pixels. All the images belong to 101 different categories, including accordion, chair, crab, and laptop. The number of images in each category ranges from 31 to 800. Caltech-256 is a data set containing 30607 images. The image is also a color image. All the images belong to 101 different categories, including cakes, CDs, coins, frogs, grapes, and so on. The number of images in each category ranges from 80 to 827.

4.4. Cifar-10 Data Set Experimental Results. The Cifar-10 data set is a relatively easy data set for image classification. One reason is that the number of images available for training in the Cifar-10 data set is huge, with a total of 60000 images, and 50000 images were used in the experiment. Second, there are only ten categories due to fewer categories. According to the theoretical research and inference of existing algorithms, after the training of the convolutional neural network model, higher accuracy can be obtained. This is supported by the data in Table 1.

It can be seen from Table 1 that the accuracy of the five models on the Cifar-10 data set is high and the difference is small. The accuracy of the training set was more than 95%, and the accuracy of the test set was about 90%. From the data, we can find that the model in this paper has the best fitting for the dataset. The accuracy of the training set and the test set is the highest among all models, which are 99.96% and 92.43%, respectively. The loss value was the lowest, only 0.00129.

It can be observed from Figure 3 that the loss values of the five models gradually decrease from the interval of 1.5 to 2 to about 0. Among them, the cyan curve of the AA-ResNet model is located at the bottom as a whole, the loss value is close to 0 at about 8 epochs, and the fitting speed is fast.

Table 1: Experimental results of Cifar-10 data set.

	AlexNet	VggNet	GoogLeNet	AA-ResNet	DenseNet
Train Acc	98.58%	98.93%	99.67%	99.96%	98.78%
Test Acc	91.42%	87.85%	90.54%	92.43%	91.11%
Loss	0.04569	0.03547	0.11288	0.00129	0.03543
Time (s)	145.71	202.68	306.90	253.71	374.37

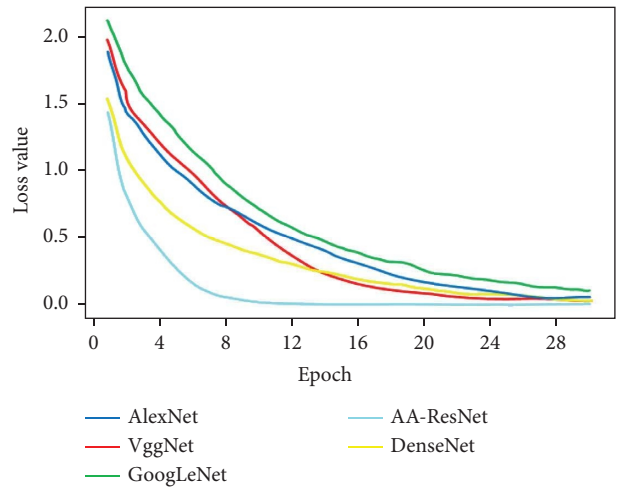

Figure 3: Loss value of Cifar-10 data set.

The accuracy broken line graph in Figure 4 reflects the changes in the training set accuracy rate train acc and the test set accuracy rate test acc as the number of epochs increases. It can be found that the accuracy starting point range of the training set and test set of AlexNet, VggNet, and GoogLeNet models is relatively consistent, between 20% and 40%, while the starting point range of AA-ResNet is relatively high, between 50% and 60%, and the initial fitting is relatively good. At the same time, it can also be seen that the accuracy rate of AA-ResNet has a large initial discount slope, which indicates that the accuracy rate is greatly improved with less epoch numbers, it is also a performance of excellent performance. It was also found that when the accuracy of the training set tends to be stable, the accuracy of the test set does not change.

In terms of data parameters and overall mapping, the classification results of the five models are excellent in the Cifar-10 dataset experiment. This is not only because the classification difficulty of the Cifar-10 data set is low but also reflects the superiority of convolutional neural networks in the field of image classification. However, there are small differences between the models. AA-ResNet has the best performance, high accuracy, and fast fitting speed in the Cifar-10 data set. The comprehensive performance of the other models is relatively consistent.

4.5. Caltech-101 Data Set Experimental Results. The classification difficulty of the Caltech-101 data set is significantly higher than that of the Cifar-10 data set. Not only has the classification category increased from 10 to 101 but also the

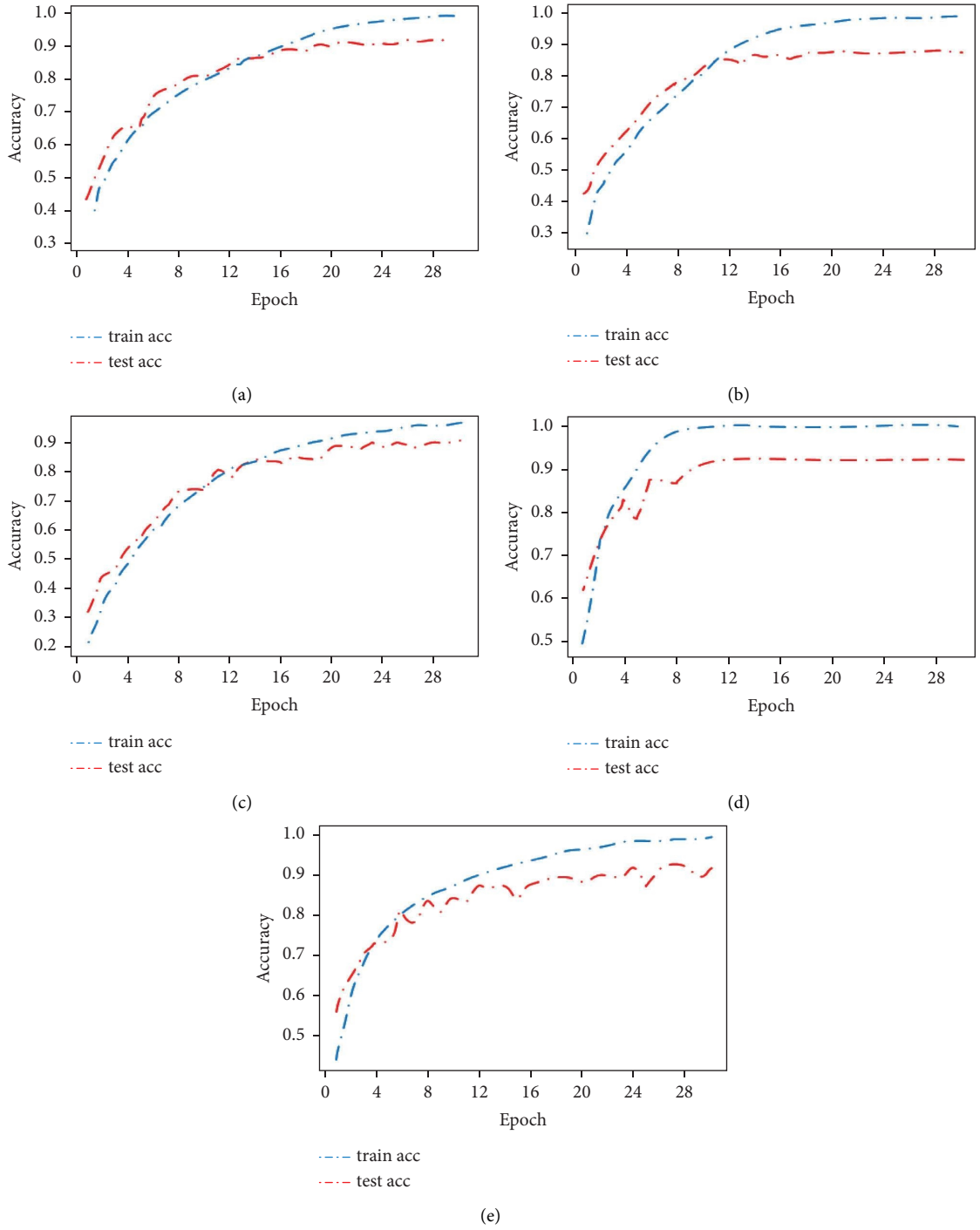

Figure 4: Accuracy rate of Cifar-10 data set. (a) AlexNet. (b) VggNet. (c) GoogLeNet. (d) AA-ResNet. (e) DenseNet.

number of categories has increased 10 times. Moreover, the number of images available for training has been reduced from 60000 to 9000, which is a great challenge to the convolutional neural network model. Generally speaking, the accuracy of image classification will be significantly reduced, and the difference between models will be more obvious. Table 2 supports this conjecture.

The data obtained in Table 2 are the results of the training Caltech-101 training set with 50 epochs. Due to the increasing difficulty of image classification in the Caltech-101 dataset, the classification accuracy of the test set is significantly lower than that of the Cifar-10 dataset. It can be found that the accuracy of the five models on the Caltech-101 test set is about 60%–70%, and the difference is also highlighted. At the same time, it can also be found that the convolution neural network can fit the training set of the dataset well, and the accuracy of the model training set is more than 98%, but the accuracy of the test set is different.

Table 2: Experimental results of Caltech-101 data set.

	AlexNet	VggNet	GoogLeNet	AA-ResNet	DenseNet
Train Acc	98.45%	99.29%	99.35%	99.96%	99.81%
Test Acc	70.07%	63.74%	63.32%	69.61%	71.28%
Loss	0.05628	0.03123	0.01042	0.00352	0.03112
Time (s)	42.55	43.56	61.27	55.82	70.91

AA-ResNet has also reached about 70%, which is the most accurate of several models. Moreover, due to the reduction in the number of images, the training time of a single epoch decreased significantly, from 253.71 seconds to 55.82 seconds, the number of training images decreased 3 times, and the training time decreased 4 times.

In Figure 5, the starting position of the loss value of the five models is near 4, which is higher than that of the previous Cifar-10 experiment. Among them, the loss value of AA-ResNet is around 0 at 14 epochs, which is far ahead of the other models. This also proves that the performance of the convolutional neural network model in the Caltech-101 data set is not as good as that in the Cifar-10 data set, because there are not many bright blocks outside the diagonal in the confusion matrix of Cifar-10, and there are no black blocks on the diagonal. At the same time, it can also be found from the confusion matrix that the classification effect of each model on small classes is inconsistent, and the classes with good and poor image classification effects of each model are inconsistent, which also shows the differences between models.

As shown in Figure 6, the Caltech-101 data set takes 50 epochs to make all models fit well, and the training set accuracy rate train acc reaches more than 95%. The corresponding Cifar-10 data set only takes 30 epochs, which also proves that the Caltech-101 data set is more complex and difficult to fit. It can be seen from the figure that AA-ResNet has a fast fitting speed and the accuracy rate of the training set is close to 100% when it is around 20 epochs. However, the GoogLeNet and DenseNet models fluctuate greatly. Even GoogLeNet has a large "*V*" shaped fluctuation, which is generally caused by a poor fitting effect. It can also be found that when the training set accuracy rate train acc and the test set accuracy rate test acc curves tend to be stable. The two lines are separated by a large distance, which also indicates that the model has not achieved a particularly good effect.

On the whole, it can also be found that Caltech-101 is more complex. The fitting effect of the model is lower than that of the previous Cifar-10 experimental model, and it shows differences. AA-ResNet performs well as a whole, with small fluctuations and fast fitting speed.

4.6. Caltech-256 Data Set Experimental Results. The Caltech-256 data set is much more complex than the Cifar-10 and Caltech-101 data sets in the above experiments. It is also a data set that is difficult to classify in all image classification data sets. The Caltech-256 dataset is composed of 256 categories, with a large number of categories, and the images in

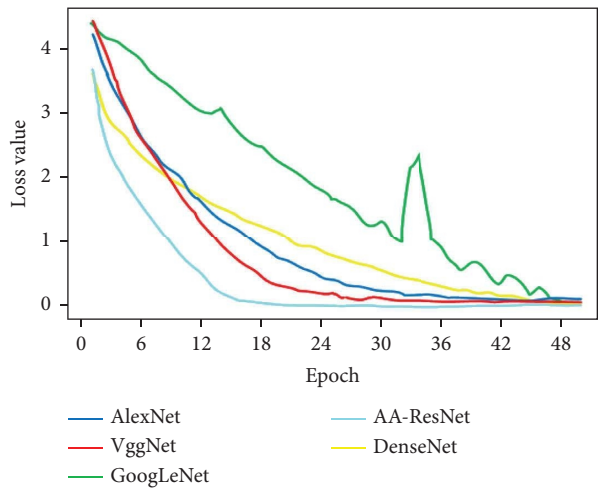

Figure 5: Loss value of Caltech-101 data set.

the dataset differ greatly in object size and position. All this means that the difficulty of classification is increased, to explore the specific performance of each network model for this complex situation and the differences in the complex situation. Table 3 shows the experimental results of the Caltech-256 data set.

The data in Table 3 are the results of the Caltech-256 training set with 50 epochs. It can be found that the accuracy rate is significantly lower than that of the above Cifar-10 and Caltech-101 data set experiments. The accuracy rate of the test sets of the five models is within the range of 30%–55%, and the difference between the models is greater. When the number of epochs trained in the Caltech-101 experiment is the same, the accuracy rate of the five model testing sets is lower, of which the accuracy rate of AA-ResNet is about 50%. Since the number of images in the Caltech-256 dataset is three times that of the Caltech-101, the training time is also greatly increased. It can be seen that the training time is in direct proportion to the number of images.

In Figure 7, the loss value of the five models gradually decreases from about 5 to about 0 with the increase in the epoch number. AA-ResNet first approaches 0 at 18 epochs, which indicates that AA-ResNet is ahead of the other models. The diagonal line of the AA-ResNet confusion matrix is brighter, so it is analyzed that the image classification effect of this model is better.

As shown in Figure 8, the accuracy starting points of the five models are all around 0%. This phenomenon is caused by the complexity of the Caltech-256 data set. Consistent with the above experiments on Cifar-10 and Caltech-101 data sets, the fitting speed of AA-ResNet is the fastest among the five models, and the fitting is completed in about 18 epochs, and the accuracy of the training set is nearly 100%. What is inconsistent with the above experiment is that the fluctuation of the model is relatively small, and the distance between the training set accuracy train acc curve and the test set accuracy test acc curve is larger. It can be seen that Caltech-256 is extremely complex and the fitting effect of the model is poor, but it shows a greater difference.

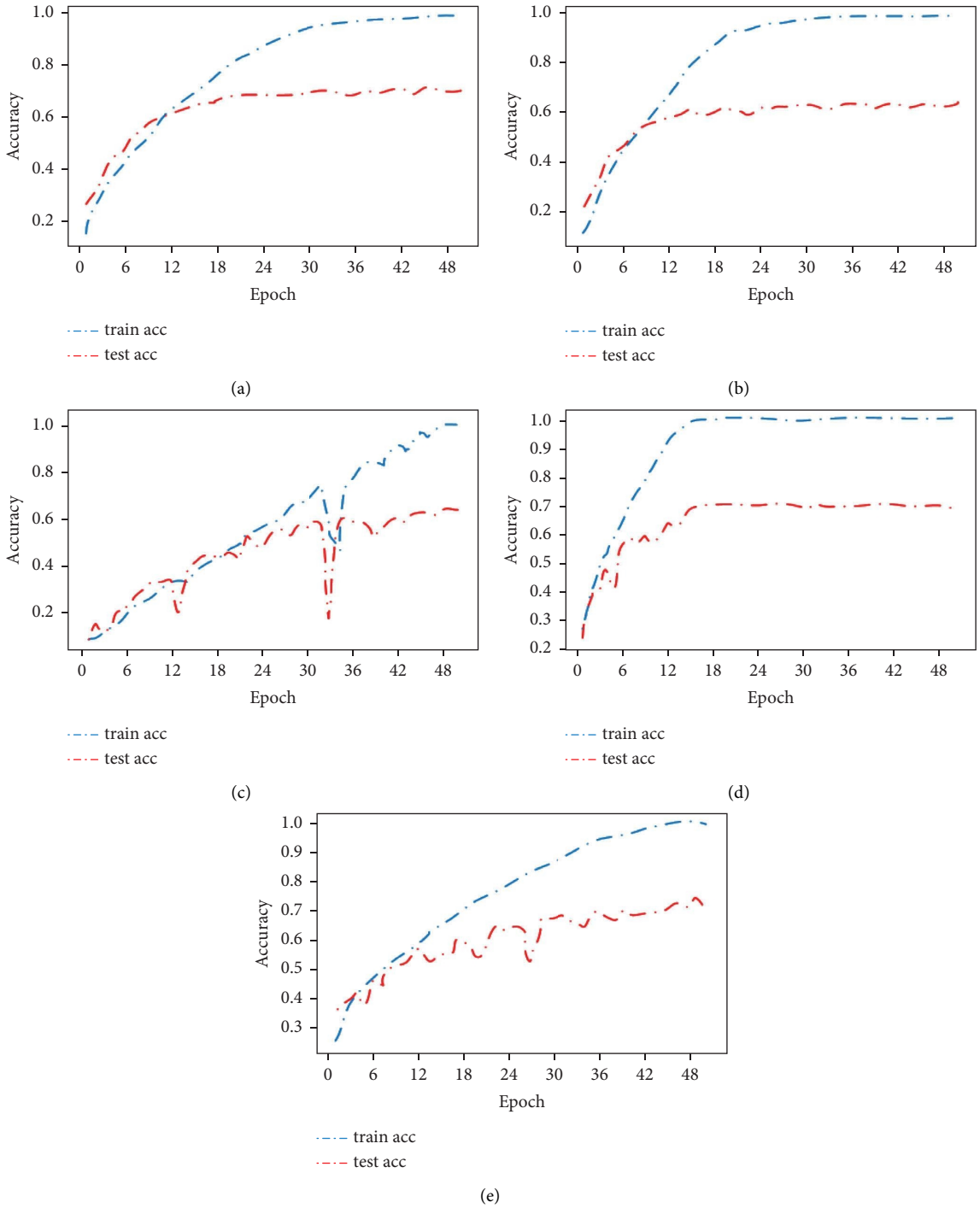

Figure 6: Accuracy rate of Caltech-101 data set. (a) AlexNet. (b) VggNet. (c) GoogLeNet. (d) AA-ResNet. (e) DenseNet.

Table 3: Experimental results of Caltech-256 data set.

	AlexNet	VggNet	GoogLeNet	AA-ResNet	DenseNet
Train Acc	96.28%	98.47%	96.34%	99.88%	93.94%
Test Acc	40.13%	33.21%	35.67%	52.29%	47.26%
Loss	0.12786	0.04983	0.14234	0.00217	0.28646
Time (s)	152.34	176.92	209.25	211.46	263.55

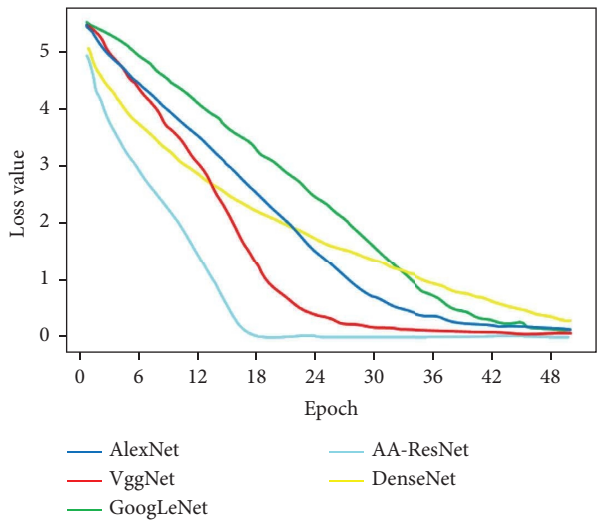

Figure 7: Loss value of Caltech-256 data set.

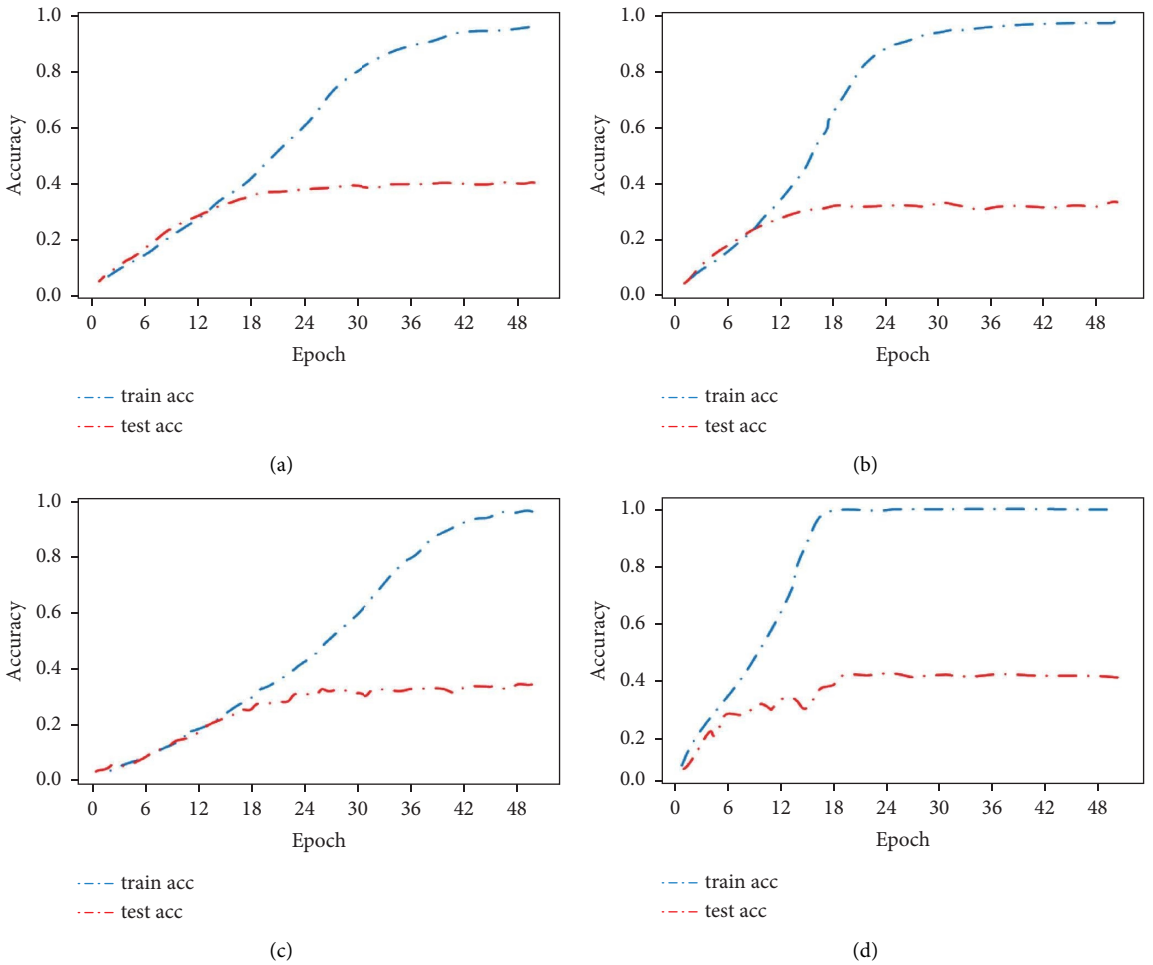

Figure 8: Continued.

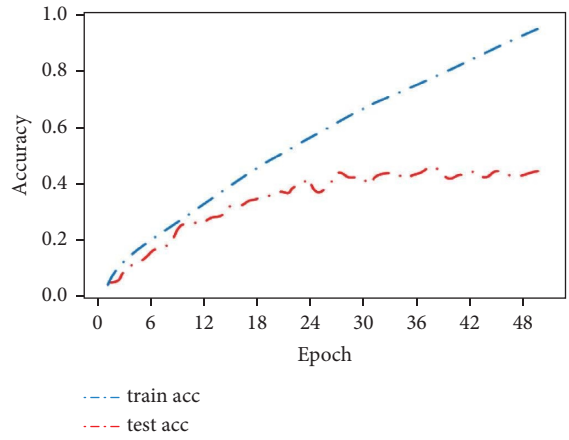

(e)

Figure 8: Accuracy rate of Caltech-256 data set. (a) AlexNet. (b) VggNet. (c) GoogLeNet. (d) AA-ResNet. (e) DenseNet.

In general, among the five models, the AA-ResNet proposed in this paper performs well. The test set has the highest accuracy, and the classification effect of each class is better.

5. Conclusions and Future Work

In the experiment, we use the data sets of Cifar-10, Caltech-101, and Caltech-256 to test the superiority of the proposed AA-ResNet model compared with the AlexNet, VggNet, GoogLeNet, and DenseNet models, and verify that AA-ResNet has better performance in image classification. By comparing the training time, accuracy and loss value parameters of the five models and drawing the confusion matrix, accuracy, and loss value change line graph, it is found that AA-ResNet has the best performance among the five convolutional neural network models, and the fitting speed of AA-ResNet is faster.

In the future, we can continue to improve the accuracy of the model by increasing the layers of AA-ResNet and spending more time to adjust the parameters of the model. Due to the limitations of the hardware and software, the relevant data for the complete model will be supplemented in the subsequent experiments. Although the convolution neural network model is applied to image classification and recognition in this paper, the running state of the relevant model on the server is not evaluated. A convolutional neural network model can not only be applied in the field of image recognition but also plays an important role in natural language processing. It needs further theoretical research and practical application.

Data Availability

The authors confirm that the data supporting the findings of this study are available within the article.

Conflicts of Interest

The authors declare that they have no conflicts of interest.

Acknowledgments

This work was supported by the Hunan Provincial Social Science Foundation Project (19YBA125).

References

[1] J. E. Liu and F. P. An, "Image classification algorithm based on deep learning-kernel function," *Scientific Programming*, vol. 2020, pp. 1–14, 2020.

[2] Y. Peng, W. T. Zhao, W. Cai, J. S. Su, B. Han, and Q. Liu, "Evaluating deep learning for image classification in adversarial environment," *IEICE - Transactions on Info and Systems*, vol. E103.D, no. 4, pp. 825–837, 2020.

[3] K. Yan, W. Y. Si, J. Hang, H. Zhou, and Q. Y. Zhu, "Multi-label garbage image classification based on deep learning," in *Proceedings of the 19th International Symposium on Distributed Computing and Applications for Business Engineering and Science (DCABES*, pp. 150–153, IEEE, Xuzhou, China, October 2020.

[4] X. B. Liu, J. S. He, L. P. Song, S. Liu, and G. Srivastava, "Medical image classification based on an adaptive size deep learning model," *ACM Transactions on Multimedia Computing, Communications, and Applications*, vol. 17, no. 3, pp. 1–18, 2021.

[5] Y. S. Chen, Y. Wang, Y. F. Gu, X. He, P. Ghamisi, and X. Jia, "Deep learning ensemble for hyperspectral image classification," *Ieee Journal of Selected Topics in Applied Earth Observations and Remote Sensing*, vol. 12, no. 6, pp. 1882–1897, JUN 2019.

[6] L. Zhang, W. Xie, F. Zhao, H. Q. Liu, and Y. P. Duan, "Deep learning based classification using semantic information for polsar image," in *Proceedings of the Igarss 2020 - 2020 IEEE International Geoscience and Remote Sensing Symposium*, pp. 196–199, IEEE, Waikoloa, HI, USA, September 2020.

[7] K. L. Gao, B. Liu, X. C. Yu, J. C. Qin, P. Q. Zhang, and X. Tan, "Deep relation network for hyperspectral image few-shot classification," *Remote Sensing*, vol. 12, no. 6, p. 923, MAR 2020.

[8] S. Tamuly, C. Jyotsna, and J. Amudha, "Deep learning model for image classification," *Computational Vision and Bio-Inspired Computing*, vol. 1108, pp. 312–320, 2020.

[9] H. Wang, F. Xu, and Y. Q. Jin, "A review of polsar image classification: from polarimetry to deep learning," in *Proceedings of the 2019 IEEE International Geoscience and Remote Sensing Symposium (IGARSS)*, pp. 3189–3192, IEEE, Yokohama, Japan, July 2019-02 August 2019.

[10] M. A. Haq, G. Rahaman, P. Baral, and A. Ghosh, "Deep learning based supervised image classification using UAV images for forest areas classification," *Journal of the Indian Society of Remote Sensing*, vol. 49, no. 3, pp. 601–606, MAR 2021.

[11] Y. Yuan, C. Z. Wang, and Z. Y. Jiang, "Proxy-based deep learning framework for spectral spatial hyperspectral image classification: efficient and robust," *IEEE Transactions on Geoscience and Remote Sensing*, vol. 60, pp. 1–15, 2022.

[12] X. Hu, T. Li, T. Zhou, Y. Liu, and Y. X. Peng, "Contrastive learning based on transformer for hyperspectral image classification," *Applied Sciences*, vol. 11, no. 18, p. 8670, 2021.

[13] X. Hu, W. J. Yang, H. Wen, Y. Liu, and Y. X. Peng, "A lightweight 1-D convolution augmented transformer with metric learning for hyperspectral image classification," *Sensors*, vol. 21, no. 5, p. 1751, MAR 2021.

[14] H. Ucuzal, A. K. Arslan, and C. Colak, "Deep learning based-classification of dementia in magnetic resonance imaging scans," in *Proceedings of the 2019 International Conference on Artificial Intelligence and Data Processing (IDAP 2019)*, IEEE, Malatya, Turkey, September 2019.

[15] S. Arena, Y. Bodrov, M. Carletti et al., "Exploiting 2D coordinates as bayesian priors for deep learning defect classification of SEM images," *IEEE Transactions on Semiconductor Manufacturing*, vol. 34, no. 3, pp. 436–439, AUG 2021.

[16] I. Jemel, S. Hassairi, R. Ejbali, and M. Zaied, "Deep stacked sparse auto-encoder based on patches for image classification," in *Proceedings of the Twelfth International Conference on Machine Vision (ICMV 2019)*, January 2020.

[17] A. Mehmood, "Understanding deep learning decision for satellite image classification," *Pattern Recognition and Tracking*, vol. 11735, 2021.

[18] S. J. Liu and Q. Shi, "Multitask deep learning with spectral knowledge for hyperspectral image classification," *IEEE Geoscience and Remote Sensing Letters*, vol. 17, no. 12, pp. 2110–2114, 2020.

[19] YB. Hou, "Breast cancer pathological image classification based on deep learning," *Journal of X-Ray Science and Technology*, vol. 28, no. 4, pp. 727–738, 2020.

[20] G. Cheng, X. X. Xie, J. W. Han, L. Guo, and G. S. Xia, "Remote sensing image scene classification meets deep learning: challenges, methods, benchmarks, and opportunities," *Ieee Journal of Selected Topics in Applied Earth Observations and Remote Sensing*, vol. 13, pp. 3735–3756, 2020.

[21] S. T. Li, W. W. Song, L. Y. Fang, Y. S. Chen, P. Ghamisi, and J. A. Benediktsson, "Deep learning for hyperspectral image classification: an overview," *IEEE Transactions on Geoscience and Remote Sensing*, vol. 57, no. 9, pp. 6690–6709, SEP 2019.

[22] X. J. Shen, Y. Jin, K. Zhou, and Y. N. Zhang, "Application analysis and prospect of deep learning in remote sensing image classification," in *Proceedings of the MIPPR 2019: Remote Sensing Image Processing, Geographic Information Systems, and Other Applications*, February 2020.

[23] T. R. Rao, X. X. Li, and M. Xu, "Learning multi-level deep representations for image emotion classification," *Neural Processing Letters*, vol. 51, no. 3, pp. 2043–2061, JUN 2020.

[24] A. Sellami and S. Tabbone, "EDNets: deep feature learning for document image classification based on multi-view encoder-decoder neural networks," *Document Analysis and Recognition, ICDAR*, vol. 12824, pp. 318–332, 2021.

[25] Q. Li, Y. J. Yang, Y. W. Guo et al., "Performance evaluation of deep learning classification network for image features," *IEEE Access*, vol. 9, pp. 9318–9333, 2021.

[26] H. Y. Chen, Q. Lv, W. Zhou, J. Zheng, and J. Wang, "Deep image classification model based on dual-branch," *Communications, Signal Processing, and Systems*, vol. 878, pp. 636–643, 2022.

[27] I. D. Gerg and V. Monga, "Structural prior driven regularized deep learning for sonar image classification," *IEEE Transactions on Geoscience and Remote Sensing*, vol. 60, pp. 1–16, 2022.

Hindawi
Computational Intelligence and Neuroscience
Volume 2022, Article ID 7842651, 14 pages
https://doi.org/10.1155/2022/7842651

Research Article

High-Discrimination Comparison Algorithm for the Comprehensive Evaluation of Innovation Ability in Colleges and Universities under Uncertain Information

Ming Fu,[1] **Lifang Wang**,[2] **Xueneng Cao**,[1] **Bingyun Zheng**,[1] **Xianxian Zhou**,[1] **and Shishu Yin**[1]

[1]*School of Management Science and Engineering, Anhui University of Finance & Economics, Bengbu 233030, Anhui, China*
[2]*School of International Trade and Economics, Anhui University of Finance & Economics, Bengbu 233030, Anhui, China*

Correspondence should be addressed to Lifang Wang; wanglifang@aufe.edu.cn

Received 16 August 2022; Accepted 24 September 2022; Published 14 October 2022

Academic Editor: Zaoli Yang

The innovation ability of students is one of the most important objectives that need to be cultivated in colleges and universities. The comprehensive evaluation of innovation ability discussed in the study can be divided into two stages: the first stage can be called preliminary evaluation and its main target is to identify students with innovative potential; in the second stage, the target objects found in the previous stage will be evaluated quantitatively and ranked. However, it is always difficult to quantitatively evaluate the innovation ability by using traditional algorithms. Based on the above analysis, the study proposes an algorithm to quantitatively evaluate the innovation ability with the help of management thought and fuzzy mathematics. Data are the basis of evaluation, and the accuracy of the data directly determines the quality of the algorithm; the data structure of the incompletely probabilistic fuzzy set is proposed in the study; the data structure can fully consider the fuzziness of the problem and the hesitation in the decision-making process; it can save the original detailed data to the maximum extent. Certainly, certain information may be lost or only the value range can be determined; there are usually some unknowns in the evaluation data, and the consistency optimization model is proposed for solving the problem. Usually, there are certain contradictions among the evaluation data; the definition of the consistency degree is proposed in the study; the consistency can be verified in time after all the unknowns are obtained, and the automatic adjustment module will be activated immediately if the value of the consistency degree exceeds the warning threshold. Finally, after verifying the data consistency, the solution can be obtained by solving the optimization model. Several experiments have been carried out to verify the effectiveness and high-discrimination ability of the algorithm proposed in the study; meanwhile, the superiority of the algorithm is further verified through comparisons with other outstanding algorithms.

1. Introduction

Innovation ability has always been an important force to promote human progress which has been recognized by more and more experts. The innovation ability of students is one of the training targets of higher education; it is also one of the core indicators to measure the quality of education. However, the quantitative measurement of the innovation ability is seriously insufficient currently.

Innovation is a kind of human creative practice from the perspective of philosophy; innovation is the activity that people discover or produce some novel, unique, valuable new products and new ideas in order to meet the needs of development from the perspective of sociology. Innovation is the behavior of creating new inventions and obtaining certain beneficial effects by using existing knowledge and materials from the perspective of economics. From the above analysis, we can see that no matter from which perspective, innovation is a relatively vague and subjective concept.

At present, academic circles have generally believed that innovation ability is composed of numerous factors, but its specific structure is still an unsolved problem. The existing research studies on the structure of innovation ability are mainly based on personality theory, competency theory, and

action theory. The personality theory holds that innovative behavior is closely related to creative personality, risk-taking spirit, and self-efficacy; on the basis of the personality theory, the competency theory mainly focuses on the combination method of personality and behavior; the action theory believes that the essence of innovation is action, and it provides theoretical support for exploring the internal logic contained in the innovation ability structure. Generally, the theoretical discussions on the innovation ability have provided important academic accumulation for this study; however, there are also shortcomings, the fault tolerance of the model is relatively low, and the accuracy of the results needs to be further improved.

Professor Zadeh first put forward the concept of fuzzy sets in 1965 [1], the emergence of fuzzy sets makes it possible to deal with fuzzy problems by mathematical methods, its core idea is to extend the characteristic function to a value in the closed interval [0, 1], and the value is used to describe the fuzzy degree of the element in a set. This idea was widely recognized by scholars, and since then, the fuzzy sets have developed rapidly and expanded into many forms, including L-type fuzzy sets, 2-type fuzzy sets, interval fuzzy sets, hesitation fuzzy sets, probability hesitation fuzzy sets, hesitation fuzzy linguistic sets, and probability hesitation fuzzy linguistic sets. The definition of the L-type fuzzy sets was proposed by Goguen in 1967 [2], different from fuzzy sets; it expands the value range of membership function into a partially ordered set. The 2-type fuzzy sets which allow membership to be a fuzzy set can be regarded as a special case of the L-type fuzzy sets. The interval fuzzy sets allow the membership to be interval values. The three fuzzy sets discussed above only consider the value of membership function; they cannot describe the information of support, opposition, and hesitation simultaneously in practical applications; moreover, due to the complexity of problems, people are often hesitant and difficult to reach consensuses in the process of collaborative decision-making and evaluation, and the data collected may be positive, negative, and hesitant; therefore, the Bulgarian scholar Atanassov extended the definition of the fuzzy set and successively proposed the concepts of intuitionistic fuzzy sets and interval intuitionistic fuzzy sets [3], and the membership, nonmembership, and hesitation can be considered simultaneously. Torra, a Spanish scholar, further expanded the fuzzy sets and proposed the definition of the hesitation fuzzy sets in 2010 [4]; when evaluating alternatives, people often hesitate among multiple values; therefore, ordinary data structures are difficult to handle this problem; fortunately, the hesitation fuzzy set can effectively solve this problem by saving all the possible values; it can be seen that the hesitant fuzzy set can more accurately and reasonably describe the uncertainty of objects; therefore, it is widely used in dealing with fuzzy problems. We find that the hesitant fuzzy set cannot directly reflect the number of experts in the group decision-making and a lot of information may be lost. Based on the above considerations, scholars proposed the definition of the probability hesitation fuzzy set which is an extension of the hesitation fuzzy set, and its basic element is composed of the evaluation value and its corresponding probability; the probability can accurately describe the importance or occurrence rate of the evaluation value. Usually, verbal words rather than mathematical symbols are more commonly used to describe evaluation opinions in real life; this is obviously beyond the capability of hesitant fuzzy sets, and for this reason, Rodriguez proposed the definition of hesitant fuzzy linguistic sets [5].

Obviously, people are better at making pairwise comparisons between alternatives in the process of decision-making; it is always easier to obtain reasonable results by pairwise comparisons; the preference relationship table which records all comparison results will be obtained after multiple pairwise comparisons. In order to describe the relative importance of comparison results, Saaty proposed the definition of the fundamental scale [6]; while each element in the fundamental scale is in the form of a single real-value, due to the complexity and uncertainty of decision-making problems and the incompleteness of information or knowledge, it is often difficult to obtain these exact values; therefore, Maji et al. used fuzzy membership functions to describe the relative importance of comparison results [7]; unfortunately, the preference relationship established by the method of Maji does not satisfy the complementary condition; in order to solve this problem, Soller et al. proposed the method of the fuzzy preference relation which can effectively overcome this defect [8]; moreover, there are inevitable contradictions among the data in the preference relationship table; the definition of the consistency is introduced to describe the contradiction degree and it is one of important concepts in the preference relationship theory; the solutions that do not satisfy consistency requirement are not feasible. Stukalina proposed a calculation method of priority weights that satisfies the consistency preference relationship [9]. Xu defined the consistency of intuitionistic fuzzy preference relationship [10].

At present, the comprehensive evaluation of innovation ability in colleges and universities is indeed a worthy problem for studying; it has not only certain theoretical value but also practical value; however, innovation ability is a vague and subjective concept, which is difficult to measure scientifically and accurately; some key indicators of the problem are often difficult to be described by single determined values; even worse, due to the limitation of cognition and the complexity of the problem, some information may be lost; therefore, traditional algorithms are hard to deal with this problem. The study combines the problem with the fuzzy theory and provides a new way to solve this problem from the perspective of management science.

2. Some Basic Definitions and Theories

Some basic definitions and theories will be briefly introduced in this section which will be helpful for other researchers to better understand the algorithm proposed in this study.

2.1. The Incompletely Probabilistic Fuzzy Set. The definition of the incompletely probabilistic fuzzy set (IPFS) is

expanded from the interval-valued fuzzy set and the probability hesitation fuzzy set, which can be described mathematically as follows:

$$l_{rs}=\left\{\gamma_l|p_l\,\gamma_l\in[0,1],p_l\in[0,1],\sum_{l=1}^{k}p_l=1,l=1,2,\cdots,k\right\}. \quad (1)$$

The symbol γ_l indicates one of the evaluation values, the symbol p_l indicates the corresponding probability value of the evaluation value γ_l, the restriction $p_l \in [0, 1]$ indicates the value range of the evaluation value γ_l, and the restriction $\sum_{l=1}^{m} p_l = 1$ indicates that the sum of all the probability values must be equal to 1. In general, any incompletely probabilistic fuzzy set l_{rs} can include several elements, the total number of elements is recorded as the symbol k, each pair of the symbols $\gamma_l|p_l$ can be called the incompletely probabilistic fuzzy element (IPFE), and the restriction $l = 1, 2, \cdots, k$ can be regarded as the value range of subscripts.

Different from other data structures, multiple values can be stored together in a single incompletely probabilistic fuzzy set, which can overcome hesitation in the evaluation process; in addition, the probability values can provide additional descriptions for the evaluation values; furthermore, it is worth noting that the evaluation values and the probability values are allowed to contain some unknowns; this improvement will further expand the application scope.

Let us illustrate the above theory with several simple examples. It can be divided into several categories according to the unknowns: the first category is that all the information is known, such as $l_{12} = \{0.32|0.42, 0.38|0.26, 0.42|0.32\}$; the second category is that some evaluation information is unknown, such as $l_{13} = \{x_1|0.42, 0.38|0.26, 0.42|0.32\}$; the third category is that some probability information is unknown, such as $l_{14} = \{0.32|0.42, 0.38|y_1, 0.42|(0.58 - y_1)\}$ and $l_{23} = \{0.32|y_2, 0.38|y_3, 0.42|(1 - y_2 - y_3)\}$; the fourth category is that some evaluation information and probability information are unknown, such as $l_{24} = \{0.32|y_3, x_2|(1 - y_3 - y_4), 0.42|y_4\}$. We must point out that the default value range of unknowns is from 0 to 1; however, if possible, it is still recommended to give the value ranges of unknowns, which can improve the accuracy of the algorithm.

Through the above analysis, we find that the data structure proposed in the paper can save the original data to the greatest extent. In addition, the expected value of the incompletely probabilistic fuzzy set may be used in the latter subsections, and the definition of the expected value is shown as follows:

$$E(l_{rs}) = \sum_{l=1}^{k} \gamma_l \cdot p_l. \quad (2)$$

The expected values of the above incompletely probabilistic fuzzy sets can be calculated according to equation (2) and are shown as follows:

$$\begin{aligned} E(l_{12}) &= E(\{0.32|0.42, 0.38|0.26, 0.42|0.32\}) = 0.3676,\\ E(l_{13}) &= E(\{x_1|0.42, 0.38|0.26, 0.42|0.32\}) = 0.2332 + 0.42 \cdot x_1,\\ E(l_{14}) &= E(\{0.32|0.42, 0.38|y_1, 0.42|(0.58 - y_1)\}) = 0.378 - 0.04 \cdot y_1. \end{aligned} \quad (3)$$

$$\begin{aligned} E(l_{23}) &= E(\{0.32|y_2, 0.38|y_3, 0.42|(1 - y_2 - y_3)\}) = 0.42 - 0.1 \cdot y_2 - 0.04 \cdot y_3,\\ E(l_{24}) &= E(\{0.32|y_3, x_2|(1 - y_3 - y_4), 0.42|y_4\}) = (0.32 - x_2) \cdot y_3 + x_2 + (0.42 - x_2) \cdot y_4. \end{aligned} \quad (4)$$

2.2. The Subtraction of Incompletely Probabilistic Fuzzy Sets. The subtraction of incompletely probabilistic fuzzy sets should be used in the following sections; however, since the definition of the incompletely probabilistic fuzzy set is first proposed in the paper, this method is rarely mentioned by other researchers; therefore, it is necessary to define the subtraction of incompletely probabilistic fuzzy sets which is shown as follows:

$$\begin{aligned} l_{xy} &= \left\{\gamma_{l_1}|p_{l_1}\,\gamma_{l_1} \in [0,1], p_{l_1} \in [0,1], \sum_{l_1=1}^{k_1} p_{l_1} = 1, l_1 = 1, 2, \cdots, k_1\right\},\\ l_{pq} &= \left\{\gamma_{l_2}|p_{l_2} \quad \gamma_{l_2} \in [0,1], p_{l_2} \in [0,1], \sum_{l_2=1}^{k_2} p_{l_2} = 1, l_2 = 1, 2, \cdots, k_2\right\},\\ l_{x394;} = l_{xy} - l_{pq} &= \bigcup_{\gamma_{l_1}\in l_{xy},\gamma_{l_2}\in l_{pq},p_{l_1}\in l_{xy},p_{l_2}\in l_{pq}} \left\{\left(\gamma_{l_1} - \gamma_{l_{12}}\right)|p_{l_1} \cdot p_{l_2} \quad l_1 = 1, 2, \cdots, k_1, l_2 = 1, 2, \cdots, k_2\right\}. \end{aligned} \quad (5)$$

Table 1: The overall structure of the original data needs to be collected.

Indicators alternatives	I_1	I_2	$\cdots$	I_t
A_1	l_{11}	l_{12}	$\cdots$	l_{1t}
A_2	l_{21}	l_{22}	$\cdots$	l_{2t}
$\vdots$	$\vdots$	$\vdots$	$\vdots$	$\vdots$
A_m	l_{m1}	l_{m2}	$\cdots$	l_{mt}

The symbols l_{xy} and l_{pq} represent two ordinary $IPFS_s$, and the symbol l_Δ records the subtraction result of the two ordinary $IPFS_s$. In particular, as a special case, the complementary set of the incompletely probabilistic fuzzy set will be frequently used in later sections; therefore, the definition of the complementary set can be given in advance which is shown as follows:

$$l_{rs}^c = 1 - l_{rs} = \left\{(1-\gamma_l)\middle| p_l\,\gamma_l \in [0,1], p_l \in [0,1], \sum_{l=1}^{k} p_l = 1, l = 1,2,\cdots,k\right\}. \tag{6}$$

Let us give a few simple examples to illustrate the above theory; the values of the $l_{12}, l_{13}, l_{14}, l_{23}, l_{24}$ have been given in the above subsection, and the specific calculation steps of the complementary sets are shown as follows:

Table 2: The structure of the comparison table.

Alternatives	A_1	A_2	$\cdots$	A_m
A_1	l_{11}	l_{12}	$\cdots$	l_{1m}
A_2	l_{21}	l_{22}	$\cdots$	l_{2m}
$\vdots$	$\vdots$	$\vdots$	$\vdots$	$\vdots$
A_m	l_{m1}	l_{m2}	$\cdots$	l_{mm}

Table 3: The simplified data structure of the comparison table.

Alternatives	A_1	A_2	$\cdots$	A_m
A_1	$\{0.5\|1\}$	l_{12}	$\cdots$	l_{1m}
A_2	$1 - l_{12}$	$\{0.5\|1\}$	$\cdots$	l_{2m}
$\vdots$	$\vdots$	$\vdots$	$\vdots$	$\vdots$
A_m	$1 - l_{1m}$	$1 - l_{2m}$	$\cdots$	$\{0.5\|1\}$

$$\begin{aligned} l_{12}^c &= 1 - l_{12} = 1 - \{0.32|0.42, 0.38|0.26, 0.42|0.32\} = \{0.68|0.42, 0.62|0.26, 0.58|0.32\},\\ l_{13}^c &= 1 - l_{13} = 1 - \{x_1|0.42, 0.38|0.26, 0.42|0.32\} = \{(1-x_1)|0.42, 0.62|0.26, 0.58|0.32\},\\ l_{14}^c &= 1 - l_{14} = 1 - \left\{0.32|0.42, 0.38\middle|y_1, 0.42\middle|0.58 - y_1\right\} = \left\{0.68|0.42, 0.62\middle|y_1, 0.58\middle|(0.58 - y_1)\right\}, \end{aligned} \tag{7}$$

$$\begin{aligned} l_{23}^c &= 1 - l_{23} = 1 - \left\{0.32|y_2, 0.38\middle|y_3, 0.42\middle|(1 - y_2 - y_3)\right\} = \left\{0.68|y_2, 0.62\middle|y_3, 0.58\middle|(1 - y_2 - y_3)\right\},\\ l_{24}^c &= 1 - l_{24} = 1 - \left\{0.32|y_3, x_2\middle|(1 - y_3 - y_4), 0.42\middle|y_4\right\} = \left\{0.68|y_3, (1 - x_2)\middle|(1 - y_3 - y_4), 0.58\middle|y_4\right\}. \end{aligned} \tag{8}$$

2.3. The Comparison Decision-Making Method. The goal of decision-making can be simply summarized as finding the best solution from multiple alternatives [11]. Specifically, the goal of this paper is to rank students according to the innovation ability. With the help of management science, every student with innovative potential can be regarded as an alternative.

All the alternatives can be recorded as mathematically. Data are always the basis of any decision-making [12]; first, several indicators will be selected from multiple interference factors which can be recorded as $I = \{I_1, I_2, \ldots, I_t\}$, the data of each indicator needs to be collected and recorded, and the data structure of the incompletely probabilistic fuzzy set mentioned above is suitable for collecting the original information. All the indicators can be classified into two categories according to the objective function: positive indicators and negative indicators. The negative indicators should be converted into positive indicators by using the complement operation mentioned in equation (3). The overall structure of the original data needs to be collected is listed in Table 1.

Generally, the alternatives can be ranked based on the data in the above table when the data are complete; unfortunately, due to the fuzziness of the problem and the hesitation of experts [13], the data in the table often contain several unknowns which will directly make the problem cannot be solved by common algorithms; for this reason, the comparison decision-making algorithm based on the incompletely probabilistic fuzzy set is proposed in the paper.

Compared with multiple alternatives, when only two alternatives are compared at a time, it is obvious that people can give the evaluation result with higher accuracy [14]. Based on this idea, the comparison table of alternatives can be created, and the structure of the comparison table is shown as Table 2.

Every element l_{ij} in Table 2 is in the form of the incompletely probabilistic fuzzy set. The elements in the above table meet the following two rules: the first one is that all the elements in the main diagonal should be recorded as $\{0.5|1\}$ which can be denoted as $l_{ii} = \{0.5|1\} \forall i = 1, 2, \cdots, m$ completely; obviously, it is the inevitable result when compared with themselves; the other rule is that the elements symmetrical to the main diagonal will meet complementary relationship which can be denoted as $l_{ij} = l_{ji}^c \forall i, j = 1, 2,$

$\cdots, m$ mathematically. After the above analysis, we can find that only the elements on the upper triangle of Table 3 need to be evaluated, and the data in Table 1 can play an important role in this process [15].

2.4. The Consistency Problem in the Process of Group Decision-Making. Every data in Table 3 is obtained separately by comparing only two alternatives at one time; all alternatives have never been compared together; therefore, there may be some inconsistencies among the data.

Inspired by Herrera [16], we believe that the data in Table 3 will meet the consistency requirement if equation (5) holds.

$$E(l_{rs}) = E(l_{rk}) - E(l_{sk}) + 0.5 \forall r, s, k = 1, 2, \cdots, m. \tag{9}$$

While, how to make equation (5) hold has become a difficult problem in front of us. Based on the theory of Chiclana et al. [17], the data $C = (l_{ij})_{m\times m}$ will meet the consistency requirement if and only if there is a set of normalized values $\omega = (\omega_1, \omega_2, \cdots, \omega_m)^T$ that make the following equations hold [18]:

$$E(l_{rs}) = In\omega_r - In\omega_s + 0.5 \forall r, s = 1, 2, \cdots m. \tag{10}$$

The symbol ω_i can also be called the comprehensive value of the alternative A_i. Generally, it can be calculated by the following equation:

$$\omega_r = \frac{e^{1/m\sum_{k=1}^{m} E(l_{rk})}}{\sum_{j=1}^{m} e^{1/m\sum_{k=1}^{m} E(l_{jk})}} \forall r, j, k = 1, 2, \cdots, m. \tag{11}$$

According to formula (6), the proof of the necessary condition is shown as follows:

$$\begin{aligned} In\omega_r - In\omega_s &= \frac{1}{m}\sum_{k=1}^{m} E(l_{rk}) - \frac{1}{m}\sum_{k=1}^{m} E(l_{sk}) \\ &= \frac{1}{m}\sum_{k=1}^{m} (E(l_{rk}) - E(l_{sk})) = \frac{1}{m}\sum_{k=1}^{m} (E(l_{rs}) - 0.5) \\ &= \frac{1}{m} \times m \times (E(l_{rs}) - 0.5) = E(l_{rs}) - 0.5. \end{aligned} \tag{12}$$

Thus, the equation $E(l_{rs}) = In\omega_r - In\omega_s + 0.5$ can be derived from the positive direction [19]. Conversely, the proof of the sufficient condition is shown as follows:

$$\begin{aligned} E(l_{rs}) &= In\omega_r - In\omega_s + 0.5 \\ &= (In\omega_r - In\omega_k + 0.5) - (In\omega_s - In\omega_k + 0.5) + 0.5. \\ &= E(l_{rk}) - E(l_{sk}) + 0.5. \end{aligned} \tag{13}$$

Thus, the equation $E(l_{rs}) = E(l_{rk}) - E(l_{sk}) + 0.5$ can be derived from the opposite direction. In addition, when the equation $E(l_{rs}) = \sum_{l=1}^{k} \gamma_l \cdot p_l = In\omega_r - In\omega_s + 0.5$ holds, then equation (7) will also hold [20], and the derivation process is shown as follows:

$$E(l_{sr}) = In\omega_s - In\omega_r + 0.5, \tag{14}$$

$$\begin{aligned} E(l_{sr}) &= E(l_{rs}^c) = E(1 - l_{rs}) \\ &= \sum_{l=1}^{k} (1 - \gamma_l) \cdot p_l \\ &= \sum_{l=1}^{k} p_l - \sum_{l=1}^{k} \gamma_l \cdot p_l \\ &= 1 - (In\omega_r - In\omega_s + 0.5) \\ &= In\omega_s - In\omega_r + 0.5. \end{aligned} \tag{15}$$

Therefore, according to the above analysis, it is only necessary to verify the consistency of the upper triangle data in Table 3.

3. The High-Discrimination Comparison Algorithm

The algorithm proposed in this paper mainly focuses on the alternatives with small differences and is difficult to be ranked directly; the algorithm and the mathematical model will be systematically introduced in this section. The flowchart of the high-discrimination comparison algorithm is shown in Figure 1.

3.1. Mathematicise the Problem. First, list all the alternatives that need to be ranked and divide them into two categories: the first category is the alternatives that can be ranked directly by common methods and the other category is the alternatives that are difficult to be ranked and need the help of the algorithm proposed in the paper [21]; these alternatives can be recorded as $A = \{A_1, A_2, \cdots, A_m\}$.

After that, several key indicators will be selected and can be denoted as $I = \{I_1, I_2, \cdots, I_t\}$; the original data of each indicator will be collected and then standardized; then, the processed data $I = (l_{ij})_{m\times t} \forall i = 1, 2, \cdots, m; j = 1, 2, \cdots, t$ will be saved in the form of the incompletely probabilistic fuzzy set.

The comparison table will be established through multiple pairwise comparisons among different alternatives. The values in the comparison table can be obtained mainly based on the key indicators of the alternatives mentioned in the above step. The data of the comparison table can be denoted as $C = (l_{ij})_{m\times m} \forall i, j = 1, 2, \cdots, m$. Since all the alternatives have not been compared together, there may be some contradictions among the data in the comparison table [22], and we must point out that the data cannot be used for ranking alternatives until it meets the requirement of consistency verification. The consistency optimization model and the adjustment algorithm will be introduced in detail in the following subsections.

3.2. The Consistency Optimization Model. Due to the complementary relationship mentioned above, the consistency optimization model is proposed according to the elements in the upper triangle of the comparison table. The consistency

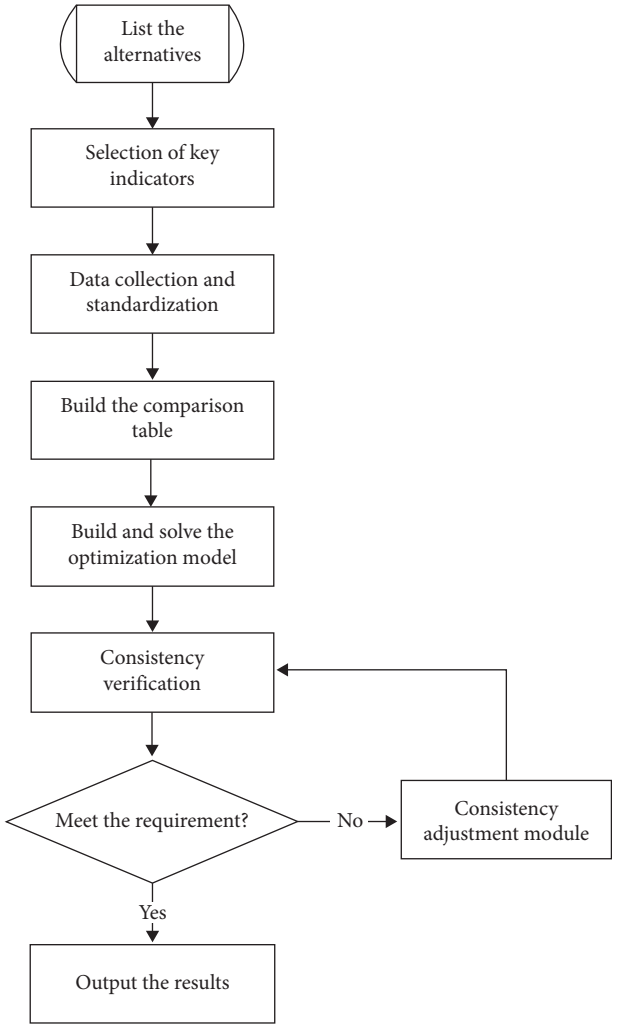

Figure 1: The flowchart of the high-discrimination comparison algorithm.

constraints can be established by introducing positive deviations and negative deviations [23]; the objective function is to minimize the sum of deviations. The model is shown as follows:

$$
\begin{aligned}
&Model\ 1:\\
&\min \xi = \min \sum_{i=1}^{m-1} \sum_{j>i}^{m} \left(d_{ij}^{+} + d_{ij}^{-}\right),\\
&s.t. \begin{cases}
In\omega_i - In\omega_j + 0.5 - \sum_{l=1}^{k} \gamma_l \cdot p_l - d_{ij}^{+} + d_{ij}^{-} = 0\\
\sum_{i=1}^{m} \omega_i = 1\\
0 \le \omega_i \le 1\\
0 \le d_{ij}^{+} \le 1\\
0 \le d_{ij}^{-} \le 1\\
i = 1, 2, \cdots, m\\
j = 1, 2, \cdots, m\\
i < j
\end{cases}
\end{aligned}
\tag{16}
$$

Although the accuracy of each comparison result obtained by such a method is relatively high from the local perspective, however, as mentioned above, only two

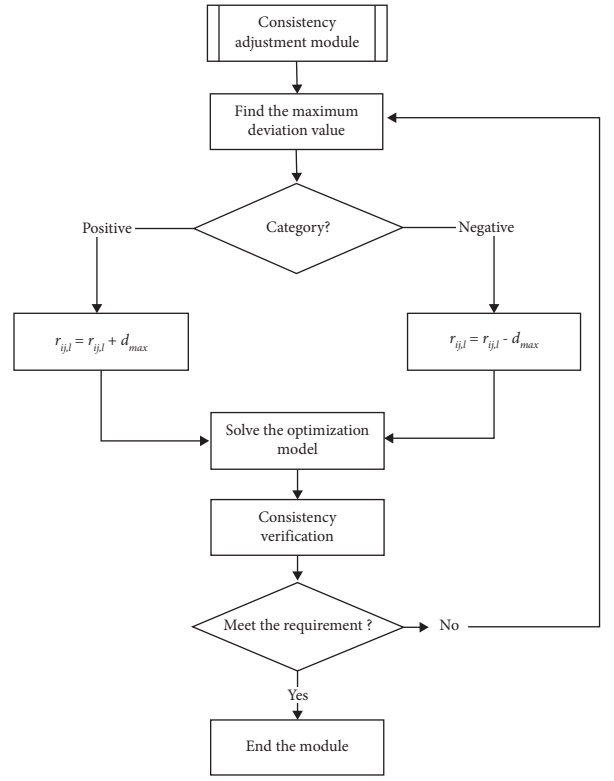

Figure 2: The flowchart of the consistency automatic adjustment algorithm.

alternatives are compared at a time, and the data may be inconsistent from the whole perspective [24]. For this reason, we propose the definition of the consistency degree which is shown as follows:

$$
CI = \frac{2}{m(m-1)} \sum_{i=1}^{m-1} \sum_{j>i}^{m} \left(d_{ij}^{+} + d_{ij}^{-}\right). \tag{17}
$$

The consistency threshold (Ω) will be set in advance, if the inequality $CI \le \Omega$ holds, which indicates that the data meet the consistency requirement, and the calculation results obtained by the model 1 will be valid [25]; on the other hand, if the inequality $CI > \Omega$ holds, it indicates that some data in the comparison table must be adjusted in time, and the specific method will be introduced in the next subsection.

3.3. The Consistency Automatic Adjustment Algorithm. The flowchart of the consistency automatic adjustment algorithm is shown in Figure 2. The adjustment method can be divided into several steps, which are introduced in detail as follows:

(1) Find the maximum deviation value which can be described as $d_{\max} = \max\left\{d_{ij}^{+}, d_{ij}^{-} | \forall i, j = 1, 2, \cdots, m; i < j\right\}$ mathematically

(2) It can be divided into two categories according to whether the maximum deviation is positive or negative [26]. If the value is positive which can be denoted as $d_{\max} = d_{ij}^{+}$, then find the maximum

Table 4: The comparison data with complete information.

	A_1	A_2	A_3	A_4
A_1	{0.5|1}	$\begin{pmatrix} 0.45\|0.36, 0.47\|0.18 \\ 0.49\|0.24, 0.52\|0.22 \end{pmatrix}$	$\begin{pmatrix} 0.46\|0.32, 0.49\|0.23 \\ 0.51\|0.45 \end{pmatrix}$	$\begin{pmatrix} 0.51\|0.23, 0.54\|0.41 \\ 0.56\|0.22, 0.58\|0.14 \end{pmatrix}$
A_2		{0.5|1}	$\begin{pmatrix} 0.51\|0.35, 0.53\|0.36 \\ 0.55\|0.29 \end{pmatrix}$	$\begin{pmatrix} 0.46\|0.44, 0.48\|0.25 \\ 0.49\|0.31 \end{pmatrix}$
A_3			{0.5|1}	$\begin{pmatrix} 0.52\|0.35, 0.54\|0.51 \\ 0.55\|0.08, 0.57\|0.06 \end{pmatrix}$
A_4				{0.5|1}

probability value in the corresponding incompletely probabilistic fuzzy set l_{ij} which can be denoted as $p_{ij,l}{}^{\max}$, and the corresponding evaluation value $r_{ij,l}$ will increase $d_{\max}$ which can be described as $r_{ij,l} = r_{ij,l} + d_{\max}$ mathematically; similarly, if the value is negative which can be denoted as $d_{\max} = d_{ij}^-$, then find the maximum probability value in the corresponding incompletely probabilistic fuzzy set l_{ij} which can be denoted as $p_{ij,l}{}^{\max}$, and the corresponding evaluation value $r_{ij,l}$ will decrease $d_{\max}$, which can be described as $r_{ij,l} = r_{ij,l} - d_{\max}$ mathematically.

(3) The consistency verification operations listed in the previous subsection will be executed repeatedly until the consistency requirement is met

(4) Finally, the alternatives will be ranked according to the values of $\omega_i (i = 1, 2, \cdots, m)$

4. A Case of the Comparison Algorithm Based on Uncertain Information

4.1. The General Description of the Problem. Innovation ability is the soul of national progress and the core of economic competition [27]. As the main institutions for cultivating innovative talents, universities or colleges have always attached great importance to the cultivation of innovation ability. Finding students with innovative potential as soon as possible is very important for the work of cultivating innovative talents; however, innovation ability is a vague concept and difficult to be measured quantitatively [28]. Based on these analyses, the algorithm proposed in this paper is suitable for dealing with such problems.

Supposing, after the first round of screening, four students with innovative potential are found out, and we hope to rank them according to their innovative ability. The four students can be denoted as $\{A_1, A_2, A_3, A_4\}$. Comparisons will be made between any two students, and the results given by experts will be recorded in the form of incompletely probabilistic fuzzy sets; thus, the comparison table will be established, and the consistency threshold is set as $\Omega = 0.015$.

According to the comparison data, it can be divided into several categories, which will be introduced, respectively, in the following subsections.

4.2. The Comparison Algorithm with Complete Information. In this category, all the data are complete, such as the data in Table 4. Due to the complementary relationship mentioned above, the elements in the lower triangle are not listed for the sake of simplicity, and the elements in the upper triangle and the main diagonal are given.

We find that it is almost impossible to rank the alternatives directly based on the data in the above table, the optimization model mentioned above will be built and its extended form is shown as follows:

$$
\begin{aligned}
&\textit{Model 2:}\\
&\min \xi_1 = d_{12}^+ + d_{12}^- + d_{13}^+ + d_{13}^- + d_{14}^+ + d_{14}^- + d_{23}^+ + d_{23}^- + d_{24}^+ + d_{24}^- + d_{34}^+ + d_{34}^-\\
&s.t. \begin{cases}
In\omega_1 - In\omega_2 + 0.5 - 0.4786 - d_{12}^+ + d_{12}^- = 0\\
In\omega_1 - In\omega_3 + 0.5 - 0.4894 - d_{13}^+ + d_{13}^- = 0\\
In\omega_1 - In\omega_4 + 0.5 - 0.5431 - d_{14}^+ + d_{14}^- = 0\\
In\omega_2 - In\omega_3 + 0.5 - 0.5288 - d_{23}^+ + d_{23}^- = 0\\
In\omega_2 - In\omega_4 + 0.5 - 0.4743 - d_{24}^+ + d_{24}^- = 0\\
In\omega_3 - In\omega_4 + 0.5 - 0.5356 - d_{34}^+ + d_{34}^- = 0\cdot\\
\sum_{r=1}^{4} \omega_i = 1\\
0 \le \omega_i \le 1,\ i = 1, 2, 3, 4\\
0 \le d_{jk} \le 1,\ j = 1, 2, 3,\ k = 2, 3, 4
\end{cases}
\end{aligned}
\tag{18}
$$

The above linear model can be solved with the help of the lingo software, and the calculation results are shown as follows:

$$\begin{aligned}&\xi_1 = 0.1082,\\&\omega_1 = 0.2506452; \omega_2 = 0.2560667; \omega_3 = 0.2510339; \omega_4 = 0.2422542\\&d_{13}^{+} = 0.00905; d_{14}^{-} = 0.00905; d_{23}^{-} = 0.00895; d_{24}^{+} = 0.08115,\end{aligned} \tag{19}$$

$$d_{12}^{+} = d_{12}^{-} = d_{13}^{-} = d_{14}^{+} = d_{23}^{+} = d_{24}^{-} = d_{34}^{+} = d_{34}^{-} = 0. \tag{20}$$

The value of the consistency degree CI can be calculated according to equation (8); the value is $CI = 0.018$ after calculation. We can find that the inequality $CI \le \Omega$ does not hold, and the data in Table 4 do not pass the consistency verification, which indicates that the reliability of the results is not enough; consequently, the consistency adjustment module will be activated immediately; the specific steps are listed as follows:

(1) The maximum deviation is found which is denoted as $d_{\max} = \max\left\{d_{ij}^{+}, d_{ij}^{-}\right\} = d_{24}^{+}$, and its type is a positive deviation.

(2) We can find that the evaluation value of the l_{24} is denoted as $l_{24} = (0.46|0.44, 0.48|0.25, 0.49|0.31)$ in the above table. The maximum probability value in the l_{24} is 0.44; therefore, the corresponding evaluation value will be increased from 0.46 to 0.54115, and the specific calculation step is $r_{ij,l} = r_{ij,l} + d_{\max} = 0.46 + 0.08115 = 0.54115$ according to the above adjustment algorithm. So, the updated value of the l_{24}' will be denoted as $l_{24}' = (0.54115|0.44, 0.48|0.25, 0.49|0.31)$ after the first adjustment.

(3) The model will be rebuilt based on the updated data, and it is shown as follows:

$$Model\ 3:\ \min \xi_1' = d_{12}^{+}{}' + d_{12}^{-}{}' + d_{13}^{+}{}' + d_{13}^{-}{}' + d_{14}^{+}{}' + d_{14}^{-}{}' + d_{23}^{+}{}' + d_{23}^{-}{}' + d_{24}^{+}{}' + d_{24}^{-}{}' + d_{34}^{+}{}' + d_{34}^{-}{}'$$

$$s.t.\begin{cases} In\omega_1' - In\omega_2' + 0.5 - 0.4786 - d_{12}^{+}{}' + d_{12}^{-}{}' = 0\\ In\omega_1' - In\omega_3' + 0.5 - 0.4894 - d_{13}^{+}{}' + d_{13}^{-}{}' = 0\\ In\omega_1' - In\omega_4' + 0.5 - 0.5431 - d_{14}^{+}{}' + d_{14}^{-}{}' = 0\\ In\omega_2' - In\omega_3' + 0.5 - 0.5288 - d_{23}^{+}{}' + d_{23}^{-}{}' = 0\\ In\omega_2' - In\omega_4' + 0.5 - 0.510006 - d_{24}^{+}{}' + d_{24}^{-}{}' = 0\\ In\omega_3' - In\omega_4' + 0.5 - 0.5356 - d_{34}^{+}{}' + d_{34}^{-}{}' = 0\\ \sum_{r=1}^{4} \omega_i' = 1\\ 0 \le \omega_i' \le 1,\ i = 1, 2, 3, 4\\ 0 \le d_{jk}' \le 1,\ j = 1, 2, 3,\ k = 2, 3, 4 \end{cases} \tag{21}$$

The model can be solved again with the help of the lingo software and the results are shown as follows: $\xi_1' = 0.072494$;

$$\begin{aligned}&\omega_1' = 0.2506452; \omega_2' = 0.2560668; \omega_3' = 0.2510339; \omega_4' = 0.2422541,\\&d_{13}^{+}{}' = 0.00905; d_{14}^{-}{}' = 0.00905; d_{23}^{-}{}' = 0.00895; d_{24}^{+}{}' = 0.045444,\\&d_{12}^{+}{}' = d_{12}^{-}{}' = d_{13}^{-}{}' = d_{14}^{+}{}' = d_{23}^{+}{}' = d_{24}^{-}{}' = d_{34}^{+}{}' = d_{34}^{-}{}' = 0.\end{aligned} \tag{22}$$

The value of the consistency degree CI can be calculated according to equation (8), and the value is $CI' = 0.01208$ after calculation. We can find that the inequality $\xi_1' < \Omega$ holds after the adjustment which indicates that the calculation

Table 5: The comparison data with unrelated unknowns.

	A_1	A_2	A_3	A_4
A_1	$\{0.5\|1\}$	$\begin{pmatrix} 0.44\|0.31, 0.46\|0.22 \\ 0.48\|0.21, x_1\|0.26 \end{pmatrix}$	$\begin{pmatrix} 0.47\|y_1, x_2\|0.26 \\ 0.53\|0.74 - y_1 \end{pmatrix}$	$(x_3\|0.46, x_4\|0.54)$
A_2		$\{0.5\|1\}$	$\begin{pmatrix} 0.46\|0.55, x_5\|0.31 \\ 0.53\|0.14 \end{pmatrix}$	$\begin{pmatrix} 0.42\|0.24, 0.45\|0.27 \\ 0.47\|0.31, 0.51\|0.18 \end{pmatrix}$
A_3			$\{0.5\|1\}$	$\begin{pmatrix} 0.51\|y_2, x_6\|0.41 \\ 0.53\|0.59 - y_2 \end{pmatrix}$
A_4				$\{0.5\|1\}$

results meet the consistency requirements; therefore, the result is reasonable, and it is $A_2 \succ A_3 \succ A_1 \succ A_4$ according to the innovative ability.

4.3. The Comparison Algorithm with Unrelated Unknowns. In this category, the data contain several unknowns and the unknowns are not related to each other, such as the data in Table 5. Each unknown may give a specific value range; if it is not given, the default value range of the unknown is $0 \le x \le 1$.

$$\begin{aligned} &0.50 \le x_1 \le 0.54; 0.48 \le x_2 \le 0.52; 0.43 \le x_3 \le 0.47; 0.49 \le x_4 \le 0.52; 0.47 \le x_5 \le 0.52 \\ &0.54 \le x_6 \le 0.56; 0 \le y_1 \le 0.74; 0 \le y_2 \le 0.59. \end{aligned} \tag{23}$$

The optimization model will be built based on the data in Table 5, and it is shown as follows:

$$\begin{aligned} &Model\ 4: \\ &\min \xi_2 = d_{12}^+ + d_{12}^- + d_{13}^+ + d_{13}^- + d_{14}^+ + d_{14}^- + d_{23}^+ + d_{23}^- + d_{24}^+ + d_{24}^- + d_{34}^+ + d_{34}^- \\ &s.t. \begin{cases} In\omega_1 - In\omega_2 + 0.5 - (0.3384 + 0.26 \times x_1) - d_{12}^+ + d_{12}^- = 0 \\ In\omega_1 - In\omega_3 + 0.5 - (0.3922 + 0.26 \times x_2 - 0.06 \times y_1) - d_{13}^+ + d_{13}^- = 0 \\ In\omega_1 - In\omega_4 + 0.5 - (0.46 \times x_3 + 0.54 \times x_4) - d_{14}^+ + d_{14}^- = 0 \\ In\omega_2 - In\omega_3 + 0.5 - (0.3272 + 0.31 \times x_5) - d_{23}^+ + d_{23}^- = 0 \\ In\omega_2 - In\omega_4 + 0.5 - 0.4598 - d_{24}^+ + d_{24}^- = 0 \\ In\omega_3 - In\omega_4 + 0.5 - (0.3127 + 0.41 \times x_6 - 0.02 \times y_2) - d_{34}^+ + d_{34}^- = 0 \\ \sum_{r=1}^{4} \omega_i = 1 \\ 0 \le \omega_i \le 1 \\ 0 \le d_{jk} \le 1 \\ 0.50 \le x_1 \le 0.54 \\ 0.48 \le x_2 \le 0.52 \\ 0.43 \le x_3 \le 0.47 \\ 0.49 \le x_4 \le 0.52 \\ 0.47 \le x_5 \le 0.52 \\ 0.54 \le x_6 \le 0.56 \\ 0 \le y_1 \le 0.74 \\ 0 \le y_2 \le 0.59 \\ i, j, k = 1, 2, 3, 4 \end{cases} \end{aligned} \tag{24}$$

The above model can be solved with the help of the Lingo software, and the results are shown as follows:

$$\begin{aligned}&\xi_2 = 0.0563,\\ &\omega_1 = 0.2444283; \omega_2 = 0.2485094; \omega_3 = 0.2553364; \omega_4 = 0.2517258,\\ &x_1 = 0.54; x_2 = 0.48; x_3 = 0.4374795; x_4 = 0.4987803; x_5 = 0.47; x_6 = 0.54;\end{aligned} \tag{25}$$

$$\begin{aligned}&y_1 = 0.74; y_2 = 0.59;\\ &d_{12}^{+} = 0.004640146; d_{23}^{-} = 0.01625985; d_{24}^{+} = 0.02734181; d_{34}^{-} = 0.008058187,\\ &d_{12}^{-} = d_{13}^{+} = d_{13}^{-} = d_{14}^{+} = d_{14}^{-} = d_{23}^{+} = d_{24}^{-} = d_{34}^{+} = 0.\end{aligned} \tag{26}$$

We can find that all unknowns can be obtained by solving the above model; moreover, the value of the consistency degree CI_2 can be calculated according to equation (8); the value is $CI_2 = 0.00938$ after calculation, and the inequality $CI_2 < \Omega$ holds which indicates that the results have met the consistency requirement; therefore, the adjustment module does not need to be activated, and the result is $A_3 \succ A_4 \succ A_2 \succ A_1$ according to the innovative ability.

4.4. The Comparison Algorithm with Related Unknowns. In this category, the data also contain several unknowns; moreover, different from the previous case, some unknowns are related to each other, and unknowns are not completely independent, such as the data in Table 6.

$$\begin{aligned}&0.50 \le x_1 \le 0.54; x_2 = x_1 + 0.2; x_3 = 1.2 \times x_1; 0.28 \le y_1 \le 0.35; y_2 + y_3 + y_4 = 1; 0.2 \le y2 \le 0.4\\ &0.3 \le y3 \le 0.45; 0.35 \le y4 \le 0.57; 0 \le x_2 \le 1; 0 \le x_3 \le 1; 0.51 \le x_4 \le 0.55; 0.53 \le x_5 \le 0.56\\ &0.3 \le y_5 \le 0.38; y_6 = y_5 - 0.1; 0 \le y_6 \le 1.\end{aligned} \tag{27}$$

Model 5:

$$\min \xi_3 = d_{12}^{+} + d_{12}^{-} + d_{13}^{+} + d_{13}^{-} + d_{14}^{+} + d_{14}^{-} + d_{23}^{+} + d_{23}^{-} + d_{24}^{+} + d_{24}^{-} + d_{34}^{+} + d_{34}^{-}$$

$$s.t. \begin{cases} In\omega_1 - In\omega_2 + 0.5 - (0.344 + 0.29 \times x_1) - d_{12}^{+} + d_{12}^{-} = 0\\ In\omega_1 - In\omega_3 + 0.5 - (0.37 + 0.26 \times x_2 - 0.02 \times y_1) - d_{13}^{+} + d_{13}^{-} = 0\\ In\omega_1 - In\omega_4 + 0.5 - 0.5206 - d_{14}^{+} + d_{14}^{-} = 0\\ In\omega_2 - In\omega_3 + 0.5 - (0.48 \times y_2 + x_3 \times y_3 + 0.52 \times y_4) - d_{23}^{+} + d_{23}^{-} = 0\\ In\omega_2 - In\omega_4 + 0.5 - 0.512 - d_{24}^{+} + d_{24}^{-} = 0\\ In\omega_3 - In\omega_4 + 0.5 - (x_4 \times y_5 + 0.55 \times y_6 + x_5 - x_5 \times y_5 - x_5 \times y_6) - d_{34}^{+} + d_{34}^{-} = 0\\ \sum_{r=1}^{4} \omega_i = 1\\ 0 \le \omega_i \le 1\\ 0 \le d_{jk} \le 1\\ 0.50 \le x_1 \le 0.54\\ x_2 = x_1 + 0.2\\ 0.28 \le y_1 \le 0.35\\ y_2 + y_3 + y_4 = 1\\ 0.2 \le y_2 \le 0.4\\ 0.3 \le y_3 \le 0.45\\ 0.35 \le y_4 \le 0.57\\ x_3 = 1.2 \times x_1\\ 0.51 \le x_4 \le 0.55\\ 0.53 \le x_5 \le 0.56\\ 0.3 \le y_5 \le 0.38\\ y_6 = y_5 - 0.1\\ i, j, k = 1, 2, 3, 4 \end{cases} \tag{28}$$

Table 6: The comparison data with related unknowns.

	A_1	A_2	A_3	A_4
A_1	{0.5|1}	$\begin{pmatrix} 0.48\|0.39, 0.49\|0.32 \\ x_1\|0.29 \end{pmatrix}$	$\begin{pmatrix} 0.48\|y_1, x_2\|0.26 \\ 0.50\|0.74 - y_1 \end{pmatrix}$	(0.51|0.47, 0.53|0.53)
A_2		{0.5|1}	$\begin{pmatrix} 0.48\|y_2, x_3\|y_3 \\ 0.52\|y_4 \end{pmatrix}$	$\begin{pmatrix} 0.49\|0.37, 0.52\|0.32 \\ 0.53\|0.31 \end{pmatrix}$
A_3			{0.5|1}	$\begin{pmatrix} x_4\|y_5; 0.55\|y_6 \\ x_5\|1 - y_5 - y_6 \end{pmatrix}$
A_4				{0.5|1}

The above model can be solved with the help of the lingo software, and the results are shown as follows:

$$\begin{aligned} &\xi_3 = 0.0708 \\ &\omega_1 = 0.2543168; \omega_2 = 0.2541642; \omega_3 = 0.2423875; \omega_4 = 0.2491315 \\ &x_1 = 0.54; x_2 = 0.74; x_3 = 0.648; x_4 = 0.51; x_5 = 0.53; \end{aligned} \tag{29}$$

$$\begin{aligned} &y_1 = 0.35; y_2 = 0.2739702; y_3 = 0.3; y_4 = 0.4260298; y_5 = 0.3; y_6 = 0.2 \\ &d_{13}^- = 0.007358808; d_{24}^+ = 0.008; d_{34}^- = 0.05544119 \\ &d_{12}^+ = d_{12}^- = d_{13}^+ = d_{14}^+ = d_{14}^- = d_{23}^+ = d_{23}^- = d_{24}^- = d_{34}^+ = 0. \end{aligned} \tag{30}$$

All unknowns can be obtained by solving the above model and all constraints are satisfied; moreover, the value of the consistency degree CI_3 can be calculated according to equation (8), the value is $CI_3 = 0.0118$ after calculation, and the inequality $CI_3 < \Omega$ holds which indicates that the results have met the consistency requirement; therefore, the adjustment module does not need to be activated; the result is $A_1 \succ A_2 \succ A_4 \succ A_3$ according to the innovative ability.

5. The Comparisons and Discussion

Several data structures and processing methods proposed by other outstanding scholars will be compared with the data structure and algorithm proposed in the paper in this section.

5.1. The Probabilistic Linguistic Fuzzy Set and Its Processing Methods. The definition of the probabilistic linguistic fuzzy set is shown as follows:

$$L_{ij} = \left\{ L_l(p_l) | L_l \in S, 0 \le p_l \le 1, l = 1, 2, \cdots, k, \sum_{l=1}^{k} p_l = 1 \right\}. \tag{31}$$

The symbol L_l represents the evaluation value, the symbol p_l represents its corresponding probability, the symbol S is called the additive linguistic set which contains all the possible evaluation values, the specific form is $S = \{s_a | a = 0, 1, \cdots, 2\tau\}$, the symbol τ indicates an integer, the constraint condition $L_l \in S$ indicates that all the evaluation values are from the additive linguistic set, the constraint condition $0 \le p_l \le 1$ gives the value range of the probability, the symbol k indicates the total number of elements, and the constraint $\sum_{l=1}^{k} p_l = 1$ indicates that the sum of all the probabilities in a set must be equal to 1 [29].

Let us give a simple example to illustrate the above definition. Supposing the additive linguistic set is $S = \{s_a | a = 0, 1, 2, 3, 4\}$, the symbol s_0 indicates "terrible," the symbol s_1 indicates "bad," the symbol s_2 indicates "moderate," the symbol s_3 indicates "good," and the symbol s_4 indicates "excellent." One of the typical probabilistic linguistic fuzzy sets can be denoted as $L_{12} = \{s_1(0.45), s_2(0.37), s_3(0.18)\}$.

We can find that there are certain similarities with the definition of the incompletely probabilistic fuzzy set proposed in the paper. However, there are also differences between them, the main difference is the total number of the possible evaluation values, specifically, the number of possible evaluations in the probabilistic linguistic fuzzy set is limited; while, the number of possible evaluations in the incompletely probabilistic fuzzy set is infinite; in addition, the processing methods of incomplete information are not mature enough, and the data structure of probabilistic linguistic fuzzy set cannot contain multiple unknowns. These defects will seriously reduce the algorithm's accuracy.

5.2. The Probabilistic Hesitation Fuzzy Set and Its Processing Methods. Although the mathematical model of the probabilistic hesitation fuzzy set and the probabilistic linguistic fuzzy set has some similarities, there are still differences between them. Comparatively speaking, the probabilistic hesitation fuzzy set has more advantages in data processing, the operation rules, and the decision-making model, while the probabilistic linguistic fuzzy set can use linguistic terms to describe the real ideas of decision makers.

The probabilistic hesitation fuzzy set is an extension of the hesitation fuzzy set; its basic element is composed of the evaluation value and the corresponding probability [30]. In the decision-making process, the preference information given by experts can be described more comprehensively, and the uncertainty of a variety of possible scenarios can be simulated [31]. The definition of the probabilistic hesitation fuzzy set can be mathematically described as follows:

$$h_r = \left\{ \gamma_i | p_i \, 0 \le \gamma_i \le 1, 0 \le p_i \le 1, \sum_{i=1}^{k} p_i = 1, i = 1, 2, \cdots, k \right\}. \tag{32}$$

Supposing that there are two probabilistic hesitation fuzzy sets which can be denoted as $h_1 = \{\gamma_i | p_i \, i = 1, 2, \cdots, k_1\}$ and $h_2 = \{\gamma_j | p_j \, j = 1, 2, \cdots, k_2\}$, respectively, the symbol λ indicates a positive real number. The basic rules of the probabilistic hesitation fuzzy set are listed as follows:

(1) $(h_1)^\lambda = \bigcup_{\gamma_i \in h_1, p_i \in h_1} \{\gamma_i^\lambda | p_i\}$

(2) $\lambda h_1 = \bigcup_{\gamma_i \in h_1, p_i \in h_1} \{1 - (1 - \gamma_i)^\lambda | p_i\}$

(3) $h_1 \oplus h_2 = \mathrm{U}\{\gamma_i + \gamma_j - \gamma_i \gamma_j | p_i p_j\}$ $\gamma_i \in h_1, p_i \in h_1$ $\gamma_j \in h_2, p_j \in h_2$

(4) $h_1 \otimes h_2 = \mathrm{U}\{\gamma_i \gamma_j | p_i p_j\}$ $\gamma_i \in h_1, p_i \in h_1$ $\gamma_j \in h_2, p_j \in h_2$

The incompletely probabilistic fuzzy set proposed in the paper is extended from the probabilistic hesitation fuzzy set [32]. It inherits the advantages of the probabilistic hesitation fuzzy set, including basic calculation methods and theoretical models; on this basis, the incompletely probabilistic fuzzy set allows some unknowns to be included and the processing scope has been further expanded.

6. Conclusions

It is widely known that a scientific and reasonable evaluation mechanism is very important to promote the cultivation of students' innovative abilities [33]. The main purpose of this paper is to establish a high-discrimination evaluation mechanism of innovative ability. The innovative ability is a fuzzy definition and difficult to be measured by common algorithms.

At present, the common methods of dealing with this problem can be simply summarized as follows: several key indicators should be selected and these indicators will be scored separately; then, the scores will be aggregated by simple algebraic operation methods, and the aggregated value represents the innovation ability of the tested student. The above method is simple and efficient, but there are also some serious shortcomings. The value of each indicator is a single real-value, and it may be difficult to fully describe the details of the indicator [34]. The information aggregation method are too simple, and it is difficult to make full use of the indicator data [35].

After the above analysis, the paper combines the problem with fuzzy mathematics and tries to propose a new way to solve this problem. The data structure of the incompletely probabilistic fuzzy set proposed in the paper is developed from several definitions of fuzzy mathematics; it can save all possible values in a single dataset which can fully consider the hesitation and fuzziness in the process of data collection; and it also can fully accommodate different opinions of multiple experts. In addition, the incompletely probabilistic fuzzy set also allows unknowns to be included which enables more data details can be saved together. Compared with traditional methods, the pairwise comparison method is also one of the improvements; obviously, it is easier to obtain scientific and reasonable results by the pairwise comparison of alternatives. Since experts mainly focus on the work of pairwise comparisons, there may be contradictions among the comparison results from the overall perspective. To solve this problem, the definition of the consistency degree is proposed in the paper; moreover, the consistency optimization model is designed to estimate the values of the unknowns. The consistency degree can be obtained through the accumulation of deviation values. The automatic adjustment module will be activated if the consistency degree exceeds the warning threshold; this mechanism is also one of the innovations; it can improve the efficiency of the algorithm and accelerate the achievement of the consistency goal. After the above steps, the ranking of alternatives can be obtained according to the checked comparison data.

In order to verify the superiority of the algorithm, various experiments have been carried out; all the results have proved the effectiveness of the algorithm proposed in the paper, and then, several outstanding algorithms have been compared with the algorithm proposed in the paper; the results show that the algorithm proposed in this paper does have some advantages for solving this problem.

Honestly, although the algorithm is efficient, but it has not been fully verified in large projects, the algorithm with a feedback mechanism will be the research object of our team in the near future.

Data Availability

The data used to support the findings of this study are included whthin the paper and are obtained through practical investigations by our team.

Conflicts of Interest

The authors declare that they have no conflicts of interest.

Authors' Contributions

M. F. conceptualized the study. L. F. W. supervised the study. X. N. C. administered project. B. Y. Z. validated the study.

X. X. Z. investigated the study. S. S. Y. was responsible for writing and original draft preparation. All authors have read and agreed to the published version of the manuscript.

Acknowledgments

This research was funded by the Excellent Young Talents Fund Program of Higher Education Institutions of Anhui Province (gxyqZD2021110), the scientific research program of Anhui University of Finance and Economics (ACKYB21014 and ACKYC19024), the humanities and social sciences research project of Anhui Provincial Department of Education (SK2021A0250), and "the six outstanding and one top-notch" outstanding talent training innovation project of Anhui University of Finance and Economics, Anhui Province (aclzy2020010 and 2020zyrc005).

References

[1] L. A. Zadeh, "Fuzzy sets," *Information and Control*, vol. 8, no. 3, pp. 338–353, 1965.

[2] J. Goguen, "L-fuzzy sets," *Journal of Mathematical Analysis and Applications*, vol. 18, no. 1, pp. 145–174, 1967.

[3] K. T. Atanassov, "Intuitionistic fuzzy sets," *Fuzzy Sets and Systems*, vol. 20, no. 1, pp. 87–96, 1986.

[4] V. Torra, "Hesitant fuzzy sets," *International Journal of Intelligent Systems*, vol. 25, no. 6, pp. 529–539, 2010.

[5] R. M. Rodriguez, L. Martinez, and F. Herrera, "Hesitant fuzzy linguistic term sets for decision making," *IEEE Transactions on Fuzzy Systems*, vol. 20, no. 1, pp. 109–119, 2012.

[6] T. L. Saaty, "Axiomatic foundation of the analytic hierarchy process," *Management Science*, vol. 32, no. 7, pp. 841–855, 1986.

[7] P. K. Maji, R. Biswas, and A. R. Roy, "Fuzzy soft sets," *Journal of Fuzzy Mathematics*, vol. 9, no. 3, pp. 589–602, 2001.

[8] B. R. Soller, M. Ca Brera, S. M. Smith, and J. P. Sutton, "Smart medical systems with application to nutrition and fitness in space," *Nutrition*, vol. 18, no. 10, pp. 930–936, 2002.

[9] Y. Stukalina, "The management of integrated educational environment resources: the factors to be considered," *European Journal of Education*, vol. 45, no. 2, pp. 345–361, 2010.

[10] Z. S. Xu, "Intuitionistic fuzzy multiattribute decision making: an interactive method," *IEEE Transactions on Fuzzy Systems*, vol. 20, no. 3, pp. 514–525, 2012.

[11] M. Andrejić, N. Bojović, and M. Kilibarda, "Benchmarking distribution centres using principal component analysis and data envelopment analysis: a case study of Serbia," *Expert Systems with Applications*, vol. 40, no. 10, pp. 3926–3933, 2013.

[12] N. Dabaghian, R. Tavakkoli-Moghaddam, A. A. Taleizadeh, and M. S. Moshtagh, "Channel coordination and profit distribution in a three-echelon supply chain considering social responsibility and product returns," *Environment, Development and Sustainability*, vol. 24, no. 3, pp. 3165–3197, 2021.

[13] T. Kovacs, "Laser welding process specification base on welding theories," *Procedia Manufacturing*, vol. 22, no. 3, pp. 147–153, 2018.

[14] X. H. Xu, Z. J. Du, and X. H. Chen, "Consensus model for multi-criteria large-group emergency decision making considering non-cooperative behaviors and minority opinions," *Decision Support Systems*, vol. 79, pp. 150–160, 2015.

[15] Z. Wu and J. Xu, "A consensus model for large-scale group decision making with hesitant fuzzy information and changeable clusters," *Information Fusion*, vol. 41, pp. 217–231, 2018.

[16] L. Martinez and F. Herrera, "A 2-tuple fuzzy linguistic representation model for computing with words," *IEEE Transactions on Fuzzy Systems*, vol. 8, no. 6, pp. 746–752, 2000.

[17] F. Chiclana, E. Herrera-Viedma, S. Alonso, and F. Herrera, "Cardinal consistency of reciprocal preference relations: a characterization of multiplicative transitivity," *IEEE Transactions on Fuzzy Systems*, vol. 17, no. 1, pp. 14–23, 2009.

[18] Y. Dong, H. Zhang, and E. Herrera-Viedma, "Integrating experts' weights generated dynamically into the consensus reaching process and its applications in managing non-cooperative behaviors," *Decision Support Systems*, vol. 84, pp. 1–15, 2016.

[19] F. Meng, S.-M. Chen, and J. Tang, "Group decision making based on acceptable multiplicative consistency of hesitant fuzzy preference relations," *Information Sciences*, vol. 524, no. 524, pp. 77–96, 2020.

[20] Y. Xue, Y. Deng, and H. Garg, "Uncertain database retrieval with measure - based belief function attribute values under intuitionistic fuzzy set," *Information Sciences*, vol. 546, pp. 436–447, 2021.

[21] K. Fiedler, B. F. Rolfe, and T. De Souza, "Integrated shape and topology optimization-applications in automotive design and manufacturing," *SAE International Journal of Materials and Manufacturing*, vol. 10, no. 3, pp. 385–394, 2017.

[22] A. Ur Rahman, M. Saeed, S. S Alodhaibi, and H. Abd El-Wahed Khalifa, "Decision making algorithmic approaches based on parameterization of neutrosophic set under hypersoft set environment with fuzzy, intuitionistic fuzzy and neutrosophic settings," *Computer Modeling in Engineering and Sciences*, vol. 128, no. 2, pp. 743–777, 2021.

[23] M. Fu, L. F. Wang, J. M. Zhu, and B. Y. Zheng, "Emergency optimization decision-making with incomplete probabilistic information under the background of COVID-19," *Complexity*, vol. 2021, pp. 1–16, 2021.

[24] F. Ming, L. F. Wang, and J. Zhou, "The identification of poverty alleviation targets based on the multiple hybrid decision-making algorithms," *IEEE Access*, vol. 8, pp. 169585–169593, 2020.

[25] M. Fu, L. F. Wang, B. Y. Zheng, and H. Y. Shao, "The optimal emergency decision-making method with incomplete probabilistic information," *Scientific Reports*, vol. 11, pp. 23400–23414, 2021.

[26] M. Unver, M. Olgun, and E. T¨urkarslan, "Cosine and cotangent similarity measures based on choquet integral for spherical fuzzy sets and applications to pattern recognition," *Journal of Computational and Cognitive Engineering*, vol. 1, pp. 1–20, 2022.

[27] L. Wang and H. Garg, "Algorithm for multiple attribute decision-making with interactive Archimedean norm operations under Pythagorean fuzzy uncertainty," *International Journal of Computational Intelligence Systems*, vol. 14, no. 1, pp. 503–527, 2020.

[28] S. Debnath, "Fuzzy hypersoft sets and its weightage operator for decision making," *Journal of Fuzzy Extension and Applications*, vol. 2, no. 2, pp. 163–170, 2021.

[29] C. Kadar, R. Maculan, and S. Feuerriegel, "Public decision support for low population density areas: an imbalance-aware hyper-ensemble for spatio-temporal crime prediction," *Decision Support Systems*, vol. 119, pp. 107–117, 2019.

[30] E. K Amir, O. R. Shahin, M. Rasha, E. A. Abd, and A. I. Taloba, "Integration of computer vision and natural language processing in multimedia robotics application," *Information Sciences Letters*, vol. 11, no. 3, pp. 765–775, 2022.

[31] Z. Yang, Y. Gao, and X. Fu, "A decision-making algorithm combining the aspect-based sentiment analysis and intuitionistic fuzzy-VIKOR for online hotel reservation," *Annals of Operations Research*, vol. 2021, pp. 1–17, 2021.

[32] Q. He, P. Xia, B. Li, and J. B. Liu, "Evaluating investors' recognition abilities for risk and profit in online loan markets using nonlinear models and financial big data," *Journal of Function Spaces*, vol. 2021, pp. 1–15, 2021.

[33] Y. Li, H. Garg, and Y. Deng, "A new uncertainty measure of discrete Z-numbers," *International Journal of Fuzzy Systems*, vol. 22, no. 3, pp. 760–776, 2020.

[34] Z. Yang, J. Chang, L. Huang, and A. Mardani, "Digital transformation solutions of entrepreneurial SMEs based on an information error-driven T-spherical fuzzy cloud algorithm," *International Journal of Information Management*, vol. 2021, pp. 102384–102419, 2021.

[35] M. Fu, L. Wang, X. Cao, B. Zheng, X. Zhou, and S. Yin, "A closed-loop method for multiperiod intelligent information processing with cost constraints under the fuzzy environment," *Computational Intelligence and Neuroscience*, vol. 2022, pp. 1–19, 2022.

Hindawi
Computational Intelligence and Neuroscience
Volume 2022, Article ID 8656013, 11 pages
https://doi.org/10.1155/2022/8656013

Research Article

Research on Domain-Specific Knowledge Graph Based on the RoBERTa-wwm-ext Pretraining Model

Xingli Liu,[1] **Wei Zhao**,[1] **and Haiqun Ma**[2]

[1]*School of Computer Science and Technology, Heilongjiang University of Science and Technology, Harbin 150020, Heilongjiang, China*
[2]*School of Information Management, Heilongjiang University, Harbin 150080, Heilongjiang, China*

Correspondence should be addressed to Haiqun Ma; mahaiqun@hlju.edu.cn

Received 6 August 2022; Accepted 6 September 2022; Published 12 October 2022

Academic Editor: Zaoli Yang

The purpose of this study is to solve the effective way of domain-specific knowledge graph construction from information to knowledge. We propose the deep learning algorithm to extract entities and relationship from open-source intelligence by the RoBERTa-wwm-ext pretraining model and a knowledge fusion framework based on the longest common attribute entity alignment technology and bring in different text similarity algorithms and classification algorithms for verification. The experimental research showed that the named entity recognition model using the RoBERTa-wwm-ext pretrained model achieves the best results in terms of recall rate and F1 value, first, and the F value of RoBERTa-wwm-ext + BiLSTM + CRF reached up to 83.07%. Second, the RoBERTa-wwm-ext relationship extraction model has achieved the best results; compared with the relation extraction model based on recurrent neural network, it is improved by about 20%~30%. Finally, the entity alignment algorithm based on the attribute similarity of the longest common subsequence has achieved the best results on the whole. The findings of this study provide an effective way to complete knowledge graph construction in domain-specific texts. The research serves as a first step for future research, for example, domain-specific intelligent Q&A.

1. Introduction

With the advent of the big data era and artificial intelligence, the knowledge graph in the domain-specific application has received widespread attention. Knowledge map is a new concept proposed by Google in 2012, which is essentially the knowledge base of semantic network. As an effective knowledge representation method of cognitive intelligence of the new generation of artificial intelligence, knowledge graph uses open-source information to train cognitive models and then applies this model for cognitive application, which is an effective formation of anthropomorphic thinking. It has not only become the most intuitive and understandable framework for knowledge representation and reasoning but also improved the efficient of knowledge discovery, such as the problem system based on the domain-specific knowledge graph. However, when the knowledge graph is successfully applied in many fields, ambiguity, difficult links, data sparsity in special fields, and other problems hinder the application task effect based on the domain-specific knowledge graph. Especially in some fields with complex data sources and limited available data, how to provide an accurate knowledge extraction model for new knowledge cognition according to the needs of the field and, at the same time, how to effectively link and fuse the discovered new knowledge with the knowledge base or how to effectively link and fuse the multisource heterogeneous data with the knowledge base is an important foundation for the application of knowledge maps in some fields at present. In view of this, since open-source intelligence such as military books and the Internet has been used as the data source to solve related problems such as the automatic construction of the domain-specific knowledge graph, this research serves as a first step for future research, for example, the construction of knowledge graphs Q&A application. The innovative contribution of this research is as follows:

(1) The RoBERTa-wwm-ext model is used to enhance the knowledge of the data in the knowledge extraction process to complete the knowledge extraction including entity and relationship

(2) This study proposes a knowledge fusion framework based on the longest common attribute entity alignment technology and brings in different text similarity algorithms and classification algorithms for verification, all of which have achieved good results

2. Related Work

The knowledge graph was proposed by Google in 2012, and its essence is a semantic network knowledge base. The knowledge graph is divided into a general knowledge graph and a domain-specific knowledge graph. For the former, it emphasizes the scope of knowledge, while for the latter, it emphasizes the accuracy of domain-specific knowledge. At present, the construction and exploration technology of knowledge graphs at home and abroad has become mature. Many research institutions have successively created some large-scale general knowledge graphs, such as YAGO [1], Wikidata [2], and DBpedia [3]. However, for knowledge graphs in professional fields, the services it provides for people are still far from meeting the needs. For this reason, academia and industry have paid more attention to the research of domain-specific knowledge graphs with high professional knowledge accuracy.

Due to the sensitivity of data and low resource information in the field of military security, knowledge graph research in this field is relatively lacking, and the research progress is slow. F. Liao et al. [4], using the knowledge extraction method based on the BiLSTM model, studied the knowledge graph construction of the US military equipment and designed and implemented the US military equipment knowledge graph system. C. Liu et al. [5], aiming at the problems of loose structure of the military equipment database, difficulty in using effectively, low storage efficiency, and chaotic management, used the entity relation extraction method of the dependency syntax tree and CRF to extract information from unstructured text data, build a knowledge map of the military equipment, and achieve good results. D. Song et al. [6] proposed a military knowledge graph construction method based on bibliographic data of military disciplines to solve the problems of sparse data distribution, weak data correlation, and difficulty in using data effectively in the retrieval process of military industrial academic research content. This method designs the structure of the knowledge graph according to the bibliographic information characteristics of the article and uses the information-rich article titles and keywords to study entity extraction, entity classification, knowledge graph storage, and visualization. Yao Yi et al. [7] relied on the structured data of the existing arsenal to build the equipment concept map, using the method of iterative learning, based on open multisource data to complete the equipment entity to ensure the breadth and depth of the concept map precision. Xing Meng et al. [8] proposed a technical framework for the construction and application of knowledge graphs in the military domain regarding the opportunities and challenges currently faced by knowledge graphs in the military domain. It also discusses the key issues and core technologies in all aspects of the knowledge life cycle, such as knowledge representation based on the ontology system, knowledge extraction based on machine learning, cross-domain-specific knowledge fusion, knowledge computing, and knowledge application. Zhao Yu et al. [9] used the BiLSTM + CRF model for military named entity recognition, extracted relation words through syntactic analysis and hierarchical Dirichlet process (HDP) clustering, and obtained entities and the relationships between entities to build a military knowledge graph.

Knowledge fusion is an important link in the process of domain-specific knowledge graph construction and an important means to ensure knowledge quality and knowledge update. At present, in the process of knowledge graph research in the military field, the technology for knowledge fusion is relatively lacking. In the general field, knowledge fusion is usually based on cross-language entity alignment and same-language knowledge base entity alignment technology research. Cross-language entity alignment techniques mainly include representation learning methods based on translation models and graph neural networks. The translation model takes TransE [10] as the basic model. Models such as JE [11], MTransE [12], IPTransE [13], and AttrE [14] have improved it by using methods such as attribute, relation information, and iterative training and obtained a good effect. The graph neural network uses the global structural information of the graph to match the entities to be aligned in the two knowledge graphs. The GCN-Align [15] model is an earlier model that uses a graph neural network algorithm for entity alignment. It proposes a cross-language knowledge graph alignment method based on a graph convolutional network. The research on entity alignment of the same language is based on the Chinese heterogeneous encyclopedia knowledge base and adopts the paired entity alignment technology with the text similarity algorithm as the core.

It can be seen from the above that most of the knowledge graphs in the military field focus on the construction of knowledge graphs of weapons and equipment. Some military knowledge graph research does not subdivide the ontology granularity and builds a military knowledge graph equivalent to an encyclopedia, which is similar to the military module in the general knowledge graph and cannot meet accurate knowledge services. At present, the only research on knowledge graph construction in the military field mainly focuses on the extraction of knowledge, and there are relatively few studies on knowledge fusion. Based on the research on the military intelligence information of major military news platforms and the suggestions of military experts, this study refines the data granularity of the knowledge graph in the military field and extracts open-source military information through the deep learning technology. Second, this study obtains the diverse and heterogeneous military domain knowledge base on the Internet, combines text similarity and machine learning algorithm, proposes a knowledge fusion algorithm

framework based on the longest common attribute entity alignment technology, which is used for knowledge fusion and updating, and then, constructs a high-quality maintainable knowledge graph of the military.

3. Key Technology

The construction of the domain-specific knowledge graph is divided into the construction of the ontology layer and the data layer. In this article, by studying the influence of data distribution and data granularity in the open-source military intelligence on the quality of knowledge graph construction, the ontology of the graph is divided into 9 entity types, including countries, aircraft carriers, missiles, radars, ships, aircraft, military bases, waters, and islands, and the relationship is divided into 5 types: country, collaboration, activity, equipment, and NULL, which are used to verify the reliability of the knowledge graph construction experiment. The definition of the relationship between entities is shown in Table 1.

The technologies of domain-specific knowledge graph data layer construction mainly include domain-specific data acquisition, knowledge extraction, knowledge fusion, knowledge storage, and graph visualization. Among them, knowledge extraction and knowledge fusion technology are the most reused, which determine the efficiency and quality of graph construction. Therefore, this study focuses on knowledge extraction and knowledge fusion technology in the construction of a knowledge graph. The technical architecture of the knowledge graph construction is shown in Figure 1.

3.1. Data Preprocessing

3.1.1. Data Collection. The knowledge extraction module of this study takes the military intelligence information data as the main research object, and the data mainly come from open-source military news. Crawler technology is used to collect unstructured text information in the global military, military forums, and military modules in various news platforms.

The external knowledge base in the knowledge fusion module of this study mainly comes from two aspects. On the one hand, it is to obtain existing external knowledge bases. For example, data in the open-source weapon and equipment knowledge graph (OpenKG.CN) and the US military knowledge base data (Heilongjiang University of Science and Technology Cognitive Intelligence Experiment) provide existing structured knowledge bases. On the other hand, crawler technology is used to crawl semistructured military data in the open-source encyclopedias, such as Weapon Encyclopedia (http://www.wuqibaike.com/) and Wikipedia.

3.1.2. Data Annotation. Data annotation is an important part of data preprocessing, which determines the quality of knowledge extraction. The entity annotation adopts the BIO annotation method; that is, the "B-entity type" indicates the mark of the beginning word of the entity, the "I-entity type" indicates the mark of the subsequent word of the entity, and "O" indicates the nonentity part. According to the definition of the ontology library, this study annotates 9 types of military entities, including NAT (country), PLA (aircraft), VES (ship), MIS (missile), WAT (water area), AIR (aircraft carrier), BAS (military base), RAD (radar), and ISL (island). An example of entity annotation is shown in Figure 2.

Relation annotation is based on entity annotation. We segment the text data with entity annotations in units of sentences and judge and annotate the relationship between entities contained in each unit according to the definition of the relational ontology library. Examples of relational annotations are shown in Table 2.

3.2. Knowledge Extraction. Knowledge extraction is an important step in the process of knowledge graph construction, which is mainly divided into two parts: named entity recognition (entity extraction) and relation extraction. In this study, the method based on deep learning is used to extract knowledge from unstructured text data, and the related structured knowledge base is extracted according to the organizational structure design rules of the knowledge base. This article mainly studies knowledge extraction from unstructured text data and uses a pretraining model to vectorize text data to enhance knowledge. The acquired text semantic feature vector is combined with the deep learning model to learn the features of a large number of texts corpus and realize the knowledge extraction of unstructured text data.

3.2.1. RoBERTa-wwm-ext Pretraining Model. The BERT [16] (Bidirectional Encoder Representation from Transformers) model is a pretraining model for encoding text characters proposed by Google in 2018, which uses the idea of transfer learning. Knowledge or patterns learned in one domain or task are applied to a different but related domain or problem. The BERT model mainly uses the encoder structure of the transformer model [17], which can better obtain the semantic relationship in the text data. The BERT model uses massive Wikipedia data for model training so that each word can obtain a better vector feature.

The RoBERTa [18] (robustly optimized BERT approach) model is an improved version of the BERT model, using more training data and improving the training method. In terms of training method, RoBERTa removes the NSP (Next Sentence Prediction) task, and at the same time, compared with BERT's static masking mechanism, RoBERTa uses a dynamic masking mechanism. Although RoBERTa has only slightly improved the model mechanism, it has achieved an effective improvement in the use effect.

WWM [19] (Whole Word Masking) is the whole word mask, which changes the method of using a single Chinese character as the unit of mask in the Chinese BERT model to mask the whole Chinese word. The advantage of such training is that the words encoded by the model have the meaning of the context words.

The Harbin Institute of Technology iFLYTEK Joint Laboratory released the Chinese RoBERTa-wwm-ext

Table 1: Interpretation of relationship labels.

Serial number	Relation label	Relationship type interpretation
1	Country	Country to which ships, aircraft carriers, aircraft, and missiles belong
2	Collaboration	Cooperative operations among ships, aircraft carriers, and aircraft
3	Activity	Ships, aircraft carriers, and aircraft are active in a certain area target
4	Equipment	Missiles and radars equipped on ships, aircraft carriers, and aircraft
5	NULL	No relationship between entities

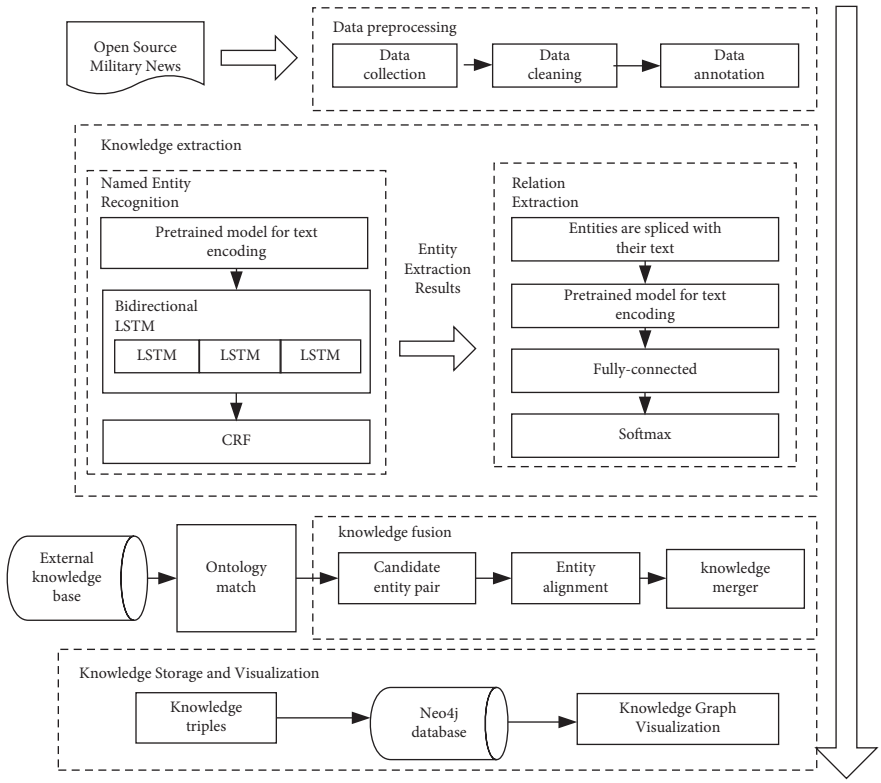

Figure 1: Technical architecture of knowledge graph construction.

pretraining model, which achieved the best results in several natural language processing tasks. Therefore, this study uses the RoBERTa-wwm-ext pretraining model open sourced by the Harbin Institute of Technology to obtain text vectors with semantic features and encode the text.

3.2.2. Named Entity Recognition Model. The named entity recognition model in this study is mainly divided into three layers, namely, the text encoding layer of the pretraining model, the bidirectional long short-term memory network layer (BiLSTM), and the conditional random field layer (CRF). The structure of the model is shown in Figure 3.

First, this model uses sentences containing military information as input data and encodes the text information of the sentences through the RoBERTa-wwm-ext model. A sequence of word vectors $(X_1, X_2, \cdots, X_n)$ with semantic information is obtained and fed into a bidirectional LSTM layer to automatically extract the features of sentences. The bidirectional LSTM layer splices the hidden state sequence $(h_1, h_2, \cdots, h_n)$ output by the forward LSTM and the sequence output by the reverse LSTM at the corresponding position according to the position, accesses the linear layer, and maps it into a K-dimensional hidden vector. Among them, K is the number of entity labels. At this time, K classification can be performed on the P vector corresponding to each character vector, and data labeling can be performed. To better obtain sentence-level annotation information, the output P vector is input into the CRF layer.

3.2.3. Relation Extraction Model. The relation extraction model consists of a text encoding layer, a fully connected layer, and a multiclassifier layer. First, we obtain entity A and entity B whose relationship needs to be determined in the text data and the text data containing these two entities and connect the three to form the input text of the model. The text encoding layer encodes the input text data to form a hidden layer state vector with semantic features. The fully connected layer is used to normalize the obtained feature

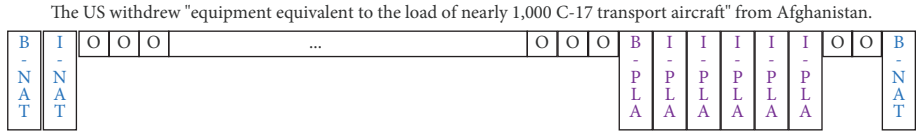

Figure 2: An example of entity annotation.

Table 2: Examples of relational annotation data.

Text	The British Royal Navy's aircraft carrier "Italia Hakujou," the Yomikoku Navy's aircraft carrier "Satone," and the "Soho Island" cruise ship to Dingyang completed a large-scale maritime military exercise
Entities	Aircraft carrier "Satone" and "Soho Island" cruise ship
Annotation	Collaboration

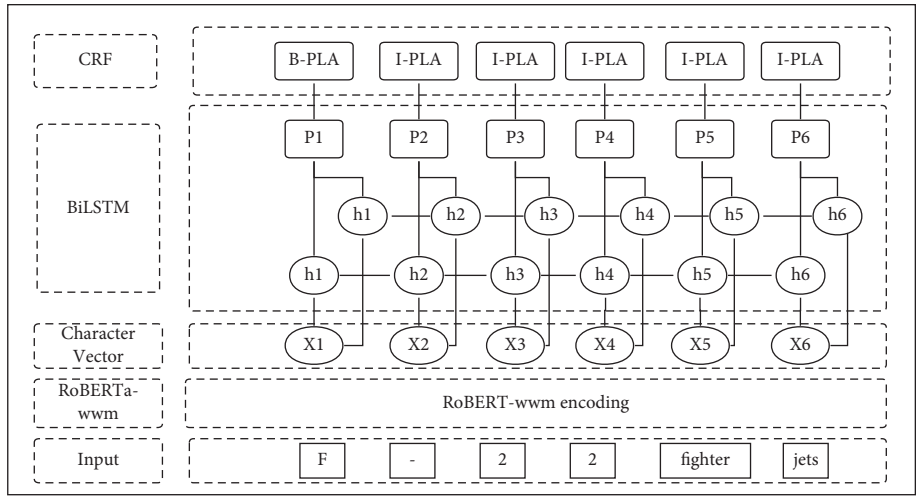

Figure 3: The named entity recognition model.

vector containing semantics, and the classification result is input through the multiclassifier layer. It is expressed in a mathematical equation as follows:

$$H = \text{RoBET}a_{wwm}[\text{concat}(\text{ent}A + \text{ent}B) + \text{txt}],$$
$$h = wH + b, p = \text{softmax}(h), \quad (1)$$

where H represents the semantic feature vector of the hidden layer obtained by the RoBERTa-wwm-ext model, h is the output of the fully connected layer, w and b are the weight and bias parameters, respectively, and p is the input probability of each relation label. The model structure is shown in Figure 4.

3.3. Knowledge Fusion. The knowledge obtained through knowledge extraction has a wide range of sources, the quality of knowledge from different sources is different, and the expression form is not uniform, which will lead to problems such as knowledge redundancy and low accuracy. Integrating multisource and heterogeneous knowledge and solving problems such as knowledge duplication is the key to improving the quality of knowledge graph construction. First, knowledge fusion is to fuse entities with different expressions of the same entity concept from multiple data sources to obtain unified knowledge. Knowledge fusion is divided into two stages. In the first stage, knowledge fusion is performed on the extracted results to ensure the formation of high-quality knowledge graphs. In the second stage, based on the constructed knowledge graph, knowledge fusion is carried out with the external knowledge base to realize the expansion and update of knowledge.

3.3.1. Knowledge Fusion Framework. The knowledge fusion architecture of this study is shown in Figure 5. The data come from two parts, namely, the result of knowledge extraction and the external knowledge base, corresponding to two stages of knowledge fusion. The data preprocessing process organizes the structured and semistructured data in the external knowledge base into unified knowledge triples, through manual ontology matching and entity classification and entity alignment within each ontology type, and finally completes knowledge fusion.

3.3.2. Entity Alignment. The entity alignment algorithm is the core of the knowledge fusion framework. This study adopts the paired entity alignment algorithm; that is, the similarity screening of entities is performed in advance, the entities that cannot be similar are filtered out, and the possibly similar entities are marked as candidate entity pairs.

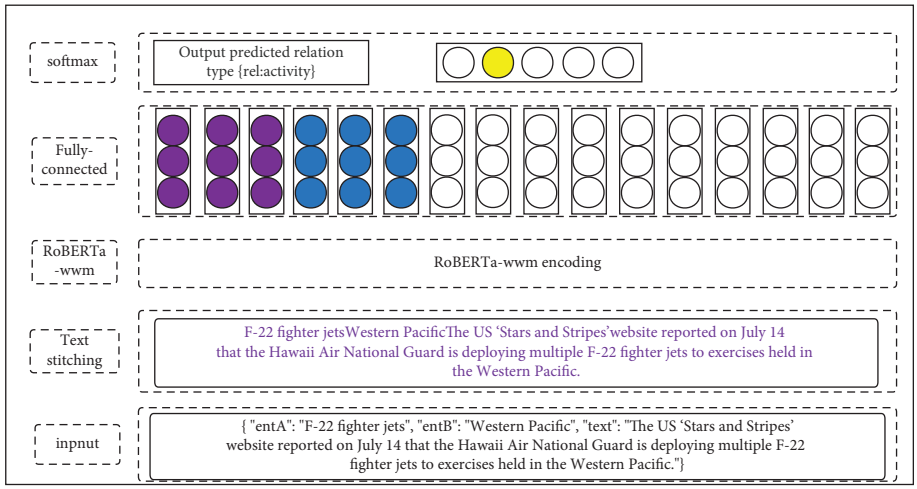

Figure 4: Relation extraction model.

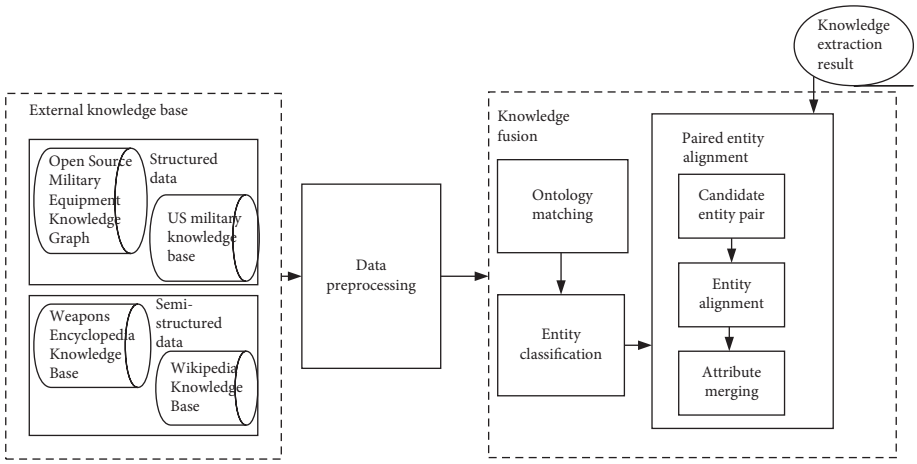

Figure 5: Framework of knowledge fusion.

According to the attribute similarity between candidate entity pairs, a machine learning algorithm is used to classify them into a matching set or a nonmatching set. The algorithm flow is shown in Figure 6.

The attribute similarity algorithm is an important part of the paired entity alignment algorithm in this study. Due to the different sources of knowledge, the attribute lengths of entities describing knowledge are inconsistent. Therefore, this study proposes a method of maximum common attribute length to calculate the similarity of attributes. We select the attribute of the maximum coincidence of two entities in the entity pair to calculate, which is expressed as follows:

$$\text{CommomPropertty}\left(e_1, e_2\right) = \text{Property}_{e_1} \cap \text{Property}_{e_2}. \quad (2)$$

Among them, e_1 and e_2 represent entities and Property_{e_1} and Property_{e_2} represent attributes corresponding to entities. The lengths of common attributes between different entity pairs are inconsistent, which leads to unequal lengths of attribute similarity feature vectors obtained from attribute similarity calculation. Therefore, the obtained feature vector is subjected to dimension reduction and normalization processing. Since the name of the entity has a high degree of identification for the entity, the entity name is used as the main attribute $\text{Property}_{\text{main}}$, and the other attributes are used as auxiliary attributes $\text{Property}_{\text{secondary}} = \{P_{s1}, P_{s2}, \cdots, P_s\}$. The auxiliary attributes are averaged to reduce the original multidimensional feature vector to two dimensions. Thereby, the similar feature quantities of the attributes can be unified. Normalizing the attribute similarity vector can represent the similarity between entity pairs. Based on the above-mentioned ideas, the similarity between entity pairs can be expressed as follows:

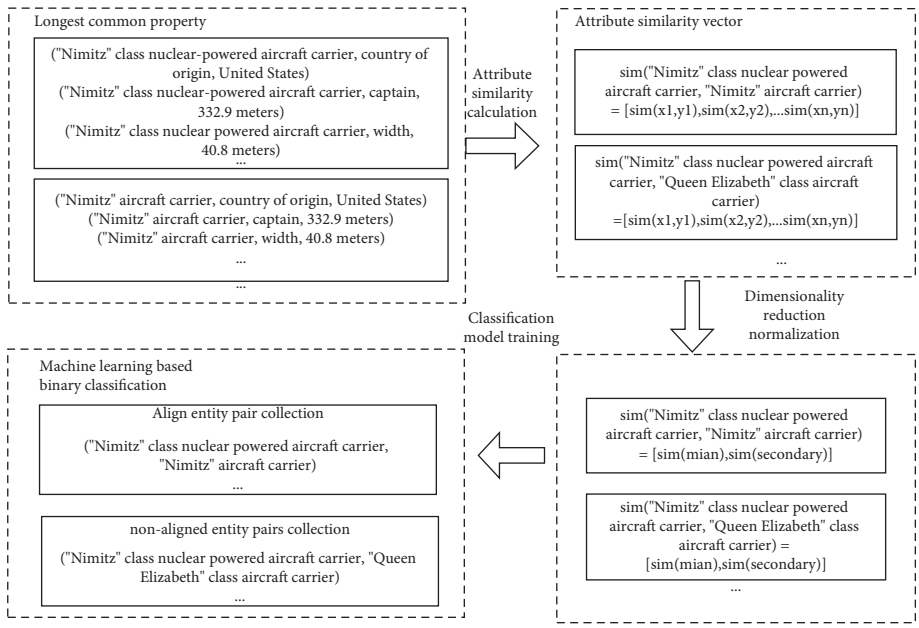

Figure 6: Entity alignment algorithm flow.

$$\begin{aligned}\mathrm{sim}_{\mathrm{Propertty}\,(e_1,e_2)} &= \left\{\mathrm{sim}\left(\mathrm{Property}_{\mathrm{main}}\right), \mathrm{ave}\left[\mathrm{sim}\left(\mathrm{Property}_{\mathrm{secondary}}\right)\right]\right\},\\ \mathrm{ave}\left[\mathrm{sim}\left(\mathrm{Property}_{\mathrm{secondary}}\right)\right] &= \frac{\sum_i^N \mathrm{sim}\left(p_{si}\right)}{N}, N = \left|\mathrm{Property}_{e_1} \cap \mathrm{Property}_{e_2}\right|.\end{aligned} \tag{3}$$

The attribute similarity algorithm adopts text similarity algorithms such as SimHash [20], edit distance, longest common subsequence, and BERT word embedding. The classification algorithm adopts machine learning algorithms such as support vector machine [21] (SVM), decision tree, logistic regression, and naive Bayes. Combined experiments with different attribute similarity algorithms and classification algorithms are used to verify the effectiveness of entity alignment.

4. Experiments

4.1. Datasets. This study takes the military intelligence information data as the main research object, and the data mainly come from open-source military news. We use crawler technology to collect unstructured text information containing the military intelligence information such as global military, military forums, and military modules in various news platforms for knowledge extraction. Second, we extract the structured and semistructured data in the open-source weapon and equipment knowledge graph, weapon encyclopedia, Wikipedia knowledge base, and the US military knowledge base for knowledge fusion. The experimental datasets in this study are divided into three parts: named entity recognition, relation extraction, and entity alignment.

4.1.1. Named Entity Recognition Dataset. The named entity recognition part of the dataset in this study is constructed by manual annotation. The dataset contains 9 types of entity labels, including a total of 53,295 entity labels and 14 MB of text data. The distribution of entity labels is shown in Table 3.

4.1.2. Relation Extraction Dataset. The relation extraction part of the dataset in this study is jointly constructed by the methods of automatic labeling of entity-relationship types and manual review. The dataset contains a total of 2251 pieces of data with 5 types of relationship labels. The distribution of relationship labels is shown in Table 4.

Since the length of the text corpus has a certain influence on the difficulty of relation extraction, the text length is counted. The text length distributions of the training set and test set are the same, as shown in Figure 7.

4.1.3. Entity Alignment Dataset. The data used in this study to verify the entity alignment algorithm in the knowledge fusion framework come from two data platforms, the open-source military weapon and equipment knowledge graph and the weapons encyclopedia. From the acquired data, a total of 1324 prealigned entity pairs were obtained by random sampling and manual alignment of four types of data, including missile weapons, aircraft carriers, vessels, and plane. These entity pairs contain a total of 28447 attribute triples. The specific data distribution is shown in Table 5.

Through the analysis of the dataset composed of two data sources, it is found that two entities have the same name in some prealigned entity pairs. In order to improve the robustness of the trained model, a new entity name is formed

Table 3: Entity label distribution.

Serial number	Entity label	Number statistics
1	NAT (nation)	34833
2	PLA (plane)	8144
3	VES (vessel)	4319
4	MIS (missile)	2597
5	WAT (waters)	1351
6	AIR (aircraft carrier)	704
7	BAS (military base)	561
8	RAD (radar)	470
9	ISL (island)	316

Table 4: Relation label distribution.

Serial number	Relation label	Number statistics
1	Country	841
2	Collaboration	491
3	Activity	262
4	Equipment	297
5	NULL	360

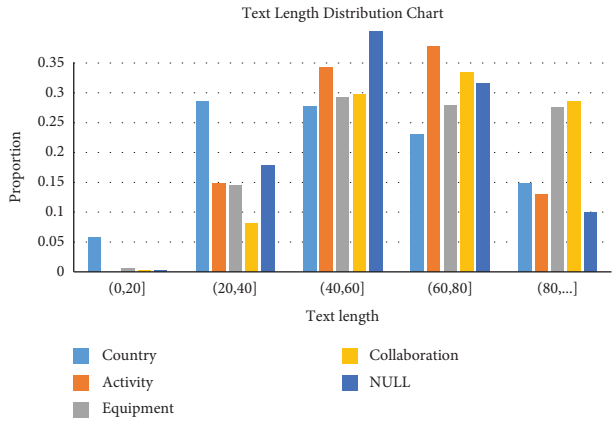

Figure 7: Distribution of text length in relation extraction.

by inserting, deleting, or replacing characters in the data from one of the sources according to the naming rules of the military field and forming a prealigned entity pair in this experiment. Negative samples are obtained by randomly replacing entities between prealigned entity pairs. The prealigned entities are scrambled by their data categories to form 50% positive and 50% negative samples, and finally, 2648 entity pairs are formed for alignment experiments.

4.2. Experimental Parameters

4.2.1. Named Entity Recognition Model Parameters. The amount of data used in the training of the named entity recognition model and the parameter volume of the pretraining model are large. Considering the hardware environment of the experiment and the reliability of model training, the main parameters of the named body recognition model in this study are shown in Table 6.

4.2.2. Relation Extraction Model Parameters. The size of the hidden layer state vector of relation extraction and the size of the number of hidden layers refer to the RoBERTa model parameters. Considering the distribution of text lengths in the dataset, we set the maximum text input (max_length) to 128 characters. Other parameters are based on the experience of deep learning model training, and the specific experimental parameter settings are shown in Table 7.

4.3. Evaluation Metrics. This experiment uses three indicators of precision, recall, and F1 value to evaluate the reliability of the model. The calculation expressions of the three indicators are as follows:

$$\text{precision} = \frac{TP}{TP + FP},$$
$$\text{recall} = \frac{TP}{TP + FN}, F1 = \frac{2 \times \text{precision} \times \text{recall}}{\text{precision} + \text{recall}}, \tag{4}$$

where TP represents the number of labels that the model can correctly detect, FP represents the number of irrelevant labels detected by the model, and FN represents the number of labels not detected by the model.

4.4. Experimental Results

4.4.1. Named Entity Recognition Experiment Results. The named entity recognition dataset is used for data, the size of the training dataset is 10.3 MB, and the test is 3.2 MB. The experimental results of the trained model on the test set are shown in Table 8. The accuracy of some of the entity labels is low, the reason is that the amount of labeled data for this part of the entity labels is small, and the number of occurrences in the military dataset used in this experiment is small. However, it does not affect the reliability of the model and can be corrected by increasing the number of corresponding labels.

To verify the effectiveness of the named entity recognition model and dataset, four groups of comparative experiments were set up in this experiment as shown in Table 9. These include the BiLSTM + CRF model, IDCCN model, BERT + BiLSTM + CRF model, and BERT-wmm-ext + BiLSTM + CRF model. From the results of the comparative experiments, it can be seen that the named entity recognition model using the RoBERTa-wwm-ext pretrained model achieves the best results in terms of recall rate and F1 value.

4.4.2. Relation Extraction Experiment Results. The relation extraction experiment uses 1800 text data for model training and 451 text data for testing. Each relationship label has achieved better results on the test set, and the experimental results of the trained model on the test set are shown in Table 10.

To verify the effectiveness of the relation extraction model and dataset, four groups of comparative experiments were set up in this experiment, and the more popular deep

Table 5: Distribution of prealigned entity pairs.

Label	Open-source knowledge graph (attribute triple)	Weapon encyclopedia (attribute triple)	Prealigned entity pairs
Missile weapon	3914	2641	349
Aircraft carrier	1593	1123	100
Vessel	5571	3546	360
Plane	10007	4927	515
Total	21085	12237	1324

Table 6: Named entity recognition model parameters.

Serial number	Parameter	Value
1	Epochs	50
2	batch_size	64
3	lstm_dim	200
4	max_seq_len	128
5	Learning rate	0.001
6	Dropout	0.5

Table 7: Relation extraction model parameters.

Serial number	Parameter	Value
1	Epochs	50
2	batch_size	50
3	hidden_size	768
5	max_length	128
6	Learning rate	0.001
7	Dropout	0.1

Table 8: Named entity model recognition results.

Label	Precision (%)	Recall (%)	F1	Number statistics
NAT (nation)	85.87	93.83	89.68	8453
PLA (plane)	79.05	76.12	77.55	1532
VES (vessel)	66.71	69.49	68.07	775
MIS (missile)	61.60	50.10	55.26	388
WAT (waters)	58.33	69.72	63.52	300
AIR (aircraft carrier)	63.64	52.34	57.44	88
BAS (military base)	50.51	48.54	49.50	99
RAD (radar)	72.46	37.88	49.75	69
ISL (island)	60.92	64.63	62.72	87
Overall	81.11	85.13	83.07	11722

learning models were selected as comparative experiments. The comparative experimental results are shown in Table 11. From the comparative experimental results, it can be seen that the BERT series of relationship extraction models have good results, and the BERT-wwm-ext relationship extraction model has achieved the best results, which is similar to the RoBERTa-wwm-ext-based relationship extraction model used in this study. Compared with the relation extraction model based on recurrent neural network, it is improved by about 20%~30%.

After further analysis, there are two reasons for the excellent effect of the experiment. On the one hand, it is the superiority of the BERT model, which is formed based on massive data training and has a good ability to express knowledge. The RoBERTa-wwm-ext model is a further improvement of the BERT model, so the experiment has achieved good results. On the other hand, the dataset used for the experiment contains fewer relationship types, which may lead to a high effect on the experiment. In the future, the relationship type of the dataset will be increased to further verify the effect of the model.

Table 9: Comparative experimental results of named entity recognition.

Model	Precision (%)	Recall (%)	F1
RoBERTa-wwm-ext + BiLSTM + CRF	81.11	85.13	83.07
BiLSTM + CRF	81.51	84.63	83.04
BERT-wmm-ext + BiLSTM + CRF	80.96	84.90	82.89
BERT + BiLSTM + CRF	81.93	84.01	82.96
IDCNN	79.46	84.73	82.01

Table 10: Test results of the relation extraction model.

Label	Precision (%)	Recall (%)	F1	Number statistics
Country	99.36	96.89	98.11	161
Activity	95.00	100	97.43	57
Equipment	96.61	95.00	98.45	60
Collaboration	96.94	100	98.07	95
NULL	98.70	97.44	98.07	78
Overall	97.32	97.87	97.57	451

4.4.3. Entity Alignment Experiment Results. The entity alignment experiment in this study is based on the scikit-learn and bert4keras framework. Combined experimental analysis of four attribute similarity algorithms of SimHash, edit distance, longest common subsequence (LCS), and BERT word embedding and four classification algorithms of support vector machine (SVM), decision tree, logistic regression (LR), and naive Bayes (NB) was conducted. The experimental results are shown in Table 12.

According to Table 12, the entity alignment algorithm based on the attribute similarity of the longest common subsequence has achieved the best results on the whole, and the combination with the classification algorithm of logistic regression has achieved the best results. Second, the algorithm based on SimHash is better overall and achieves the

Table 11: Comparative experimental results of relation extraction.

Model	Precision (%)	Recall (%)	F1
RoBERTa-wwm-ext	97.32	97.87	97.57
BERT	96.46	96.56	96.50
BERT-wwm-ext	98.11	98.14	98.13
BiGRU-ATT	77.87	74.22	75.74
BiLSTM-ATT	68.36	66.61	67.47

Table 12: Comparison of the experimental results of entity alignment.

Similarity	Classification	Precision (%)	Recall (%)	F1
SimHash	SVM	97.79	97.66	97.72
SimHash	Decision tree	98.31	98.28	98.29
SimHash	LR	97.79	97.66	97.72
SimHash	NB	98.00	97.84	97.91
Edit distance	SVM	97.58	97.49	97.53
Edit distance	Decision tree	97.24	97.08	97.15
Edit distance	LR	97.37	97.31	97.34
Edit distance	NB	95.40	95.65	95.46
LCS	SVM	99.27	99.21	99.24
LCS	Decision tree	99.59	99.65	99.62
LCS	LR	99.80	99.81	99.81
LCS	NB	99.27	99.21	99.24
Word embedding	SVM	82.75	80.17	80.46
Word embedding	Decision tree	92.41	92.40	92.41
Word embedding	LR	91.47	91.44	91.45
Word embedding	NB	67.02	63.40	59.84

local optimum when combined with the decision tree classification algorithm.

5. Discussion

This study aims to provide an efficient and reliable method for the construction of knowledge graphs in specific fields. Taking the military field as an example, the two modules of knowledge extraction and knowledge fusion mentioned in the study are experimentally verified. Different from previous studies, this study uses the pretrained model RoBERTa-wwm-ext for knowledge enhancement, which improves the effect of knowledge extraction. In addition, this article studies the knowledge fusion module that is less studied in the construction of domain knowledge graphs in the past and proposes a knowledge fusion framework based on the longest common attribute entity alignment technology. In the process of graph construction, it is used to ensure its quality, and it is used for knowledge expansion and update in the process of graph maintenance.

In the knowledge extraction module, this study uses the RoBERTa-wwm-ext model to vectorize text data, which is different from the previous random initialization or word2vec for text vectorization. The advantage of this is that the vector of the knowledge extraction model in the data input stage has excellent semantic expression ability, so the effect of the trained knowledge extraction model will be greatly improved. Most of the previous research on domain knowledge graph construction focused on knowledge extraction, but this research not only studies knowledge extraction but also studies knowledge fusion and proposes a knowledge fusion framework. The framework brings in different text similarity algorithms and machine learning classification algorithms, all of which have achieved good results.

There are also some limitations in this study. First, this study uses the manual annotation method in the data preprocessing stage to annotate the named body recognition dataset and relation extraction dataset, which increases a lot of labor costs. Although the most effective method is manual annotation at present, semiautomatic annotation methods will be considered in the future, for example, annotating a small number of correct seed data and using the seed data to iteratively annotate most of the data.

Second, in the knowledge extraction stage of this study, the recognition effect of some entity labels in the named entity recognition experiment is not good. After analyzing the experimental process, in the named entity recognition experiment, due to the small number of annotations for some labels, the data distribution of each label in the data samples used for training is unbalanced, resulting in poor recognition of some labels. In the future, we will continue to optimize the datasets of each experimental module to improve the experimental effect of each module.

Third, in the knowledge fusion stage, a large amount of text similarity between entity attributes needs to be calculated in the process of entity alignment, which will inevitably lead to the low computational efficiency of the knowledge fusion framework. In the future, the domain synonym dictionary and stop word dictionary will be added to the text similarity calculation process, which can reduce the number of text similarity calculations and optimize the efficiency of the knowledge fusion framework.

6. Conclusion

This study combines the machine learning and deep learning technology to study the automatic construction technology of knowledge graphs in the military domain and focuses on the knowledge extraction and knowledge fusion technology in the process of domain-specific graph construction. The RoBERTa-wwm-ext model is used to enhance the knowledge of the data in the knowledge extraction process to complete the knowledge extraction. Second, this study proposes a knowledge fusion framework based on the longest common attribute entity alignment technology and brings in different text similarity algorithms and classification algorithms for verification, all of which have achieved good results. The recognition effect of some labels in the named entity recognition model in this study is not good. In the future, the model training dataset and the architecture of the model will be improved to improve the effect of entity extraction. In knowledge fusion, a large amount of data calculation needs to be performed. The current knowledge fusion framework

has low computational efficiency. In the future, a domain synonym dictionary and a stop word dictionary will be added to perform word segmentation calculation on attribute information to improve computational efficiency.

Data Availability

The data supporting the findings of this study are available within the article.

Conflicts of Interest

The authors declare that they have no conflicts of interest.

Acknowledgments

This article is an outcome of the major project "Research on Public Data Open Utilization System and Capacity Building Orienting Digital Development" (No. 21&ZD336) supported by the National Social Science Foundation of China and "Research on the Institutional Innovation of National Intelligence Work under the Overall National Security View" (No. 20ATQ004) supported by the National Social Science Foundation of China, and this project was undertaken by Professor Ma Haiqun.

References

[1] F. Mahdisoltani, J. Biega, and F. Suchanek, "Yago3: a knowledge base from multilingual wikipedias," in *Proceedings of the 7th Biennial Conference on Innovative Data Systems Research*, Asilomar, CA, USA, 2014.

[2] R. Navigli and S. P. Ponzetto, "BabelNet: the automatic construction, evaluation and application of a wide-coverage multilingual semantic network," *Artificial Intelligence*, vol. 193, pp. 217–250, 2012.

[3] S. Auer, C. Bizer, G. Kobilarov, J. Lehmann, R. Cyganiak, and Z. Ives, "DBpedia: a nucleus for a web of open data," *Semantic Web*, vol. 4825, pp. 722–735, 2007.

[4] F. Liao, L. Ma, and D. Yang, "Research on construction method of knowledge graph of US military equipment based on BiLSTM model," in *Proceedings of the 2019 International Conference on High Performance Big Data and Intelligent Systems (HPBD&IS)*, pp. 146–150, Shenzhen, China, May 2019.

[5] C. Liu, Y. Yu, X. Li, and P. Wang, "Application of entity relation extraction method under CRF and syntax analysis tree in the construction of military equipment knowledge graph," *IEEE Access*, vol. 8, Article ID 200581, 2020.

[6] D. Song, Y. Li, and Q. Wang, "Construction of Military Knowledge Graph Based on Paper Bibliographic Data," in *Proceedings of the 2021 33rd Chinese Control And Decision Conference (CCDC)*, pp. 2297–2301, Kunming, China, May 2021.

[7] Y. Yao, F. Yang, Y. Liu, and Q. Yuan, "The construction and application research of military equipment concept graph," *Fire Control and Command Control*, vol. 46, no. 9, pp. 125–132, 2021.

[8] X. Meng, C. H. Yang, and J. Q. Bi, "Construction and application of domain-speific knowledge graph in military field," *Command Control &Simulation*, vol. 42, no. 4, 2020.

[9] Y. Zhao, Z. K. Chen, and C. Yang, "Construction Knowledge Graph Method for Military Field Based on Open Source Data," *Command Information System and Technology*, vol. 10, pp. 64–69, 2019.

[10] A. Bordes, N. Usunier, A. Garcia-Duran, J. Weston, and O. Yakhnenko, "Translating embeddings for modeling multi-relational data," *Advances in Neural Information Processing Systems*, vol. 26, 2013.

[11] Y. Hao, Y. Zhang, S. He, K. Liu, and J. Zhao, "A Joint embedding method for entity alignment of knowledge bases," *China Conference on Knowledge Graph and Semantic Computing*, vol. 650, pp. 3–14, 2016.

[12] M. Chen, Y. Tian, M. Yang, and C. Zaniolo, "Multilingual Knowledge Graph Embeddings for Cross-Lingual Knowledge Alignment," in *Proceedings of the Twenty-Sixth International Joint Conference on Artificial Intelligence*, Melbourne, Australia, August 2017.

[13] H. Zhu, R. Xie, Z. Liu, and M. Sun, "Iterative entity alignment via knowledge embeddings," in *Proceedings of the International Joint Conference on Artificial Intelligence (IJCAI)*, Melbourne, Australia, August 2017.

[14] B. D. Trisedya, J. Qi, and R. Zhang, "Entity alignment between knowledge graphs using attribute embeddings," *Proceedings of the AAAI Conference on Artificial Intelligence*, vol. 33, no. 1, pp. 297–304, 2019.

[15] Z. Wang, Q. Lv, X. Lan, and Y. Zhang, "Cross-lingual knowledge graph alignment via graph convolutional networks," in *Proceedings of the 2018 Conference on Empirical Methods in Natural Language Processing*, pp. 349–357, Brussels, BE, Europe, 2018.

[16] J. Devlin, M. W. Chang, K. Lee, and K. Toutanova, "Bert: pre-training of deep bidirectional transformers for language understanding," 2018, https://arxiv.org/abs/1810.04805.

[17] A. Vaswani, N. Shazeer, N. Parmar et al., "Attention is all you need," *Advances in Neural Information Processing Systems*, vol. 30, 2017.

[18] Y. Liu, M. Ott, N. Goyal et al., "Roberta: A Robustly Optimized Bert Pretraining Approach," 2019, https://arxiv.org/abs/1907.11692.

[19] Y. Cui, W. Che, T. Liu, B. Qin, and Z. Yang, "Pre-training with whole word masking for Chinese BERT," *IEEE/ACM Transactions on Audio, Speech, and Language Processing*, vol. 29, pp. 3504–3514, 2021.

[20] M. S. Charikar, "Similarity estimation techniques from rounding algorithms," in *Proceedings of the Thiry-fourth Acm Symposium on Theory of Computing*, pp. 380–388, Montreal, Quebec, Canada, May 2002.

[21] H. M. Wallach, "Conditional Random fields: An Introduction," Technical Reports MS-CIS-04-21, University of Pennsylvania CIS, Philadelphia, PA, USA, 2004.

Hindawi
Computational Intelligence and Neuroscience
Volume 2022, Article ID 5904043, 12 pages
https://doi.org/10.1155/2022/5904043

Research Article

A Generative Image Inpainting Model Based on Edge and Feature Self-Arrangement Constraints

Fan Yao[1] **and Yanli Chu**[2]

[1]*College of Information Engineering, Xizang Minzu University, Xian Yang, Shaanxi, China*
[2]*College of Equipment Management and Support, Engineering University of PAP, Xi'an 710086, China*

Correspondence should be addressed to Fan Yao; fannyaoo@xzmu.edu.cn

Received 31 August 2022; Accepted 27 September 2022; Published 12 October 2022

Academic Editor: Zaoli Yang

At present, the image inpainting method based on deep learning has achieved a better inpainting effect than traditional methods, but the inpainting results still have problems such as local structure disorder and blurred texture when the images involving a large defect area are processed. This paper proposes a second-order generative image inpainting model based on edge and feature self-arrangement constraints. The model consists of two parts: edge repair network and image repair network. Based on the self-encoder, the edge repair network generates the edges in the defect area according to the known information of the image and improves the edge repair effect by minimizing the adversarial loss and feature matching loss. The image inpainting network fills the defect area with the edge repair result as a priori condition. On the basis of U-Net, the feature self-arrangement module (FSM) is proposed to reconstruct the coding features of a specific scale, and the reconstructed feature skips to connect the decoding layer of the same scale, and it is fused with the upper layer underlying features for decoding. Meanwhile, guide loss, adversarial loss, and reconstruction loss are introduced to narrow the difference between the repaired image and the original image. The experimental results show that the inpainting results of the proposed model have stronger structural connectivity and clearer textures and the performance of PSNR, SSIM, and mean L1 loss in the Celeba, Facade, and Places2 is better than other inpainting methods, indicating that the algorithm can produce an inpainting effect with highly connected structure, reasonable semantics, and fine details.

1. Introduction

Image inpainting can synthesize visually realistic and semantically correct content for the missing area by using the prior information in the missing image or image training data. It is a crucial research direction in the domain of computer vision, which can be used in a variety of application scenarios, for instance, target removal, damaged or occluded area inpainting, etc.

According to different utilization characteristics, current inpainting strategies can be classified into two types: nonsemantic inpainting and semantic inpainting. Nonsemantic inpainting is a traditional image inpainting method that gradually fills the pixel information of the nondefective region of the image into the defective area through the diffusion or pixel block matching mechanism, which does not cover the generation and completion of semantic targets but only focuses on the connection and duplication and the filling of local structure and texture information. Semantic inpainting is based on deep learning. Through learning massive training data, the deep model constructs the complete mapping relationship from the damaged image to the repaired image based on the high-level semantic information extracted from the broken image and can generate semantic targets that do not exist in the background area of the broken image [1], achieving great performance in large-scale defect work that cannot be completed by traditional methods.

The current mainstream deep models all adopt generative adversarial networks (GANs) [2]. Through a

continuous adversarial game between the generator and the discriminator, the repaired image quality is gradually improved. Pathak et al. [3] applied deep learning to the field of image restoration for the first time and proposed a deep network based on an autoencoder structure. By mapping the broken image features to the low-dimensional feature space by the encoder, the output signal is reconstructed with deconvolution, and the 64×64 rectangular defect area with the resolution of 128×128 image center can be repaired. However, there are obvious traces in the inpainting results. Based on the research of Pathak et al. [3], Iizuka et al. [4] used dilated convolution [5] to replace the ordinary convolution in the fully connected layer to enhance the receptive field and introduced a local discriminator to enhance the quality of details of the generated content. Finally, it is able to repair rectangular defect areas of any size. However, the model requires postprocessing similar to Poisson fusion [6] to reduce inpainting traces, and the inpainting results are significantly degraded when dealing with irregular defect area. Yu et al. [7] divided the inpainting into two stages, including rough estimation of damaged images and introducing an attention mechanism to further refine the rough inpainting result, but the inpainting effect was significantly reduced when dealing with the irregular broken area. For the poor performance of deep model when processing irregular defect area, Liu et al. [8] proposed a special convolution method and applied it in the U-Net [9] architecture, which can fill the defect area by only using the known pixel information and effectively reducing inpainting traces and chromatic aberration. Zeng et al. [10] put forward a pyramid context encoder network, which reconstructed the encoding features of each layer to constrain the decoder, obtaining high-quality inpainting results. However, there was a problem of structure disorder when repairing irregular broken images with the complex structure.

In general, the current mainstream depth model is able to generate semantically plausible content in defect regions, but there are problems of local pixel discontinuity, structure disorder, and texture blur when repairing large-area irregular broken images. For these problems, the image inpainting is decomposed into two parts in this paper: edge repair and image inpainting, and a second-order image inpainting network is proposed, which is composed of two parts: edge repair network and image repair network. First, the edge repair network extends the edge in the defect area according to the pixel information and edge information around the defect area to obtain the edge repair map and then guides the image inpainting with the edge repair map as a priori condition. In order to improve the contextual and semantic consistency of potential features at all levels in the process of image inpainting and reduce the structural features loss, U-NET network architecture is adopted to transfer the coding features at all levels to the corresponding decoding layer through skip connection, using the rich structural information and texture features in the low-level features as much as possible. Meanwhile, the feature self-arrangement module (FSM) is proposed to reconstruct the specified coding features and fuse them with the potential features and coding features of corresponding scales for the next step of decoding so as to restrict the generator to improve the final inpainting effect.

Overall, the contribution of this paper is as follows:

(1) *The edge repair network is proposed*. The edge repair network generates edges in the defect area according to the high-frequency information features of the background area of the broken image, repairs the overall semantic contour of the image, perfects the local structure details, and completes the edge repair.

(2) *The feature self-arrangement module (FSM) is proposed*. The feature self-arrangement module refills reasonable information in defective areas of latent features according to the correlation between the pixel block in the coded feature background area and the pixel block in the corresponding decoded feature defect area to effectively reconstruct the decoded feature.

(3) *An image inpainting network is proposed*. The image inpainting network fills the pixel with output of the edge repair network as a priori condition and restricts the decoder by introducing a feature self-arrangement module on the basis of U-Net. Combining the influence of edge information and reconstruction features, high-quality repair results with complete semantics, connected structure, and clear texture can be obtained by using the image inpainting network.

2. Related Work

Traditional repair strategies mainly use low-level nonsemantic features in the background area of the defect image to fill in the defect area. The diffusion-based method [11–13] spreads the pixel information around the defect area from the outside region to the inside region, which can only fill in small missing areas similar to scratches and ink dots. The patch matching-based method [14, 15] can be applied into more image inpainting. The method based on pixel block matching fills the pixel information in the defect area sequentially by calculating the similarity between the boundary of the defect area and the pixel block of the background area. The traditional restoration methods only use the existing pixel information of the defect image to carry out diffusion or weighted copying, which lacks the high-level semantic understanding of the image and cannot generate the content with structural connectivity and clear texture when faced with the repair work with a complex structure and large defect area [16].

The image repair strategy based on deep learning learns high-level semantic representation from large-scale data, which greatly improves the inpainting effect. However, early convolutional neural network-based methods [6, 7] cannot handle structure and texture information separately and cannot effectively use context information to reconstruct missing content. Therefore, these methods often produce inpainting results with noise or texture artifacts when dealing with irregular defects. In order to solve these problems, many scholars conducted research from different

perspectives. Liu et al. [17] divided the inpainting into two stages: rough estimation and refinement, and they proposed a coherent semantic attention layer that predicted missing content by modeling the correlation between semantic features. It is embedded in the encoder of the image refinement network to improve the inpainting ability of image details, but this method is more time-consuming and it lacks the influence of advanced context information in the attention operation. Sagong et al. [18] simplified the coarse-to-fine second-order repair network to a single-level codec network containing a contextual attention module, greatly reducing training time and computing resources and achieving high-quality inpainting results. The model proposed by Liu et al. [19] treated the deep and shallow convolution features as the structural features and texture features of the input image separately for inpainting. The two types of repaired features are balanced, fused, and transferred to the decoding layer of each scale to constrain the generated network. The semantic target with complete outline and clear texture in the large-area irregular defect area is effectively reconstructed [20].

Aiming at the above problems, this paper proposes a second-order image inpainting model that combines edge guidance and feature self-arrangement constraints. The edge repair map generated by the edge repair network ensures the structural connectivity of the final inpainting result; the feature self-arrangement module fills in the effective pixel information in the defective area of the feature level; and the skip connection fuses the coding features of each level and the FSM reconstruction features with the corresponding decoding features to guide the decoding of the next layer. The method makes full use of the context feature information on both sides of the U-Net architecture "bottleneck," effectively reducing the blocked feature propagation in the decoding process. The image inpainting network can finally generate content with reasonable semantics, highly connected structure, and exquisite details.

3. Generative Image Inpainting Model

3.1. Model Framework. The proposed second-order image inpainting model includes the edge repair network and the image inpainting network. The edge repair network adopts a generative confrontation network structure, which is classified into a generator G_1 and a discriminator D_1. The image inpainting network includes a generator G_2 and a discriminator D_2. The edge repair network generates a reasonable edge contour in the defect area according to the gray value of the pixels around the broken image and the edge information of the undefected area; taking the edge generation map as a priori condition, the image inpainting network outputs all levels of coding features to the corresponding decoding layer combined with skip connections and fuses with the corresponding potential features for layer decoding, which effectively uses the context information in the encoding and decoding process, reducing the information loss during feature propagation; taking the output of the specified coding layer and the underlying features of the corresponding decoding layer as input, the feature self-arrangement module fills the defect part at the image feature level to obtain the FSM reconstruction feature map. Then it is fused with the underlying features and coding features of the corresponding decoding layer for the next step decoding to improve the final inpainting effect. The specific model framework is shown in Figure 1.

3.2. Feature Self-Arrangement Module. For the broken image I, Ω is defined as the missing area and $\overline{\Omega}$ is the known area. The U-Net frame of L-th layer is taken as an example. $\varphi^l(I)$ represents the coding feature of the l-th layer, $\varphi^{L-l}(I)$ represents the decoding feature of the $(L-l)$-th layer, and $F(\cdot)$ represents the feature self-arrangement operation. The corresponding output FSM reconstruction feature is

$$\phi^{L-l} = F\left(\varphi^l, \varphi^{L-l}\right). \tag{1}$$

As shown in Figure 2, the feature self-arrangement module predicts $\phi^{L-l}(I)$ through $\varphi^l(I)$ and $\varphi^{L-l}(I)$, making it closer to the output feature $\varphi^l(I_{gt})$ of the original image I_{gt} in the corresponding coding layer. For each $(\varphi^{L-l}(I))_\beta (\beta \in \Omega)$, its related nearest neighbor search in $(\varphi^l(I))_\alpha (\alpha \in \overline{\Omega})$ can be derived by the following formula:

$$\alpha^*(\beta) = \arg\max_{\alpha \in \overline{\Omega}} \frac{\left\langle \left(\varphi^{L-l}(I)\right)_\beta, \left(\varphi^l(I)\right)_\alpha \right\rangle}{\left\| \left(\varphi^{L-l}(I)\right)_\beta \right\|_2 \left\| \left(\varphi^l(I)\right)_\alpha \right\|_2}. \tag{2}$$

At the same time, the displacement vector of the feature self-arrangement patch block is defined as $\mu_\beta = \alpha^*(\beta) - \beta$, and then $(\phi^{L-l}(I))_\beta$ is predicted by copying and filling the patch block of encoding feature $(\varphi^l(I))_\alpha$, that is

$$\left(\phi^{L-l}(I)\right)_\beta = \left(\varphi^l(I)\right)_{\beta+\mu_\beta}. \tag{3}$$

The feature auto-arrangement module can use the pixel block in the defective region of the decoded feature to perform matching calculation with the known pixel value of the corresponding encoding feature and refill the defective region of the decoded feature, effectively improving the content rationality at the feature level and providing a good guiding foundation for the next step of decoding.

3.3. Edge Repair Network. The edge repair network adopts a generative confrontation network structure, which is classified into a generator G_1 and a discriminator D_1. The generator adopts a self-encoder structure, and the input is composed of the mask, the gray image of the broken image, and the edge binary image which are used to obtain the shallow features through the encoder of subsampling twice. The shallow features are sent to the feature extraction area composed of eight residual blocks combined with expansion convolution (expansion factor is 2), and then the complete image is decoded by a decoder that is up-sampled twice. Spectral normalization is used for each layer in the generator network [21, 22]. Apart from the last layer of convolution of each residual block and the last layer of convolution of the decoder, the ReLU activation function is used after each layer of convolution. The network parameters of the edge generator are shown in Table 1.

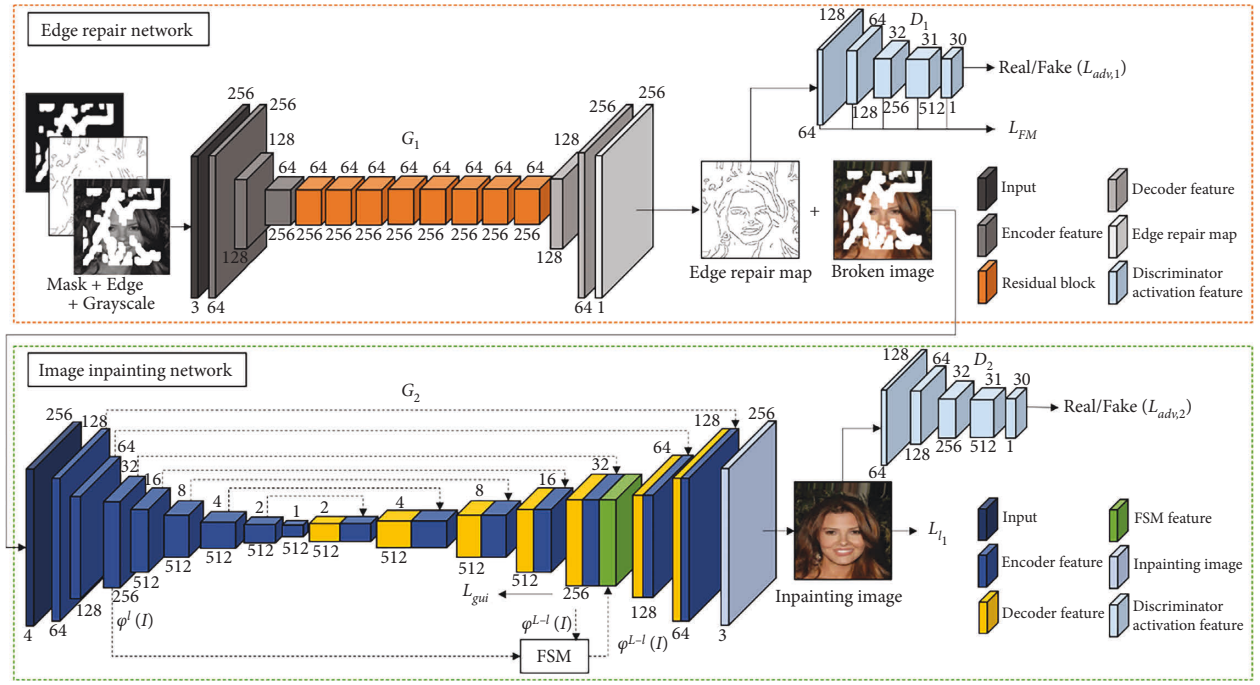

Figure 1: Generative image inpainting model framework.

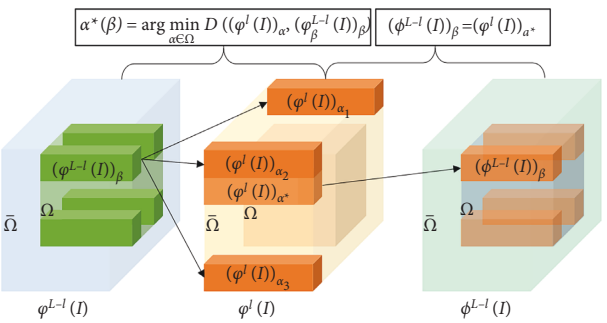

Figure 2: Feature self-arrangement module.

Table 1: The network parameters of the edge generator.

Layer	Inputs ($H \times W \times C$)	Kernel size	Stride	Padding	Dilation	Activation function	Outputs ($H \times W \times C$)
ReflectionPad	$256 \times 256 \times 3$	—	—	3	—	—	$262 \times 262 \times 3$
Conv	$262 \times 262 \times 3$	7×7	1	0	1	ReLU	$256 \times 256 \times 64$
Conv	$256 \times 256 \times 64$	4×4	2	1	1	ReLU	$128 \times 128 \times 128$
Conv	$128 \times 128 \times 128$	4×4	2	1	1	ReLU	$64 \times 64 \times 256$
Residual Blocks × 8							
ReflectionPad	$64 \times 64 \times 256$	—	—	2	—	—	$68 \times 68 \times 256$
Res-conv	$68 \times 68 \times 256$	3×3	1	0	2	ReLU	$64 \times 64 \times 256$
ReflectionPad	$64 \times 64 \times 256$	—	—	1	—	—	$66 \times 66 \times 256$
Res-conv	$66 \times 66 \times 256$	3×3	1	0	1	—	$64 \times 64 \times 256$
ConvTranspose	$64 \times 64 \times 256$	4×4	2	1	1	ReLU	$128 \times 128 \times 128$
ConvTranspose	$128 \times 128 \times 128$	4×4	2	1	1	ReLU	$256 \times 256 \times 64$
ReflectionPad	$256 \times 256 \times 64$	—	—	3	—	ReLU	$262 \times 262 \times 64$
Conv	$262 \times 262 \times 64$	7×7	1	0	1	—	$256 \times 256 \times 1$

The edge discriminator uses the Path GAN [23] architecture. Path GAN maps the input image to a matrix X of $N \times N$ through convolution, and each point of the matrix X; that is, the value of $X_{i,j}$ stands for the evaluation of a small area of the input image. Finally, the average value of $X_{i,j}$ is the output of the discriminator. The introduction of Path GAN can make the edge repair network attach importance to image details in training. The training process is stabilized

Table 2: Network parameters of the edge discriminator.

Layer	Inputs ($H \times W \times C$)	Kernel size	Stride	Padding	Dilation	Activation function	Outputs ($H \times W \times C$)
Conv	$256 \times 256 \times 2$	4×4	2	1	1	Leaky ReLU	$128 \times 128 \times 64$
Conv	$128 \times 128 \times 64$	4×4	2	1	1	Leaky ReLU	$64 \times 64 \times 128$
Conv	$64 \times 64 \times 128$	4×4	2	1	1	Leaky ReLU	$32 \times 32 \times 256$
Conv	$32 \times 32 \times 256$	4×4	1	1	1	Leaky ReLU	$31 \times 31 \times 512$
Conv	$31 \times 31 \times 512$	4×4	1	1	1	—	$30 \times 30 \times 1$

by adding spectral normalization to each layer of the discriminator network [21]. After the first four layers are convolved, the slope parameters of Leaky ReLU are set to 0.2, and the sigmoid activation function is utilized before the discriminator outputs the final result. The network layer parameters of the edge discriminator are shown in Table 2.

3.4. Image Inpainting Network. Similar to the edge generation network, the image inpainting network includes a generator G_2 and a discriminator D_2. Skip connection is applied at each coding layer of the generator to transfer the output of each coding layer to the corresponding decoding layer, and it is fused with the underlying features to decode layer by layer, which takes full advantage of the context information in the encoding and decoding process to decrease the information loss during the layer-by-layer transmission of features at all levels. In addition, in order for the generator to generate content with consistent contextual semantics and rich low-level details in the decoding process, a feature self-arrangement module is proposed, which performs pixel rearrangement and fills in the defect areas with the coding features and decoding features of the same scale as input. Finally, FSM feature map with a complete semantic and structural connection can be reconstructed. This method fills reasonable information in the defect area at the feature level, playing a positive role in improving and guiding the subsequent decoding at all levels. By minimizing the introduced guidance loss, the specific decoding layer of the generator is obliged to output a feature map that conforms to the real situation as much as possible. Meanwhile, reconstruction loss and counter loss are applied to the final output image to train the network, thereby continuously improving the inpainting effect of the network.

The image repair network generator is divided into encoding and decoding. $Enc(\cdot)$ represents the encoding process, I_{gt}^{brk} represents the broken RGB image, and E_{pred} represents the edge repair map. The input of the image repair network is represented as $I = I_{gt}^{brk} \oplus E_{pred}$. The encoding features at all levels are expressed as

$$\varphi^1(I) = Enc(I), \tag{4}$$

$$\varphi^2(I) = Enc\left(\varphi^1(I)\right), \tag{5}$$

$$\varphi^3(I) = Enc\left(\varphi^2(I)\right), \tag{6}$$

$$\varphi^8(I) = Enc\left(\varphi^7(I)\right). \tag{7}$$

By introducing skip connections, the coding features and corresponding decoding features at each decoding layer are fused for decoding. $Dec(\cdot)$ represents the decoding operation. $F(\cdot)$ represents the feature self-arrangement operation. The decoding features at all levels are expressed as

$$\varphi^9(I) = \mathrm{Dec}\left(\varphi^8(I)\right), \tag{8}$$

$$\varphi^{10}(I) = \mathrm{Dec}\left(\varphi^9(I) \oplus \varphi^7(I)\right), \tag{9}$$

$$\phi^{13}(I) = F\left(\varphi^{13}(I) \oplus \varphi^3(I)\right), \tag{10}$$

$$\varphi^{14}(I) = \mathrm{Dec}\left(\left(\varphi^{13}(I) \oplus \varphi^3(I)\right) \oplus \phi^{13}\right), \tag{11}$$

$$\varphi^{15}(I) = \mathrm{Dec}\left(\varphi^{14}(I) \oplus \varphi^2(I)\right). \tag{12}$$

Instance normalization is applied to each convolution layer of the image generator network except the first and last layers [24]. The slope parameters of Leaky ReLU are set to 0.2. The network parameters of the image generator are shown in Table 3.

The image discriminator D_2 and the edge discriminator D_1 adopt the same network architecture and parameter settings, and the generator generates content that looks like the raw image by minimizing the adversarial loss.

4. Loss Function

4.1. Overall Loss Function. The overall loss function of the proposed model is

$$\begin{aligned} L_{\mathrm{Gen}} &= L_{\mathrm{edge}} + L_{\mathrm{img}} = \lambda_{\mathrm{adv},1} L_{\mathrm{adv},1} + \lambda_{\mathrm{FM}} L_{\mathrm{FM}} \\ &\quad + \lambda_{\mathrm{adv},2} L_{\mathrm{adv},2} + \lambda_{\mathrm{gui}} L_{\mathrm{gui}} + \lambda_{l_1} L_{l_1}, \end{aligned} \tag{13}$$

where L_{edge} is the overall loss function of the edge repair network; L_{img} is the overall loss function of the image repair network; $L_{\mathrm{adv},1}$ is the adversarial loss of the edge discriminator, which is applied to train the edge generation network; L_{FM} is the feature matching loss of the edge generation network; $L_{\mathrm{adv},2}$ is the adversarial loss of the image repair network; L_{gui} is the guiding loss of the output by the specific decoding layer of the constrained image repair network; L_{l_1} is the reconstruction loss of the image repair network. $\lambda_{\mathrm{adv},1}$, λ_{FM}, $\lambda_{\mathrm{adv},2}$, λ_{gui}, and λ_{l_1} are the corresponding weight parameters. Each loss function is described in detail below.

4.2. Edge Loss. I_{gt}, I_{gray}, and E_{gt}, respectively, represent the original image of the input edge repair network and its grayscale image and edge binary image; in the mask M, the missing area is marked as 1, and the background area is marked as 0. The broken image is expressed as $I_{\mathrm{gt}}^{\mathrm{brk}} = I_{gt} \odot (1 - M)$, and the defect grayscale image is

Table 3: Network parameters of the image generator.

Layer	Inputs ($H \times W \times C$)	Kernel size	Stride	Padding	Dilation	Activation function	Outputs ($H \times W \times C$)
Conv	$256 \times 256 \times 4$	4×4	2	1	1	—	$128 \times 128 \times 64$
Conv	$128 \times 128 \times 64$	4×4	2	1	1	Leaky ReLU	$64 \times 64 \times 128$
Conv	$64 \times 64 \times 128$	4×4	2	1	1	Leaky ReLU	$32 \times 32 \times 256$
Conv	$32 \times 32 \times 256$	4×4	2	1	1	Leaky ReLU	$16 \times 16 \times 512$
Conv	$16 \times 16 \times 512$	4×4	2	1	1	Leaky ReLU	$8 \times 8 \times 512$
Conv	$8 \times 8 \times 512$	4×4	2	1	1	Leaky ReLU	$4 \times 4 \times 512$
Conv	$4 \times 4 \times 512$	4×4	2	1	1	Leaky ReLU	$2 \times 2 \times 512$
Conv	$2 \times 2 \times 512$	4×4	2	1	1	Leaky ReLU	$1 \times 1 \times 512$
DeConv	$1 \times 1 \times 512$	4×4	2	1	1	ReLU	$2 \times 2 \times 512$
DeConv	$2 \times 2 \times 1024$	4×4	2	1	1	ReLU	$4 \times 4 \times 512$
DeConv	$4 \times 4 \times 1024$	4×4	2	1	1	ReLU	$8 \times 8 \times 512$
DeConv	$8 \times 8 \times 1024$	4×4	2	1	1	ReLU	$16 \times 16 \times 512$
DeConv	$16 \times 16 \times 1024$	4×4	2	1	1	ReLU	$32 \times 32 \times 256$
DeConv	$32 \times 32 \times 768$	4×4	2	1	1	ReLU	$64 \times 64 \times 128$
DeConv	$64 \times 64 \times 256$	4×4	2	1	1	ReLU	$128 \times 128 \times 64$
DeConv	$128 \times 128 \times 128$	4×4	2	1	1	Tanh	$256 \times 256 \times 3$

expressed as $I_{\text{gray}}^{\text{brk}} = I_{\text{gray}} \odot (1 - M)$, and the defect edge binary image is expressed as $E_{\text{gt}}^{\text{brk}} = E_{gt} \odot (1 - M)$; $\odot$ is the Hadamard product, which means that the corresponding elements of the matrix are multiplied. $G_1(\cdot)$ stands for the operation of the edge generator, and $D_1(\cdot)$ stands for the operation of the edge discriminator, then the edge repair map is expressed as $E_{\text{pre d}} = G_1(I_{\text{gray}}^{\text{brk}}, E_{\text{gt}}^{\text{brk}}, M)$.

The adversarial loss $L_{\text{a dv},1}$ [1] is defined as follows, which is used to train the edge repair network:

$$L_{\text{a dv},1} = \mathbb{E}_{\left(E_{\text{gt}}, I_{\text{gray}}\right)} \log\left[D\left(E_{\text{gt}}, I_{\text{gray}}\right)\right] + \mathbb{E}_{I_{\text{gray}}} \log\left[1 - D\left(E_{\text{pre d}}, I_{\text{gray}}\right)\right]. \tag{14}$$

The feature matching loss is introduced [25]. By comparing the activation features of the edge repair image and the original image edge in the middle layer of the discriminator, the generator is forced to produce more realistic and reasonable results to stabilize the training process. L represents the number of convolutional layers of D_1, N_i represents the number of elements in the i-th active layer of D_1, and $D_1^{(i)}$ represents the activation feature map of the i-th layer in the discriminator. By comparing the activation maps of the middle layer of the discriminator, the generator is forced to produce results closer to the raw image to stabilize the training process. The feature matching loss is as follows:

$$L_{\text{FM}} = \mathbb{E}\left[\sum_{i=1}^{L} \frac{1}{N_i} \left\| D_1^{(i)}\left(E_{\text{gt}}\right) - D_1^{(i)}\left(E_{\text{pre d}}\right) \right\|_1\right]. \tag{15}$$

The overall loss function of the edge generation network is

$$L_{\text{e dg e}} = \lambda_{\text{a dv},1} L_{\text{a dv},1} + \lambda_{\text{FM}} L_{\text{FM}}, \tag{16}$$

where $\lambda_{\text{a dv},1}$ and λ_{FM} are the weight parameters. $\lambda_{\text{a dv},1} = 1$, $\lambda_{\text{FM}} = 15$.

4.3. Image Inpainting Loss. $G_2(\cdot)$ stands for the operation of the image generator, and $D_2(\cdot)$ stands for the operation of the image discriminator; the generated image is expressed as $I_{pre\,d} = G_2(I_{\text{gt}}^{\text{brk}}, E_{\text{pre d}}, M)$. The final output of the entire inpainting network is the fused image, defined as $I_{\text{gt}}^{\text{comp}} = I_{\text{gt}}^{\text{brk}} + I_{\text{pre d}} \odot M$.

The adversarial loss [2] $\lambda_{\text{a dv},2}$ is introduced, which is used to train the image inpainting network.

$$L_{\text{a dv},2} = \mathbb{E}_{\left(I_{\text{gt}}, I_{\text{pre d}}\right)} \log\left[D_2\left(I_{\text{gt}}, E_{\text{pre d}}\right)\right] + \mathbb{E}_{E_{\text{pre d}}} \log\left[1 - D_2\left(I_{\text{pre d}}, E_{\text{pre d}}\right)\right]. \tag{17}$$

In the decoding process, in order to retain more of the raw information of the image, the guidance loss is introduced to judge the output feature of the $L - l$-th layer, so as to reduce the difference between the output $\varphi^{L-l}(I)$ and $\varphi^{l}(I_{gt})$ of the decoding layer and enhance the decoding capability of the model. The guidance loss is as follows:

$$L_{\text{gui}} = \sum_{\beta \in \Omega} \left\| \left(\varphi^{L-l}(I)\right)_\beta - \left(\varphi^{l}\left(I_{gt}\right)\right)_\beta \right\|_2^2. \tag{18}$$

The reconstruction loss is introduced to evaluate the final repaired image, so as to make the content generated by the image generator closer to the real image. The reconstruction loss is as follows:

$$L_{l_1} = \left\| I_{\text{pre d}} - I_{\text{gt}} \right\|_1. \tag{19}$$

The overall loss function of this module is

$$L_{\text{img}} = \lambda_{\text{a dv},2} L_{\text{a dv},2} + \lambda_{\text{gui}} L_{\text{gui}} + \lambda_{l_1} L_{l_1}, \tag{20}$$

where $\lambda_{\text{a dv},2} = 0.1$, $\lambda_{\text{gui}} = 0.01$, and $\lambda_{l_1} = 0.5$.

5. Experimental Comparison and Analysis

5.1. Experimental Set-Up. This network runs under the Windows10 platform, Intel Xeon E5 is used by the CPU, NVIDIA RTX 2070 is used by the GPU, the GPU memory is 8G; the depth learning development frame is PyTorch, and the CUDA installed version is V10.0. Two networks are trained by using the mask set offered by Liu et al. [8], and the image size of the input network is uniformly

Figure 3: Comparison results on the Celeba.

adjusted to 256 × 256, and the mask required for each image was randomly selected from the mask library published by Liu et al. [8]. The mask library contained 12,000 irregular masks, and the mask rate was divided into six categories: (0, 0.1], (0.1, 0.2], [(0.3, 0.4, 0.2, 0.3]], (0.4, 0.5], and (0.5, 0.6]. When the edge repair network is trained, the batchsize is 8, the Adam optimizer with parameter: beta1 = 0, beta2 = 0.9 is used for optimization. The ratio of the learning rate of the generator to the discriminator is 0.1. At the beginning of network training, the learning rate uses 1×10^{-4}, and when the loss tends to be stable, the learning rate is changed to 1×10^{-5}, and then training until convergence is realized. When the image inpainting network is trained, batchsize is set to 4, and the remaining training parameters and strategies are consistent with the edge repair network.

Experiments are conducted on three datasets with different styles: Celeba [26], Façade [27], and Places2 [28], and GL [4] PCONV [8], and PEN-Net [10] are selected to compare with the proposed model.

5.2. Wavelet Filterbank Theory

5.2.1. Qualitative Comparison. GL performs poorly in color consistency and structural connectivity when repairing irregular and defective face images. Although two discriminators are used to evaluate the overall semantic information and local detailed features of the inpainting results, GL does not perform targeted filling and inpainting of the defect area at the feature level, and the performance of GL in the large-area irregular broken image inpainting is inferior to that in regular rectangular area. The content generated by PConv in the defect area is close to the original image in color, but there is an obvious blur. Moreover, due to the lack of the guidance of the marginal prior conditions, there is structural disorder in the inpainting result. PEN-Net is not stable enough to repair such irregular face images. It can generate semantic targets (such as eyes) in the defect area that are not found in the surrounding background area, but lacking prerequisite guidance for the edge results in the generated content with reasonable semantics but disorderly location,

Figure 4: Comparison results on the Facade.

which affects the inpainting effect. Taking the edge repair map as the guiding factor, through the flexible combination of the feature self-arrangement module and the skip connection, the context feature information is fully used, and then the clear and reasonable content can be obtained. The specific inpainting effect is shown in Figure 3.

The inpainting result of the image with the complex structure such as the exterior wall of the building by GL is relatively blurred. PConv can generate content with similar structure and color to the raw image in the defect area, but there are still obvious artifacts. The attention shift mechanism applied by PEN-Net can generate pixel content similar to the original image at the defect location, and the artifact is significantly improved. However, due to the lack of guidance from the edge, the structure connectivity of the generated content is insufficient. When the algorithm in this paper repairs such irregular broken images with complex structures, the edge generation map repaired by the edge repair network plays a very important guiding role. Because the edge repair network can generate a well-structured edge in the defect area, the final inpainting result avoids structural disorder. The specific inpainting effect is shown in Figure 4.

Both GL and PCONV have different degrees of artifacts in the inpainting of natural images. Pen-Net performs well in repairing solid color background areas, but the model has poor performance when processing natural image texture synthesis, resulting in color distortion and serious blurring, which generates content with poor structural connectivity and unreasonable color content. The edge repair network in this paper generates reasonable structural information in the broken area to ensure the structural connectivity of the final inpainting effect. Through skip connection and feature matching rearrangement network, the potential feature information at all levels is fully utilized to ensure the semantic coherence and color rationality of the final inpainting effect. The specific inpainting effect is shown in Figure 5.

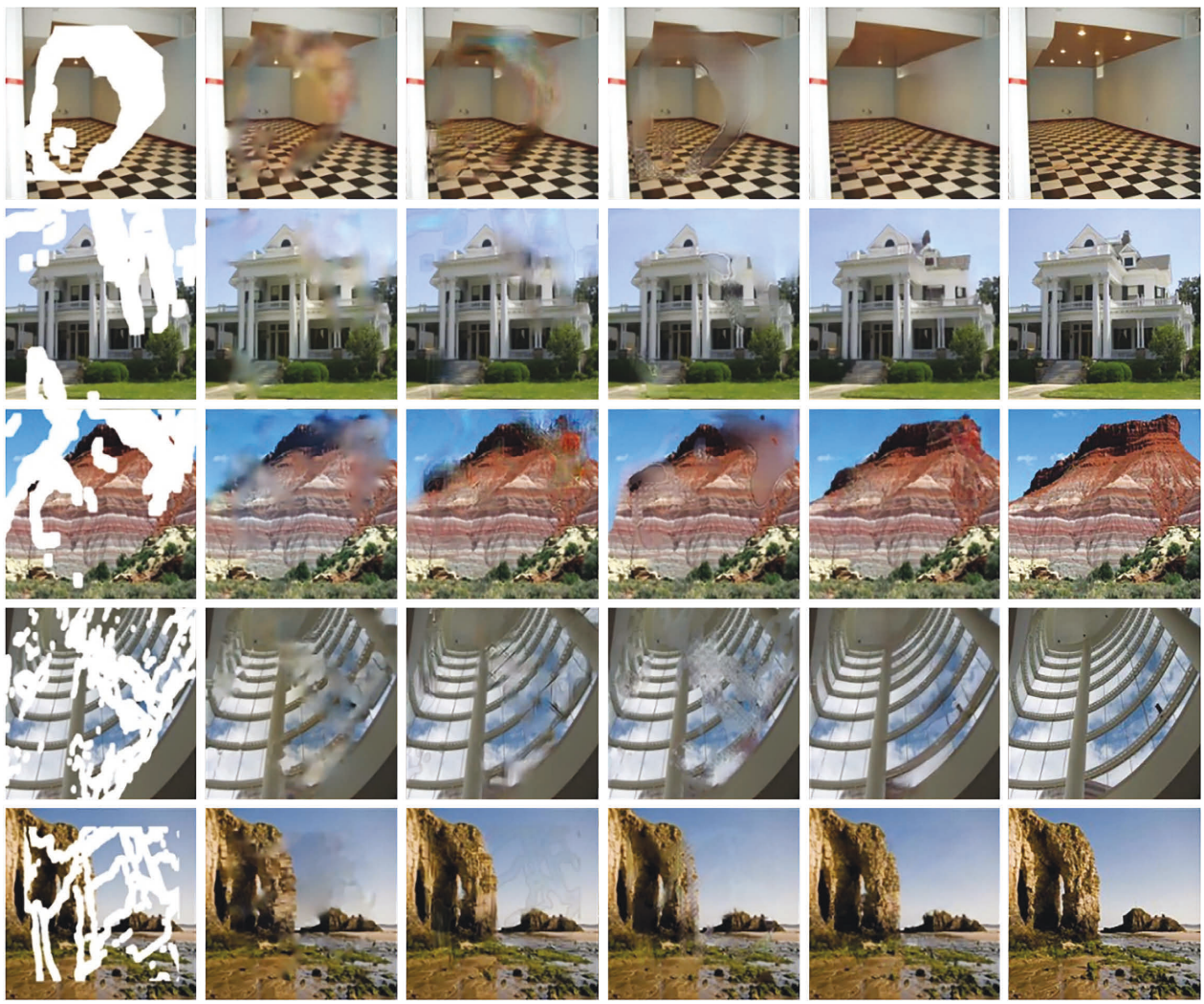

Figure 5: Comparison results on the Places2.

Table 4: Quantitative comparison of algorithms.

Data set	Mask rate	Mean L1 loss†				PSNR¶				SSIM¶			
		GL	PConv	PEN-Net	Ours	GL	PConv	PEN-Net	Ours	GL	PConv	PEN-Net	Ours
Celeba	10% ~ 20%	0.035	0.031	0.026	**0.012**	25.11	26.29	27.69	**31.65**	0.853	0.885	0.912	**0.931**
	20% ~ 30%	0.062	0.051	0.041	**0.036**	23.96	24.21	26.44	**30.21**	0.811	0.817	0.826	**0.839**
	30% ~ 40%	0.081	0.055	0.051	**0.037**	23.64	23.85	23.86	**27.03**	0.795	0.811	0.811	**0.841**
	40% ~ 50%	0.101	0.089	0.072	**0.065**	22.21	21.47	22.37	**26.41**	0.713	0.786	0.797	**0.823**
Facade	10% ~ 20%	0.043	0.033	0.031	**0.019**	23.08	23.59	24.19	**32.36**	0.801	0.857	0.841	**0.943**
	20% ~ 30%	0.047	0.073	0.045	**0.044**	23.57	23.21	23.91	**27.17**	0.774	0.863	0.861	**0.889**
	30% ~ 40%	0.088	0.091	0.073	**0.055**	21.15	22.19	22.57	**25.33**	0.766	0.712	0.854	**0.871**
	40% ~ 50%	0.101	0.113	0.076	**0.067**	21.67	22.31	21.34	**23.57**	0.714	0.751	0.836	**0.857**
Places2	10% ~ 20%	0.037	0.021	0.023	**0.011**	21.61	23.61	25.33	**30.19**	0.784	0.835	0.814	**0.919**
	20% ~ 30%	0.057	0.054	0.040	**0.031**	21.17	22.71	24.74	**27.47**	0.776	0.797	0.804	**0.814**
	30% ~ 40%	0.051	0.058	0.053	**0.046**	20.53	22.15	23.87	**25.31**	0.751	0.779	0.789	**0.826**
	40% ~ 50%	0.071	0.083	0.075	**0.066**	20.27	21.94	21.61	**22.92**	0.737	0.764	0.778	**0.793**

The bold values are the experimental results in this paper.

5.2.2. Quantitative Comparison. In order to objectively compare the repair effects of this model and other algorithms, mean L1 loss, peak signal-to-noise ratio (PSNR), and structural similarity index measurement (SSIM) are adopted to evaluate the inpainting results. The mean L1 loss is used to compare the L1 distance between the raw image

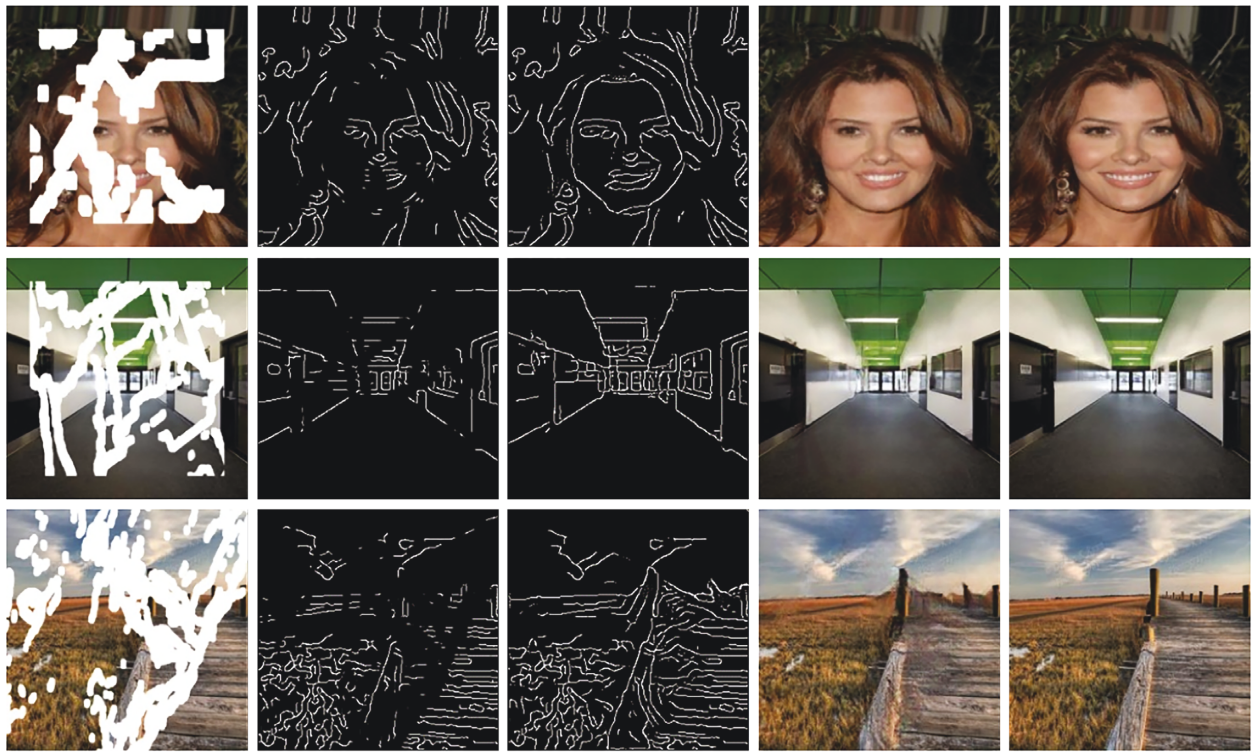

Figure 6: Edge repair network validity test.

Figure 7: Validity test of edge prior conditions.

and the repaired image. PSNR focuses on the difference between image pixels, and the SSIM is selected to compare the difference between the two images in brightness, contrast, and structure. The quantitative comparison results are shown in Table 4. The lower the value of mean L1 loss is, the better. The higher the value of PSNR and SSIM are, the better. The method with the optimal inpainting effect under different mask rates has been shown in bold († indicates that the lower the value is, the better, and ¶ indicates that the higher the value is, the better).

5.3. Model Validity Analysis

5.3.1. Validity Analysis of Edge Repair Network. Under the condition of given gray information and edge

Figure 8: FSM feature validity test.

information around the broken area, the edge repair network can extend the edge in the broken area and generate a partially closed and coherent semantic contour. The comparison of the broken edge map and the edge repair map in Figure 6 shows that the edge repair network can connect the two ends of the broken structure in the broken area, which fully indicates that the edge repair network can accurately reconstruct high-frequency structural information. At the same time, the analysis of the repaired image by the edge repair map shows that the semantic target structure in the broken area is highly consistent with that of the edge generated map in the broken area, which proves the validity of image inpainting with the edge repair map as a prior condition.

5.3.2. Validity Analysis of Edge Prior Conditions. With the edge repair map as a priori condition, the model can finally generate semantically coherent content in the broken area. Without the edge repair map as a guide condition, the model cannot generate content with reasonable semantics and connected structure. It fully illustrates the important role of the edge generated map in the image inpainting to insure the structural connectivity and semantic coherence of the inpainting effect, as shown in Figure 7.

5.3.3. FSM Feature Validity Analysis. Without FSM feature guiding inpainting, the final inpainting result generated in this paper is quite distinct from the background region in color, which does not conform to the human visual characteristics; when the FSM feature guidance is introduced in the decoding process, the content generated by the model in the broken area is highly consistent with the background area in color, and the texture blur in the broken area is effectively reduced, indicating that the introduction of FSM features in the decoding process enables the model to generate content with more reasonable color and clearer details, as shown in Figure 8.

6. Conclusions

A generative image inpainting model combining edge and feature self-arrangement module is proposed. The edge repair network can effectively reconstruct structural information in the broken area and output a highly connected and semantically coherent edge repair map; the image inpainting network uses edge generation map as prior conditions and fuses the encoding features at all levels with the corresponding decoding features to decode layer by layer through skip connection, which effectively utilizes the context feature information in the process of encoding and decoding, avoiding the loss of part of semantic information and local details when the context features are transmitted among convolutional layers; meanwhile, a feature self-arrangement module is proposed to fill the broken area with effective information at the feature level, and it fuses the reconstruction features into the decoding process of the corresponding layer to restrain the subsequent decoding. Combined with the influence of the above three aspects, the model of this article can eventually generate the content with the same semantics, valid structure, and clear texture features as the original image.

Data Availability

The datasets analyzed during the current study are available from the corresponding author on reasonable request.

Conflicts of Interest

The authors declare no conflicts of interest.

Acknowledgments

This work was supported by Natural Science Foundation of China (NO. 62062061).

References

[1] S. Yingnan, F. Yao, and Z. Ningjun, "A generative image inpainting network based on the attention transfer network across layer mechanism," *Optik*, vol. 242, Article ID 167101, 2021.

[2] H. Jeong, J. Yu, and W. Lee, "Poster abstract: a semi-supervised approach for network intrusion detection using generative adversarial networks," in *Proceedings of the IEEE Conference on Computer Communications Workshops (INFOCOM WKSHPS)*, pp. 1-2, IEEE, Paris, France, May 2019.

[3] D. Pathak, P. Krähenbühl, J. Donahue, T. Darrell, and A. Efros, "Context encoders: feature learning by inpainting," in *Proceedings of the IEEE conference on computer vision and pattern recognition*, pp. 2536–2544, IEEE, Las Vegas, NV, USA, June 2016.

[4] S. Iizuka, E. Simo-Serra, and H. Ishikawa, "Globally and locally consistent image completion," *ACM Transactions on Graphics*, vol. 36, no. 4, pp. 1–14, 2017.

[5] F. Yu and K. Vladlen, "Multi-scale context aggregation by dilated convolutions," in *Proceedings of the 4th Internatinal Conference on Learning Representations (ICLR 2016)*, IEEE, San Juan, Puerto Rico, May 2016.

[6] J. M. Di Martino, G. Facciolo, and E. Meinhardt-Llopis, "Poisson image editing," *Image Processing On Line*, vol. 6, pp. 300–325, 2016.

[7] J. H. Yu, Z. Lin, J. M. Yang, X. H. Shen, X. Lu, and T. Huang, "Generative image inpainting with contextual attention," in *Proceedings of the IEEE Conference on Computer Vision and Pattern Recognition(CVPR 2018)*, pp. 5505–5514, IEEE, Salt Lake City, UT, USA, 2018.

[8] G. L. Liu, F. A. Reda, K. J. Shih, T. C. Wang, A. Tao, and B. Catanzaro, "Image inpainting for irregular holes using partial convolutions," in *Proceedings of the European Conference on Computer Vision (ECCV 2018)*, pp. 85–100, IEEE, Munich, Germany, September 2018.

[9] O. Ronneberger, F. Philipp, and B. Thomas, "U-net: convolutional networks for biomedical image segmentation," in *Proceedings of the International Conference on Medical image computing and computer-assisted intervention*, vol. 9351, pp. 234–241, Singapore, October 2015.

[10] Y. H. Zeng, J. L. Fu, H. Y. Chao, and B. N. Guo, "Learning pyramid-context encoder network for high-quality image inpainting," in *Proceedings of the IEEE/CVF Conference on Computer Vision and Pattern Recognition (CVPR 2019)*, pp. 1486–1494, IEEE, Long Beach, CA, USA, June 2019.

[11] M. Bertalmio, G. Sapiro, V. Caselles, and C. Ballester, "Image inpainting," in *Proceedings of the 27th Annual Conference on Computer Graphics and Interactive Techniques*, pp. 417–424, IEEE, New Orleans, LA, USA, July 2000.

[12] J. H. Shen and T. F. Chan, "Mathematical models for local nontexture inpaintings," *SIAM Journal on Applied Mathematics*, vol. 62, no. 3, pp. 1019–1043, 2002.

[13] T. F. Chan and J. Shen, "Nontexture inpainting by curvature-driven diffusions," *Journal of Visual Communication and Image Representation*, vol. 12, no. 4, pp. 436–449, 2001.

[14] C. Barnes, E. Shechtman, A. Finkelstein, and D. B. Goldman, "Patch match: a randomized correspondence algorithm for structural image editing," *ACM Transactions on Graphics*, vol. 28, no. 3, pp. 1–11, 2009.

[15] A. Criminisi, P. Perez, and K. Toyama, "Region filling and object removal by exemplar-based image inpainting," *IEEE Transactions on Image Processing*, vol. 13, no. 9, pp. 1200–1212, 2004.

[16] P. Li and Y. Chen, "Research into an image inpainting algorithm via multilevel attention progression mechanism," *Mathematical Problems in Engineering*, vol. 2022, Article ID 8508702, 12 pages, 2022.

[17] H. Y. Liu, B. Jiang, Y. Xiao, and C. Yang, "Coherent semantic attention for image inpainting," in *Proceedings of the IEEE/CVF International Conference on Computer Vision(ICCV 2019)*, pp. 4170–4417, IEEE, Seoul, Korea, November 2019.

[18] M. C. Sagong, Y. G. Shin, S. W. Kim, S. Park, and S. J. Ko, "Pepsi: fast image inpainting with parallel decoding network," in *Proceedings of the IEEE/CVF Conference on Computer Vision and Pattern Recognition (CVPR 2019)*, pp. 11360–11368, IEEE, Long Beach, CA, USA, June 2019.

[19] H. Y. Liu, B. Jiang, Y. B. Song, W. Huang, and C. Yang, "Rethinking image inpainting via a mutual encoder-decoder with feature equalizations,"vol. 12347, pp. 725–741, in *Proceedings of the 16th European Conference Computer Vision (ECCV 2020)*, vol. 12347, pp. 725–741, IEEE, Glasgow, UK, August 2020.

[20] S. Mahpod, R. Das, E. Maiorana, Y. Keller, and P. Campisi, "Facial landmarks localization using cascaded neural networks," *Computer Vision and Image Understanding*, vol. 205, no. 3, pp. 103171–103463, 2021.

[21] T. Miyato, T. Kataoka, M. Koyama, and Y. Yoshida, "Spectral normalization for generative adversarial networks," 2018, http://arXiv.org/abs/1802.05957.

[22] D. Hu, H. Shi, and W. Jiang, "Infrared Infrared and visible image fusion based on empirical curvelet transform and phase congruency," *Ukrainian Journal of Physical Optics*, vol. 22, no. 3, pp. 128–137, 2021.

[23] I. Phillip, J. Zhu, T. Zhou, and A. Alexei, "Efros. Image-to-image translation with conditional adversarial networks," in *Proceedings of the IEEE Conference on Computer Vision and Pattern Recognition (CVPR 2017)*, pp. 1125–1134, IEEE, Honolulu, HI, USA, July 2017.

[24] D. Ulyanov, V. Andrea, and L. Victor, "Instance normalization: the missing ingredient for fast stylization," 2016, http://arXiv.org/abs/1607.08022.

[25] J. Johnson, A. Alexandre, and F. F. Li, "Perceptual losses for real-time style transfer and super-resolution," in *Proceedings of the European Conference on Computer Vision(ECCV 2016)*, vol. 9906, pp. 694–711, Amsterdam, The Netherlands, October 2016.

[26] Z. W. Liu, P. Luo, X. G. Wang, and X. O. Tang, "Deep learning face attributes in the wild," in *Proceedings of the IEEE International Conference on Computer Vision (ICCV 2015)*, pp. 3730–3738, IEEE, Santiago, Chile, December 2015.

[27] R. Tyleček, "Spatial pattern templates for recognition of objects with regular structure," in *Proceedings of the German Conference on Pattern Recognition*, vol. 8142, pp. 364–374, Saarbrücken, Germany, September 2013.

[28] B. Zhou, A. Lapedriza, A. Khosla, A. Oliva, and A. Torralba, "Places: a 10 million image database for scene recognition," *IEEE Transactions on Pattern Analysis and Machine Intelligence*, vol. 40, no. 6, pp. 1452–1464, 2018.

Hindawi
Computational Intelligence and Neuroscience
Volume 2022, Article ID 6989374, 9 pages
https://doi.org/10.1155/2022/6989374

Research Article

Learning of Short Video Text Description of Nursing Teaching Based on Transformer

Xuenan Cao

Nursing and Health College, Shanghai Zhongqiao Vocational and Technical University, Shanghai 201514, China

Correspondence should be addressed to Xuenan Cao; caoxn@shzq.edu.cn

Received 19 August 2022; Revised 17 September 2022; Accepted 20 September 2022; Published 10 October 2022

Academic Editor: Zaoli Yang

Nursing is an important task in modern medical treatment, which can assist patients in the treatment and rehabilitation process. Nursing practitioners' skills and mentality can affect patient recovery and the speed of treatment. Therefore, there are already a large number of colleges and universities to carry out nursing teaching work. However, the current nursing teaching work still adopts the traditional teaching mode, which is no longer in line with the nursing work of the present era. Nursing teaching not only imparts nursing expertise to students, but it also requires higher practical ability. This study considers the integration of short video technology and text teaching mode into the teaching work of nursing. This study also used the transformer method to extract and predict the characteristics of nursing knowledge, nursing actions, and student satisfaction in short nursing teaching videos and texts. This study also explores the temporal characteristics existing in short videos of nursing teaching. The results show that the T-CNN-L method has higher accuracy than the T-CNN method in predicting the relevant features of nursing teaching short videos. The T-CNN-L method can also accurately and efficiently extract and predict nursing knowledge features and nursing action features.

1. Introduction

With the continuous improvement of living standards, the level of medical care also continues to improve. Nursing is an important stage in patient recovery and treatment. Effective nursing work and the attitude of nursing staff can affect the recovery process of the patient and the degree of treatment of the condition [1, 2]. Therefore, the method of nursing and the professionalism of nursing are a stage that cannot be ignored for medical treatment. For patients, most of the time is in the process of being cared for. It requires effective nursing work, both during the initial hospitalization phase and after the surgical phase. Therefore, the learning and teaching process of nursing is particularly important. The scope of nursing professional learning is also relatively wide because the nursing mode and nursing methods required by different diseases are different. There is a gap between the teaching work of nursing and traditional disciplines [3, 4]. Nursing students not only need to learn professional nursing knowledge and nursing actions, but also focus on practice. Professional nursing knowledge is the foundation of nursing practice. Through textbooks, nursing students can only learn the basic knowledge and precautions of nursing [5, 6]. Successful nursing work also requires more practice and internship process, which can improve the practical and clinical nursing ability of nursing students. At present, most colleges and universities use the form of textbooks and PPT to transmit relevant knowledge, and nursing students will also be exposed to practical links [7, 8]. However, the time for nursing students to be exposed to the practice link is relatively small, so it is necessary to consider other ways to integrate them into the teaching work of nursing [9, 10]. With the advancement of science and technology, video technology and text technology can be well transmitted through the Internet, and students or teachers can obtain more relevant video and text information about nursing knowledge through Internet technology.

Video technology is a technology that integrates vision and hearing. It can display relevant information in the form of images and sounds. At the same time, video technology

can help nursing students to fully watch and learn the movements in the nursing process. Compared with textbooks and PPT teaching methods, visual teaching methods can be more easily accepted by nursing students [11, 12]. This video technology has been used in teaching work in many disciplines. It has also been proven that video teaching methods can adequately impart knowledge. Unlike the textbook method, video technology only transmits more important knowledge, it can transmit the nursing professional knowledge in a comparatively complete manner. For a more practical discipline such as nursing, video technology will be more helpful. However, related videos in nursing teaching have many complex features. The memory occupied by video is larger than that of the image method, and the short video of the nursing profession is also a kind of continuous information expression, which shows that the short video method of nursing teaching will have a lot of characteristics. Simple neural network methods cannot effectively extract the spatial and temporal features of short nursing teaching videos, which requires deepening the number of network layers. Therefore, this study considers the application of transformer technology to achieve the task of extracting short nursing teaching videos and text features.

Artificial intelligence technology has been successfully applied in various fields for many years. It also exhibits some excellent algorithms [13, 14]. Among these algorithms, the most successful and mature algorithms are mainly Convolutional Neural Network (CNN) and Recurrent Neural Network (RNN) theory. RNN is mainly used in the field of speech recognition, which can extract time-related features and research objects. CNN is mainly used in the field of image recognition-related research objects, it can complete the mapping of input and output features and the task of spatial feature extraction of research objects [15, 16]. Although the CNN method can use the weight-sharing mechanism to reduce the amount of operation parameters, the RNN method still has a large amount of parameter operation. This will lead to a relatively long training and learning process and time of RNN, which will limit the depth of the number of layers of RNN, which also limits the scope of use of RNN and the accuracy of feature extraction. In order to increase the scope of use of RNN and increase the depth of RNN, researchers have successfully added the self-attention mechanism to the RNN network layer, which is the so-called transformer technology. Transformer technology is actually an encoder-decoder structure. The encoder and decoder also include feedforward neural network structures such as CNN and RNN [17, 18]. Transformer technology can further deepen the number of RNN network layers, which can also reduce the amount of parameters in the RNN learning and training process. For the short video and text feature extraction tasks of nursing teaching, the transformer technology can fully extract the relevant features of nursing teaching tasks on the basis of reducing the amount of parameters. Transformer techniques is a deep learning method that combines CNN and RNN methods, and it also includes an attention mechanism. This will further improve its accuracy and generalization ability in extracting features from short nursing teaching videos.

The main task of this research is to use transformer technology to achieve feature extraction and related prediction in short nursing videos and text knowledge. This study designs a transformer structure according to the needs of nursing specialty feature extraction and analyzes the ability of this method in the extraction of nursing knowledge features, nursing action features, and student satisfaction features. This study presents research on transformers and nursing short videos and texts from five different aspects. Section 1 mainly describes the importance of the nursing profession and the development background of transformer technology. Section 2 investigates the related research status of nursing and the research status of nursing teaching. The application of transformer technology in feature extraction of nursing short videos and the related structures and expressions of transformer technology is illustrated in Section 3. Section 4 presents the accuracy of the transformer technique in nursing short videos and text feature extraction through some statistical parameters. Section 5 is the last section to summarize and illustrate the value and significance of transformer technology for nursing teaching and research.

2. Related Work

Nursing is an important job in medicine, and it is a guarantee for patients to restore their health. Different patients have different requirements for nursing, which requires nursing students to master the common sense of nursing and nursing methods. Different conditions are treated differently. It is precisely because of the importance of nursing for the rehabilitation of medical patients that a large number of researchers have conducted research on the methods and methods of nursing. Hynes et al. [19] believed that there are still many needs to improve work efficiency and methods in the nursing work of intensive care, which is related to the speed and effect of recovery of patients with the disease. This study used a questionnaire to collect a large number of nursing-related data in the Australian intensive care unit setting. The findings suggest that the attitudes of nursing professionals and the psychological role of nurses can have a powerful effect on the rehabilitation and treatment of critically ill patients. This study suggests that nursing work should give more psychological care and a positive and optimistic nursing attitude to critically ill patients. The study also sheds light on how family care works. Al-Hakim et al. [20] studied investigated the relationship between nursing workload and job satisfaction, mainly from the perspective of psychological attitude and perception. It also uses the form of a questionnaire to study intensive care work in a large number of hospitals. It tested the relationship between nursing work and satisfaction using SPSS method and univariate measurement model. The research results show that there is a direct relationship between the psychological attitude of nursing work and nursing job satisfaction, and the perception of the author plays a certain moderating role. Using a quantitative approach to explore the relationship, the study allows nursing workers to see the key role between workload and satisfaction, which can also help increase their

psychological motivation at work. Oikarainen et al. [21] present guidance on clinical safety and cultural aspects of nursing work for nursing students from diverse backgrounds. It believes that evaluating educational interventions will diversify the culture and language of nursing teaching, which will help nursing students deepen their knowledge and understanding of nursing work. It designed two different controlled experiments using data from two hospitals in Finland, and it examined the difference between the two using a repeated-measures mixed model. The results of the study show that improving teachers' guidance ability can help improve students' cognition of clinical nursing profession, and it can also increase their enthusiasm for nursing profession. It also has important implications for increasing the linguistic diversity that leads to teaching and for understanding the wishes of nursing students. Plaza et al. [22] believed that the growth of the Spanish immigrant population has changed the traditional medical care model, which has brought certain difficulties for nursing students. It also considers the literacy of nursing students to be important. It uses high-fidelity simulation to study ways and means to improve nursing student literacy. This study also employs a qualitative approach to explain phenomena. The results of the study show that the high-fidelity simulation method can improve the learning experience of nursing students, which can also improve nursing students' care and understanding of patients with different cultural backgrounds, which is beneficial to the development of nursing work. This research also helps to improve nursing satisfaction and communication skills in nursing jobs. Martin-Delgado et al. [23] explore the student approach of clinical nursing students during COVID-19, and it mainly uses online clinical training to teach nursing students. It is mainly to improve the health education ability of nursing students. This study explores the changing roles of nursing students and the content of their training during the pandemic. It qualitatively investigates issues related to nursing students using survey methods. The results of the study found that clinical reductions did not bring much emotion to nursing work. Cognitive teaching is also an essential knowledge for nursing students for clinical practice. This study better guides nursing students' learning styles and psychological changes during a period of COVID-19. The traditional nursing teaching work has certain defects. This study will use the T-CNN-L method to extract the temporal and spatial correlations in short nursing teaching videos. This is a more efficient and accurate way. It will save a lot of time resources.

3. Application and Research of Transformer in Nursing Short Video and Text Teaching

3.1. The Importance of Transformers in Nursing Teaching Application. This study mainly explores the role of short videos and text content on nursing teaching tasks. It is difficult to qualitatively and quantitatively analyze the ability and effect of nursing students to absorb short videos and text content, which makes it difficult to ensure that short videos and texts are important for nursing. At the same time, short videos and texts are a new way of teaching that is different from traditional books, which requires nursing teachers to fully explore the relevant nursing professional knowledge contained in nursing short videos and nursing texts. However, nursing short videos and texts will contain rich text knowledge, graphic knowledge, and video action knowledge, which requires nursing students and teachers to grasp the key content. Transformer can realize the extraction of short nursing videos and nursing text features and the mapping of complex relationships, which can help nursing students and teachers quickly absorb the nursing actions and key content of nursing knowledge contained in short videos and texts. This allows nursing students to learn and apply nursing-related knowledge and related nursing actions in a targeted manner. This can not only improve students' awareness of nursing content, but also enhance students' interest in learning nursing knowledge.

3.2. The Scheme Design of Transformer in Nursing Short Video Teaching and the Principle of Transformer. Different diseases have great differences in nursing expertise and nursing actions. This requires nursing students to learn more nursing knowledge and nursing actions. However, the task of nursing care in real life is more complex because everyone's condition and physical state are different. Cumbersome nursing knowledge can easily make students lose interest in learning. This research mainly uses transformer technology to learn the characteristics of nursing knowledge, nursing action, and student satisfaction contained in nursing short videos and nursing texts. Transformer is also a kind of artificial intelligence technology. It also requires a large amount of data for training and testing, which can improve the accuracy of extracting nursing short videos and nursing text features. In this study, an intelligent feature recognition scheme of nursing short videos and text features was designed to achieve this purpose. Figure 1 shows the application scheme of nursing short video and text features based on transformer technology. First, it needs to divide the collected dataset into three features: nursing knowledge, nursing action, and nursing student satisfaction, which will be used as the input layer of the transformer technology. Transformer technology is actually a structure that includes a variety of convolutional neural networks and long and short-term memory neural networks. After the nursing-related features are extracted, it can recommend nursing-related learning knowledge and actions to students and teachers using a computer system. In Figure 1, the transformer technique can not only extract the spatial features of nursing short videos, but it can also extract the temporal features of nursing short videos. This is mainly because short video technology is also a feature similar to the field of speech recognition, which contains relatively rich temporal features. When the weight and bias of this intelligent algorithm are determined, it can be applied in practical nursing teaching tasks. It only needs to provide short videos and textual knowledge related to nursing. In practical nursing teaching tasks, the optimal weights and biases in transformer techniques have been determined. When the test set is applied it does not go through the

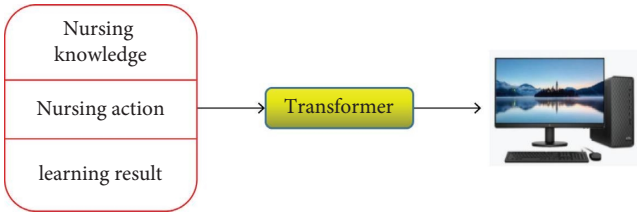

Figure 1: Transformer technology in nursing short video and text feature extraction process.

training and iterative process, it will directly perform the matrix calculation using the weights and biases.

3.3. Principles of Transformer Technology and Related Structures. Transformer technology is also a kind of big data technology. It also uses the distribution of weights and biases to realize the prediction and feature extraction of related features. It can be applied to the feature extraction tasks of short videos and texts in the nursing profession. Transformer technology is a solution proposed to solve the training time comparison field problem of recurrent neural network (RNN), which is equivalent to adding an attention mechanism to the traditional neural network. Figure 2 shows the basic structure of the transformer technology, which mainly consists of multiple layers of decoders and encoders. The input layer will be connected to the encoder, and the output layer will be connected to the decoder.

Decoder and encoder are also common network structures. Each layer of decoder or encoder will contain CNN method and LSTM method, and one layer of encoder may contain multiple layers of CNN and LSTM layers. Transformer techniques add attention mechanisms to this encoder and decoder structure. Figure 3 shows the detailed structure of the encoder and decoder. It can be seen from Figure 3 that the encoder mainly includes the attention mechanism layer and the feedforward neural network layer. The feedforward neural network layer can use the CNN method and the LSTM method to extract the spatial and temporal features of the research object. The decoder mainly includes three parts: attention mechanism layer, feedforward neural network layer, and encoding-decoding attention layer. Transformer techniques include CNN and LSTM structures, these two common deep learning methods are just an important part of transformer techniques. It will use CNN to form an encoder and decoder. It is the similarities and differences between CNN and transformer techniques.

3.4. Transformer and Encoder-Decoder Expression Introduction and Working Process. In this study, in order to achieve the extraction of short nursing videos and text features, CNN and LSTM methods are used in the feedforward neural network layers in the encoder and decoder of the transformer. The detailed self-attention representation and the representation of the feedforward neural network layers are presented below.

For the structure of the transformer, whether it is an encoder or a decoder, it is a superposition of an attention mechanism and a feedforward network layer. Expressions 1 and 2 show a computational relationship between the attention mechanism layer and the feedforward network layer.

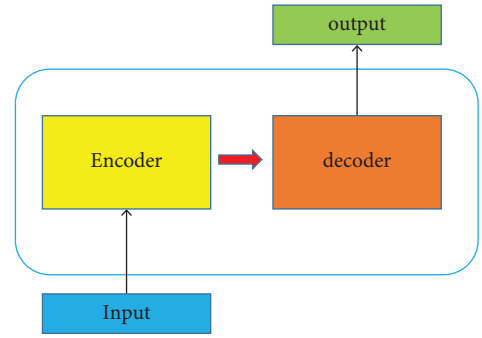

Figure 2: Schematic diagram of the basic structure of transformer technology.

$$Z^l = \text{Layer} - \text{Norm}\left(\text{Anomaly} - \text{Attention}\left(\chi^{l-1} + \chi^{l+1}\right)\right), \tag{1}$$

$$\chi^l = \text{Layer} - \text{Norm}\left(\text{Feed} - \text{Forward}\left(Z^{l-1} + Z^{l+1}\right)\right). \tag{2}$$

It is similar to RNN and CNN neural networks, there is also an excitation function for attention. Expression 3 shows the calculation method of the excitation function of the transformer technique. Expression 4 shows one way of computing the output layer of the transformer technique. It will do matrix operations.

$$S^l = \text{Softmax}\left(\frac{Q\kappa^T}{\sqrt{d_{\text{model}}}}\right), \tag{3}$$

$$\dot{Z}^l = S^l \nu. \tag{4}$$

In the transformer technology, there is a distribution between different layers of the self-attention mechanism layer. This study uses the Gaussian distribution to process the distribution of the attention mechanism layer. Expression 5 shows the Gaussian distribution function of the attention mechanism layer.

$$G\left(|j-i|;\sigma_i\right) = \frac{1}{\sqrt{2\pi\sigma_i}}\exp\left(-\frac{|j-i|^2}{2\sigma_i}\right). \tag{5}$$

For the transformer technology, the feedforward neural network layer can be a CNN or RNN method, which involves derivative calculations. The derivation calculation will process the existing features of nursing teaching short videos with the distribution of weights and biases. Expressions 6 and 7 show the derivation process of the weights and biases of the feedforward neural network layer in the transformer technique.

$$\Delta\omega_{ji} = -\eta\frac{\partial E}{\partial\omega_{ji}}, \tag{6}$$

$$\Delta u_{ij} = -\eta\frac{\partial E\partial}{\partial u_{ij}}. \tag{7}$$

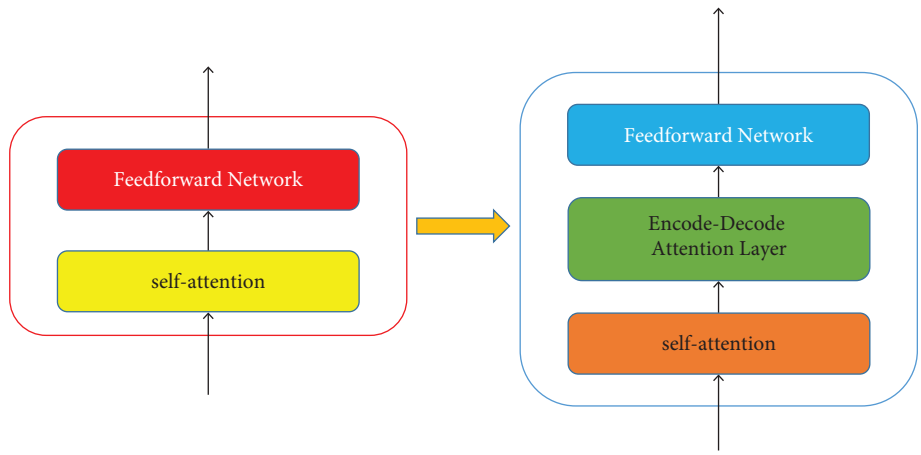

Figure 3: Detailed structure introduction of the encoder and decoder.

Expression 8 shows the loss function of the feedforward neural network in the transformer technique. It will be responsible for calculating the error between the predicted value and the actual value of the relevant features of nursing teaching short videos, and the iterative process of the feedforward neural network will iterate according to the direction of minimizing the loss function. The loss function will calculate the error distribution between the predicted value and the actual value of a feature, and it is also a continuous process with iterations. The three kinds of feature data will be separately calculated for the loss function. The three characteristics do not mix.

$$E = \frac{1}{2}\left(d_{\text{out}} - O_{\text{real}}\right)^2 = \frac{1}{2}\sum_{\kappa=1}^{t}\left(d_{\kappa} - O_{\kappa}\right)^2. \tag{8}$$

Expressions (9) and (10) show the loss function calculation method for the self-attention layer of the transformer technique. This is somewhat different from common loss functions.

$$L_{\text{Total}}\left(\chi, p, S_{\text{detach}}, -\lambda, \overline{\chi}\right), \tag{9}$$

$$L_{\text{Total}}\left(\chi, p, S, \lambda, \overline{\chi}\right). \tag{10}$$

For the feedforward neural network of the transformer, it requires convolution operations. Expression 11 shows how the convolution of the feedforward neural network layer is calculated.

$$V = \text{conv2}\left(W, X, \text{"valis"}\right) + b. \tag{11}$$

4. Result Analysis and Discussion

This research mainly uses transformer technology to study the related characteristics of short videos and texts in the nursing teaching process. In the design process of transformer technology, the feedforward neural network structure used in this study is CNN and LSTM methods. These two algorithms belong to the category of big data technology, which requires a large amount of data of short nursing teaching videos and text features to support transformer technology for training and testing. In order to better analyze the important knowledge and characteristics of nursing teaching, this study divides the characteristics of nursing short videos and texts into three characteristics: nursing knowledge characteristics, nursing action characteristics, and nursing student satisfaction for related research. It considers data related to multiple medical specialties in Beijing as the dataset for this study. These datasets will be divided into a training set and a test set of nursing teaching features in a ratio of 7 : 3. In order to improve the parameters and network layers and other characteristics in the training process of nursing features, this study uses a part of the dataset in the training set as the validation set. The presence of a validation set can reduce the time in the nursing feature extraction process.

In the process of extracting nursing short videos and text-related features using transformers, this study will consider the influence of with and without LSTM neural network layers. This is also a sufficient reason to illustrate the temporal characteristics contained in nursing short videos and nursing textual knowledge. In this study, the transformer technique with a single CNN feedforward neural network layer is marked as T-CNN, and the transformer technique with CNN and LSTM feedforward neural network is marked as T-CNN-L. First, the prediction errors of the T-CNN method in predicting the three characteristics of short nursing teaching videos and texts are shown in Figure 4. From Figure 4, it can be seen that the prediction errors of the three characteristics of short nursing videos and texts are all about 3%. For the nursing knowledge characteristics of short nursing videos, this part of the prediction error has reached 3.12%. For the nursing action characteristics of nursing short videos and texts, this part of the prediction error has also reached 3.24%. Although the prediction errors of the three characteristics of nursing teaching short videos and texts are all within 5%, this only shows that the T-CNN method can predict the short video characteristics of nursing teaching, but the accuracy is relatively low.

This study uses the T-CNN-L method to study the temporal characteristics of short nursing teaching videos and texts. It also compares the difference in accuracy

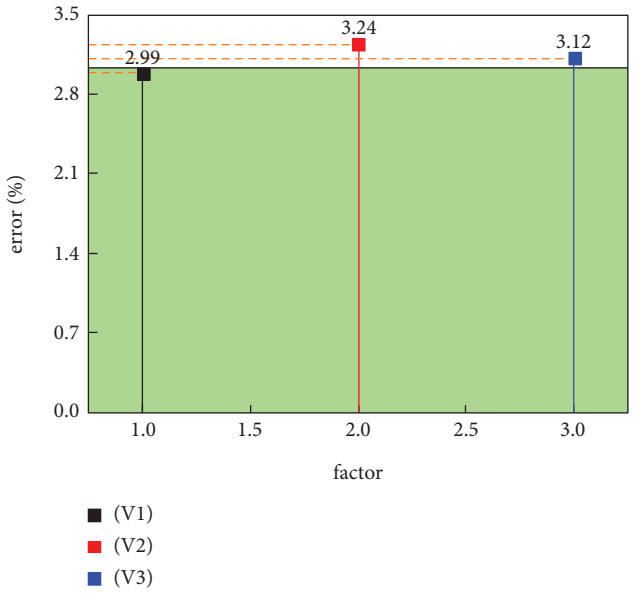

Figure 4: Prediction errors of short videos and text-related features in nursing teaching using the T-CNN method.

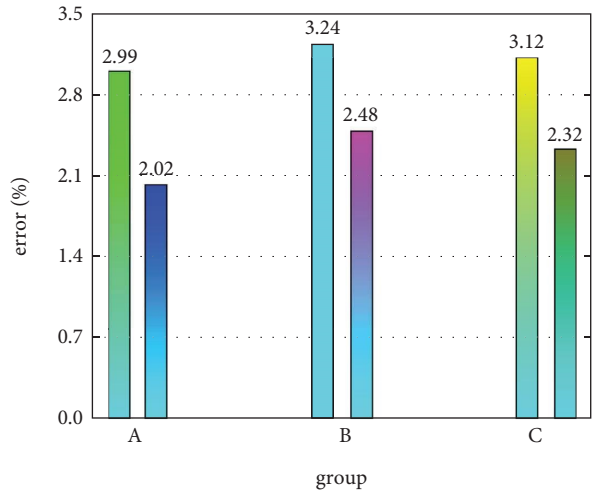

Figure 5: Prediction errors of nursing teaching short videos and text features using T-CNN-L method.

between T-CNN and T-CNN-L methods in predicting short nursing videos as well as text features. Figure 5 shows the prediction errors of short nursing teaching videos and text-related features using the T-CNN-L method. It can be seen from Figure 5 that the prediction errors of the three characteristics of the short nursing teaching videos have been greatly reduced. This fully demonstrates that the T-CNN-L method has obvious advantages over the T-CNN method in predicting the relevant features of nursing short videos. This is mainly because the T-CNN-L method can fully consider the temporal features contained in short videos and text information. It is difficult for the T-CNN method to capture temporal correlations in short videos of nursing teaching. For the nursing action characteristics of short nursing teaching videos, the prediction error of this part is reduced from 3.24% to 2.48%. The prediction error of the nursing knowledge feature was reduced from 3.12% to 2.32%. The prediction error of learning effect characteristics in short nursing teaching videos was reduced by 0.97%, and the reduction rate of nursing action characteristics was 0.76%. Nursing knowledge characteristics decreased by 0.8%. The prediction errors of these three features were reduced by a relatively large margin. This fully demonstrates the effectiveness of the T-CNN-L method in predicting the relevant features of short nursing teaching videos.

Figures 4 and 5 compare the accuracy and difference of two types of transformer techniques in predicting and extracting nursing short videos and text features in the form of mean error. Through the above study, we determined that the T-CNN-L method was used to study the features present in nursing teaching. In order to fully study the differences in the prediction of the three teaching characteristics by the T-CNN-L method, this study used different statistical parameters to analyze the three characteristics of nursing teaching. First, Figure 6 shows the data distribution of nursing action features of short videos and texts of nursing teaching. In Figure 6, the red part represents the predicted value of the nursing action feature, and the green part represents the actual value of the nursing action feature. Overall, the trends and data values in the red areas are consistent with the green areas. It can be seen from Figure 6 that there is a certain degree of fluctuation in the data value of the nursing action, whether it is the predicted value of the nursing action or the characteristic value of the actual nursing action. In general, the T-CNN-L method can more accurately grasp the characteristic data values of nursing actions and the changes in nursing action characteristics in short nursing teaching videos. The distribution of the eigenvalues of nursing actions can prove that the T–CNN–L method has enough confidence to help nursing students to find the knowledge of nursing actions corresponding to different diseases.

Nursing teaching short videos will have more relevant nursing knowledge, and nursing students can extract relevant knowledge and characteristics from it. This study uses the T-CNN-L method to extract nursing knowledge from short nursing videos and texts. Figure 7 shows the data distribution of nursing knowledge in nursing short videos. There is a large fluctuation in the prediction errors of nursing knowledge features, which indicates that the number of different nursing knowledge features is different in the dataset. It can also show that the data in the test set is reasonably distributed. From Figure 7, it can be seen that most of the predicted values of nursing knowledge are distributed within 2%, and some predicted eigenvalues of nursing knowledge are distributed below 1%. Only a small subset of nursing knowledge characteristics had prediction errors distributed above 4%. Most of the errors are distributed within a reasonable range for nursing teaching tasks. Part of the reason for the larger error may be that the characteristics of this part of nursing knowledge are special and the characteristics of this part of nursing knowledge are relatively sparse in the training set. Through the error distribution of nursing knowledge, it

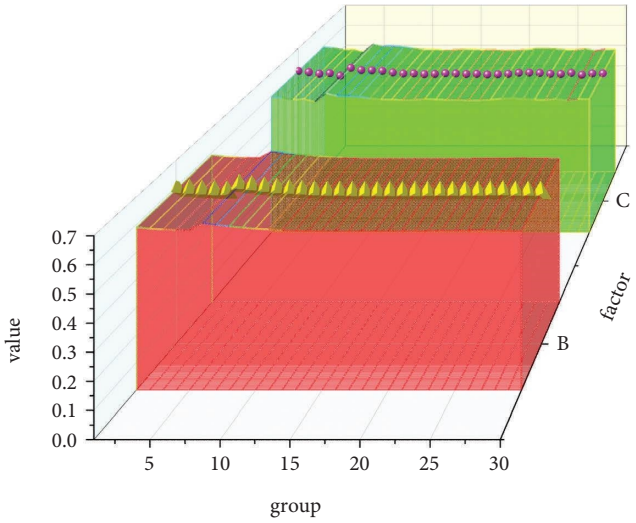

Figure 6: Predicted distribution of nursing actions in short nursing teaching videos and texts.

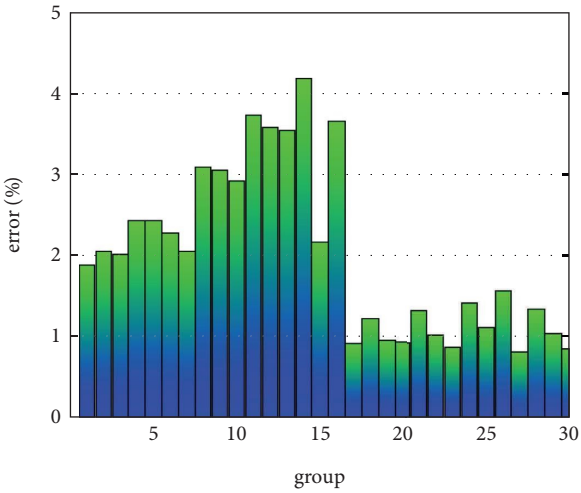

Figure 7: Prediction error distribution of nursing knowledge existing in nursing teaching short videos and texts.

can be seen that T-CNN-L can effectively help nursing students and teachers to extract useful nursing-related knowledge. Students in nursing teaching can not only observe detailed nursing actions through short videos, but also efficiently acquire nursing professional knowledge through the T-CNN-L method. The reason for the large differences in nursing knowledge characteristics of different groups may be that the disease characteristics in the dataset are relatively small, which limits the learning and training of transformer technology.

In the short nursing video and text teaching scheme designed in this study, there is a teaching feedback mechanism. It provides feedback on student satisfaction to teachers and students based on student performance as well as clinical performance. This method not only allows students to fully understand their learning level of nursing knowledge, but also shows the students' adaptability to

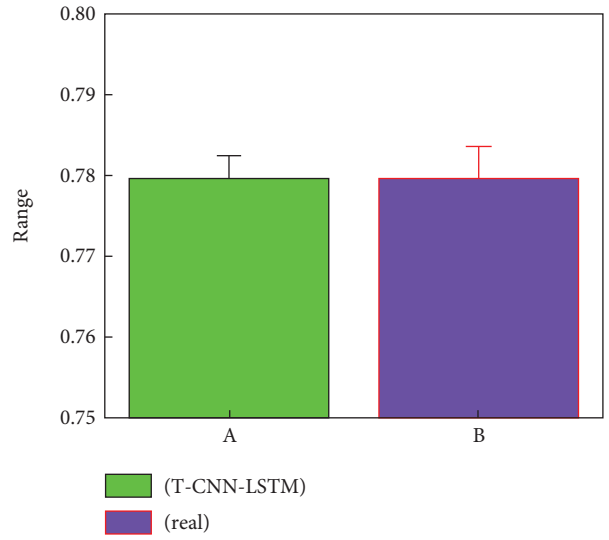

Figure 8: Data distribution of student satisfaction characteristics in nursing teaching short videos.

this transformer technology. Figure 8 shows the data distribution of student satisfaction features of short nursing videos and texts. Figure 8 introduces the effect of T-CNN-L on predicting student satisfaction features in the form of a predicted box plot. If the distribution and form of the box plots are consistent, this can illustrate the reliability of the T-CNN-L method in predicting the characteristics of student satisfaction. From Figure 8, it can be seen that the predicted value of the short nursing video and the text's student satisfaction characteristics are in good agreement with the actual value. This also fully proves that the T-CNN-L method can extract the characteristics of students' satisfaction from nursing teaching programs. This is a beneficial feedback mechanism for both teachers and students. At the same time, the average value of student satisfaction in the short nursing teaching videos is in good agreement with the predicted average value.

5. Conclusions

With the continuous improvement of medical levels and people's requirements for living standards, nursing work has become an important part of medical work. Nursing work is not only related to the speed of the patient's recovery, but it is also related to the level of recovery of the patient with the disease. Positive optimism and more professional nursing workers will have a positive effect on the recovery of patients with the disease. Nursing teaching work has also been carried out in many colleges and universities. However, there is still a big difference between nursing teaching work and traditional disciplines. Nursing teaching work not only needs to learn nursing professional knowledge, but also needs more input into nursing practice. Nursing teaching short videos contain relatively rich features. Students can only perceive relevant nursing knowledge and nursing

actions through sight and hearing, but it is difficult for students and teachers to grasp relevant important features, which is difficult to practice manually.

This study integrates short video and text technology into nursing teaching work. At the same time, in order to carry out the teaching of nursing more efficiently, this study considers embedding artificial intelligence technology into the teaching of nursing. Considering the huge amount of data in short videos and texts of nursing teaching, this requires deeper network layers. Therefore, this study utilizes the transformer technique to solve this problem, which needs to take into account the self-attention mechanism. Through the above research, it can be found that the T-CNN-L method has higher accuracy than the T-CNN method in predicting and extracting short nursing teaching videos and text features. Although the T-CNN method can also predict the characteristics of nursing knowledge and nursing actions in short nursing teaching videos and texts, the maximum prediction error has reached 3.24%. For the teaching work of nursing, this is an unfavorable error value. This is because the T-CNN method does not fully extract the temporal features in short nursing teaching videos. After using the T-CNN-L method, the prediction error of nursing knowledge was reduced to 2.32%. The prediction error for nursing actions was reduced to 2.48%. The error of the learning effect feature is also reduced to 2.02%. The T-CNN-L method can effectively integrate short nursing videos and texts to assist nursing students in their learning. The T-CNN-L method can help people to identify and predict the characteristics of nursing knowledge and nursing actions in short nursing teaching videos. This is a more effective and rapid method, and it has high value.

Data Availability

The data used to support the findings of this study are available from the author upon request.

Conflicts of Interest

The author declares no conflicts of interest.

References

[1] J. C. Tee, S. J. McLaren, and B. Jones, "Sports injury prevention is complex: we need to invest in better processes, not singular solutions," *Sports Medicine*, vol. 50, no. 4, pp. 689–702, 2020.

[2] A. Donaldson, A. Callaghan, M. Bizzini, A. Jowett, P. Keyzer, and M. Nicholson, "A concept mapping approach to identifying the barriers to implementing an evidence-based sports injury prevention programme," *Injury Prevention*, vol. 25, no. 4, pp. 244–251, 2019.

[3] C. Bolling, B. S. Delfino, M. W. Van, and H. R. Pasman, "Letting the cat out of the bag: athletes, coaches and physiotherapists share their perspectives on injury prevention in elite sports," *British Journal of Sports Medicine*, vol. 54, no. 14, pp. 871–877, 2020.

[4] B. Ferrell, P. Mazanec, P. Malloy, and R. Virani, "An innovative end-of-life nursing education consortium curriculum that prepares nursing students to provide primary palliative care," *Nurse Educator*, vol. 43, no. 5, pp. 242–246, 2018.

[5] E. Gatewood, C. Broholm, J. Herman, and C. Yingling, "Making the invisible visible: implementing an implicit bias activity in nursing education," *Journal of Professional Nursing*, vol. 35, no. 6, pp. 447–451, 2019.

[6] P. Marsh, R. Polster, G. Ricco, and S. A. Kemery, "Factors influencing faculty decisions to teach LGBTQ content in undergraduate nursing programs," *Nursing Education Perspectives*, vol. 43, no. 4, pp. 228–232, 2022.

[7] A. D. Mahoney, K. K. Westphaln, A. F. Covelli, and F. Mullan, "Advancing social mission in nursing education: recommendations from an expert advisory board," *Journal of Nursing Education*, vol. 59, no. 8, pp. 433–438, 2020.

[8] Q. Phan, N. Johnson, J. Hillman, D. Geller, L. P. Kimble, and B. A. Swan, "Assessing baccalaureate nursing students' knowledge and attitudes of social determinants of health after a health equity simulation," *International Journal of Nursing Education Scholarship*, vol. 17, no. 1, Article ID 2020024, 2020.

[9] M. L. Lim and S. Y. Ang, "A time–motion observation study to measure and analyse clinical nursing workload in an acute care hospital in Singapore," *Proceedings of Singapore Healthcare*, vol. 28, no. 2, pp. 124–128, 2019.

[10] W. E. Rosa, C. Dahlin, V. Battista et al., "Primary palliative care clinical implications: oncology nursing during the COVID-19 pandemic," *Clinical Journal of Oncology Nursing*, vol. 25, no. 2, pp. 119–125, 2021.

[11] R. A. Smiley, C. Ruttinger, C. M. Oliveira et al., "The 2020 national nursing workforce survey," *Journal of Nursing Regulation*, vol. 12, no. 1, pp. 91–96, 2021.

[12] M. E. Hoogendoorn, S. Brinkman, R. J. Bosman, J. Haringman, N. F. de Keizer, and J. J. Spijkstra, "The impact of COVID-19 on nursing workload and planning of nursing staff on the Intensive Care: a prospective descriptive multicenter study," *International Journal of Nursing Studies*, vol. 121, Article ID 104005, 2021.

[13] A. Mohamed, M. K. Najafabadi, Y. B. Wah, E. A. K. Zaman, and R. Maskat, "The state of the art and taxonomy of big data analytics: view from new big data framework," *Artificial Intelligence Review*, vol. 53, no. 2, pp. 989–1037, 2020.

[14] B. Fang, Y. Li, H. Zhang, and J. Chan, "Hyperspectral images classification based on dense convolutional networks with spectral-wise attention mechanism," *Remote Sensing*, vol. 11, no. 2, p. 159, 2019.

[15] J. M. Haut, M. E. Paoletti, J. Plaza, A. Plaza, and J. Li, "Visual attention-driven hyperspectral image classification," *IEEE Transactions on Geoscience and Remote Sensing*, vol. 57, no. 10, pp. 8065–8080, 2019.

[16] S. Li, W. Song, L. Fang, Y. Chen, P. Ghamisi, and J. A. Benediktsson, "Deep learning for hyperspectral image classification: an overview," *IEEE Transactions on Geoscience and Remote Sensing*, vol. 57, no. 9, pp. 6690–6709, 2019.

[17] C. Yu, R. Han, M. song, C. Liu, and C. I. Chang, "A simplified 2D-3D CNN architecture for hyperspectral image classification based on spatial–spectral fusion," *Ieee Journal of Selected Topics in Applied Earth Observations and Remote Sensing*, vol. 13, pp. 2485–2501, 2020.

[18] H. Wang, Y. Zhu, B. Green, H. Adam, A. Yuille, and L. C. Chen, "Axial-deeplab: stand-alone axial-attention for panoptic segmentation," in *Proceedings of the European Conference on Computer Vision*, pp. 108–126, Glasgow, Scotland, October 2020.

[19] L. Hynes, T. Coventry, and K. Russell, "Intensive care nurses' perceptions on barriers impeding the provision of end of life

care in the intensive care setting: a quantitative analysis," *Australian Journal of Advanced Nursing*, vol. 39, no. 1, pp. 7–17, 2022.

[20] L. Al-Hakim, Y. P. Zhang, J. F. Jin, and N. Sevdalis, "The effect of psychological meaningfulness and perceived organisational support on the relationship between nursing workload and job satisfaction: a prospective, cross-sectional investigation," *International Journal of Nursing Studies*, vol. 133, no. 7, Article ID 104274, 2022.

[21] A. Oikarainen, V. Kaarlela, M. Heiskanen et al., "Educational intervention to support development of mentors' competence in mentoring culturally and linguistically diverse nursing students: a quasi-experimental study," *Nurse Education Today*, vol. 116, no. 7, Article ID 105424, 2022.

[22] D. Plaza, O. Arrogante, and S. Javier, "Use of high-fidelity clinical simulation for the development of cultural competence of nursing students," *Nurse Education Today*, vol. 116, no. 7, Article ID 105465, 2022.

[23] L. Martin-Delgado, B. Goni-Fuste, C. Monforte-Royo, M. de Juan, M. L. Martin-Ferreres, and P. Fuster, "A teaching role practicum during the COVID-19 for final year nursing students in Spain: a qualitative study," *Journal of Professional Nursing*, vol. 42, no. 6, pp. 51–57, 2022.

Hindawi
Computational Intelligence and Neuroscience
Volume 2022, Article ID 5503153, 14 pages
https://doi.org/10.1155/2022/5503153

Research Article

Analysis and Construction of the User Characteristic Model in the Adaptive Learning System for Personalized Learning

Xuekong Zhao,[1] Shirong Long,[1] and Defa Hu[2]

[1]*Education Technology and Information Management Center, Guangxi College of Education, Nanning 530023, China*
[2]*Hunan University of Technology and Business, Changsha 410205, Hunan, China*

Correspondence should be addressed to Shirong Long; longshirong@nnnu.edu.cn

Received 7 September 2022; Accepted 28 September 2022; Published 10 October 2022

Academic Editor: Zaoli Yang

Adaptive Learning System (ALS) is a supportive environment, which dynamically provides learners with services that can satisfy their demand for personalized learning in accordance with the differentiation of their individual traits. At present, study on ALS is still in the exploratory stage, and there are still many fields that deserve to be studied thoroughly. User characteristic model is the foundation and core of ALS and the key to the implementation of intelligent and personalized recommendation service. Based on this, this paper intends to analyze learners' characteristics in ALS through several dimensions, such as basic information, interest, preference, cognitive level and learning style, through which learners' user characteristic model is established. In the end, ALS, which supports the function of personalized recommendation, is implemented based on this model. It is suggested by the result of the simulation experiment that ALS, which is developed through this model, demonstrates a satisfying effect in recommendation, and it can dynamically recommend appropriate learning resources in accordance with learners' personalized demands through which learners' quality and efficiency of learning can be effectively enhanced to a certain extent.

1. Introduction

With the rapid development of Internet information and communication technology, E-learning, which is based on digitalized network, has gradually become an important learning style in the information era. Since E-learning demonstrates many advantages in timeliness, convenience, interaction, and resource-sharing, it makes learning activities more flexible, open, and liberal, and becomes quite popular among an increasing number of scholars. However, it is suggested by survey data that the current implementation of E-learning has not achieved a satisfying learning effect. This can be mainly attributed to the fact that many E-learning systems provide modularized or fixed functions and learning resources, and fail to provide accurate and superior learning resources in accordance with learners' demand for personalized learning. Consequently, there are such phenomena as poor quality and efficiency in learning, which leads to unsatisfying effect in the practical application. Hence, how to build an E-learning system to support personalized learning, and provide better and further services for users' learning has attracted extensive attention of many of researchers.

At present, many researchers have implemented a great deal of exploratory research work in certain fields, such as intelligent tutoring system, adaptive learning system, personalized virtual learning environment, and E-learning personalized recommendation technology. They have been making attempts to explore an optimal personalized solution to E-learning system through theoretical and practical research. Researchers, who hold the objective of making E-learning system more intelligent and personalized, and enabling it to dynamically recommend appropriate learning resources based on the accurate "understanding" of current learners' personalized demands, and further implementing the effect of systematic and personalized learning, have proposed their own viewpoints from different perspectives. Voiskovskii et al. [1] invented a method which can improve the algorithms in navigation systems, and they analyzed the configuration of the hardware and software in the prototype

integrated navigation system. Ghadirli and Rastgarpour [2] introduced a simple E-learning system which determines learning style and characteristics of learners by a questionnaire and then makes learners' model. Kaziev and Glukhova [3] analyzed key methods, approaches, and technologies of adapting and intellectualizing web-learning, and they introduced a special model of adaptive learning decision-making. Alghofaily and Ding [4] took into consideration the dataset features in the QoS-based service recommendation process, and then used a meta-learning algorithm to incorporate dataset features in the recommendation process and study the use of different machine learning algorithms. Rafiq et al. [5] introduced the possibility of disaggregating query/question information in E-learning system online lectures or course recommendations, and then proposed a method for improving the classification of action verbs to a more accurate level in E-learning system. Sridharan et al. [6] invented an adaptive learning management system, which can create a customized course for every student based on their level of knowledge, preferred mode of learning, and continuously updating the course based on their learning speed. However, for accurate and personalized recommendation of learning resources, Tarus et al. [7] proposed that learner's context and sequential access patterns should be incorporated into the recommender system, and then introduced a hybrid recommendation approach for recommending learning resources. In addition, an idea of case-based reasoning has been adapted suitable for web page recommendation. Bhavithra and Saradha [8]suggested that apply weighted association rule mining to recommendation system for enhancing its accuracy. Collaborative filtering is an important approach to build a recommendation system. Ambulgekar et al. [9] introduced the recommendation technology of collaborative filtering and believed that this technology can be utilized in E-learning system to acquire learners' feedback information to learning resources, through which a personalized recommendation system can be implemented, etc.

Adaptive Learning System (ALS) is a personalized E-learning system solution. It can use data analysis technology to judge the characteristic attributes or behavioral tendencies of current learners in real time, and then use relevant teaching strategies, recommendation technologies, algorithms, and other technical means to dynamically provide learners with appropriate learning paths or learning resources to meet their personalized learning needs. For example, when learners prefer to browse video resources, the system will recommend more video resources for learners; when learners' cognitive level is high, the system will recommend some resources with higher difficulty level for learners. At present, a few achievements on the research of ALS are mostly concentrated on recommendation technology, recommendation algorithm, system modeling, adaptive engine, data mining, and cluster analysis. Specifically speaking, the commonly utilized recommendation technology mainly includes content-based recommendation, collaborative filtering recommendation, association rule recommendation, and integrated recommendation [10]. In terms of ALS modeling, there are also some typical representative achievements: Babori et al. suggested that the frameworks model of ALS should be composed of three components: learner model, domain model, and adaptation model, and then invented a framework based on self-regulated learning (SRL) [11]. Vesin et al. [12] considered that an intelligent tutoring system should provide smart and interactive content, personalization options, adaptive features, and then they presented the interactive learning analytics component developed in ProTu, so as to deeply discuss the key technologies of ALS recommendation.

By comparing and analyzing the above theoretical-practical research achievements, it is clear that the achievements can provide reference for our subsequent research in relevant fields. At the same time, it is also found that although many researchers have proposed various ideas for building the ALS system framework, their research results or conclusions are still being explored and improved. For example, some researchers focus on recommendation algorithms, adaptive engines, or data mining, but their thinking on the user model of ALS system is not comprehensive and in-depth enough, which leads to the unsatisfactory recommendation effect of the ALS system [13]. Based on this, we believe that it is necessary to conduct a comprehensive and in-depth study on the user feature model of the ALS system. In this study, we will focus on more comprehensive analysis and construction of user feature model from multiple dimensions such as user basic information, interest preference, cognitive level, and learning style, so as to explore a new approach to personalized recommendation in the ALS system. In order to carry out in-depth research, we will model and analyze the attribute structure, behavior characteristics, and construction process of the user model of the ALS system based on other research results, and we will propose a more comprehensive user feature model structure. On this basis, we focus on exploring the representation mode, matching relationship, and computational reasoning process of user feature model from multiple dimensions, and propose the multiple-tuple representation method and calculation formula of user basic model, interest preference model, cognitive level model, and learning style model. Finally, a simulation experiment scheme is proposed to verify the personalized recommendation effect of the research results. It is suggested by the result of the simulation experiment that the ALS system, which is developed through this model, demonstrates a satisfying effect in recommendation. Furthermore, it can dynamically recommend appropriate learning resources in accordance with learners' personalized demands, which can effectively enhance learners' quality and efficiency of learning to a certain extent.

2. Analysis of the User Characteristic Model for Personalized ALS

In accordance with the characteristics and demands of personalized learning, ALS users generally include learners and resource managers. Specifically speaking, learners are the acquirer of learning resources in ALS and the main object of the implementation of personalized

recommendation service; managers are mainly in charge of the management and update of ALS learning resources, and this position is generally taken by system managers or class teachers. During the process of E-learning, there are significant differences among individual learners in knowledge base, disciplinary background, age, gender, learning style, and personal abilities, which will further lead to constant changes and development of the learning process and the grasp of knowledge. In consideration of these, whether the system can accurately acquire and analyze current learners' status and information is the premise of the recommendation of personalized learning materials to current learners and the implementation of intelligence and adaptability. Based on this, a user feature model for ALS learners is mainly established and analyzed in this paper.

User feature model is a specific representation of system users in the computer field. In the ALS system, the user feature model plays a fundamental role. It is not only the core component of the system to achieve intelligence and adaptability but also an important basis for the system to accurately recommend personalized resources. When the ALS system is running, it will generally analyze and judge the characteristic attributes of the current user, and then use them as the basis for user learning needs to dynamically recommend personalized learning paths or learning resources. Generally, user feature model has many characteristics of learning behavior attributes, so many researchers have explored it based on the perspective of learner model. For example, there are many viewpoints on the description of learner model: Sweta and Lal [14] believed that learners' learning style and behaviour to provide suitable learning paths are important to the accuracy of ALS recommendation, so they suggested that learning style and learning behavior should be able to be dynamically detected in ALS, and then constructed a personalized adaptive learner model (PALM). By experimental research, Fatahi [15] proposed that personality and emotion are important parts of learner feature model, and play important roles in the adaptive learning system. Lwande et al. [16] believe that learning style is very important for the definition of learner model. Through learning behavior log analysis, learners' style preference can be predicted, which can be used as the basis for learning system recommendation. By the analysis of the abovementioned viewpoints, it is believed that the learner model is a mathematical model, which is established to present learners' individual traits, such as personal information, knowledge base, and cognitive structure, with the objective of reflecting learners' learning through the E-learning system. In the practical application, since ALS attaches much importance to the development of current learners' cognitive dimension, learner model's accurate acquisition of learners' understanding of knowledge and content is of great importance. Learners' cognitive state is generally their grasp of learning resources and an important constituent part of the learner model.

Based on the consideration of the general attribute characteristics, behavior operation and learning needs of learner users in the E-learning environment, and on the basis of reference to other research results, this study analyzes the IMS LIP modeling standard of learner information package in the international integrated management system, and then proposes the basic structure of user feature model of adaptive learning system from a more comprehensive perspective. The user feature model mainly includes four dimensions: basic information, learning preference, cognitive level, and learning style, which can basically meet the general needs of personalized recommendation in the ALS system. Of course, in the future research work, we will continue to enrich and improve the model in this field to provide more scientific and comprehensive research results. In the user feature model, basic information features mainly represent some static information of students, such as student number, name, gender, age, major, learning experience, etc. Interest and preference is mainly utilized to describe learners' preference of the type of learning resources. As the key to the learner model, learning style and cognitive level are utilized to store learners' dynamic information and jointly represent learners' state. After sorting out the personalized recommendation function of the ALS system and its implementation technical scheme, we will explore to build a learner model framework with dynamic updating effect. Please see the modeling process from Figure 1.

It can be seen from Figure 1 that the construction of a learner model is a dynamic updating process, which mainly includes three links: user initial model, user dynamic model, and user evolution model. Among them, the user initial model is mainly used to represent the basic-static information of learners, such as student number, name, major, etc. User dynamic model is mainly used to represent the dynamic change characteristics of learners in the learning process, such as learning preference, cognitive level, learning style, etc. User evolution model is mainly used to represent the change of learners' learning behavior, and its analysis results can be used as an important data source for updating user dynamic model. In the ALS system, users' basic information, interest preferences, cognitive level, and learning style characteristics can be stored in the form of two-dimensional relationship tables or log files. For example, the user's basic information can be stored in the user table, and the user's learning behavior record can be stored in the log file. When the ALS system is running, the user's ID index can be used to query the current learner's basic personal information, and the data mining technology can also be used to analyze and obtain the latest learning state characteristics of the current learner from the user's behavior log file, such as learning preference, cognitive level, etc. According to the dynamic construction process of the user model, after the ALS system obtains various user feature information, the system will usually use the program algorithm to dynamically update the user model in real time, and use this as the basis for subsequent judgment and analysis of user feature status, and then recommend personalized learning materials for them.

In the E-learning environment, each user often has different behavior activities in the learning process. These behavior activities can reflect varied implicit information such as the learning style characteristics, cognitive level,

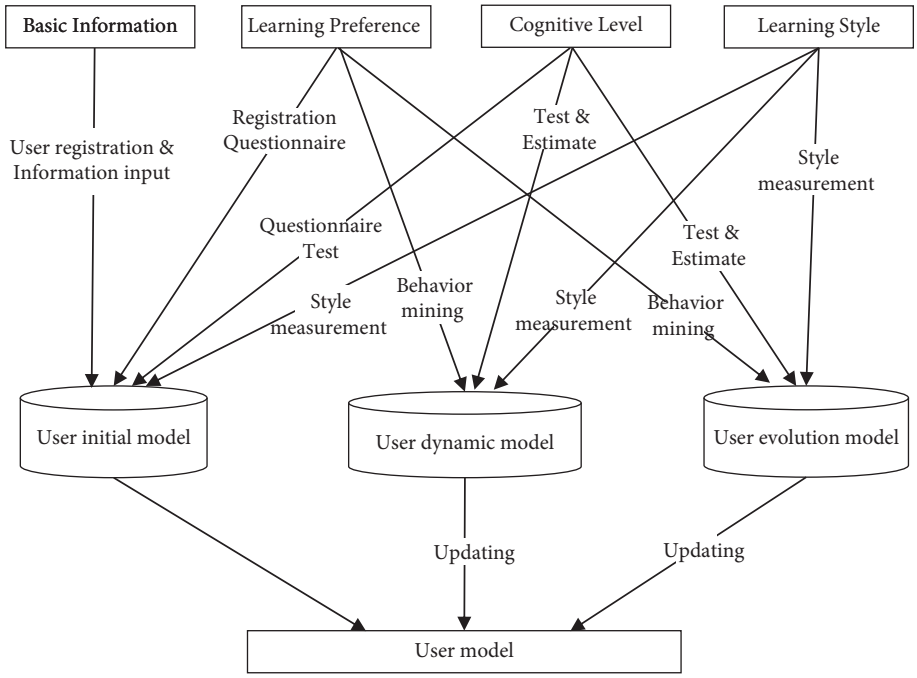

Figure 1: Construction of learners' user model.

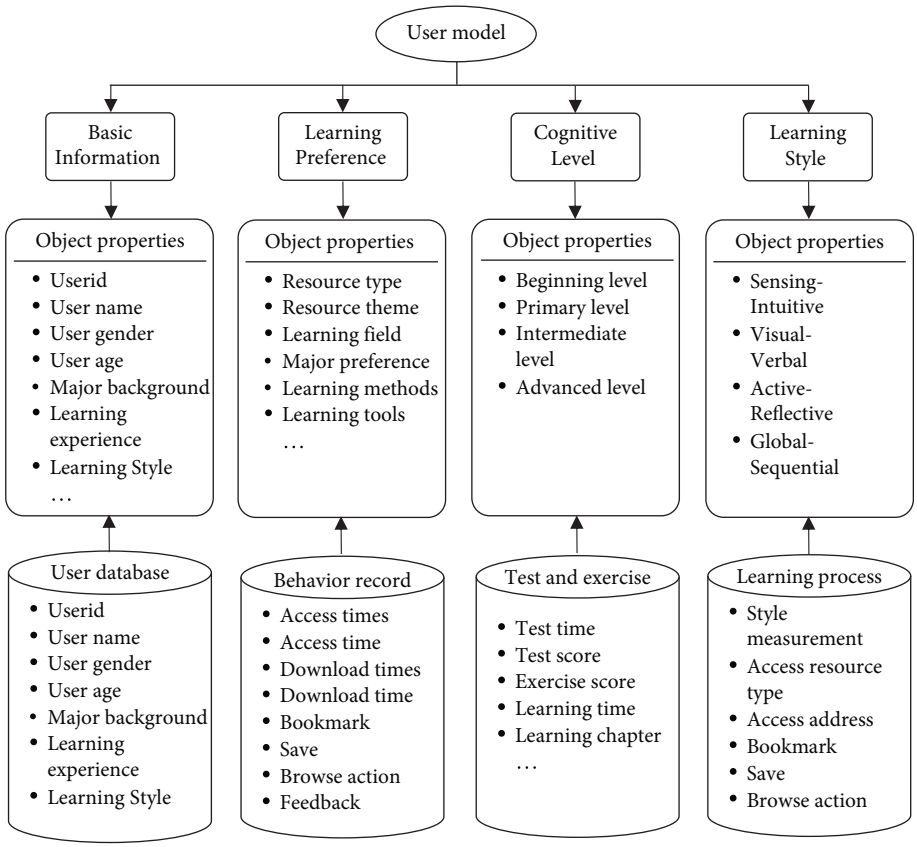

Figure 2: User behavior characteristic-based user model.

interest preference, etc. For instance, if a user browses a certain knowledge point for a long time during the learning process, it indicates that this user has a high degree of interest or demand for such knowledge point content. If a user frequently accesses, downloads, or saves a certain type of resource during the learning process, it indicates that the

user prefers this type of learning resources. Thus, it can be seen that it is very important to start with the behavior activities of users in the E-learning environment, explore the individual behavior characteristics of users hidden behind these behavior activities, and further explore their value and build user models. On this basis, an attempt is made to further describe user behavioral model from four dimensions, namely, basic information, learning preference, cognitive level, and learning style. Please see the constructed user model from Figure 2 [17, 18].

The user behavior characteristic model (Figure 2) shows that the modeling of users' basic information dimension is acquired directly through the user database. User's learning preference model includes resource type, resource theme, learning field, major preference, learning methods, learning tools, etc. It excavates data through behavior record during user's E-learning. User's cognitive level model, which includes beginning level, primary level, intermediate level, and advanced level, is acquired from testing and exercise database. Learning style model, which includes four properties as sensing-intuitive, visual-verbal, active-reflective, and global-sequential, can be comprehensively assessed and acquired through the result of user's learning style measurement, the type of access resources, and the excavation of browsing behavior. Specifically speaking, user behavior characteristic includes access times, access time, download times, download time, add bookmark, save, browse action, and feedback. User's browsing behavior mainly includes the times of clicking the mouse, scrolling the scroll bar, and pressing the up and down button. Under normal circumstances, more operation behaviors during webpage-browsing can indirectly reflect that the user is more interested in this web page, for example, if a user shows behaviors like frequently accessing a website, saving a website, adding a bookmark, and downloading resources, this user's interest in this web page can be confirmed [19, 20].

After the above analysis of the dimensions of constructing a user characteristic model, relevant matching rules, expressions, and algorithms can be utilized to analyze user's demand for learning resources, and confirm user's characteristic model in ALS. The specific methods of construction will be described in the next article.

3. Methods of Constructing User Characteristic Model for Personalized ALS

3.1. Basic User Model. Substantively speaking, personalized recommendation forwards and presents appropriate resources in accordance with the current users' personalized demands. Learner's user model is the foundation of ALS modeling. When constructing the user basic model, the user's characteristic attribute may include static information such as name and gender, and also dynamic information such as interest preference or learning experience. The user model can be constructed by the following method [21, 22]:

$$\text{UserModel} = (\text{BasicInformation}, \text{LearningPreference}, \text{CognitiveLevel}, \text{LearningStyle}). \quad (1)$$

In expression (1), "BasicInformation" represents user's basic-static information, which includes student no., name, gender, age, professional background, learning experience, user name, password for login, etc. "LearningPreference" represents user's learning preference, which is represented through user's interest in learning resources. "CognitiveLevel" represents user's current cognitive level or learning ability. "LearningStyle" represents user's learning style. Learning Preference, Cognitive Level, and Learning Style, which store user's dynamic information, are the key to ALS modeling and the implementation of personalized recommendation. Furthermore, real-time dynamic update is realized in the value with the changes of the status of E-learning. Next, an emphasis will be placed on the elaboration of the specific modeling method for Learning Preference, Cognitive Level, and Learning Style.

3.2. User Interest and Preference Model. User interest model is an integrated description of user's information and demand during the learning after logging into the system, which reflects the current user's preference or interest tendency for a certain learning content. For example, if the user's browsing time or download times for a learning resource increases, it indicates that the user prefers the learning resource. User interest information can generally be obtained by user active description and user behavior record mining. In order to ensure that the ALS system can more accurately support personalized learning, based on the thinking of the dynamic updating process of the user feature model, we believe that it is an important way to build the current user's interest preference model based on user behavior records. Here, we will conduct a comprehensive modeling and analysis of all learning behaviors related to learners' interests and preferences in the ALS system, such as the access times, access time, download times, bookmark actions, mouse events, etc., to ensure the integrity and scientific nature of the data recording user behavior characteristics. After the ALS system records the user behavior preference information in the database table or log file, the system will use the user learning preference model as the basis to obtain more accurate interest values by mining the user's implicit learning behavior, and then recommend appropriate personalized learning resources. In this section, we will focus on how to calculate the user's interest in the current learning resources based on the user's learning behavior characteristics, and build its interest preference model.

In accordance with the above analysis, the calculation of user's interest mainly takes the attention to the web page or learning resources as the main basis, which can be calculated and reflected through user's behavior characteristic. The more attention that a user pays to the learning resources, the more interest he or she holds in the learning resources. Meanwhile, it is also a reflection of the user's increasing demand for the learning resources. With the purpose of calculating user's interest, the mode of tuple is adopted to construct a calculation model of user's attention. The user interest model and the calculation method of its interest degree are given as follows [23, 24]:

$$InterestDegree(n) = \left\{ < R_1, A_1 >, < R_2, A_2 >, \cdots, < R_i, A_i >, \cdots, < R_p, A_p > \right\}. \tag{2}$$

In expression (2), R_i represents the collection of webpages or resources for learning, A_i represents user's attention to R_i, and p is the quantity of the collection of webpages or resources for learning, $i = 1, 2, 3, \cdots p$. User's attention to the resources can be acquired through the accurate feedback information and access pattern. Please see the method of presenting the degree of attention in the following expression:

$$A_i = A(U, R_i, T_i). \tag{3}$$

In expression (3), $0 \le A_i \le 1$, U represents learner user, R_i represents the learning resources being accessed, T_i represents the type of user's behavior characteristic, i represents the number of learning resources, and $i = 1, 2, 3, \cdots p$, A_i represents user (U)'s attention to the learning resources R_i. In accordance with the above analysis of user's behavior characteristic, the value range of T_i in expression (3) is $T_i \in$ {Access times, Access time, Download times, Bookmark, Save, Browse action, Feedback, ...}. Access times represent the times of accessing webpages or learning resources; Access time represents the time of accessing webpages or learning resources; Download times represents the times of downloading learning resources; Bookmark represents the behavior and action of adding learning webpages to the bookmark; Save represents the behavior and action of saving learning webpages; Browse action represents the behavior and action of browsing learning webpages, such as scrolling the mouse, clicking the mouse, moving forward and backward, etc.; Feedback represents user's feedback to the given resources.

In accordance with the above user's behavior characteristic model, data matching and switching is needed in the model of attention degree, namely, expression (3), so that user's interest in learning resources can be calculated. With regard to the model of attention degree, the rules of data matching and switching are set up as follows: if a user downloads resources, adds webpages to the bookmark, and saves webpages, it suggests that this user holds a higher degree of expectation and interest in the learning resources presented through the webpages, and under this circumstance, the user's degree of interest is set as 1; if none of these behaviors or actions happen, the user's interest in this kind of learning resources can be calculated through other behaviors. Please see the method of calculation from the following expression:

$$ID = \begin{cases} 1, & T_i \in \{\text{Downloa dB ookmarkSave}\}, \\ f_1(ats, dts), & T_i \in \{\text{Access timesDownloa dt imes}\}, \\ f_2(at, sc, cc), & T_i \in \{\text{Access timeBrowseaction}\}. \end{cases} \tag{4}$$

In expression (4), ID represents the degree of interest; T_i represents the type of user's behavior characteristic, {Downloa d, Bookmark, Save} represents the collection of a group of behaviors that the user might show during webpage-browsing, including downloading resources, adding webpages to a bookmark and saving learning webpages; ats represents the times of accessing webpages or learning resources; $dt\ s$ represents the times of downloading resources; at represents the time of accessing webpages, namely, the learning time; sc represents the times of scrolling the scroll bar when the user is browsing webpages; cc represents the times of mouse-clicking when the user is browsing webpages; $f_1(ats, dts)$ represents the mapping function from ats and dts to RD; $f_2(at, sc, cc)$ represents the mapping function from at, sc, and cc to ID [23, 24].

As for the mapping function $f_1(ats, dts)$ in expression (4), since user's times of accessing resources ats and times of downloading resources dts cannot objectively demonstrate user's interest in the resources, the average times of accessing and downloading resources need to be quoted to evaluate the current user's interest degree. Therefore, the function $f_1(ats, dts)$ can be replaced with expression (5). Please see the specific expression as follows:

$$f_1(ats, dts) = \begin{cases} 1, & \left(ats > \overline{ats_0}, dts > \overline{dts_0}\right), \\ \dfrac{\alpha ats}{\overline{ats_0}} + \dfrac{\beta\, dts}{\overline{dts_0}}, & \left(ats < \overline{ats_0}, dts < \overline{dts_0}\right). \end{cases} \tag{5}$$

In expression (5), ats represents the times of accessing webpages or learning resources; dts represents the times of downloading resources; $\overline{ats_0}$ represents the average times of accessing webpages or learning resources; $\overline{dts_0}$ represents the average times of downloading resources; α and β represents weighing parameters. The modes of calculating $\overline{ats_0}$ and $\overline{dts_0}$ are listed, respectively, as follows:

$$\overline{ats_0} = \frac{ats\_\text{num}}{\text{usernum}} \overline{dts_0} = \frac{dts\_\text{num}}{\text{usernum}}. \tag{6}$$

In expression (6), ats_num represents the total times of accessing learning webpages or resources; user_num represents the total number of users in the system; dts_num represents the total times of accessing learning webpages or resources. When $\alpha ats/ats_0 + \beta dts/\overline{dts_0} \geq 1$, the value of $f_1(ats, dts)$ is set as 1; when $0 < \alpha ats/ats_0 + \beta dt\, s/dts_0 < 1$, the value of $f_1(ats, dts)$ is $\alpha ats/ats_0 + \beta dts/\overline{dts_0}$.

As for the mapping function $f_2(at, sc, cc)$ in expression (4), the time of accessing webpages at is under the influence of various factors, such as reading speed, length of content and form of expression on the webpages. More content generally means longer accessing time; more video resources also mean longer accessing time. In addition, since the mode of reading pictures and video resources manifests substantial difference from the mode of reading texts, it is quite difficult to simply quantify the time of accessing webpages at. In consideration of this, the text resource is emphatically taken as an example in this paper, and the access time ratio is adopted to eliminate the influence brought about by the length of content of user's own factors. Please see the method of calculation from the following expression:

$$atr = \frac{at}{\overline{at_0}} = \frac{at \times trs}{cl}. \tag{7}$$

In expression (7), atr represents access time ratio; at represents user's access time; $\overline{at_0}$ represents the average access time, and the mode of calculation is $\overline{at_0} = cl/trs$. cl represents content length; trs represents user's text reading speed, and it can adopt the average standard value of reading speed.

In accordance with user's access behavior and habit, the maximum and minimum threshold value of the average access time is set as $atr_{\min}$ and $tr_{\max}$, respectively. If the abovementioned function $f_2(at, sc, cc)$ is replaced by $f_2(atr, sc, cc)$, a piecewise function can be achieved. Please see the method of expression as follows:

$$f_2(atr, sc, cc) = \begin{cases} 0, & (atr < atr_{\min}) \\ atr, & (atr_{\min} < atr < atr_{\max}), \\ f_3(sc, cc), & (atr > atr_{\max}). \end{cases} \tag{8}$$

Expression (8) suggests that when $atr < atr_{\min}$, it signifies that the user spends very little time accessing the webpages, and the interest degree can be recorded as 0; when $atr_{\min} < atr < atr_{\max}$, it signifies that the user spends a normal length of time accessing the webpages, and the interest degree can be acquired through normal calculation, namely, $f_2(atr, sc, cc) = atr$; when $atr > atr_{\max}$, it signifies that the user spends a lot of time accessing the webpages, and the state of access might be abnormal, for example, the user forgets to close the web page after clicking open. Under this circumstance, another behavioral function $f_3(sc, cc)$ can be adopted to acquire the interest degree. Function $f_3(sc, cc)$ mainly involves such behavioral characteristics as scrolling the scroll bar and clicking the mouse. Under general circumstances, the times of scrolling the scroll bar and clicking the mouse should be directly proportional to the length of the content. In other words, if there is much content on the web page, the times of scrolling the scroll bar and clicking the mouse will be more. With the purpose of calculating the user's interest degree more accurately and objectively, the function $f_3(sc, cc)$ is expressed through piecewise function. Please see the mode of expression from the following expression:

$$f_3(sc, cc) = \begin{cases} 0, & (f_3(sc, cc)' < 0), \\ f_3(sc, cc)', & (0 \leq f_3(sc, cc)' \leq 1), \\ 1, & (f_3(sc, cc)' \geq 1). \end{cases} \tag{9}$$

In expression (9), $f_3(sc, cc)'$ is the binary regression of user's behavior characteristic of scrolling the scroll bar and clicking the mouse during webpage-browsing, and its method of calculation is $f_3(sc, cc)' = \alpha \times sc/cl + \beta \times cc/cl + \gamma/cl$. sc represents the times of scrolling the scroll bar; cc represents the times of clicking the mouse; cl represents the length of content; α, β, and γ represent weighting parameters that are about to be estimated.

3.3. User Cognitive Level Model. User cognition level indicates the ability of individual users to understand and process information. In the ALS system, the user's cognitive level reflects the user's mastery of the learning content, which provides a decision-making basis for the ALS system to recommend learning materials of various difficulty levels. In order to make the ALS system determine the current cognitive level of users more accurately, it is usually possible to conduct a comprehensive evaluation from multiple dimensions such as learners' user test scores, test duration, learning duration, and learning behavior. For example, if the user's current unit test score is very good, it indicates that the user's cognitive level of the unit knowledge is high. If the user's current unit test lasts for a long time, it indicates that the user's cognitive level of the unit knowledge is not high enough. When the ALS system is running, it will dynamically obtain the user's current cognitive level information, update the user's cognitive level model in a timely manner, and then match the learning resources in the system on this basis to recommend learning materials suitable for users. An attempt is made to adopt the method of four-level classification to determine the user's cognitive level based on the test performance. The four levels are the beginning level, primary level, intermediate level, and advanced level, respectively. And, the sectional range is set as {[0–59], [60–69], [70–89], [90–100]} accordingly, and the corresponding

cognitive level is recorded as {1, 2, 3, 4}. Thus, user cognitive level model can be defined as follows [21, 25]:

$$\text{CognitiveLevel}(U) = (U, CL_i). \tag{10}$$

In expression (10), Urepresents learner user; CL_i represents user's cognitive level, and it is under the range of $CL_i \in \{1, 2, 3, 4\}$.

Likewise, the grade of difficulty also needs to be set up to implement the function of recommending learning materials of different grades of difficulty in accordance with user's cognitive level. In consideration of this, we hereby divide the grade of difficulty into four grades, namely, easy, relatively easy, average, and difficult. The grade of difficulty is recorded as {1, 2, 3, 4} accordingly. Thus, the level model of learning materials can be defined as follows:

$$\text{CognitiveLevel}(R) = (R, DL_i). \tag{11}$$

In expression (11), R represents learning material; DL_i represents the level of learning material, and it is under the range of $DL_i \in \{1, 2, 3, 4\}$. Under general circumstances, the value of DL_i is set up by the course teacher or system manager during the establishment of curriculum resources on the back-stage management web page.

After the above cognitive level and the grade of difficulty of the learning materials are confirmed, the screening of resources can be implemented through matching rules. Please see the specific method as follows:

$$\text{CognitiveLevel}(CL_U, CL_R) = \begin{cases} CL_R X > 0 \\ CL_U X \le 0 \end{cases} (X = CL_U - CL_R). \tag{12}$$

In expression (12), CL_U represents user's cognitive level, namely, the value of $\text{CognitiveLevel}(U) = (U, CL_i)$. CL_R represents the grade of difficulty, namely, the value of $\text{CognitiveLevel}(R) = (R, DL_i)$. $\text{CognitiveLevel}(CL_U, CL_R)$ represents the matching degree of user (U)'s cognitive level and the grade of difficulty of learning materials R. If the learner's current cognitive level is higher than the difficulty level of the learning materials presented by the system, the personalized learning materials will be randomly recommended based on the system. On the contrary, if the learner's current cognitive level is lower than the difficulty level of the learning materials presented by the system, the personalized learning content that meets the cognitive ability of the users will be recommended based on the learner's current cognitive level.

To a certain extent, the length of online testing also reflects user's cognitive level. Hence, the length of online testing also needs to be taken into consideration during the assessment of the cognitive level. Longer length of online testing generally signifies lower cognitive level. On the contrary, if the length of online testing is shorter, it signifies higher cognitive level. Under this circumstance, the function $F(T)$ can be adopted to manifest the relationship between user's cognitive level and the length of online testing [25, 26].

$$F(T) = \begin{cases} 1, & T \le T_r, \\ 1 - \dfrac{T}{(T_r + T_m)}, & T_r < T \le T_m, \\ 0, & T \ge T_m. \end{cases} \tag{13}$$

In expression (13), T_r represents the normal length of testing; T_m represents the maximum length of testing. Expression (13) shows that when the length of testing is shorter than the normal length, it can be deemed that the user's cognitive level is higher, and the value is set as 1; on the contrary, when the length of testing is longer than the maximum length, it can be deemed that the user's cognitive level is relatively lower, and the value is set as 0. Likewise, the relationship between user's cognitive level and the length of online testing can be achieved. Please see the method of calculation as follows:

$$H(T) = \begin{cases} 1, & T \le P_r, \\ 1 - \dfrac{T}{(P_r + P_m)}, & P_r < T \le P_m, \\ 0, & T \ge P_m, \end{cases} \tag{14}$$

In expression (14), P_r represents the normal length of learning a certain chapter or knowledge point; P_m represents the maximum length of learning.

In conclusion, the matching degree between the user and learning materials can be calculated through the user's cognitive level, the grade of difficulty of learning materials, and the length of online testing and learning. Please see the expression as follows:

$$\begin{aligned} \text{CognitiveLevel}(U, R) = {} & \alpha \text{CognitiveLevel}(CL_U, CL_R) \\ & + \beta F(T) + \gamma H(T). \end{aligned} \tag{15}$$

In expression (15), $\text{CognitiveLevel}(U, R)$ represents the matching degree between the user and learning materials, and greater value represents higher matching degree here. α, β, γ are weighing parameters that can be set up by course teacher (or system manager) through the system management web page.

3.4. User Learning Style Model. Learning style is one of the research fields of pedagogy and psychology. In recent years, it has also attracted the attention of computer science. Especially, in the aspect of adaptive personalized recommendation system, many researchers try to explore it deeply. Learning style generally refers to an inherent or biased characteristic pattern of individual learners' perception, acquisition, and processing of information in the learning process. It is an important embodiment of individual differences of learners. For example, some learners prefer to browse video learning resources, while others prefer to browse text learning resources, which reflects the different learning styles of learners. As for the types of learning styles,

Table 1: Felder-Silverman learning style model.

Dimension	Values	Description
Perception	Sensitive—intuitive	Sensitive style shows inclination towards concreteness or practice, and is good at remembering details, facts, and figures; intuitive style shows inclination towards concept or innovation, and is good at theoretical learning
Input	Visual—verbal	Visual style shows an inclination to visual expression, such as chart, picture and flow diagram, and other media information; verbal style shows an inclination towards documents and verbal expression
Processing	Active—reflective	Active style shows an inclination to practical activities, collaborative learning, activity, and exchange; reflective style shows an inclination to independent thinking and learning
Understanding	Global—sequential	Global style shows an inclination towards macroscopic blueprint and the grasp of overall concept; sequential style shows an inclination towards specific steps and gradual learning by logical sequence

Sensing	{"Text", "Audio"} : {"Concept", "Formula", "Theory"}
Intuitive	{"Image", "Video"} : {"Concept", "Formula", "Theory"}
Visual	{"Image", "Animation", "Video"} : {"Concept", "Formula", "Case", "Theory"}
Verbal	{"Text", "Audio"} : {"Concept", "Case", "Theory"}
Active	{"Animation", "Audio", "Video"} : {"Concept", "Case", "Theory", "Activity"}
Reflective	{"Text","Audio", "Video"} : {"Concept", "Case", "Theory", "Problem"}
Global	{"Text", "Image", "Video"} : {"Concept", "Case", "Theory"}
Sequential	{"Text", "Image"} : {"Concept", "Formula", "Case"}

Figure 3: Matching relation between learning style and resource type.

many researchers agree with the classification method of learning styles proposed by psychologist Felder et al., which divides learning styles into four categories based on the four dimensions of learners' perception, input, processing, and understanding of information: sensing-intuitive, visual-verbal, active-reflective, and global-sequentia (see Table 1). In the ALS system, the user learning style model is mainly used to represent the characteristics of the user learning style, which has an important reference basis for the system to recommend personalized learning paths or learning resources. In order to accurately represent the learning style model of learners in the ALS system, this study constructs learner personality attributes based on four dimensions of Felder's learning style model: perception, input, processing, and understanding, and each dimension is corresponding with two opposite style types, respectively. When the ALS system is running, it can extract the current user's learning style type from the user's learning style model, and match the user's learning style with the learning resources in the system for associated attributes, and then provide personalized learning services for the current user by recommending resources that match the user's learning style. For example, users of visual learning style will be mainly recommended for video or animation resources, while users of verbal learning style will be mainly recommended for text or audio resources. Next, we will focus on the representation method and construction process of user learning style model in the ALS system [19, 27, 28].

Based on Felder's four-dimensional learning style model, an attempt is made to adopt the form of tetrad to construct user learning style model. Please see the method of expression as follows [20]:

$$\text{LearningStyle}(U) = <D_1, ls_1>, <D_2, ls_2>, <D_3, ls_3>, <D_4, ls_4>. \tag{16}$$

In expression (16), $<D_i, ls_i> (1 \le i \le 4)$ represents learner's value in a certain dimension under Felder's learning style, D_i represents the type of style value ($D_i \in$ {"Sensing-Intuitive," "Visual-Verbal," "Active-Reflective," and "Global-Sequential"}), ls_i is fuzzy value ($ls_i \in [0, 1]$), which represents the value of the dimension learning style D_i.

With the purpose of matching the rules of the user's learning style and learning resource model, the correlation between the type of learning resources and learning style also needs to be taken into consideration in the establishment of the system model. In consideration of this, the following learning resource model is established:

$$\text{ResourceModel} = (\text{ResourceInformation}, \text{ResourceStyle}). \tag{17}$$

In expression (17), ResourceInformation represents basic information of resources, such as name, size, uploader, time and path of uploading, etc.; ResourceStyle represents the type of decision style. ResourceStyle can be represented

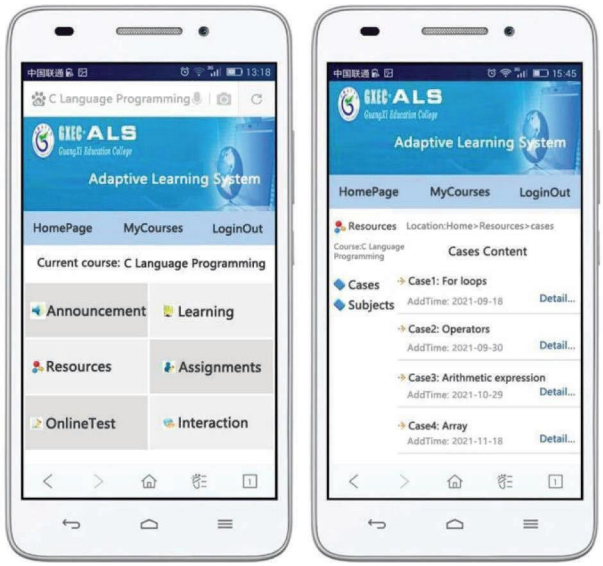

Figure 4: Effect of ALS course learning page via a mobile phone.

as $\text{ResourceStyle}(i) = \{\langle rs_i, rt_i \rangle\}$ in the form of two-tuples. Specifically speaking, rs_i represents the media type, and $rs_i \in \{"Text", "\text{Image}", "\text{Animation}", "\text{Au di o}", "\text{Vi de o}"\}$; rt_i represents the strategy type, and $rt_i \in \{"\text{Concept}", "\text{Formula}", "\text{Case}", "\text{Theory}", "\text{Problem}", "\text{Activity}"\}$. For instance, $\text{Resource Style}(p) = \{< "\text{Image}", "\text{Case}" >\}$ represents that the decision style type of resource p is picture and case-oriented. After this, a resource model is established, Felder-Silverman style dimension can be taken as a reference to build a matching relation between learning style and resource model. Please see the rule of relation in Figure 3 [20, 29].

Figure 3 suggests the relation between learning resource type and learning style. It cannot accurately calculate the matching relation between learning style and resources through the method of quantitative processing. Hence, the matching relation between learning resource model and learning style needs to be further converted into an expression that is of mathematical significance. An attempt is made to construct the learning resource style model through the form of tetrad. Please see the specific method of expression as follows [20, 25].

$$\text{ResourceStyle}(R) = < D_1, rs_1 >, < D_2, rs_2 >, < D_3, rs_3 >, < D_4, rs_4 >. \tag{18}$$

In expression (18), $< D_i, rs_i > (1 \le i \le 4)$ represents the value of knowledge object in a certain dimension under Felder's learning style, D_i represents the style type ($D_i \in$ {"Sensing-Intuitive," "Visual-Verbal," "Active-Reflective," "Global-Sequential"}), the value of rs_i is −1 or 1. The value of rs_i is generally set up by course teacher or system manager in light of the matching rules of Figure 3 during the establishment of curriculum resources.

It can be inferred from expression (16) and expression (18) that the style matching degree of the learning and learning materials is decided by the sum of the numerical value on the diagonal line of the matrix multiplication of Learning Style and Resource Style.

The process of inference: tetrad expression (16) and expression (18) that are defined above are converted into 4×1 column matrix and 1×4 row matrix, respectively, and

$$\begin{aligned} \text{LearningStyle}(U, R) &= \text{LearningStyle}(U) \times \text{ResourceStyle}(R) \\ &= \begin{pmatrix} ls_1 \\ ls_2 \\ ls_3 \\ ls_4 \end{pmatrix} \times \begin{pmatrix} rs_1 & rs_2 & rs_3 & rs_4 \end{pmatrix} \\ &= \begin{pmatrix} lrs[1,1] & lrs[1,2] & lrs[1,3] & lrs[1,4] \\ lrs[2,1] & lrs[2,2] & lrs[2,3] & lrs[2,4] \\ lrs[3,1] & lrs[3,2] & lrs[3,3] & lrs[3,4] \\ lrs[4,1] & lrs[4,2] & lrs[4,3] & lrs[4,4] \end{pmatrix}. \end{aligned} \tag{19}$$

In expression 19, $\textit{LearningSt yle}(U, R)$ is the product of two matrixes and a fourth-order matrix. A greater sum of the numerical value of the diagonal line signifies the higher matching degree between the learning and learning resources. This value can be achieved from

$$\begin{aligned} \textit{LearningSt yle}(U, R) = {} & (ls_1 - C) \times rs_1 + (ls_2 - C) \times rs_2 \\ & + (ls_3 - C) \times rs_3 + (ls_4 - C) \times rs_4. \end{aligned} \tag{20}$$

In expression (20), C is a constant, and it is the median of the data range of $ls_i (ls_i \in [0, 1])$.

4. Simulation Experiment and Discussion

4.1. Simulation Experiment Design. With the purpose of examining the validity of the research achievement, a user characteristic model is constructed based on UML modeling standard and XML + SQL Server database technology after the analysis and organization of the user characteristic model for personalized ALS. And then, NET Framework environmental development is utilized on this basis to implement the prototype of ALS. The development language mainly utilizes C#, C, VBScript, JavaScript, SQL query language, etc. In terms of the function of system implementation, the current ALS can provide different functions to students and teachers. It can not only satisfy the demands of general classroom teaching but also support students' online personalized and independent learning. When a student user logs in the system, he or she can select courses online, study courses, browse resources, submit assignment, take online tests, etc. When a teacher user logs in the system, he or she can examine and verify students who are selecting courses, manage curriculum resources, correct assignments, etc. Figure 4 suggests the effect of course learning page when a student user utilizes the mobile phone to log in the system. [29].

With the purpose of examining whether ALS can dynamically recommend personalized learning materials in

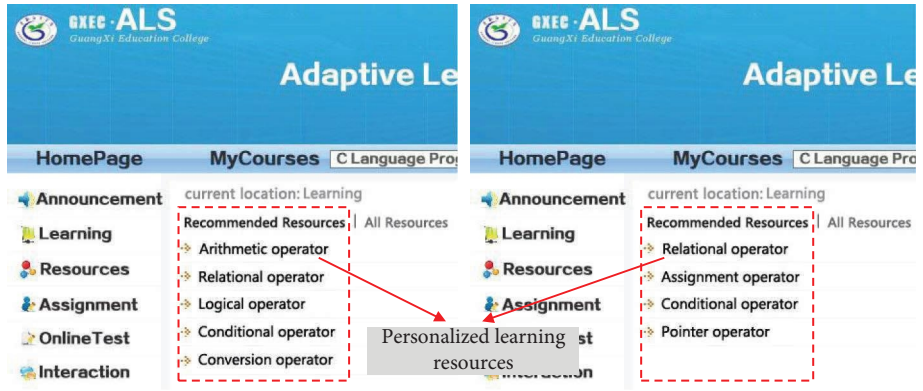

Figure 5: Personalized learning page of two students from group *T*1.

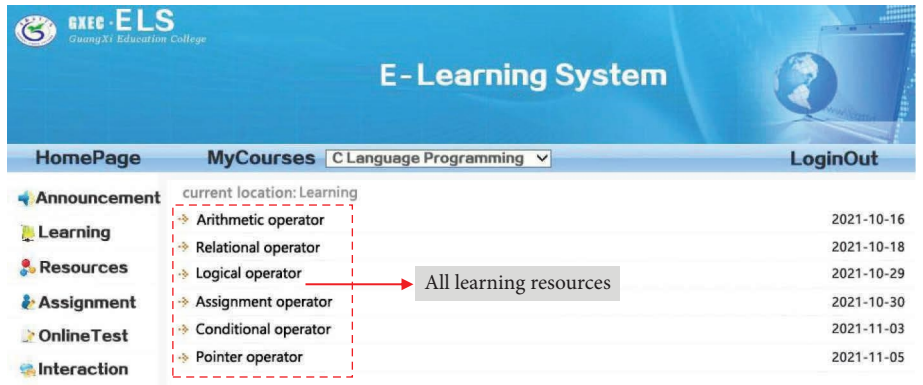

Figure 6: Personalized learning page of two students from group *T*2.

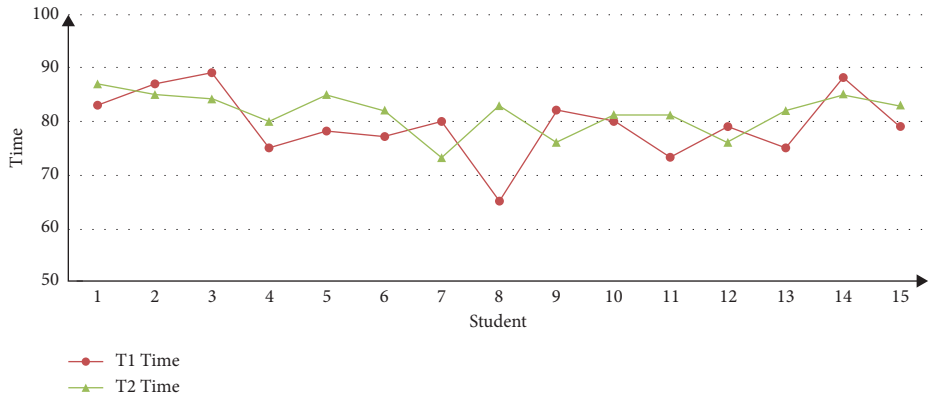

Figure 7: Distribution of learning length in groups *T*1 and group *T*2.

accordance with the user characteristic model, an attempt is made to design and implement a series of experiments. Before the experiment, 30 students were randomly selected from two classes of educational technology major in our school as experimental samples. And then, these students are randomly divided into two groups, namely, *T*1 group (experimental group) and *T*2 group (control group). Meanwhile, account number and password are distributed to all the students in Group *T*1. During the implementation of the experiments, students in Group *T*1 and Group *T*2 are arranged in the same computer network classroom. Students in Group *T*1 are required to log in the personalized ALS that is developed in this research through the previously given account and password, and students in Group *T*2 are required to access ALS system directly through the computer browser without logging into the account. The learning contents for the two groups of students are the second chapter (operator and expression) of Programming in *C*. And, the students are required to learn all the knowledge points in the appointed chapter within 90 minutes, and take

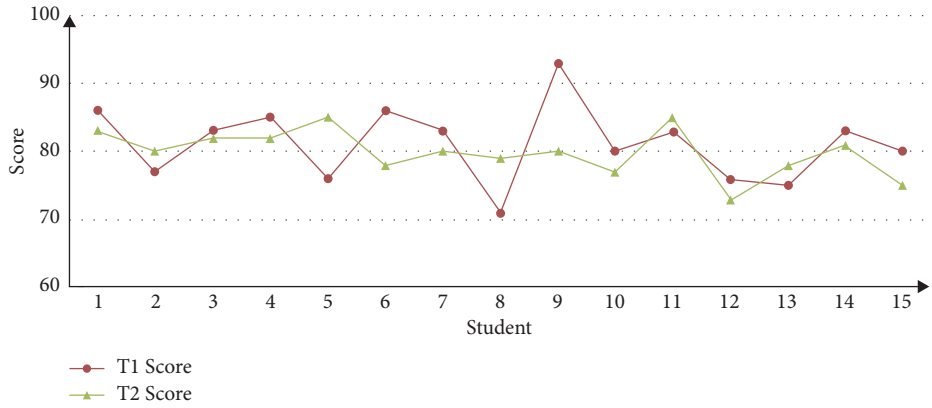

Figure 8: Distribution of test result in groups $T1$ and group $T2$.

an online test afterwards. During the learning, individual students' learning pages are captured in the two groups, respectively, to examine whether the system can recommend appropriate learning resources in accordance with students' demand for personalized learning. Please see the effect from Figures 5 and 6. After the experiments, all the learning records in the system database are collected to form a sample dataset. And then, the sample data are organized and analyzed.

4.2. Experiment Result Analysis and Discussion. With the comparison and analysis of the above experiments, it can be found that the contents of different students' learning resources in the ALS system are not the same, and all the learning resources can be browsed by clicking the button "All Resources" during the learning. After the students logged in ALS, there is no such button as "All Resources" in Figure 6, and the system presents the same learning resources to each student. This is because students in Group $T1$ are registered users, so that ALS could recommend personalized resources in accordance with the user characteristic model; on the contrary, students in Group $T2$ are not registered, and ALS cannot recommend personalized resources because it could not have access to the user characteristic model. Thus, it can be preliminarily judged that ALS developed in this research has the function of personalized recommendation to a certain extent. With the purpose of further analyzing the effect of ALS recommendation, the sample data collected from the experiments are organized and analyzed. And then, the effect of ALS recommendation is analyzed through two-dimension indexes, namely, learning length and test result. Please see the analysis result from Figures 7 and 8.

Figure 7 shows the distribution of students' online learning length in Group $T1$ and Group $T2$. This figure suggests that the time of learning is mainly between 70 and 90 mins, and the distribution track of $T1$ is generally below $T2$, which preliminarily suggests that students in $T1$ spend shorter time, while students in $T2$ spend longer time. Figure 8 suggests the distribution of test result in Group $T1$ and Group $T2$. This figure shows that the test result of the two groups is mainly between 70 and 90, and the distribution track of $T1$ is generally above $T2$, which preliminarily suggests that students in $T1$ have better academic performance. Therefore, we believe that the reason why $T1$ group students generally get higher test scores is that they have used the ALS system, which also shows that the system has better personalized recommendation effect. With the purpose of analyzing whether there is a difference between the two groups in the distribution learning length and test result more scientifically and accurately, SPSS is conducted in t-test analysis. Please see the result from Table 2.

Table 2 shows that the average learning time of $T1$ and $T2$ is 78.27 and 82.87 respectively, which suggests that students in $T1$ spend shorter time than students in $T2$ on average. The standard deviation (Std. deviation) of learning time of the two groups is 6.995 and 5.012, which indicates that students in $T2$ group have relatively long concentrated performance in learning time. The significance Sig. (2-tailed) of the average time is 0.049 (less than 0.05), which suggests that there is a difference between $T1$ and $T2$ in the length of learning time. In addition, it is found through the comparison of the test result that the average score of $T1$ and $T2$ is 82.67 and 79.83, respectively, which demonstrates that the average score of $T1$ is higher than the average score of $T2$. The standard deviation (Std. deviation) of test score of the two groups is 5.960 and 8.205, which indicates that students in $T1$ group have relatively high scores in the test results. The significance Sig. (2-tailed) of the average score is 0.046 (less than 0.05), which demonstrates that there is a difference between $T1$ and $T2$ in the test result. Thus, it can be inferred from Table 2 that the quality and efficiency of learning in $T1$ is superior to $T2$.

Hence, Figures 7 and 8 and Table 2 are considered comprehensively, and a conclusion is reached. The personalized ALS that is developed in this research manifests a satisfying function of recommendation, and it can recommend relatively ideal personalized learning resources in accordance with user characteristic model, which can effectively enhance learner's learning quality and efficiency to a certain extent. Based on the inference, this can be mainly

Table 2: *T* sample test analysis result.

	Group statistics					*t*-test for equality of means	
	Group	*N*	Mean	Std. deviation	Std. error. mean	*t*	Sig. (2-tailed)
Time	*T*1	15	78.27	6.995	1.806	−2.083	0.049
	*T*2	15	82.87	5.012	1.294		
Score	*T*1	15	82.67	5.960	1.539	2.088	0.046
	*T*2	15	79.83	8.205	2.118		

attributed to the fact that ALS can analyze the current learner's demand in accordance with the user characteristic model and recommend personalized learning resources accordingly, which is conducive to learner's efficient and high-quality online learning.

5. Conclusions

With the purpose of implementing the effect of intelligent and personalized recommendation in accordance with user's different demands via ALS, many domestic and overseas scholars have conducted a great deal of theoretical and practical research and yielded substantial achievements. However, the current research on ALS is still in the exploratory stage, and there are a lot of fields that need to be further studied. In consideration of this, this paper intends to specifically analyze learners' traits through several dimensions, such as basic information, interest and preference, cognitive level, and learning style, and construct a user characteristic model on this basis. It is found through the research that user's demand for learning resources can be calculated through the excavation of behavior records based on the multi-dimensional modeling of learner user, through which a personalized recommendation mechanism for the learning system can be realized. In the end, an attempt is made to design and develop a prototype of the personalized ALS to test and verify the recommendation effect. And then, a series of experiments are implemented. It is suggested by the result of the experiments that ALS, which is developed, based on user characteristic model, manifests satisfying effect in recommendation, and it can dynamically recommend appropriate learning resources in accordance with learners' personalized demand, which can effectively enhance learners' learning quality and efficiency to a certain extent.

Data Availability

The data supporting the findings of this study are included within the article.

Conflicts of Interest

The authors declare that they have no conflicts of interest.

Acknowledgments

The study was supported by Guangxi Higher Education and Teaching Reform Project: "Research and Practice on Individualized Training of Post-Capacity-Oriented Educational Technology Ability of High Normal Students" (Project no. 2022JGZ192).

References

[1] A. P. Voiskovskii, K. V. Kuznetsov, and V. A. Yakimenko, "Adaptive algorithms in a universal integrated navigation system based on low-cost instruments," *Russian Engineering Research*, vol. 41, no. 1, pp. 68–71, 2021.

[2] H. M. Ghadirli and M. Rastgarpour, "A web-based adaptive and intelligent tutor by expert systems," *Advances in Computing and Information Technology*, vol. 177, pp. 87–95, 2013.

[3] V. M. Kaziev and L. V. Glukhova, "Adaptive and intelligent web-based learning and control technologies," *Handbook on Intelligent Techniques in the Educational Process*, vol. 29, 2022.

[4] B. I. Alghofaily and C. Ding, "Data mining service recommendation based on dataset features," *Service Oriented Computing and Applications*, vol. 13, no. 3, pp. 261–277, 2019.

[5] M. S. Rafiq, X. Jianshe, M. Arif, and P. Barra, "Intelligent query optimization and course recommendation during online lectures in E-learning system," *Journal of Ambient Intelligence and Humanized Computing*, vol. 12, no. 11, pp. 10375–10394, 2021.

[6] S. Sridharan, D. Saravanan, A. K. Srinivasan, and B. Murugan, "Adaptive learning management expert system with evolving knowledge base and enhanced learnability," *Education and Information Technologies*, vol. 26, no. 5, pp. 5895–5916, 2021.

[7] J. K. Tarus, Z. Niu, and D. Kalui, "A hybrid recommender system for e-learning based on context awareness and sequential pattern mining," *Soft Computing*, vol. 22, no. 8, pp. 2449–2461, 2018.

[8] J. Bhavithra and A. Saradha, "Personalized web page recommendation using case-based clustering and weighted association rule mining," *Cluster Computing*, vol. 22, no. S3, pp. 6991–7002, 2019.

[9] H. P. Ambulgekar, M. K. Pathak, and M. B. Kokare, "A survey on collaborative filtering: tasks, approaches and applications," in *Proceedings of the International Ethical Hacking Conference 2018. Advances in Intelligent Systems and Computing*, vol. 811, Kolkata, India, October 2019.

[10] L. Iaquinta, M. Gemmis, and P. Lops, *Can a Recommender System Induce Serendipitous Encounters*, InTech, London, UK, 2010.

[11] A. Babori, N. Falih, and H. Ouchitachen, "A framework for adaptive E-learning systems based on self-regulated learning strategies," in *Proceedings of the International Conference on Digital Technologies and Applications Digital Technologies and Applications. ICDTA 2022*, vol. 454, Fez, Morocco, January 2022.

[12] B. Vesin, K. Mangaroska, and M. Giannakos, "Learning in smart environments: user-centered design and analytics of an

adaptive learning system," *Smart Learn. Environ*, vol. 5, no. 1, 2018.

[13] Y. Wang, "User behavior identification and personalized recommendation based on web data mining," *International Journal of Circuits, Systems and Signal Processing*, vol. 15, pp. 643–650, 2021.

[14] S. Sweta and K. Lal, "Personalized adaptive learner model in E-learning system using FCM and fuzzy inference system," *International Journal of Fuzzy Systems*, vol. 19, no. 4, pp. 1249–1260, 2017.

[15] S. Fatahi, "An experimental study on an adaptive e-learning environment based on learner's personality and emotion," *Education and Information Technologies*, vol. 24, no. 4, pp. 2225–2241, 2019.

[16] C. Lwande, R. Oboko, and L. Muchemi, "Learner behavior prediction in a learning management system," *Education and Information Technologies*, vol. 26, no. 3, pp. 2743–2766, 2020.

[17] X. M. Zhao, "Research on learner model of adaptive learning system," in *Proceedings of the International Conference on Computer Science & Education (ICCSE)*, Lancaster, UK, May 2021.

[18] J. Joy and R. V. G. Pillai, "Review and classification of content recommenders in E-learning environment," *Journal of King Saud University - Computer and Information Sciences*, vol. 34, no. 9, pp. 7670–7685, 2022.

[19] R. M. Felder and J. Spurlin, "Applications, reliability and validity of the index of learning styles," *Journal of Engineering Education*, vol. 21, pp. 103–112, 2005.

[20] X. K. Zhao, L. Cen, S. R. Long, and P. Wang, "Study on and realization of hybrid recommendation-based adaptive learning system," *Journal of Software Engineering*, vol. 9, no. 4, pp. 886–894, 2015.

[21] X. K. Zhao and S. R. Long, "Research on Key Technologies of constructing personalized learning environment based on Web," *University Education*, vol. 3, pp. 67–70, 2018.

[22] F. Dag and K. Erkan, "A personalized learning system based on semantic web technologies," *Intelligent Tutoring Systems in E-Learning Environments*, pp. 258–284, 2011.

[23] Z. Song, *Research on User Interest Model Based on Web Browsing Behavior"*, Southwest University of science and Technology, Mianyang, China, 2016.

[24] L. Xing, Z. Song, and Q. Ma, "User interest model based on hybrid behaviors interest rate," *Application Research of Computers*, vol. 33, no. 3, pp. 661–665, 2016.

[25] X. K. Zhao, X. D. Xu, and S. R. Long, "Research on personalized recommendation service of adaptive learning system based on B/S mode," *China distance education*, vol. 10, pp. 71–80, 2015.

[26] X. Liu, H. Wu, R. Sun, and W. Jiang, "A fast multipole boundary element method for half-space acoustic problems in a subsonic uniform flow," *Engineering Analysis with Boundary Elements*, vol. 137, pp. 16–28, 2022.

[27] L. Cen, "Research on personalized recommendation service of e-learning system based on user learning style," *Journal of Guangxi Institute of Education*, vol. 5, pp. 139–143, 2017.

[28] H. Liu, W. Zhao, and M. Liang, "Pedagogical strategy model in adaptive learning system focusing on learning styles," *Entertainment for Education. Digital Techniques and Systems*, vol. 6249, pp. 156–164, 2010.

[29] L. Cen and X. K. Zhao, "A personalized recommendation service in E-learning system from the perspective of learning style," *Boletin Tecnico/Technical Bulletin*, vol. 55, no. 9, pp. 448–456, 2017.

Hindawi
Computational Intelligence and Neuroscience
Volume 2022, Article ID 9889292, 12 pages
https://doi.org/10.1155/2022/9889292

Research Article

Research on Decision-Making of Hybrid Dominant Closed-Loop Supply Chain considering Different Logistics Modes

Wanxian Wu and Lin Miao

Business School of Liming Vocational University, Quanzhou 362000, China

Correspondence should be addressed to Lin Miao; 1611407089@stu.hqu.edu.cn

Received 18 August 2022; Revised 5 September 2022; Accepted 19 September 2022; Published 10 October 2022

Academic Editor: Zaoli Yang

Based on the mode of manufacturers dominating in the forward supply chain and retailers dominating in the backward supply chain, a hybrid leading closed-loop supply chain structure with different two-way dominance is constructed to study the advantages and disadvantages of supply chain decision-making under logistics self-supporting and logistics outsourcing modes. Stackelberg game theory is used to solve the equilibrium solution and optimal profit of the forward and backward supply chains under different logistics modes. On this basis, the profits of manufacturers and retailers in the forward and backward closed-loop supply chains are compared, and finally, the conclusion is verified by numerical examples. The influence of different logistics modes on pricing decisions of manufacturers and retailers is studied based on the dual-agent hybrid dominant supply chain model, and then, the logistics mode selection of manufacturers and retailers under different conditions of forward dominant body and backward dominant body.

1. Introduction

When the whole world begins to gradually enter the post-industrial era, it is urgent to reduce environmental pollution and improve the efficiency of resource utilization. Therefore, the government proposes to strongly support enterprises to recycle waste products for remanufacturing. Compared with traditional supply chain systems, the recycling and remanufacturing closed-loop supply chain has a complex structure, and dominant enterprises, recycling channels, and logistics services have a cross-impact on the selection of closed-loop supply chain mode. Based on the reproduction capacity or recycling capacity, the closed-loop supply chain is mostly dominated by manufacturers or retailers [1]. The closed-loop supply chain dominated by different players needs support from different recycling channels and decides whether to adopt logistics outsourcing [2]. Savaskan and Wassenhove [3] studied the closed-loop supply chain with different recycling channels established by manufacturers, sellers, and third parties in charge of recycling, respectively, and the results showed that sellers in charge of recycling were more effective than manufacturers and third parties. Han [4] and Gao et al. [5] studied three recovery channel strategies of retailer recovery, manufacturer recovery, and third-party recovery in the closed-loop supply chain dominated by sellers. Gong [6] designed four supply chain modes based on the cross-combination of manufacturer- or seller-dominant mode and recovery mode and then analyzed the relationship between sales price, sales volume, recovery rate, and profit under different modes to determine the stability of the four supply chains. Meanwhile, the above dominant modes combine logistics self-supporting or outsourcing to form a new combination, and its stability is evaluated through the total profit of the supply chain [7]. Zhang et al. [8] proposed that enterprises in the forward and backward processes of the closed-loop supply chain had different concerns, so the dominant enterprises in the supply chain should choose different logistics strategies to achieve the stability of the supply chain.

The cross-combination of different dominant modes, recovery modes, and logistics strategies forms closed-loop supply chains with different structures. The structure of the

closed-loop supply chain affects supply chain pricing, main income (profit distribution), and supply chain stability and ultimately influences the choice of supply chain model. Karakayali et al. [9] studied the pricing service decision of the backward supply chain from the perspective of the power structure of different channels. Ma et al. [10] studied the two closed-loop supply chains with or without government subsidies and explored the benefits that consumers obtained from them. Gao et al. [11] studied the product pricing and member enterprises' profit distribution in the closed-loop supply chain under three situations: manufacturers' dominance, retailers' dominance, and manufacturers and retailers' rights, and believed that retailers' profits were the largest rights when they dominated, and under the condition of equal rights, this was most favorable for consumers, and at this time, the product sales price was the lowest. Liu and Liu [12] analyzed the dual-channel closed-loop supply chain system in which the original manufacturers and the third-party remanufacturing coexisted, analyzed the differential pricing methods of new products and remanufactured products by using the game model, and then obtained the best pricing strategies under different modes. Sun et al. [13] constructed a closed-loop supply chain structure of three recycling channels based on the influence of sales quantity and recycling price. Based on the closed-loop supply chain structure with double sales and double recovery as two competitive channels, Lin and Cao [14] explored the pricing strategy model of the closed-loop supply chain with manufacturers and retailers as the dominant players. Xie [15] believed that revenue sharing contract could provide support for supply chain cooperation and proposed that forward sales revenue and backward recovery revenue should be distributed simultaneously based on contract theory, which would help maximize the profits of both in the closed-loop supply chain system cooperated by a single manufacturer and single retailer. Ding and Ma [16] conducted a comparative analysis on pricing decisions and benefits of the two closed-loop supply chain models in which suppliers chose to participate in parts recycling and remanufacturing under the situation of supplier dominance. Xu et al. [17] analyzed the dual-channel supply chain model and obtained several management suggestions on delivery lead time decision-making. Matsui [18] used an observable delay game framework in noncooperative game theory to analyze pricing decisions in dual-channel supply chains. By modeling the demand function of the two channels as a linear function of the retail price and direct price, when manufacturers should set their direct price and wholesale price in the dual-channel supply chain was revealed. Batarfi et al. [19] extended the two-channel supply chain to a setup where standard and customized products were sold through retailers and online channels, respectively. The paper took demand as a linear function of sales price, quoted delivery time, and product difference and determined the best business strategy to maximize the total profit of the system. Besides, they also studied the impact of dual-channel strategy on supply chain performance when inventory costs were incorporated into the system. Meng et al. [20] used Stackelberg game theory to establish a dual-channel green supply chain model of consumers' green preference and channel preference. The research results show that the higher the consumer's green preference or the lower the offline channel preference, the greater the demand for green products. Zhang et al. [21] studied the dynamic pricing strategy problem of a dual-channel supply chain composed of manufacturers and retailers under consumers' green preferences. The research structure shows that the market demand is concave with the selling price, and when the selling price is equal to the reference price, the market demand reaches the maximum value, so the manufacturer should strategically decide to change the price in real time according to the previous period price. Considering consumer product differentiation preferences, Zhang and Zheng [22] studied the company's optimal customization strategy and commodity diversification pricing decisions under both online and offline channels, as well as the impact of customization strategies on company pricing decisions, profits, and consumer welfare. It is shown that, under unified pricing, the only factor affecting the customization strategy of a single-channel company is its cost efficiency, and the customization strategy is likely to play a strategic role in correctly guiding consumers' "total traffic" level.

In conclusion, the closed-loop supply chain structure or mode is influenced by the dominant enterprises, recycling channels, logistics services, and other factors [23–25], and the closed-loop supply chain structure affects the dominant enterprises' choice of closed-loop supply mode based on product pricing, enterprise benefits, and other factors. These conclusions have reached a consensus in the academic community, which is also the basis of this study. Existing studies may have the following shortcomings: (1) most of them focus on the closed-loop supply chain structure of single logistics service of logistics self-supporting or logistics outsourcing, and there are few studies on the selection and comparison of logistics self-supporting and logistics outsourcing services; (2) most of the studies on the closed-loop supply chain considering logistics services do not reflect the impact of logistics cost on the selection of recovery channel and supply chain mode; (3) existing studies are mainly manufacturer-dominant or retailer-dominant closed-loop supply chain systems, without distinguishing the leading enterprises of forward and backward supply chain systems, but in the actual environment, different dominant enterprises lead their respective supply chains; and (4) the research perspective of the closed-loop supply chain mode selection is relatively single, most of them are based on the pricing strategy and profit distribution strategy, and there are few studies on closed-loop supply chain mode selection from the perspective of logistics mode.

In the current recycling and remanufacturing cycle system, the forward supply chain is usually still dominated by manufacturers, while the backward supply chain is dominated by retailers who control recycling channels [26, 27]. Based on this, this paper mainly studies the forward closed-loop supply chain structure dominated by manufacturers and the backward closed-loop supply chain structure dominated by retailers. Based on the profit distribution mechanism, this paper discusses the logistics mode

selection of manufacturers and retailers in the mixed dominant closed-loop supply chain. The research framework is as follows: Section 2 analyzes the closed-loop supply chain model and puts forward basic assumptions. In Section 3, the game model of the closed-loop supply chain model is constructed and the equilibrium solution is obtained. Section 4 is a comparative analysis of the closed-loop supply chain under different logistics modes. In Section 5, numerical examples are used to verify the research results.

2. Model Assumption

Based on a single sales channel and a single recycling channel, this paper studies the more reasonable logistics mode selection in the closed-loop supply chain. In the forward supply chain, the manufacturer sells the product to retailers, who then provide the product for consumers. In the backward supply chain, recycling retailers recycle the waste products and finally deliver them to the manufacturer for remanufacturing. In the whole closed-loop supply chain process, logistics outsourcing is mainly provided by the third-party logistics enterprises or self-supporting logistics mode. The closed-loop supply chain structure under different logistics modes studied in this paper is shown in Figure 1.

In Figure 1, the manufacturer acts as the front end of the forward supply chain and the end of the reverse supply chain, the consumer market and the recycling market belong to the intermediate links, and the retailer acts as the channel of the forward supply chain and the reverse supply chain. The logistics circulation link between manufacturers and retailers in Figure 1(a) relies on the logistics team of the core enterprise in the supply chain; the logistics circulation link between manufacturers and retailers in Figure 1(b) relies on the third party outside the supply chain. Different logistics operation modes have a great impact on the decision-making of the entire supply chain. On this basis, this paper will further explore which decision-making scheme should be selected by supply chain enterprises under different logistics operation modes to make the overall supply chain operation optimal:

(1) The closed-loop supply chain studied in this paper is composed of a single manufacturer, a single retailer, and a single third-party logistics service provider (if logistics outsourcing is selected); it only considers a circulated closed-loop supply chain constituted by single manufacturing, sales forward supply chain and single recovery, and remanufacturing reverse supply chain.

(2) As retailers and manufacturers have different statuses in the closed-loop supply chain, core enterprises are usually the leading party in the supply chain. Therefore, this paper sets two situations: manufacturers dominate in a forward supply chain, and retailers dominate in a backward supply chain; retailers dominate in a forward supply chain, and manufacturers dominate in a backward supply chain.

(3) Assuming that the demand of the consumer market is determined, the market demand is a linear subtraction function of demand price. $Q = \alpha - \beta p_r$, where α is the maximum possible demand of the market, i.e., the market size, and $\beta > 0$ is the price sensitivity coefficient; the quantity of recycled products is $\overline{Q}$, and the expression is $\overline{Q} = k + \gamma h_r$, where $k\,(k > 0)$ represents the number of products recycled by consumers' environmental awareness [28].

(4) When the closed-loop supply chain chooses self-supporting logistics, its unit logistics cost is θ. Based on the scale efficiency and professional operation of outsourcing logistics, the forward and backward unit logistics costs of third-party logistics service providers are $s\theta\,(0 \le s \le 1)$, respectively, and $s\theta \le p_l \le \theta$, $s\theta \le p_l' \le \theta$.

(5) As dominant enterprises are at the core of the closed-loop supply chain and have decision-making power, logistics costs are borne by subordinate enterprises in both the forward and backward supply chains. Whether the manufacturer dominates the supply chain or the retailer dominates the supply chain, manufacturers, retailers, and third-party logistics service providers (under logistics outsourcing) in the supply chain will choose decisions that are in line with their own interests.

According to the above assumptions, the profits of manufacturers, retailers, and third-party logistics service providers under the logistics outsourcing mode are as follows:

$$\begin{aligned} \pi_m &= \pi_{m1} + \pi_{m2} = (p_m - c_m)Q + (\Delta - \omega - p_l')\overline{Q}, \\ \pi_l &= \pi_{l1} + \pi_{l2} = (p_l - s\theta)Q + (p_l' - s\theta)\overline{Q}, \\ \pi_r &= \pi_{r1} + \pi_{r2} = (p_r - p_m - p_l)Q + (\omega - h_r)\overline{Q}. \end{aligned} \tag{1}$$

Under the self-supporting logistics mode, the profits of manufacturers and retailers are as follows:

$$\begin{aligned} \pi_m &= \pi_{m1} + \pi_{m2} = (p_m - c_m)Q + (\Delta - \omega - \theta)\overline{Q}, \\ \pi_r &= \pi_{r1} + \pi_{r2} = (p_r - p_m - \theta)Q + (\omega - h_r)\overline{Q}. \end{aligned} \tag{2}$$

3. Model Building

3.1. Game Model and Equilibrium Solution of Logistics Outsourcing Closed-Loop Supply Chain

3.1.1. Forward Supply Chain Game Equilibrium Dominated by Manufacturers (MO)

$$\max_{p_m} \pi_{m1} = (p_m - c_m)Q, \tag{3}$$

$$s.t.\ \max_{p_l} \pi_{l1} = (p_l - s\theta)Q, \tag{4}$$

$$s.t.\ \max_{p_r} \pi_{r1} = (p_r - p_m - p_l)Q. \tag{5}$$

Based on the reverse solving method of Stackelberg game, in the forward supply chain system dominated by

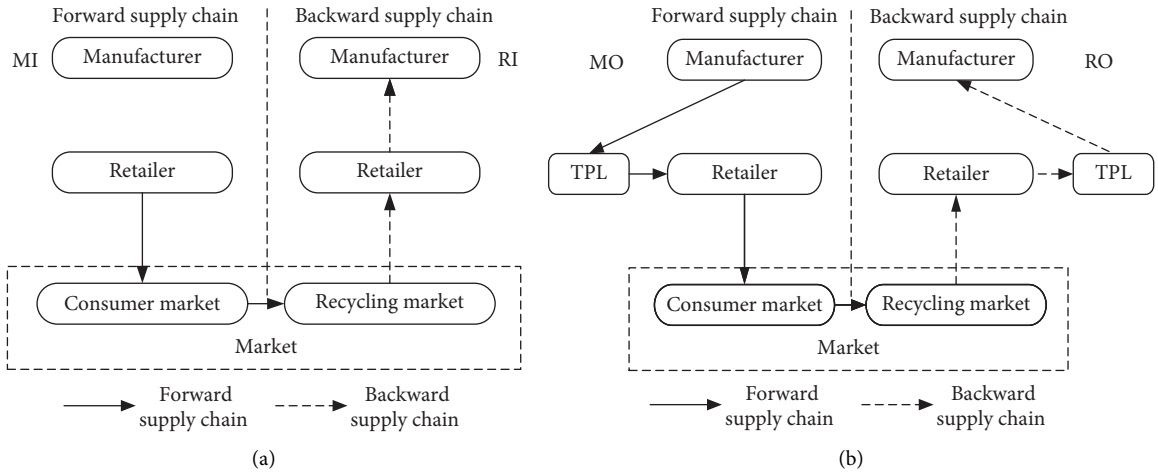

Figure 1: (a) Closed-loop supply chain structure under the logistics self-supporting mode. (b) Closed-loop supply chain structure under the logistics outsourcing mode.

manufacturers, first of all, manufacturers predict market demand and then determine their production plan and wholesale price. Secondly, the third-party logistics service providers determine the price of logistics services according to product transportation scale. Finally, sellers determine the product's sales price according to the wholesale and logistics service price. Therefore, it is easy to get the following statement (see Table 1 for equilibrium solutions).

Proposition 1. *Under the logistics outsourcing mode, when the forward supply chain reaches game equilibrium under the leadership of the manufacturer, the wholesale price of the manufacturer, the sales price of the retailer, the service price of the third-party logistics service provider, the market demand, the manufacturer's profit, the retailer's profit, and the logistics service provider's profit are as follows:*

$$
\begin{aligned}
p_m &= \frac{\alpha + \beta c_m - \beta s\theta}{2\beta},\\
p_l &= \frac{\alpha + 3\beta s\theta - \beta c_m}{4\beta},\\
p_r &= \frac{7\alpha + \beta s\theta + \beta c_m}{8\beta},\\
Q &= \frac{\alpha - \beta s\theta - \beta c_m}{8},\\
\pi_{m1} &= \frac{(\alpha - \beta s\theta - \beta c_m)^2}{16\beta},\\
\pi_{r1} &= \frac{(\alpha - \beta s\theta - \beta c_m)^2}{64\beta},\\
\pi_{l1} &= \frac{(\alpha - \beta s\theta - \beta c_m)^2}{32\beta}.
\end{aligned}
\tag{6}
$$

Proof. The reverse solution is carried out according to Stackelberg game theory. The retailer's decision should be optimized first. Because $d^2\pi_{r1}/dp_r^2 = -2\beta < 0$, the first-order condition $d\pi_{r1}/dp_r = 0$ is the retailer's optimal decision. Thus, according to $d\pi_{r1}/dp_r = 0$, $p_r(p_m, p_l) = \alpha + \beta p_m + \beta p_l/2\beta$. After substituting $p_r(p_m, p_l)$ into (4), the first-order condition is $p_l(p_m) = \alpha - \beta p_m + \beta s\theta/2\beta$. After substituting $p_l(p_m)$ into $p_r(p_m, p_l)$, $p_r(p_m) = 3\alpha + \beta p_m + \beta s\theta/4\beta$ can be obtained, and then $p_r = 7\alpha + \beta s\theta + \beta c_m/8\beta$ and $p_l = \alpha + 3\beta s\theta - \beta c_m/4\beta$. After substituting p_m, p_r, p_l into (3), (4), and (5), the profits of manufacturers, third-party logistics service providers, and retailers can be obtained as follows: $\pi_{m1} = (\alpha - \beta s\theta - \beta c_m)^2/16\beta$, $\pi_{l1} = (\alpha - \beta s\theta - \beta c_m)^2/32\beta$, and $\pi_{r1} = (\alpha - \beta s\theta - \beta c_m)^2/64\beta$.

The first-order derivative of the optimal price to the logistics cost θ is conducted to obtain the following results: $\partial p_m/\partial\theta = -(s/2) < 0$, $\partial p_l/\partial\theta = (3s/4) > 0$, and $\partial p_r/\partial\theta = (s/8) > 0$. This shows that the optimal prices p_l and p_r increase as the logistic cost θ increases and decrease as the logistic cost θ increases. According to $\partial Q/\partial\theta = -(\beta s/8) < 0$, it can be known that Q increases with the increase of logistics cost θ. In addition, we also know $\partial\pi_{m1}/\partial\theta = -(s/8)(\alpha - \beta s\theta - \beta c_m)$,$\partial\pi_{r1}/\partial\theta = -(s/32)(\alpha - \beta s\theta - \beta c_m)$, and $\partial\pi_{l1}/\partial\theta = -(s/16)(\alpha - \beta s\theta - \beta c_m)$. As $\alpha - \beta s\theta - \beta c_m > 0$, it can be known that $\partial\pi_{m1}/\partial\theta$,$\partial\pi_{r1}/\partial\theta$, and $\partial\pi_{l1}/\partial\theta$ are less than 0. This indicates optimal profits π_{m1},π_{r1}, and π_{l1} decrease as the logistics cost θ increases. Besides, the trend of change of p_m, p_r, p_l, Q, π_{m1}, π_{r1}, and π_{l1} is related to the value of S, which is caused by logistics outsourcing.

According to Proposition 1, it can be found that, in the forward supply chain, when the logistics cost S of the third-party logistics service provider is high, the wholesale price of the manufacturer will decrease, the price of the retailer will increase, and the product demand will decrease. This is because in the forward supply chain, the manufacturer is in a dominant position, and retailers of affiliate companies need to bear the cost of logistics. To let retailers gain profit margins, the manufacturer will lower wholesale prices. At

Table 1: Equilibrium solutions of closed-loop supply chain under different logistics modes.

	Logistics outsourcing		Logistics self-supporting	
	MO	*RO*	*MI*	*RI*
Q	$\alpha - \beta s\theta - \beta c_m/8$	—	$\alpha - \beta\theta - \beta c_m/4$	—
$\overline{Q}$	—	$k + \gamma\Delta - \gamma s\theta/8$	$k + \gamma\Delta - \gamma\theta/4$	$k + \gamma\Delta - \gamma\theta/4$
π_m	$(\alpha - \beta s\theta - \beta c_m)^2/16\beta$	$(k + \gamma\Delta - \gamma s\theta)^2/64\gamma$	$(\alpha - \beta\theta - \beta c_m)^2/8\beta$	$(k + \gamma\Delta - \gamma\theta)^2/16\gamma$
π_r	$\frac{(\alpha-\beta s\theta-\beta c_m)^2}{64\beta}$	$(k + \gamma\Delta - \gamma s\theta)^2/16\gamma$	$(\alpha - \beta\theta - \beta c_m)^2/16\beta$	$(k + \gamma\Delta - \gamma\theta)^2/8\gamma$
π_l	$\frac{(\alpha-\beta s\theta-\beta c_m)^2}{32\beta}$	$(k + \gamma\Delta - \gamma s\theta)^2/32\gamma$	—	—

the same time, retailers will increase retail prices and transfer costs to consumers in order to deal with high logistics costs, which will produce a vicious cycle. Therefore, consumers will buy fewer products, resulting in a lower quantity of product demand. Finally, the profits of the manufacturers and retailers will decrease. Thus, manufacturers and retailers need to strengthen cooperation with third-party logistics service providers to reduce logistics costs as much as possible and gain more profits. □

3.1.2. Backward Retailer-Dominated Supply Chain Game Equilibrium (RO)

$$\max_{h_r} \pi_{r2} = (\omega - h_r)\overline{Q} \tag{7}$$

$$\text{s.t. } \max_{p_l'} \pi_{l2} (p_l' - s\theta)\overline{Q} \tag{8}$$

$$\text{s.t. } \max_{\omega} \pi_{m2} = (\Delta - \omega - p_l')\overline{Q}. \tag{9}$$

Based on the reverse solving method of the Stackelberg game, in a backward retailer-dominated supply chain system, the seller first determines the recycling price according to the recycling amount of waste products. Then, the third-party logistics service providers determine the price of logistics according to the number of waste products. Finally, the manufacturer determines the transfer price according to the recycling price and service price. Meanwhile, when the manufacturer brings recycled products to the market at the same wholesale price, it is easy to get the following proposition (see Table 1 for equilibrium solutions).

Proposition 2. *Under the logistics outsourcing mode, when the backward supply chain reaches game equilibrium under the dominance of retailers, the manufacturer's transfer price, retailers' recovery price, third-party logistics service providers' service price, market demand, manufacturer's profit, retailers' profit, and logistics service providers' profit are as follows:*

$$\begin{aligned}
\omega &= \frac{-3k + 5\gamma\Delta - 5\gamma s\theta}{8\gamma},\\
h_r &= \frac{-7k + \gamma\Delta - \gamma s\theta}{8\gamma},\\
p_l' &= \frac{k + 3\gamma s\theta + \gamma\Delta}{4\gamma},\\
\overline{Q} &= \frac{k + \gamma\Delta - \gamma s\theta}{8},\\
\pi_{m2} &= \frac{(k + \gamma\Delta - \gamma s\theta)^2}{64\gamma},\\
\pi_{r2} &= \frac{(k + \gamma\Delta - \gamma s\theta)^2}{16\gamma},\\
\pi_{l2} &= \frac{(k + \gamma\Delta - \gamma s\theta)^2}{32\gamma}.
\end{aligned} \tag{10}$$

Proof. The reverse solution is carried out according to Stackelberg game theory, and unit expected revenue of the retailer is set as f, then $\omega = h_r + f$. $\omega = h_r + f$ is substituted into (9). The first step is to make the manufacturer's decision optimal, because $d^2\pi_{m2}/d\omega^2 = -2\lambda < 0$, as the first order is 0, $\omega(f, p_l') = -k + \gamma f + \gamma\Delta - \gamma p_l'/2\gamma$. After substituting $\omega(f, p_l')$into $\omega = h_r + f$,$h_r(f, p_l') = -k - \gamma f + \gamma\Delta - \gamma p_l'/2\gamma$ can be obtained, and then it is substituted into (8), $p_l'(f) = k - \gamma f + \gamma\Delta + \gamma s\theta/2\gamma$can be obtained by the first-order condition. Substituting $p_l'(f)$ and $h_r(f, p_l')$ into (7), $p_r(p_m) = 3\alpha + \beta p_m + \beta s\theta/4\beta$ can be obtained. Substituting $p_r(p_m)$ into (9), the first-order condition is 0, and then $f = k + \gamma\Delta - \gamma s\theta/2\gamma$, so $\omega = -3k + 5\gamma\Delta - 5\gamma s\theta/8\gamma$, $h_r = -7k + \gamma\Delta - \gamma s\theta/8\gamma$, and $p_l' = k + 3\gamma s\theta + \gamma\Delta/4\gamma$. By

substituting ω, h_r, p_l' into (7), (8), and (9), the profits of manufacturers, third-party logistics service providers, and retailers can be obtained: $\pi_{m2} = (k + \gamma\Delta - \gamma s\theta)^2/64\gamma$, $\pi_{l2} = (k + \gamma\Delta - \gamma s\theta)^2/32\gamma$, and $\pi_{r2} = (k + \gamma\Delta - \gamma s\theta)^2/16\gamma$.

The first-order derivative of the optimal price to the logistics cost θ can be obtained: $\partial\omega/\partial\theta = -(5s/8) < 0$, $\partial p_l'/\partial\theta = 3s/4 > 0$, and $\partial h_r/\partial\theta = -(s/8) < 0$. This indicates that the optimal price p_l increases with the increase of logistics cost θ, while ω and $h_r$decrease with the increase of logistics cost θ. From the equation $\partial\overline{Q}/\partial\theta = -(\gamma s/8) < 0$, it can be seen that Q increases with the increase of logistics cost θ. Besides, $\partial\pi_{m2}/\partial\theta = -(s/32)(k + \gamma\Delta - \gamma s\theta)$, $\partial\pi_{r2}/\partial\theta = -(s/8)(k + \gamma\Delta - \gamma s\theta)$, and $\partial\pi_{l2}/\partial\theta = -(s/16)(k + \gamma\Delta - \gamma s\theta)$. As $k + \gamma\Delta - \gamma s\theta > 0$, $\partial\pi_{m2}/\partial\theta$, $\partial\pi_{r2}/\partial\theta$, and $\partial\pi_{l2}/\partial\theta$ are less than 0. This indicates that the optimal profits π_{m2},π_{r2}, and π_{l2}decrease as the logistics cost θ increases, while the variation tendency of ω, h_r, $\overline{Q}$, π_{m2}, π_{r2}, and π_{l2} is related to S, which is correlated with logistics outsourcing.

According to Proposition 2, it can be found that, in the backward supply chain, the larger the logistics cost(S) is, the larger the transfer price of the manufacturer is, and the higher the recycling price of the retailer is, but the lower the number of recycled waste products will be. This is because the backward supply chain is dominated by retailers and the manufacturers bear the cost of logistics outsourcing; to obtain certain profits from remanufacturing, manufacturers reduce the transfer price. At this time, the profits obtained by the manufacturers from retailers will also reduce, thus resulting in a declined recycling price and eventually leading to a decline in enterprises' profits. Therefore, backward recycling channels also need to take corresponding measures to reduce logistics costs. □

3.2. Game Model and Equilibrium Solution of Logistics Self-Supporting Closed-Loop Supply Chain

3.2.1. Forward Supply Chain Game Equilibrium Dominated by Manufacturers (MI)

$$\max_{p_m} \pi_{m1} = (p_m - c_m)Q, \tag{11}$$

$$\text{s.t. } \max_{p_r} \pi_{r1} = (p_r - p_m - \theta)Q. \tag{12}$$

According to the reverse solution method of the Stackelberg game, in the forward manufacturer-dominated supply chain system, the manufacturer first predicts the market demand to determine its production plan and wholesale price, and the seller decides the sales price of the product according to the wholesale price; thus, the following proposition can be easily obtained (see Table 1 for equilibrium solutions).

Proposition 3. *Under the logistics self-supporting mode, when the forward supply chain reaches game equilibrium under the leadership of the manufacturer, the wholesale price of the manufacturer, the selling price of the retailer, the market demand, the manufacturer's profit, and the retailer's profit are as follows:*

$$\begin{aligned} p_m &= \frac{\alpha - \beta c_m + \beta\theta}{2\beta}, \\ p_r &= \frac{3\alpha + \beta c_m + \beta\theta}{4\beta}, \\ Q &= \frac{\alpha - \beta c_m - \beta\theta}{4}, \\ \pi_{m1} &= \frac{(\alpha - \beta c_m - \beta\theta)^2}{8\beta}, \\ \pi_{r1} &= \frac{(\alpha - \beta c_m - \beta\theta)^2}{16\beta}. \end{aligned} \tag{13}$$

Proof. According to the reverse solution, the first order of (12) is 0, so $p_r(p_m) = \alpha + \beta p_m/2\beta$. Substituting $p_r(p_m)$ into (11), as the first order is 0, $p_m = \alpha + \beta c_m - \beta\theta/2\beta$, and then $p_r = 3\alpha + \beta c_m + \beta\theta/4\beta$, $Q = \alpha - \beta c_m - \beta\theta/4$, $\pi_{m1} = (\alpha - \beta c_m - \beta\theta)^2/8\beta$, and $\pi_{r1} = (\alpha - \beta c_m - \beta\theta)^2/16\beta$.

The first-order derivative of the optimal price to the logistics cost θ can be obtained: $\partial p_m/\partial\theta = -(1/2) < 0$, $\partial p_r/\partial\theta = (1/4) > 0$. This indicates that the optimal price $p_r$increases with the increase of logistics cost θ, while $p_m$decreases with the increase of logistics cost θ. From $\partial Q/\partial\theta = -(\beta/4) < 0$, it can be seen that Q decreases with the increase of logistics cost θ. Besides, $\partial\pi_{m1}/\partial\theta = -(1/4)(\alpha - \beta\theta - \beta c_m)$and $\partial\pi_{r1}/\partial\theta = -(1/8)(\alpha - \beta\theta - \beta c_m)$. As $\alpha - \beta\theta - \beta c_m > 0$, both $\partial\pi_{m1}/\partial\theta$ and $\partial\pi_{r1}/\partial\theta$ are less than 0, which indicates that the optimal profits π_{m1} and π_{r1}decrease as the logistics cost θ increases.

According to Proposition 3, it can be found that, in the forward supply chain, when the logistics cost is higher, the wholesale price and sale price will rise, and the demand of the market can also be reduced accordingly, eventually resulting in a decrease of profits of retailers and manufacturers. Therefore, enterprises must consider the impact of logistics cost on their operation when carrying out self-supporting logistics and then use various management techniques and methods to reduce logistics cost. □

3.2.2. Backward Retailer-Dominated Supply Chain Game Equilibrium (RI)

$$\max_{h_r} \pi_{r2} = (\omega - h_r)\overline{Q}, \tag{14}$$

$$\text{s.t. } \max_{\omega} \pi_{m2} = (\Delta - \omega - \theta)\overline{Q}. \tag{15}$$

According to the reverse solution method of the Stackelberg game, in the backward retailer-dominated supply chain system, the retailer firstly determines the recycling price according to the recycling amount of waste products, and the manufacturer determines the transfer price according to the recycling price, and then the manufacturer flows the recycled products into the market at the

same wholesale price; thus, the following proposition can be easily obtained (see Table 1 for equilibrium solutions).

Proposition 4. *Under the self-supporting logistics mode, when the backward supply chain achieves game equilibrium under the dominance of retailers, the manufacturer's transfer price, retailer's recovery price, market demand, manufacturer's profit, and retailer's profit are as follows:* $\omega = -k - 3\gamma\theta + 3\gamma\Delta/4\gamma$, $h_r = -3k + \gamma\Delta - \gamma\theta/4\gamma$, $\overline{Q} = k + \gamma\Delta - \gamma\theta/4$, $\pi_{m2} = (k + \gamma\Delta - \gamma\theta)^2/16\gamma$, *and* $\pi_{r2} = (k + \gamma\Delta - \gamma\theta)^2/8\gamma$.

Proof. Reverse solving, assume that the unit revenue expected by the retailer is f, then $h_r = \omega - f$. Then, it is substituted into Equation (152), and according to the condition that the first order is 0, $\omega(f) = -k + \gamma f - \gamma\theta + \gamma\Delta/2\gamma$ and $h_r(f) = -k - \gamma f + \gamma\Delta - \gamma\theta/2\gamma$ can be obtained. After substituting$h_r(f)$ into (14), $f = k + \gamma\Delta - \gamma\theta/2r$ can be obtained. So, $\omega = -k - 3\gamma\theta + 3\gamma\Delta/4\gamma$, $h_r = -3k + \gamma\Delta - \gamma\theta/4\gamma$, $\overline{Q} = k + \gamma\Delta - \gamma\theta/4$, $\pi_{m2} = (k + \gamma\Delta - \gamma\theta)^2/16\gamma$, and $\pi_{r2} = (k + \gamma\Delta - \gamma\theta)^2/8\gamma$.

The first-order derivative of the optimal price to the logistics cost θ is obtained: $\partial\omega/\partial\theta = -(3/4) < 0$, $\partial h_r/\partial\theta = -(1/4) < 0$. This indicates that the optimal prices ω and h_r decrease as the logistics cost θ increases. From $\partial\overline{Q}/\partial\theta = -(\gamma/4) < 0$, it can be seen that $\overline{Q}$ increases as the logistics cost θ increases. Besides, the following equations can be obtained: $\partial\pi_{m2}/\partial\theta = -(1/8)(k + \gamma\Delta - \gamma\theta)$ and $\partial\pi_{r2}/\partial\theta = -(1/4)(k + \gamma\Delta - \gamma\theta)$. As $k + \gamma\Delta - \gamma\theta > 0$, it can be known that $\partial\pi_{m2}/\partial\theta$ and $\partial\pi_{r2}/\partial\theta$ are less than 0, which indicates that the optimal profits π_{m2} and π_{r2} decrease as the logistics cost θ increases.

According to Proposition 4, it can be found that, in the backward supply chain, when the transfer price and recycling amount of waste products are smaller, the profit of enterprises will decrease with the increase of logistics cost. Therefore, in the logistics self-supporting closed-loop supply chain, manufacturers and distributors should strengthen cooperation to reduce logistics costs. Meanwhile, the higher the cost saving of remanufacturing is, the larger the transfer price and recovery price will be, and the greater the recycling amount will be. Therefore, the manufacturers of recycling and reprocessing should improve the technical level and increase the cost saving of remanufacturing to improve their profits. □

4. Comparative Analysis of Closed-Loop Supply Chain under Different Logistics Modes

From the perspective of social and economic value, selecting an appropriate logistics mode can improve the profits of the closed-loop supply chain. For the convenience of description and expression, in this paper, H, T, $\overline{H}$, and $\overline{T}$ are introduced as replacement variables to compare the profits of manufacturers and retailers based on different logistics services. $H = \alpha - \beta s\theta - \beta c_m$, $T = \mathrm{k} + \gamma(\Delta - s\theta)$, $\overline{H} = \alpha - \beta\theta - \beta c_m$, and $\overline{T} = \mathrm{k} + \gamma(\Delta - \theta)$. As $0 \le s \le 1$, $H \ge \overline{H}$ and $T \ge \overline{T}$. Then, the following conclusions are drawn.

Conclusion 1. In the forward supply chain, when $H/\overline{H} \ge 2$, the product demand of the market under logistics outsourcing is greater than that under self-supporting logistics; when $1 < H/\overline{H} < 2$, the product demand of the market under the logistics self-supporting mode is greater than that under the logistics outsourcing mode. In the backward supply chain, when $T/\overline{T} \ge 2$, the product demand of the market under the logistics outsourcing mode is greater than that under the self-supporting logistics mode; when $1 < T/\overline{T} < 2$, the product demand of the market under the self-supporting logistics mode is greater than that under the logistics outsourcing mode.

Proof. As $Q^{MO} - Q^{MI} = H/8 - H/4$, when $Q_{m1}^{MO} \ge Q_{m1}^{MI}$, $H/\overline{H} \ge 2$. On the contrary, when $Q_{m1}^{MO} < Q_{m1}^{MI}$, $H/\overline{H} < 2$, and $H \ge \overline{H}$, then $1 < H/\overline{H}$, so $1 < H/\overline{H} < 2$. Similarly, $\overline{Q}^{RO} - \overline{Q}^{RI} = T/8 - T/4$, when $\overline{Q}^{RO} \ge \overline{Q}^{RI}$, $T/\overline{T} \ge 2$ and $\overline{Q}^{RO} < \overline{Q}^{RI}$, $1 < T/\overline{T} < 2$. □

Conclusion 2. In the forward supply chain, when $1 \le H/\overline{H} < \sqrt{2}$, the profits of manufacturers and retailers when they choose self-supporting logistics are greater than those when they choose outsourcing logistics; when $\sqrt{2} \le H/\overline{H} < 2$, the manufacturer chooses logistics outsourcing, whose profit is greater than that of logistics self-supporting, while the retailer chooses logistics self-supporting, whose profit is higher than that of logistics outsourcing. When $H/\overline{H} \ge 2$, the profits of manufacturers and retailers choosing logistics outsourcing are greater than those choosing logistics self-operating.

Proof. As $\pi_{m1}^{MO} - \pi_{m1}^{MI} = H^2/16\beta - \overline{H}^2/8\beta$, $\pi_{r1}^{MO} - \pi_{r1}^{MI} = H^2/64\beta - \overline{H}^2/16\beta$, when $\pi_{m1}^{MO} \ge \pi_{m1}^{MI}$, $H/\overline{H} \ge \sqrt{2}$, and when $\pi_{r1}^{MO} \ge \pi_{r1}^{MI}$, $H/\overline{H} \ge 2$. On the contrary, when $\pi_{m1}^{MO} < \pi_{m1}^{MI}$, $\pi_{m1}^{MO} < \pi_{m1}^{MI}$, $1 \le H/\overline{H} < \sqrt{2}$ and $1 \le H/\overline{H} < 2$ $(H \ge \overline{H})$. □

Conclusion 3. In the backward supply chain, when $1 \le T/\overline{T} < \sqrt{2}$, the profits of manufacturers and retailers when they choose self-supporting logistics are greater than those when they choose outsourcing logistics. When $\sqrt{2} \le T/\overline{T} < 2$, the profit of the manufacturer when choosing self-supporting logistics is greater than that when choosing logistics outsourcing, but the retailer has a high profit when choosing logistics outsourcing. When $T/\overline{T} \ge 2$, the profit of manufacturers and retailers under the logistics outsourcing mode is greater than that under the logistics self-supporting mode.

Proof. As $\pi_{m2}^{RO} - \pi_{m2}^{RI} = T^2/64\beta - \overline{T}^2/16\beta$, $\pi_{r2}^{RO} - \pi_{r2}^{RI} = T^2/16\beta - \overline{T}^2/8\beta$, when $\pi_{m2}^{RO} \ge \pi_{m2}^{RI}$, $T/\overline{T} \ge 2$, and when $\pi_{r2}^{RO} \ge \pi_{r2}^{RI}$, $T/\overline{T} \ge \sqrt{2}$. On the contrary, when $\pi_{m2}^{RO} < \pi_{m2}^{RI}$, $\pi_{r2}^{RO} < \pi_{r2}^{RI}$, $1 \le T/\overline{T} < 2$ and $1 \le T/\overline{T} < \sqrt{2}$ $(T \ge \overline{T})$. □

5. Numerical Simulation

The logistics mode of the closed-loop supply chain is affected by sales market scale α, recycling market base amount k, consumer price sensitive coefficients β and γ, and

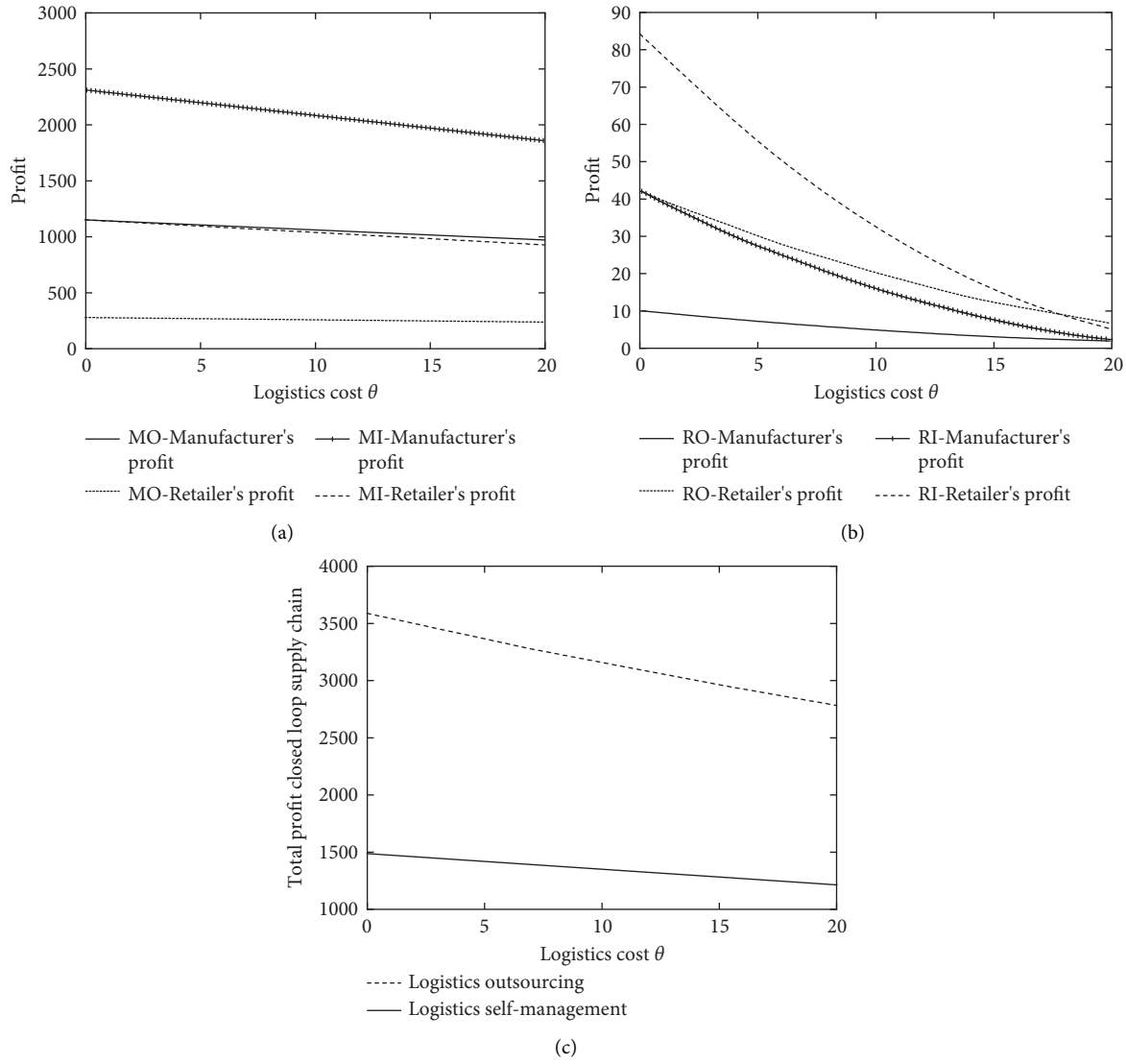

Figure 2: (a) Profit comparison between manufacturers and retailers in the reverse supply chain under different logistics modes ($s = 0.8$). (b) Profit comparison between manufacturers and retailers in the reverse supply chain under different logistics modes ($s = 0.8$). (c) Comparison of total profit of the closed-loop supply chain under different logistics modes ($s = 0.8$).

outsourcing logistics cost ratio s, but the fundamental starting point of choosing logistics outsourcing or self-supporting is to reduce logistics cost θ and thereby improve the profits of enterprises. Therefore, this paper starts from the perspective of logistics cost θ, and the decision-making of the closed-loop supply chain is explored based on the proportion s of self-operated logistics and outsourcing logistics costs. The optimal equilibrium solutions under different closed-loop supply chain modes are obtained through numerical simulation, and then the analysis and comparison are carried out.

To simplify the model and facilitate the analysis, the corresponding parameters are assigned as follows: the marginal cost per unit of the manufacturer's production is $c_m = 8$ and the marginal cost per unit of manufacturer remanufacturing is $c_m' = 2$, so the cost saved by remanufacturing is $\Delta = c_m - c_m' = 6$, $\alpha = 100$, $k = 20$, $\beta = 0.5$, $\gamma = 1$, $Q = 100 - 0.5p_r$, and $\overline{Q} = 20 + h_r$. In this paper, the values when $s = 0.8$, $s = 0.5$, and $s = 0.2$ are selected and the analysis results are shown in Figures 2–4.

It can be seen from Figures 2(a), 3(a), and 4(a) that, in the forward closed-loop supply chain, as the logistics cost θ increases, the profits of manufacturers and retailers under different logistics modes will gradually decrease. When the logistics cost is very low, the profits of manufacturers and retailers when selecting the logistics outsourcing mode are lower than those when selecting the logistics self-supporting mode, and manufacturers and retailers are more willing to accept the self-supporting logistics mode. However, as the logistics cost θ rises, although the profits of manufacturers and retailers choosing logistics outsourcing and logistics self-supporting modes all decline, the decline speed of the profits under the logistics outsourcing mode is far less than that under the logistics self-supporting mode,

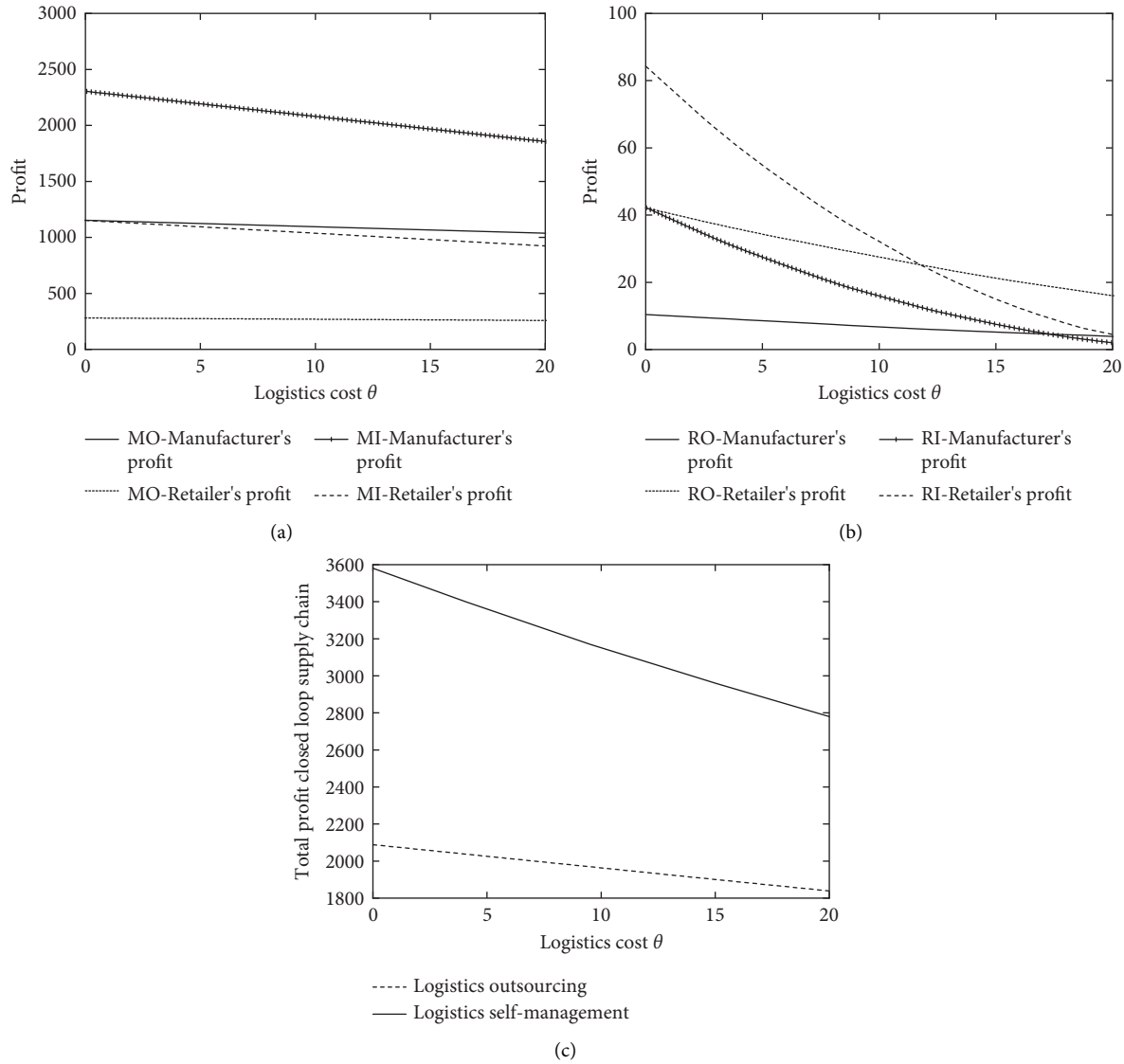

Figure 3: (a) Profit comparison between manufacturers and retailers in the reverse supply chain under different logistics modes ($s = 0.5$). (b) Profit comparison between manufacturers and retailers in the reverse supply chain under different logistics modes ($s = 0.5$). (c) Comparison of total profit of the closed-loop supply chain under different logistics modes ($s = 0.5$).

which means that when the logistics cost is very high, the advantages of logistics outsourcing are very outstanding, so at this time, it is better to choose logistics outsourcing. Similarly, in the backward supply chain, according to Figures 2(b), 3(b), and 4(b), it can be known that, under different values of s, when the logistics cost rises slowly, the economic benefits of logistics outsourcing become more obvious, and enterprises are more willing to choose the outsourcing logistics mode.

This is consistent with the reality. Generally, supply chain companies are in the period of business growth. Due to the small business volume, the logistics and transportation of goods between manufacturers and retailers will choose the self-operated logistics mode, which is highly flexible and convenient. However, as the business volume of the enterprise increases, the circulation pressure borne by the own logistics team increases, the original logistics investment cannot meet the existing business volume, and the logistics cost will continue to rise. At this time, logistics outsourcing can effectively relieve the operating pressure of enterprises. At the same time, allowing a professional logistics team to operate will improve efficiency, which can effectively reduce logistics costs and achieve a win-win situation.

According to Figures 2(c), 3(c), and 4(c), it can be found that the total profit of the closed-loop supply chain decreases with the increase of logistics cost, which is consistent with the willingness of enterprises to reduce logistics cost vigorously in reality. In the comparison of logistics outsourcing and logistics self-supporting, it can be found when the logistics cost is low, the total profit of the closed-loop supply chain when selecting logistics outsourcing is far lower than that when selecting logistics self-supporting, which suggests that, under the low logistics cost, logistics outsourcing cannot bring enough profits to enterprises in the supply

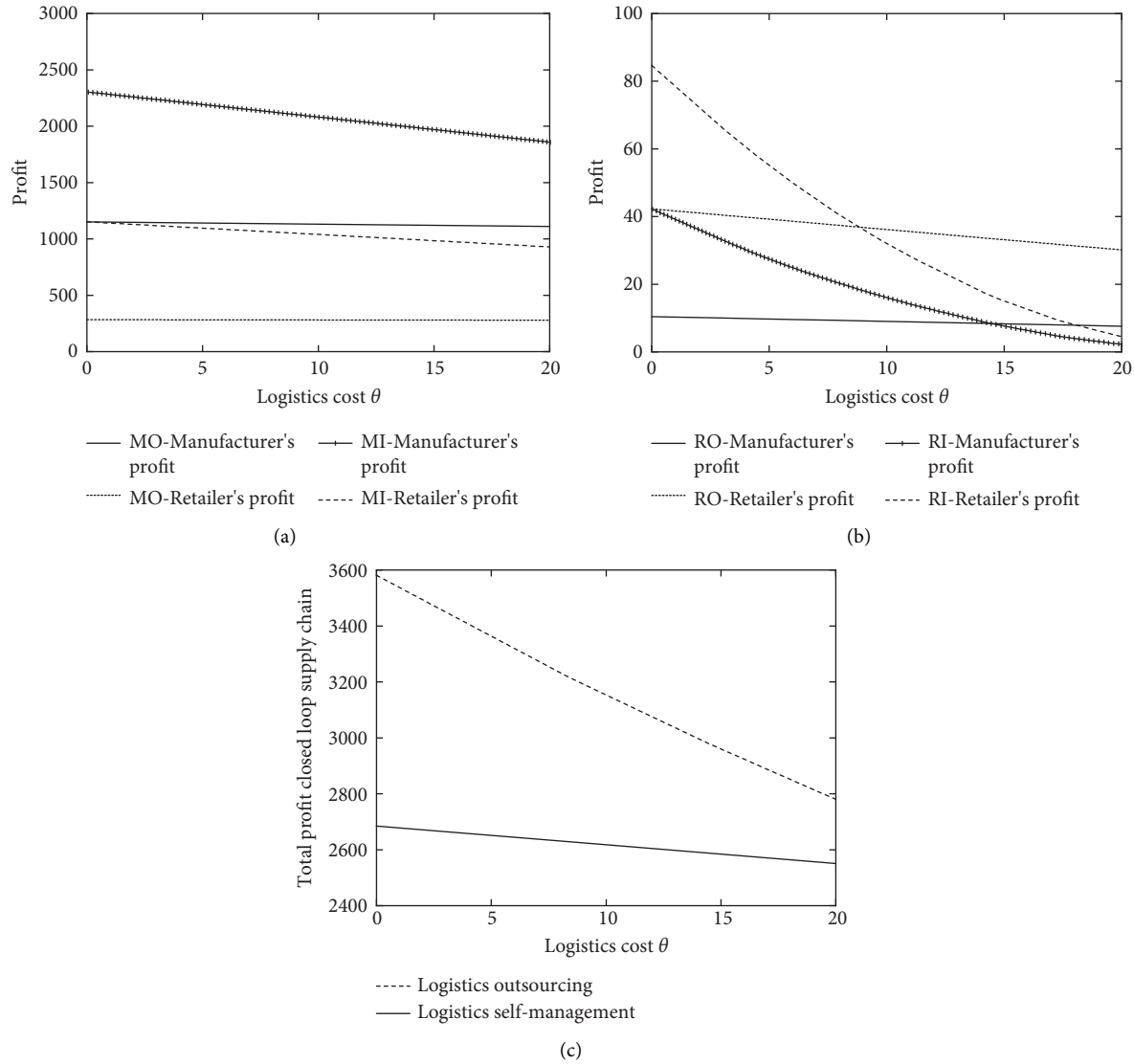

Figure 4: (a) Profit comparison between manufacturers and retailers in the reverse supply chain under different logistics modes ($s = 0.2$). (b) Profit comparison between manufacturers and retailers in the reverse supply chain under different logistics modes ($s = 0.2$). (c) Comparison of total profit of the closed-loop supply chain under different logistics modes ($s = 0.2$).

chain, and on the contrary, self-supporting logistics can make enterprises gain more profits. As can be seen from the straight downward trend in the figure, when the logistics cost is high enough, no matter what the value of s is, the profit of logistics outsourcing will gradually exceed that of self-supporting logistics, and at this time, the professionalism and scale of logistics outsourcing will be reflected.

As a whole, at different levels of s, with the increase of logistics cost θ, both the forward product demand and the reverse backward product recovery will decrease when the logistics cost increases, regardless of the self-supporting logistics mode or the logistics outsourcing mode. This is because logistics cost, as the main component of enterprise circulation (including recycling) cost, directly affects products' sales (recycling) price, thus further influencing the profits of enterprises. The high cost of self-supporting logistics will increase the burden of manufacturing enterprises or retail enterprises, which will lead to enterprises preferring the logistics outsourcing mode.

For the overall closed-loop supply chain, the level of logistics costs will affect the total profit of the overall supply chain. Pursuing the maximization of the overall profit of the closed-loop supply chain, it is necessary to take into account the profits of each subject in the closed-loop supply chain. At this time, how to control the logistics cost becomes an effective way to expand the profit. When the logistics cost is low, choosing the self-operated logistics mode is beneficial to reducing the total cost of the closed-loop supply chain, thereby increasing the profit of the closed-loop supply chain. Scale and specialization improve the efficiency of the overall

closed-loop supply chain, which can also achieve the goal of reducing costs and increasing efficiency in the closed-loop supply chain.

6. Conclusion

In this paper, a closed-loop supply chain structure of a single manufacturer and retailer was constructed, in which the forward supply chain is dominated by the manufacturer, while the backward supply chain is dominated by the seller. By considering logistics outsourcing and logistics self-supporting modes simultaneously, the impact of choosing a logistics mode for the supply chain under a hybrid dominant mode on the pricing decisions of manufacturers and retailers was studied. Based on the analysis of market demand, recycling volume, and profits of manufacturers and retailers under the two logistics modes, which logistics mode was more reasonable under different leading enterprises in the forward and backward supply chains was analyzed, and numerical simulation was used to verify the conclusions. The conclusions are as follows:

(1) Decision-making when market demand and recovery volume are the largest: In the forward supply chain link, when $H/\overline{H} \geq 2$, logistics outsourcing is superior to logistics self-supporting; when $1 < H/\overline{H} < 2$, logistics self-supporting is better than logistics outsourcing decision. In the backward supply chain, when $T/\overline{T} \geq 2$, logistics outsourcing is superior to logistics self-supporting; when $1 < T/\overline{T} < 2$, logistics self-supporting is better than logistics outsourcing.

(2) Manufacturer's optimal decision: In the forward supply chain, when $1 \leq H/\overline{H} < \sqrt{2}$, the manufacturer had a higher profit when choosing a self-supporting logistics strategy; when $H/\overline{H} \geq \sqrt{2}$, the manufacturer had a higher profit when choosing logistics outsourcing. In the backward supply chain, the manufacturer had a higher profit when choosing the logistics outsourcing mode; when $1 \leq T/\overline{T} < 2$, the manufacturer had a higher profit when choosing the logistics self-supporting mode.

(3) Retailer's optimal decision: In the forward supply chain, when $1 \leq H/\overline{H} < 2$, the manufacturer had a higher profit when choosing a self-supporting logistics strategy; when $H/\overline{H} \geq 2$, the manufacturer had a higher profit when choosing logistics outsourcing. In the backward supply chain, when $T/\overline{T} \geq \sqrt{2}$, the manufacturer had a higher profit when choosing the logistics outsourcing mode; when $1 \leq T/\overline{T} < \sqrt{2}$, the manufacturer had a higher profit when choosing the logistics self-supporting mode.

As the decision-making of the forward supply chain and backward supply chain is dominated by different enterprises, the forward supply chain and backward supply chain can be seen as two separate supply chains. The decision is made according to the optimal combination, and the closed-loop supply chain eventually formed can be a closed-loop supply chain outsourcing and whole self-supporting, which also can be said to make the forward supply chain outsourcing and the backward supply chain self-supporting, and the principle is to maximize corporate profits.

Future research can be carried out from the following perspectives: on the one hand, the decision-making problem of the closed-loop supply chain under uncertain market demand should be studied, and at the same time, the choice mode of logistics mode under two-way and dual-channel, namely, two-way sales channel and two-way recovery channel, should be further studied; on the other hand, the closed-loop supply chain constructed by a single manufacturer and a single retailer should be extended to a competitive closed-loop supply chain constituted by multiple manufacturers and multiple retailers, and carrying out an in-depth study on this type of supply chain decision-making will have stronger theoretical and practical significance.

Data Availability

The experimental data used to support the findings of this study are available from the corresponding author upon request.

Conflicts of Interest

The authors declare that there are no conflicts of interest.

Acknowledgments

This work was supported by the Fujian Southwest Collaborative Development Platform for Interworking Smart Logistics Project (No. 2021FX06) and Fujian University Application Technology Engineering Center of E-Commerce project (No. DZSW22-05).

References

[1] R. C. Savaskan, S. Bhattacharya, and L. N. V. Wassenhove, "Closed-loop supply chain models with product remanufacturing," *Management Science*, vol. 50, no. 2, pp. 239–252, 2004.

[2] Y. Lu, X. Xu, and X. Ai, "Research on double channel recovery decision of closed-loop supply chain under the third-party scale effect," *Journal of Management in Engineering*, vol. 32, no. 2, p. 11, 2018.

[3] R. C. Savaskan and L. N. V. Wassenhove, "Reverse channel design: the case of competing retailers," *Management Science*, vol. 52, no. 1, pp. 1–14, 2006.

[4] X. Han, "Decision analysis of recycling channel in closed-loop supply Chain with uncertainty," *Industrial Technical Economics*, vol. 29, no. 02, pp. 20-21, 2010.

[5] P. Gao, Z. Xie, and Y. Xie, "Collaboration mechanism of closed-loop supply Chain led by retailer under asymmetric information," *Industrial Engineering*, vol. 16, no. 01, pp. 79–85, 2013.

[6] Y. D. Gong, "Optimal combination of dominant mode and recycling mode and supply chain stability," *Journal of Systems Engineering*, vol. 29, no. 1, pp. 85–95, 2014.

[7] Y. Gong and Q. Da, "Research on combination of closed-loop Supply chain dominant mode and logistics service," *Journal of Management Science*, vol. 18, no. 10, pp. 14–25, 2015, (in Chinese).

[8] F. Zhang, Q. Da, and Y. Gong, "Research on logistics strategy and subsidy mechanism of closed-loop supply chain considering different two-way dominance," *China management science*, vol. 24, no. 10, pp. 44–51, 2016, (in Chinese).

[9] I. Karakayali, H. Emir-Farinas, and E. Akcali, "An analysis of decentralized collection and processing of end of life products," *Journal of Operations Management*, vol. 25, no. 6, pp. 1161–1183, 2007.

[10] W. M. Ma, Z. Zhao, and H. Ke, "Dual-channel closed-loop supply chain with government consumption-subsidy," *European Journal of Operational Research*, vol. 226, no. 2, pp. 221–227, 2013.

[11] J. Gao, H. Han, L. Hou, and H. Wang, "Pricing and effort decisions in a closed-loop supply chain under different channel power structures," *Journal of Cleaner Production*, vol. 112, pp. 2043–2057, 2016.

[12] G. Liu and W. Liu, "Dual-channel remanufacturing closed-loop supply Chain differential pricing strategy," *Chinese Journal of Management*, vol. 14, no. 4, pp. 625–632, 2017.

[13] J. Sun, C. Teng, and Z. Chen, "Channel selection model of remanufacturing closed-loop supply chain based on recovery price and sales quantity," *Systems Engineering Theory & Practice*, vol. 33, no. 12, pp. 3079–3086, 2013.

[14] J. Lin and K. Cao, "Pricing model of closed-loop supply chain under dual channel competition environment," *Systems engineering theory & practice*, vol. 34, no. 6, pp. 1416–1424, 2014.

[15] J. Xie, L. Liang, and Y. Li, "Research on Revenue sharing contract mechanism strategy in closed-loop supply chain," *Journal of Management in Engineering*, vol. 31, no. 2, pp. 185–193, 2017, (in Chinese).

[16] B. Ding and H. Ma, "Decision-making and performance analysis of s-m closed-loop supply chain based on two-stage remanufacturing," *Chinese journal of management science*, vol. 23, no. 06, pp. 118–125, 2015.

[17] H. Xu, Z. Z. Liu, and S. H. Zhang, "A strategic analysis of dual-channel supply chain design with price and delivery lead time considerations," *International Journal of Production Economics*, 2012.

[18] K. Matsui, "When should a manufacturer set its direct price and wholesale price in dual-channel supply chains?" *European Journal of Operational Research*, vol. 258, no. 2, pp. 501–511, 2017.

[19] R. Batarfi, M. Y. Jaber, and S. Zanoni, "Dual-channel supply chain: a strategy to maximize profit," *Applied Mathematical Modelling*, vol. 40, no. 21-22, pp. 9454–9473, 2016.

[20] Q. Meng, M. Li, W. Liu, Z. Li, and J. Zhang, "Pricing policies of dual-channel green supply chain: considering government subsidies and consumers' dual preferences," *Sustainable Production and Consumption*, vol. 26, no. 6, pp. 1021–1030, 2021.

[21] C. Zhang, Y. Liu, and G. Han, "Two-stage pricing strategies of a dual-channel supply chain considering public green preference," *Computers & Industrial Engineering*, vol. 151, no. 6, p. 106988, 2021.

[22] C. Zhang and X. Zheng, "Customization strategies between online and offline retailers," *Omega*, vol. 100, no. 1, p. 102230, 2021.

[23] R. H. Niu, X. Zhao, I. Castillo, and T. Joro, "Pricing and inventory strategies for a two-stage dual-channel supply chain," *Asia Pacific Journal of Operational Research*, vol. 29, no. 1, pp. 409–340, 2012.

[24] B. Yan, T. Wang, Y. P. Liu, and Y. Liu, "Decision analysis of retailer-dominated dual-channel supply chain considering cost misreporting," *International Journal of Production Economics*, vol. 178, pp. 34–41, 2016.

[25] F. Soleimani, A. A. Khamseh, and B. Naderi, "Optimal decisions in a dual-channel supply chain under simultaneous demand and production cost disruptions," *Annals of Operations Research*, vol. 243, no. 1-2, pp. 301–321, 2016.

[26] B. Zheng, C. Yang, and C. Liu, "Impact of cost allocation on manufacturer Recycling closed-loop supply Chain," *Systems Engineering Theory & Practice*, vol. 37, no. 9, pp. 2344–2354, 2017.

[27] Y. Huang, H. Sun, and Q. Da, "Research on pricing and production strategy of closed-loop supply chain based on product life cycle in competitive environment of manufacturers," *China Management Science*, vol. 21, no. 3, pp. 96–103, 2013.

[28] J. Ge, P. Huang, and Z. Wang, "Coordination problem of closed-loop supply chain based on game theory," *Journal of Systems Management*, vol. 16, no. 5, pp. 549–552, 2007.

Hindawi
Computational Intelligence and Neuroscience
Volume 2022, Article ID 2519035, 10 pages
https://doi.org/10.1155/2022/2519035

Research Article

Forecasting Slope Displacement of the Agricultural Mountainous Area Based on the ACO-SVM Model

Juan Chen,[1] **Yiliang Wei**,[2] **and Xiaohui Ma**[1]

[1]*Shanxi Vocational University of Engineering Science and Technology, Taiyuan 030031, Shanxi, China*
[2]*Taiyuan Design Institute of Railway Engineering Consulting Group Co Ltd, Taiyuan 030000, Shanxi, China*

Correspondence should be addressed to Juan Chen; chenjuan3@sxgkd.edu.cn

Received 15 July 2022; Accepted 6 September 2022; Published 29 September 2022

Academic Editor: Zaoli Yang

Due to the combined influence of complex engineering geological conditions and environmental factors from agricultural mountainous areas, the evolution of slope deformation is complicated and nonlinear. Support vector machine (SVM) technology could effectively solve the technical problems of small sample, high dimension, and nonlinear, so it is applied to data mining of the measured slope displacement and the prediction and analysis of the slope deformation trend. In order to avoid blindness of human choice of SVM parameters and to improve the prediction accuracy and generalization ability of the model, an ACO-SVM model is built by adopting an improved ant colony algorithm (ACO) to optimize parameters in association with the rolling forecasting method of displacement time series. The model was applied to two engineering examples. The research results showed that the ACO-SVM model was correct with high accuracy. The ACO-SVM model had higher accuracy of prediction and stronger generalization ability than optimizing SVM based on the genetic algorithm or particle swarm optimization. The forecasting results were more reasonable. It has certain engineering application values for slope deformation prediction.

1. Introduction

Landslides are one of the most harmful natural disasters in the world and pose a serious threat to human beings and society. Monitoring and early warning of the slope displacement is the main technical means to avoid this hazard [1]. According to the displacement monitoring data, the future evolution and regular development trend of the slope will be predicted. It is of great significance to grasp the slope deformation law for engineering management in the future. At present, the prediction methods of displacement of time series mainly include time series analysis, grey system, artificial neural network, support vector machine (SVM), and various combinations of prediction methods [2]. In all methods, time series analysis is difficult to determine the parameter of an autocorrelation coefficient r, a partial correlation coefficient q, and reasonable identification to the model. The grey system is mainly suitable for the time series of exponentials, and the prediction results often have large errors for complex nonlinear slope displacement series [3]. An artificial neural network is based on the heuristic algorithm, and its disadvantage is that there is no complete theoretical basis. When the number of samples is limited, it is difficult to guarantee the accuracy, while when there are many learning samples, it is easy to fall into the dimension disaster, and the generalization ability of the algorithm is not high. A support vector machine (SVM) based on the principle of structural risk minimization has strong generalization ability and effectively solves problems such as small sample, high dimension, and nonlinear. SVM can realize adaptive decomposition according to the data scale and obtain the displacement of the trend term, periodic term, and random term by setting a static component, which has the advantages of high decomposition precision, strong robustness, and clear physical meaning.

One of the outstanding problems of SVM is that it is difficult to determine the parameters of penalty parameter C and kernel function γ and the accuracy of SVM is directly related to the ability of model prediction and generalization. Previous studies have conducted a lot of research on the

optimization of SVM model parameters, mainly involving metaheuristic algorithms, such as the simulation of the living habits of the American monarch butterfly, and the monarch butterfly optimization (MBO) [4] migration operator biased to local search. A slime mould algorithm (SMA) [5] was proposed based on the oscillating predation behavior of slime mould individuals. Proposed by Al-Attar Ali Mohamed in 2016, a moth swarm algorithm (MSA) [6] was designed inspired by the photo taxis and flight patterns of moths. Hunger games search (HGS) [6] based on animal hunger-driven activities and behavior was proposed. The Runge–Kutta method (RUN) is a high-precision single-step algorithm widely used in engineering. Kok Meng of Malaysia proposed the swarm predation algorithm (CPA) [6] in 2020, inspired by how carnivorous plants adapt to harsh environments such as insect hunting and pollination. The weighted mean of vectors algorithm (INFO) is a new intelligent optimization algorithm proposed in 2022, which achieves optimization through different weighted average rules of vectors. Harris hawks optimization (HHO) [7] is a swarm optimization algorithm proposed by Heidari in 2019, which simulates the predation behavior of Harris hawks. Ant colony optimization (ACO) is a new method to simulate biological evolution and has the advantages of parallel computing, positive feedback searching, and good adaptability [8]. The feature parameter dimension of parameter data in an SVM model is higher. In order to avoid "dimension disaster," overfitting phenomenon, and improve the classification accuracy and efficiency of the model, feature selection is necessary. Feature selection is essentially a combinatorial optimization problem, so an ACO algorithm can be used to reduce dimension.

In this paper, the improved ant colony optimization algorithm is proposed on the basis of existing research, and support vector machine (SVM) technology is used to optimize the prediction model so as to reduce the blindness of model parameter selection. This technique is applied to slope monitoring, displacement training and learning, and rolling prediction of displacement change time sequences [9]. In this paper, several commonly used algorithms and the improved ACO-SVM are applied to slope treatment technology, and the efficiency of the algorithm is analysed and compared; in the end, the superiority of the improved ACO-SVM is verified. The specific research work includes the following three aspects: (1) monitoring the changes of horizontal displacement data of slope of a hydropower station and determining monitoring parameters; (2) based on the improved ACO-SVM algorithm model, the slope stability is analysed; (3) the slope displacement is predicted and analysed based on the improved algorithm model. The improved ACO-SVM model has higher prediction accuracy, stronger generalization ability, and more reasonable prediction results, which has certain engineering application values in slope deformation prediction.

2. Materials and Methods

2.1. Research Status of Slope Deformation. In recent years, slope deformation accidents caused by engineering construction, earthquakes, and rainfall have occurred in many places in China. Many scholars in the world have performed relevant work. For example, a GM (1, 1) model was successfully applied to the north slope of a tunnel by using the grey system model for beneficial exploration [10]. Combining the relevant scientific knowledge with traditional grey theory, the unbiased grey fuzzy Markov prediction model is constructed and applied to the slope displacement prediction of a mine. The least-squares support vector machine and radial basis kernel function were used to train and predict slope data, and the optimal model parameters were found by a quantum particle swarm optimization algorithm [11].The results show that the prediction accuracy is improved. Numerical simulation and slope stability analysis were used to evaluate and predict the high slope stability of tailings. The Gaussian kernel function and polynomial kernel function were combined to construct the mixed kernel function, and the particle swarm optimization algorithm was applied to find the best parameters of the least-squares support vector machine [12]. Finally, the PSO-LSSVM model of the slope displacement sequence was established, and it was applied to the left bank slope data of a hydropower station [13]. After the slope stability parameters were determined, the limit equilibrium method and discrete element numerical simulation were adopted to analyse the stability and failure mode of the open-pit mine slope [14, 15]. Considering six influencing factors of the research object, the slope stability of an open-pit mine could be judged and calculated by gene expression. Tan et al. proposed a new method to measure slope stability, which is to calculate the permanent displacement of slope by the stiffness reduction method [16].

It can be seen that there are many factors affecting slope deformation, and some models have to take many factors into account in slope prediction, which undoubtedly increases the difficulty of slope deformation prediction [17].

2.2. Support Vector Machine Regression Prediction Model. SVM is a small sample intelligent learning algorithm proposed by Vapnik based on statistical theory. This algorithm uses kernel snapping from transforming the known space to higher dimensional space through nonlinear mapping so that the samples of higher dimensional space could be linearly separable [3].

For the regression problem, let the training sample set be expressed as $\{(x_i, y_i)|x_i \in R_d, I = 1, 2, ..., n\}$, x_i is the d-dimensional vector of input, y_i is the output value, R is the set space of all real numbers, and n is the number of samples. Make nonlinear mapping: $R_d \longrightarrow H$, where is a high-dimensional feature mapping and H is a high-dimensional feature space, and we construct the optimal decision function in this feature space, the formula is as follows:

$$y(x) = w\varphi(x_i) + b, \tag{1}$$

In the formula, w is the weight vector in an H space and b is the offset term. The fitting error and the insensitive function ε are considered, and the relaxation factors and are introduced to minimize the objective function (2) of the error.

$$J(x_i, \xi_i, \xi_i^*) = \frac{1}{2} w.w^T + C \sum_{i=1}^{n} (\xi_i + \xi_i^*). \quad (2)$$

In formula (2), C is the penalty parameter and $(C > 0)$ is the sample penalty beyond ε. The constraint condition of formula (2) is as follows:

$$\begin{cases} y_i - w \bullet \varphi(x_i) - b \le \xi_i + \varepsilon, \\ w.\varphi(x_i) + b - y_i \le \varepsilon + \xi_i^*, \\ \xi_i \ge 0, \xi_i^* \ge 0. \end{cases} \quad (3)$$

Aiming at the convex quadratic optimization problem, the Lagrange function is introduced for partial differentiation so as to obtain the dual form of the optimization target and the maximization function.

$$W(\alpha, \alpha^*) = -\frac{1}{2} \sum_{i,j=1}^{n} (\alpha_i - \alpha_i^*)(\alpha_j - \alpha_j^*)(x_i \bullet x_j) + \sum_{i=1}^{n} (\alpha_i - \alpha_i^*) y_i - \sum_{i=1}^{n} (\alpha_i - \alpha_i^*) \varepsilon. \quad (4)$$

The constraint condition is as follows:

$$\begin{cases} \sum_{i=1}^{n} (\alpha_i + \alpha_i^*) = 0, \\ 0 \le \alpha_i, \alpha_i^* \le C. \end{cases} \quad (5)$$

In formula (5), α and α^* are Lagrange multipliers. In the dual problem, the optimization of the objective function only involves the inner product operation between training samples $(x_{i,} y_j)$, so the inner product operation is actually carried out in higher dimensions. This operation can be realized by using the functions in the original space. According to functional theory, as long as a kernel function $K(x_{i,} y_j)$ satisfies the Mercer condition, it will correspond to the inner product of the spatial transformation. SVM constructed by different kernel functions is different [18].The key point of SVM classification lies in the construction and selection of kernel functions. Appropriate kernel functions can effectively solve the problem of dimension disasters in a high-dimensional space and reduce the complexity of calculation in a high-dimensional space. There are four kernel functions commonly used in SVM: linear kernel function, polynomial kernel function, RBF kernel function, and sigmoid kernel function. When the ACO-SVM model is used, the accuracy of parameter selection and the classification time are taken as the effective indexes to evaluate the parameter model. In order to make the results more close to its real performance, a grid optimization method and cross validation of ten-fold are adopted. It can be found from Figure 1 that the ACO-SVM model has the highest efficiency when an RBF kernel function is adopted, and no matter which kernel function is adopted, its accuracy is improved compared with SVM classification directly. Specifically, when linear, polynomial, RBF, and sigmoid kernel functions are adopted, accuracy increases by 1.6%, 3.34%, 2.5%, and 2.5%, respectively. As can be seen from Table 1, in terms of selection efficiency, no matter which kernel function is used, the classification efficiency of the ACO-SVM model is significantly improved compared with that of direct selection, indicating that the ACO-SVM selection model is very effective for slope displacement prediction. Its expression is as follows:

$$K(x_{i,} y_j) = \exp\left(-\gamma \left\| x_i - y_j \right\|^2\right). \quad (6)$$

Then, formula (4) can be converted to the following formula, which is expressed as follows:

$$W(\alpha, \alpha^*) = -\frac{1}{2} \sum_{i,j=1}^{n} (\alpha_i - \alpha_i^*)(\alpha_j - \alpha_j^*) K(x_i \bullet x_j) + \sum_{i=1}^{n} (\alpha_i - \alpha_i^*) y_i - \sum_{i=1}^{n} (\alpha_i - \alpha_i^*) \varepsilon, \quad (7)$$

$w = \sum_{i=1}^{n} (\alpha_i - \alpha_i^*) \varphi(x_i)$, and solving the convex quadratic programming problem to nonlinear mapping is represented by the following formula:

$$y(x) = \sum_{i=1}^{n} (\alpha_i - \alpha_i^*) K(x_i \bullet x_j) + b. \quad (8)$$

From (5) and (6), it can be seen that the parameters in penalty functions C and $K(x_i \bullet x_j)$ kernel functions in support vector machines have great influence on the generalization ability and calculation efficiency of the algorithm. Generally, it is blind and inefficient to determine two parameters manually. Based on the situation, the paper uses the ant colony algorithm (ACO) to search for parameters to find the optimal support vector machine parameters [14].

2.3. Continuous Domain's Ant Colony Algorithm. The ant colony algorithm (ACO) is a new intelligent optimization algorithm proposed by Italian scholar Dorigo in the early 1990s [19]. The algorithm was first used to solve the discreteness optimization problem. The optimization of support vector machine parameters is to solve the problem of continuous domains. In this paper, the ant colony algorithm is improved by optimizing parameters of continuous domain model, and the model parameters of the continuous domain are optimized. The key factors of the ant colony algorithm are the movement rule and pheromone update. The ant colony searches for positive feedback of volatile accumulation of pheromone and selects the optimal path [20].

Suppose the objective function of the continuous field is as follows:

$$\begin{cases} \min Q = f(x), x = (x_1, x_2, \cdots, x_D), \\ x_b^1 \le x_b \le x_b^u; b = 1, 2, \cdots, D. \end{cases} \quad (9)$$

In the formula, xu/b and $x1/b$ are the upper and lower limits of the independent variable x_b and D is the number of independent variables. The search optimization steps for formula (9) by using the ant colony algorithm are as follows:

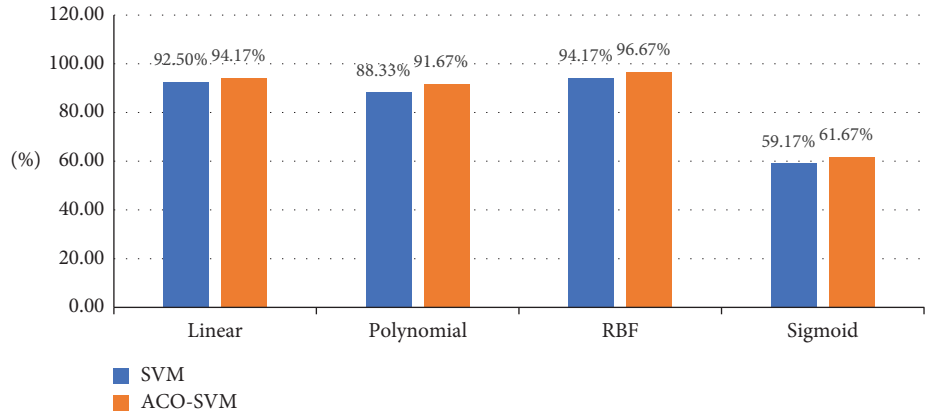

Figure 1: Comparison of model selection accuracy with four different kernel functions.

Table 1: Comparison of model classification efficiency using four different kernel functions.

Classification model	Time (s)			
	Linear	Polynomial	RBF	Sigmoid
SVM	183.39	148.22	170.48	159.21
ACO-SVM	7.37	7.6	7.17	7.01

(1) Ant colony initialization. The ant colony size is set as N, the number of cycles is K, and the ant colony is randomly distributed in the optimization space [21]. As the starting point for each ant to search, the continuous domain is discretized into a number of intervals, and the length matrix of each variable quantum interval is expressed as formula:

$$\mathrm{Len}(b) = \frac{x_b^1 - x_b^u}{N} \tag{10}$$

According to the current location situation of ants and different types of optimization goals, we make sure the initial pheromone concentration vector $\mathrm{T}(i)$ of the ant i is as follows:

$$\mathrm{T}(i) = \exp(-f(x_i)). \tag{11}$$

In formula (11), $x_i = xi/1, xi/2, \cdots, xi/j, \cdots, xi/D$, $i = 1, 2, \cdots, N$, N is the initial position of the ant i. From formula (10), it can be known that the target function value $f(x_i)$ is smaller, and more pheromones are left by the position x_i of the ant i.

(2) Movement rules of ant colony: When all ants complete searching, they will start the next searching according to the corresponding movement rules. In the paper, the dynamic global selection factor and the dynamic volatile factor are introduced to improve the global searching ability [22].

The basic rules of searching: After the ant colony completes a cycle, one ant will find the optimal solution of the cycle, namely, the head ant, and its position is x leader. The other ants in the next cycle will use the head ant position as the target for transfer searching, which is called global search. The leader with the optimal solution is randomly searched in the neighbourhood to obtain a better solution, which is called local searching [23]. The transfer probability of the ant i at the position $x_i (i = 1, 2, \ldots, N, i \neq \text{leader})$ to the position x_{leader} of the head ant is $P(i)$:

$$P(i) = \frac{\exp(T(\text{leader}) - T(i))}{\exp(T(\text{leader}))}. \tag{12}$$

In formula (12), $\tau(\text{leader})$ is a t pheromone concentration of the first ant's location and $\tau(i)$ is a pheromone concentration of the location of the ant i.

In the global searching, the selection factor of the dynamic global P_0 is introduced into the step size transferred from the ant i to the optimal solution position x_{leader}. The specific expression is

$$x_i = \begin{cases} (1-\lambda)x_i + \lambda \mathrm{x}_{\text{leader}} P(i) < P_0, \\ x_i + \mathrm{ran\,d}(-1, 1) \times \mathrm{Len} P(i) \geq P_0. \end{cases} \tag{13}$$

The local searching is a random searching in the x_{leader} neighborhood of the ant leader. Let the new search location be x_{temp}. If x_{temp} is better than x_{leader}, we replace x_{leader} with x_{temp}. Otherwise, we keep the original location. In order to obtain the optimal solution of later fine searching, the step size is introduced to update a parameter w, so the searching step size decreases with the increase of iteration times.

Specifically, it is expressed as follows:

$$x_{\text{leader}} = \begin{cases} x_{\text{temp}}, T(\text{leader}) < T(\text{temp}), \\ x_{\text{leader}}, else. \end{cases} \tag{14}$$

In formula (14), $\tau(\text{temp})$ is a pheromone concentration of the ant location x_{temp}.

$$x_{\text{temp}} = \begin{cases} x_{\text{leader}} + w \times \text{step}, \mathrm{ran\,d}(1) < 0.5, \\ x_{\text{leader}} - w \times \text{step}, \text{else}, \end{cases} \tag{15}$$

In formula (15), step = 0.1 × rand(D, N, K) is the local search step size, and the w step size updating rule is as follows:

$$w = w_{\max} - (w_{\max} - w_{\min})\frac{k}{K}. \tag{16}$$

In formula (16), $w_{\max}$ an d $w_{\min}$ are the initial setting values, generally $w_{\min} \in (0.2, 0.8)$ and $w_{\max} \in (1.2, 1.4)$; k is an iteration number of the current ant colony; K is the maximum iteration number of the ant colony.

(3) Pheromone updating rules. In the completion of global searching and local searching, ants will update the pheromone $\tau(i)$ of the location of the ant i. The pheromone updating rules can be expressed as follows:

$$T(i) = (1 - \rho)T(i) + \Delta T(i). \tag{17}$$

In formula (17), $\Delta T(i)$ is a pheromone increment and $\Delta T(i) = \exp(-f(x_i))$. ρ is a pheromone volatilization factor ($\rho \in (0,1)$) and, and the dynamic change is first small and then large with the number of iterations. The reason is to expand the global searching capability in the early stage and accelerate the convergence rate in the later stage.

2.4. Slope Displacement Prediction. The comprehensive prediction model of the slope displacement needs to consider emphatically:(1) how to choose the influencing factors of the slope displacement and the corresponding relationship between them and the slope displacement; (2) how to realize the time series decomposition of the slope displacement and whether the decomposition quantity has physical significance; (3) construction of an efficient and reliable slope displacement prediction model [24]. The combination of three methods can effectively improve the accuracy of slope displacement prediction. In order to obtain the random term of the slope displacement, the commonly used methods include empirical mode decomposition (EMD), ensemble empirical mode decomposition (EEMD), and wavelet analysis. However, their decomposition components are usually more than five, and the physical meaning represented by each component is difficult to understand [25]. To solve the above problems, SVM is used to extract the displacement component of slope random terms. SVM can achieve adaptive decomposition according to the data scale and obtain the displacement of the trend term, periodic term, and random term by setting the modal component, which has the advantages of high decomposition accuracy, strong robustness, and clear physical meaning. Therefore, SVM can be combined with time sequence analysis to achieve effective extraction of a random term displacement. In this process, the optimal decomposition parameters can be further determined by introducing an ACO algorithm. The double exponential smoothing (DES) method was used to predict the trend term displacement [26]. As a special weighted moving average method, DES is more suitable for the prediction of time series with a certain trend. Its characteristic is that the weight of the latest data is higher than that of early data, and the factor of this weight decreases exponentially with aging of data, taking into account the timeliness of landslide displacement data.

The abovementioned ant colony algorithm is used to optimize the parameter searching in the kernel functions of penalty functions C and $K(x_i, x_j)$ in the support vector machine [27]. First, the objective function is determined as follows:

$$\begin{cases} \min f(C, \gamma) = \sqrt{\dfrac{1}{n}\sum_{i=1}^{n}(z_i - \widehat{z}_i)}, \\ \\ C \in [C_{\min}, C_{\max}], \gamma = [\gamma_{\min}, \gamma_{\max}]. \end{cases} \tag{18}$$

In formula (18), z_i is the measured displacement of its sample and $\widehat{z}_i$ is a predictive value for samples. In formula (8), n is the total number of training samples. Due to the monitoring displacement, $\{x_1, x_2, \ldots, x_n\}$ is a time series, and its phase space is reconstructed to find the $i + p$ time displacement sequence value and the sequence value (x_i, x_{i+1} ...x_{i+p-1}) at the previous p months, namely, $x_{i+p} = g(x_i, x_{i+1}, x_{i+p-1})$. p is the number of historical steps, and g is the nonlinear mapping function. According to SVM theory, the nonlinear relation of displacement time series can be described as follows:

$$\widehat{z}(x_{m+n}) = \sum_{i=1}^{n-p}(\alpha_i - \alpha_i^*) - K(x_{m+n}, x_{i+p}) + b. \tag{19}$$

In formula (19), $\widehat{z}(x_{m+n})$ represents the predicted displacement at time $m + n$; x_{m+n} represents the measured displacement time series value x at p moments before time $m + n$ $x_{m+n} = (x_{m+n-p}, x_{m+n-p+1}, \ldots, x_{m+n-1})$; x_{i+p} represents the measured displacement time series value $x_{i+p} = (x_i, x_{i+1}, \ldots, x_{i+p-1})$ at p moments before the $(i + p)$ moment. It should be noted that the predicted value is used as the training and learning sample of the next prediction. After all, the predicted value is not measured and has a certain range of application. In the actual engineering process, the prediction model can be updated in real time with the acquisition of the monitoring value [16]. In the algorithm model, ACO optimizes the parameters in SVM. The main idea is to search for the smallest set of parameters by defining a set of parameters (C, γ) in the domain as the position vector of ants so that the predicted value can be closer to the monitored value. The specific steps are as follows:

An ACO-SVM prediction model was built based on the deep learning toolbox framework of MATLAB2020a software and completed on the computer with Intel Core I5–9400F CPU and 16G RAM.

(1) According to the monitored displacement data, the historical step size p and the predicted step size m are normalized, learning samples and test samples are established, and the dataset is normalized by min-max.

(2) We set the initialization of the system, including ant colony size N, cycle iteration times K, the value range of the parameter C and γ to be optimized, the number of steps, and the location of the ant. Each position value corresponds to a set of parameters (C, γ).

(3) The optimization support vector machine (SVM) learning prediction model is established based on the theory in Section 2 of this paper, and the corresponding objective function of each ant individual is calculated, as shown in formula (18). Global searching and local searching are conducted, and pheromones are updated to determine the optimal solution.

(4) First, we determine the appropriate number of iterations through multiple iterations and then judge whether the value of the objective function meets the conditions. If the conditions are met, the optimization is finished, and the optimal parameters C and γ are output. Otherwise, we return to step (3).

(5) The optimized parameters C and γ are used to establish a support vector machine (SVM) prediction model to carry out rolling prediction of displacement time series and fulfil engineering prediction requirements.

The process of optimization ACO-SVM for prediction of the slope displacement is shown in Figure 2.

2.5. Model Evaluation Index. The coefficient of determination (R^2) and the root mean square error (RMSE) are often used to evaluate the performance of slope displacement prediction models. Therefore, the performance of the prediction model is analysed based on these indicators, which are defined as follows:

$$R^2 = 1 - \frac{\sum_{t=1}^{N} (y_t - \hat{y}_t)^2}{\sum_{t=1}^{N} (y_t - \overline{y_t})^2}, \tag{20}$$

$$\text{RMSE} = \sqrt{\frac{1}{N} \sum_{t=1}^{N} (y_t - \hat{y}_t)^2}. \tag{21}$$

In formula (20) and (21), t denotes the time, N denotes the predicted time, $y_t$denotes the actual observed value of the landslide displacement, $\hat{y}_t$ denotes the predicted value of the landslide displacement in our model, and $\overline{y_t}$ denotes the average of the observed values of the displacement in the predicted time. The value range of RMSE is $[0, \infty]$, and the smaller the value , the stronger the model fitting ability. The value of R^2 is usually [0, 1], and the larger the value, the better the surface model fitting degree. When the value of RMSE is smaller and the value of R^2 is larger, the prediction effect of the model is better.

3. Algorithm Application

3.1. Shallow Deformation Prediction of the Left Bank Slope of the Hydropower Station. In the paper, the improved ant colony algorithm is used to optimize the support vector machine (ACO-SVM) to predict the displacement of the monitoring displacement sequence of the slope in reference 10. Monitoring data are the orifice displacement of the M4-7 multipoint displacement meter (elevation 1886 m) of the left bank cable crane platform slope at the exposed part of f42-9 fault[10].

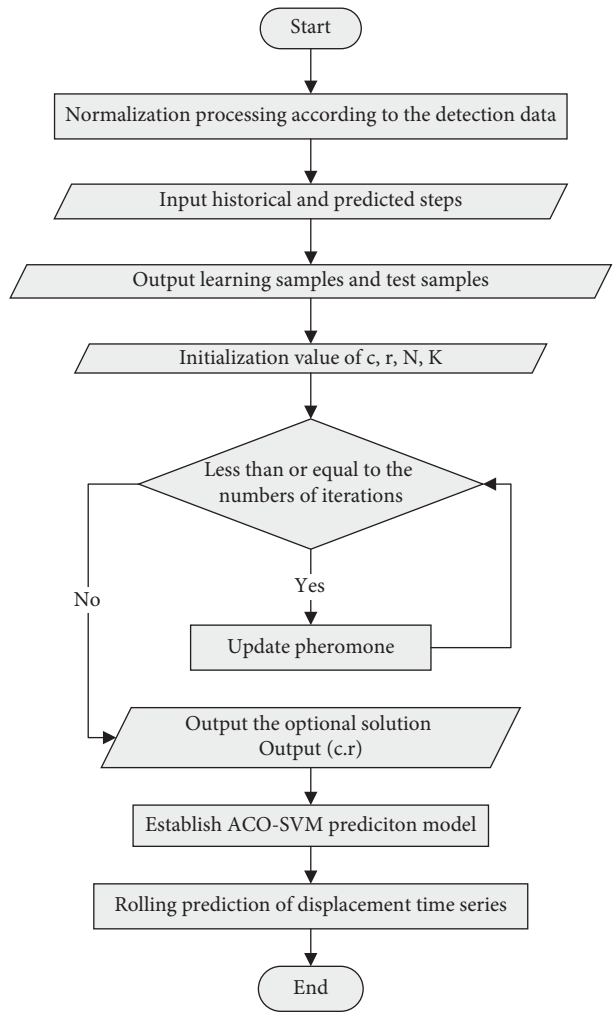

Figure 2: Flowchart of ACO-SVM optimization for prediction of the slope displacement.

The learning samples are shown in Table 2 to verify the accuracy of the ACO-SVM prediction model.

In this paper, the improved ACO algorithm is used for feature selection and combined with the SVM data model, and comparative simulation experiments are carried out. In the experimental steps, the history of the selected feature set is set to 10, the prediction step is set to 1, the maximum number of iterations is set to 100, and the classification error rate is taken as the adaptive value of the fitness function. The performance of the feature selection algorithm is evaluated by the support vector machine (SVM) classifier (mesh optimization method is used to calculate the optimal parameter values) and the adaptive values obtained by cross-validation. The lower the adaptive value, the better the performance of the feature selection algorithm. The relation between the ACO iteration number and adaptive value is shown in

Table 2: Training data of multipoint extensometer M4-7.

ID	Measured value (mm)	ID	Measured value (mm)	ID	Measured value (mm)
1	7.65	11	10.55	21	12.21
2	8.04	12	10.70	22	12.26
3	8.28	13	10.83	23	12.18
4	8.66	14	10.83	24	12.53
5	9.04	15	11.34	25	12.56
6	9.38	16	11.20	26	12.70
7	9.93	17	11.44	27	12.72
8	10.04	18	11.35	28	12.85
9	10.15	19	11.59	29	12.88
10	10.34	20	11.71	30	13.11

Figure 3. The optimal result is 0.025, and the earliest algebra value of the optimal result is 39. In order to reduce the computational overhead without significantly reducing the optimization effect, it is appropriate to set the maximum iteration number to 50. By calculating the evaluation indexes R^2 and RMSE of the SVM data model, the prediction result of the periodic displacement can be obtained. With the increase of the training set data, the prediction accuracy of the model is also improved. For periodic datasets, ACO-SVM can achieve the best effect for random datasets. The model parameters (C, γ) obtained by the ACO optimization method proposed in this paper are 20.305 and 2.514, respectively. The prediction results of the ACO-SVM model are shown in Table 3. Compared with the prediction results of the improved SVM (hybrid kernel least-squares support vector machine) in literature [14], the accuracy of the ACO-SVM prediction is better than that of the improved SVM except for a few points. The maximum relative error of the ACO-SVM prediction is 2.23%, less than 3.19% of the improved SVM, which proves the correctness of the ACO-SVM prediction model proposed in the paper.

3.2. Prediction Grey Model for the Slope Displacement in the Hydropower Station. The first-level hydropower project of HuaGuangTan is located in the middle and lower reaches of the Juxi River, Lin'an city, Zhejiang province. The first-level plant is located on the right bank of Juxi, and the overall flow direction of the nearby rivers is 120°~130°. The slope behind the plant was fully developed, and the gully direction is 40°~50°, which is nearly orthogonal to the Juxi River. The upper and lower reaches of the workshop have a cutting depth of 50~70 m, forming a long and narrow ridge facing the air and spreading in the northeast direction. The surface of the slope body is quaternary colluvial deposit, the middle part is the broken rock body with strong unloading action, and the lower part is fresh Jurassic fused tuff. During the heavy rainfall from May to June 2018, subsidence and external bulge occurred in 250 raceways of the plant area, and multiple tensile cracks were found in the middle and upper part of the slope body during a subsequent supplementary survey. In order to grasp the law and development trend of slope deformation, a safety monitoring system for slope deformation was established. In the established slope surface observation system, a total of 14 surface displacement observation points are arranged, and the number of displacement observation points is 1# to 14# according to elevation.

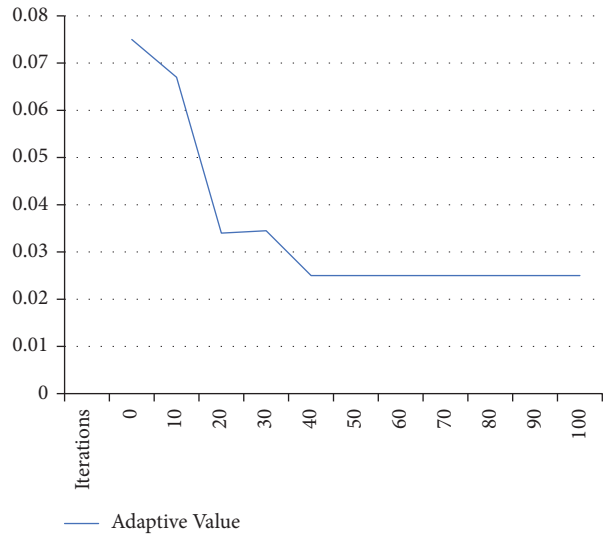

Figure 3: Performance evaluation of the ACO feature selection algorithm.

In the paper, the horizontal displacement data of measuring point 7# on the direction of the main slide are selected to predict and analyse the slope deformation. Through trial calculation, the optimal historical step p is 4, the predicted step m is 1, the ant colony size is 200, the total number of iterations is 50, and the optimal objective function value is $f < 1 \times 10^{-6}$. 30 displacement timing series monitored from the measuring point 7#, 2019-01-20 to 2019-08-11 (as shown in Table 4) were constructed into 26 training samples, and the next 10 displacement timing series were predicted with a time interval. The new prediction value was added to the training sample, the first training sample was deleted and the number of samples was kept unchanged, then the next prediction was performed, and so on.

Using ACO-SVM model research on the monitoring data in Table 3 for training and prediction analysis, at the same time in order to compare the accuracy of the models respectively, the traditional SVM, GA to optimize SVM and PSO to optimize SVM to forecast the monitoring data analysis and comparison of model parameter optimization (C, γ) is shown in Table 5, and the corresponding prediction results are shown in Table 6.

According to Table 5, it can be seen that most of the prediction results of the ACO-SVM model are better than

Table 3: Comparison of prediction results among different models for extensometer M4-7.

ID	Measured value/mm	Predicted value (mm)			Relative error (%)		
		SVM	Improved SVM	ACO-SVM	SVM	Improved SVM	ACO-SVM
31	12.83	13.27	13.02	13.01	3.40	1.45	1.41
32	13.01	13.30	13.05	13.00	2.20	0.55	0.57
33	12.76	13.27	12.99	12.91	4.03	1.79	1.17
34	12.86	13.30	13.06	12.99	3.42	1.56	1.02
35	13.14	12.50	12.72	12.74	4.91	3.19	2.23
36	13.13	12.66	12.96	12.94	3.62	1.40	1.47
37	13.01	13.28	13.01	12.92	2.09	0.73	0.72

Table 4: Horizontal resultant displacement of monitoring point 7#.

Date	Measured values (mm)	Date	Measured values (mm)	Date	Measured values (mm)
2019-01-20	10.06	2019-03-31	14.01	2019-06-09	16.27
2019-01-27	10.34	2019-04-07	13.83	2019-06-16	16.52
2019-02-03	10.62	2019-04-14	15.42	2019-06-23	16.28
2019-02-10	10.90	2019-04-21	15.75	2019-06-30	16.63
2019-02-17	11.73	2019-04-28	15.53	2019-07-07	17.50
2019-02-24	12.55	2019-05-05	16.01	2019-07-14	18.18
2019-03-03	13.38	2019-05-12	16.33	2019-07-21	18.24
2019-03-10	13.74	2019-05-19	16.65	2019-07-28	18.21
2019-03-17	13.78	2019-05-26	15.70	2019-08-04	17.68
2019-03-24	14.20	2019-06-02	16.27	2019-08-11	18.22

Table 5: Optimal parameters of different prediction models.

Model name	C	γ
SVM	128.00	0.001
GA-SVM	99.30	0.005
PSO-SVM	100.00	0.010
ACO-SVM	44.68	2.990

Table 6: Comparison of prediction results among different models for monitoring point 7#.

Date	Measured value (mm)	Predictive value (mm)				Relative error (%)%			
		SVM	GA-SVM	PSO-SVM	ACO-SVM	SVM	GA-SVM	PSO-SVM	ACO-SVM
2019-08-18	18.10	18.09	18.43	18.51	18.36	0.06	1.86	2.26	1.46
2019-08-25	18.00	18.03	18.49	18.59	18.41	0.17	2.76	3.30	2.29
2019-09-01	18.30	18.01	18.58	18.66	18.50	1.56	1.53	2.00	1.08
2019-09-08	18.45	18.03	18.72	18.82	18.61	2.30	1.42	1.96	0.85
2019-09-15	18.84	18.01	18.83	18.96	18.71	4.39	0.04	0.64	0.71
2019-09-22	18.79	18.00	18.93	19.08	18.79	4.19	0.76	1.53	0.01
2019-09-29	18.45	18.00	19.03	19.18	18.88	2.46	3.14	3.96	2.31
2019-10-06	18.89	17.99	19.12	19.29	18.96	4.76	1.24	2.09	0.36
2019-10-13	18.85	17.98	19.21	19.39	19.03	4.61	1.91	2.82	0.96
2019-10-20	18.76	17.98	19.3	19.48	19.11	4.19	2.84	3.8	1.82

those of the other three prediction models in Figure 4, with higher prediction accuracy, the maximum relative error is 2.31%, which is smaller than the maximum relative error of the other three models. The average relative error rate of the ACO-SVM algorithm is 1.19%, which is obviously lower than that of the other three algorithms in Figure 5. The traditional SVM model has high short-term prediction accuracy but weak generalization ability and large prediction error. The improved ACO-SVM model overcomes the problems of generalization ability and prediction error. The generalization ability of the three SVM models using the optimization algorithm is better than that of the traditional SVM model.

By comparing the predicted value of the ACO-SVM model with the measured value in Figure 6, it can be seen from the change law that the slope displacement changes little at the later stage, the deformation trend is gentle, and the displacement tends to converge, which proves that the slope is relatively stable. The measured value of the slope displacement at the later stage also verifies that the displacement tends to converge, so the predicted result meets the actual demand of the project.

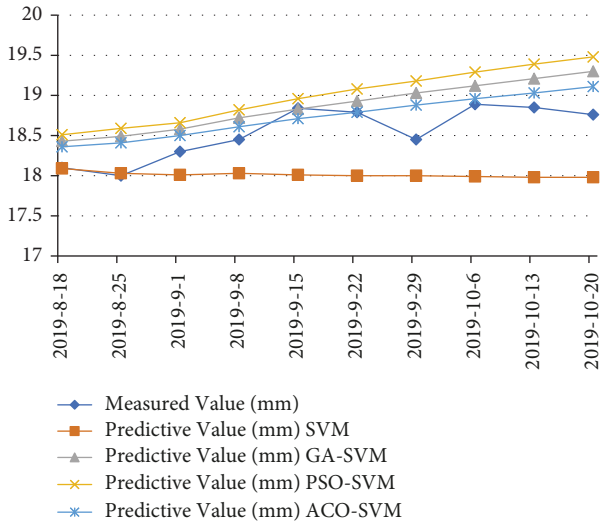

Figure 4: Comparison diagram between the measured value and predicted value (four algorithms).

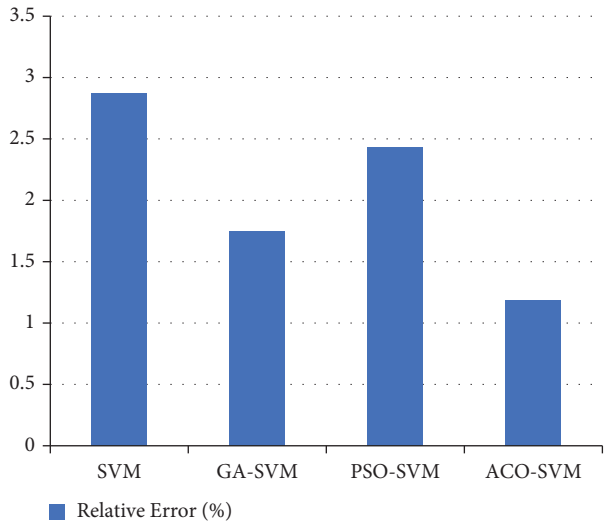

Figure 5: Comparison diagram of the relative error between ACO-SVM and three algorithms.

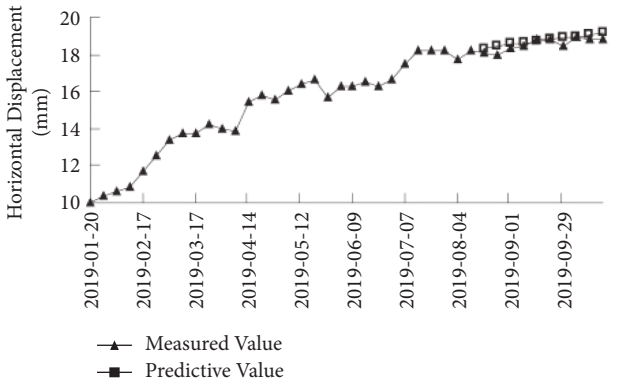

Figure 6: Comparison between the measured value and the predicted value for monitoring point 7#.

4. Conclusions

It is of great significance for engineering construction and safe operation to predict the future deformation trend of the slope based on displacement monitoring data. In view of the influence of model parameters (C, γ) of the support vector machine (SVM) on prediction accuracy and generalization ability, in order to avoid the blindness of artificial parameter selection, the paper proposed the improved ant colony algorithm to optimize SVM, search for optimal parameters, and apply the model to deformation prediction of slope engineering examples. It is found that the ACO-SVM model is able to predict the slope deformation and meet the demand of engineering prediction.

In the prediction of shallow deformation of the left bank slope of a first-stage hydropower station, the accuracy of the ACO-SVM model and the hybrid kernel least-squares SVM model is similar, which is more accurate than the traditional SVM model, indicating the accuracy of the ACO-SVM model.

The ACO-SVM model has higher prediction accuracy and stronger generalization ability than the genetic algorithm and particle swarm optimization to optimize SVM prediction results.

The comparison between the predicted value of the improved ACO-SVM model and the measured value shows that according to its variation law, the slope displacement changes little in the late stage, the deformation trend is gentle, and the displacement tends to converge, which proves that the slope is relatively stable. The measured value of the slope displacement in the later period also verifies that the displacement tends to converge, so the predicted results meet the actual engineering needs.

The ACO-SVM also has some shortcomings. For example, the searching time of this algorithm is longer than that of other optimization algorithms, which is a process of balancing accuracy and time consumption in optimization problems, which needs further research.

Data Availability

The data supporting the findings of this study are available within the article.

Conflicts of Interest

The authors declare that they have no conflicts of interest.

Acknowledgments

This work was supported by the Shanxi Province Higher Education Reform and Innovation Project (Grant no. J2020440), the Shanxi Province Educational Science Planning Project (Grant No. GH-220794 and No. GH-220970), and the Shanxi Vocational University of Engineering Science and Technology Scientific Research Fund Project (Grant No. KJ-202204).

References

[1] M. R. Daneshvar, C. S. Clay, and M. K. Savage, "Passive seismic imaging using microearthquakes," *Geophysics*, vol. 60, no. 4, pp. 1178–1186, 1995.

[2] T. Chen, N. Yang, and Y. Duan, "A fast total variation method for micro-seismic signal enhance," *Acta Microscopica*, vol. 28, no. 1, pp. 113–118, 2019.

[3] M. Umadevi and M. Malathi, "Distributed scheduling for spectrum sensing in congnitive radio networks," *Revista Tecnica de la Facultad de Ingenieria Universidad*, vol. 34, no. 2, pp. 16–21, 2018.

[4] I. Ullah, X. Su, X. Zhang, and D. Choi, "Evaluation of localization by extended kalman filter, unscented kalman filter, and article filter-based techniques," *Wireless Communications and Mobile Computing*, vol. 31, no. 6, pp. 153–159, 2020.

[5] G. G. Wang, S. Deb, and Z. Cui, "Monarch Butterfly Optimization," *Neural computing and applications*, vol. 31, no. 7, pp. 1995–2014, 2019.

[6] A.-A. Ali Mohamed, Y. S. Mohamed, A. M. EI-Gaafary Ahmed, and M. Ashraf, "Optimal power flow using moth swarm algorithm," *Electric Power Systems Research*, vol. 31, no. 1, pp. 190–206, 2017.

[7] W. A. H. M. Ghanem and A. Jantan, "Hybridizing artificial bee colony with monarch butterfly optimization for numerical optimization problems," *Neural Computing & Applications*, vol. 30, no. 1, pp. 163–181, 2018.

[8] X. Zhu, Q. Xu, M. Tang, H. Li, and F. Liu, "A hybrid machine learning and computing model for forecasting displacement of multifactor-induced landslides," *Neural Computing & Applications*, vol. 30, no. 12, pp. 3825–3835, 2017.

[9] M. ChenJuan, "Ant colony algorithm based on solving strongly heterogeneous container loading problem," *Metallurgical and Mining Industry*, vol. 7, no. 5, pp. 331–338, 2015.

[10] C. Zhou, Y. Cao, K. Yin, E. Intrieri, F. Catani, and L. Wu, "Characteristic comparison of seepage-driven and buoyancy-driven landslides in Three Gorges Reservoir area," *Engineering Geology*, vol. 30, no. 1, pp. 106–150, 2022.

[11] G. Jiang, L. I. N. Lu-sheng, and Z. d. Liu, "Grey forecasting model for slope is placement," *Rock and Soil Mechanics*, vol. 21, no. 3, pp. 244–246, 2020.

[12] L. Li, Y. Wu, and F. Miao, "Displacement prediction of landslides based on variational mode decomposition and GWO-MIC-SVR model," *Chinese Journal of Rock Mechanics and Engineering*, vol. 37, no. 06, pp. 1395–1406, 2018.

[13] N. Li, Y. J. Chen, D. D. Kong, and S. Tan, "Force-based tool condition monitoring for turning process using v-support vector regression," *International Journal of Advanced Manufacturing Technology*, vol. 91, no. 1-4, pp. 351–361, 2017.

[14] C. Zhou, Y. Cao, X. Hu, K. l. Yin, Y. Wang, and F. Catani, "Enhanced dynamic landslide hazard mapping using MT-InSAR method in the Three Gorges Reservoir Area," *Landslides*, pp. 1–13, 2022.

[15] A. Panizzo, P. De Girolamo, M. Di Risio, A. Maistri, and A. Petaccia, "Great landslide events in Italian artificial reservoirs," *Natural Hazards and Earth System Sciences*, vol. 5, no. 5, pp. 733–740, 2005.

[16] T. Carlà, E. Intrieri, F. Di Traglia, T. Nolesini, G. Gigli, and N. Casagli, "Guidelines on the use of inverse velocity method as a tool for setting alarm thresholds and forecasting landslides and structure collapses," *Landslides*, vol. 14, no. 2, pp. 517–534, 2017.

[17] F. L. Tan, X. L. Hu, C. C. He et al., "Identifying the main control factors for different deformation stages of landslides," *Geotechnical & Geological Engineering*, vol. 35, pp. 1–14, 2017.

[18] F. C. Panwala, "Modeling and Analysis of asymmetric Sieve shaped Skewed type microchannel network in BioMEMS for mass and size based mammalian cell separation and sorting using filtration method," *Revista Tecnica de la Facultad de Ingenieria Universidad*, vol. 34, no. 4, pp. 111–116, 2019.

[19] Y. U. Jun-ping, Z. j. Chen, L. j. Wu, Y. U. S. yuan, and S. Wang, "Forecasting slope displacement based on support vector machine optimized by ant colony algorithm," *Journal of Yangtze River Scientific Research Institute*, vol. 32, no. 4, pp. 22–27, 2015.

[20] B. S. Gan, T. Hara, A. Han, S. W. Alisjahbana, and S. As'ad, "Evolutionary ACO Algorithms for Truss Optimization Problems," *Procedia Engineering*, vol. 171, pp. 1100–1107, 2017.

[21] F. Zheng, A. C. Zecchin, J. P. Newman, H. R. Maier, and G. C. Dandy, "An adaptive convergence-trajectory controlled ant colony optimization algorithm with application to water distribution system design problems," *IEEE Transactions on Evolutionary Computation*, vol. 21, no. 5, pp. 773–791, 2017.

[22] ChenJuan, "Parameters evaluation of ant colony algorithm based on TSP," *Revista Tecnica de la Facultad de Ingeniera*, vol. 39, no. 4, pp. 121–126, 2016.

[23] M. R. Bonyadi and Z. Michalewicz, "Particle swarm optimization for single objective continuous space problems:A review," *Evolutionary Computation*, vol. 25, no. 1, pp. 1–54, 2017.

[24] C. Juan, "ANT colony algorithm based on solving continuous space optimization problem," *Metallurgical and Mining Industry*, vol. 7, no. 8, pp. 463–467, 2015.

[25] C. Zhou, Y. Cao, K. Yin et al., "Landslide characterization applying sentinel-1 images and InSAR technique: the muyubao landslide in the three gorges reservoir area, China," *Remote Sensing*, vol. 12, no. 20, pp. 3385–85, 2020.

[26] M. R. Daneshvar and C. S. Clay, "Imaging of rough surfaces for impulsive and continuously radiating sources," *Journal of the Acoustical Society of America*, vol. 82, no. 1, pp. 360–369, 1987.

[27] F. Xu, Y. Wang, and J. Du, "Study of displacement prediction model of landslide based on time series analysis," *Chinese Journal of Rock Mechanics and Engineering*, vol. 30, no. 4, pp. 746–751, 2018.

[28] A. Arabameri, B. Pradhan, K. Rezaei, M. Sohrabi, and Z. Kalantari, "GIS-based landslide susceptibility mapping using numerical risk factor bivariate model and its ensemble with linear multivariate regression and boosted regression tree algorithms," *Journal of Mountain Science*, vol. 16, no. 3, pp. 595–618, 2019.

Hindawi
Computational Intelligence and Neuroscience
Volume 2022, Article ID 7291735, 19 pages
https://doi.org/10.1155/2022/7291735

Research Article

Optimal Control of False Information Clarification System under Major Emergencies Based on Differential Game Theory

Bowen Li,[1] Hua Li ,[2] Qiubai Sun,[2] and Rongjian Lv[1]

[1]*School of Electronic and Information Engineering, University of Science and Technology Liaoning, Anshan, China*
[2]*School of Business Administration, University of Science and Technology Liaoning, Anshan, China*

Correspondence should be addressed to Hua Li; lh1@ustl.edu.cn

Received 23 July 2022; Accepted 20 August 2022; Published 23 September 2022

Academic Editor: Zaoli Yang

To further study the issue of false information classification on social platforms after major emergencies, this study regards opinion leaders and Internet users as a false-information classification system and constructs three differential game models of decentralized, centralized, and subsidized decision-making based on optimal control and differential game theory. Comparison analyses and numerical simulations of optimal equilibrium strategies and the optimal benefit between opinion leaders and Internet users, the optimal trajectory and the steady-state value of the total volume of real information, and the optimal benefit of the false information clarification system are carried out. It is found that under centralized decision-making, equilibrium strategy and total benefit of opinion leaders and Internet users, system total benefit, and total volume of real information can achieve Pareto optimality. Although subsidized decision-making fails to achieve Pareto optimality, with opinion leaders providing cost subsidies for Internet users, it is possible to reach relative Pareto improvement compared with decentralized decision-making.

1. Introduction

With the rapid development of the Internet, the public is now able to quickly learn of, and exchange information about, major emergencies in some places via social platforms of new media, such as Facebook, Instagram, Tiktok, and Weibo. With major emergencies featuring abruptness, the wildness of dissemination, and high levels of danger [1], relevant departments find it hard to carry out overall research effectively, therefore failing to release any relevant information to the public in the first place. This leads to a lack of accurate and real information about major emergencies from the public view, who are interested in those emergencies. It is possible that the public, influenced by false information disseminated on social platforms, becomes panicked causing severe online cluster behavior or even the appearance of cluster events, which will obstruct the process of relevant government departments dealing with major emergencies and negatively impact social stability and prosperity. Therefore, to develop countermeasures against false information of major emergencies on social platforms, opinion leaders are encouraged to clarify false information by releasing real information, channeling Internet users' attention, and advising them to adopt real information. It is also very important to establish a false-information clarification system, so that any panic among Internet users could be eliminated, and any repeating impact could be reduced.

Academic circles have carried out multi-perspective research on different clusters' behavior under the background of major emergencies. Kang et al. [2] studied the influence of support provided by e-commerce platforms to businesses after major emergencies. Wu et al. [3] studied social influence and public voice after major emergencies and constructed a public opinion evolution model between the public and the government by means of information entropy. Cao et al. [4] studied the influence of extremist behavior on cluster decision-making and particularly focused on cluster decision-making under major emergencies. Din et al. [5] investigated the impact of Internet customers' behavior on food supply chains. Other scholars carried out research on major emergencies' influence on the public; for example, Akatu et al. [6] studied the public's negative

emotions after the COVID-19 pandemic. From the perspective of emergencies, Hong et al. [7] proposed that panic emotions could be disseminated via both the virtual world and the real world when information is exchanged. Liu [8] suggested that the quality of information released by social media is in inverse proportion to the amount of panic behavior caused by major emergencies. McElroy et al. [9] discovered that the level of anxiety caused by major emergencies is related to an individual's age, gender, and health status.

In terms of false-information clarification, Liao and Wang [10] believed that a timely and effective clarification of false information could reduce the negative impact of major emergencies and promote cooperation among the public to disseminate real information. Hosseini and Zandvakili [11] held the view that the dissemination of false information negatively affects the stability of society. Pal and [12] studied individuals with different levels of risk preference and their selection of false information or real information. It was concluded that the individuals were more interested in false information regardless of the level of their risk preference. Bordia et al. [13] proposed effectively limiting the dissemination of false information by clarifying it. Buchanan and Benson [14] found that the dissemination of false information was affected by the level of recognition the receiver had of the disseminator, as well as the receiver's own risk preference. Guess et al. [15] believed that the dissemination of false information affects the public judgment. Vosoughi et al. [16] found that the scope and speed of the dissemination of false information are higher than those of real information. Agarwal et al. [17] thought that after major emergencies, timely clarification of false information should be carried out so that its negative impact could be ameliorated. Ozturk et al. [18] found that clarification of false information could effectively control its dissemination.

Differential game theory has been widely applied in various fields including military science [19], cybernetics [20], science of management [21], and economics [22]. This study mainly applies differential game theory to research on false information clarification systems after major emergencies. Combining classical game theory and cybernetics theory, differential game theory was first applied in modern war to deal with optimal control theory between two or multiple parties. Later, with the improvement of its theoretical framework, differential game theory has become a tool for analyzing different participants' decision behavior. Differential game theory was applied by Shchelchkov [23] to study the issue of chase-and-run among individuals, Machowska et al. [24] to study the business reputation of advertisers, Biancardi et al. [25] to study the recovery of underground water by peasants and water supply institutions, and Garcia-Meza [26] to study the behavior of enterprises and workers in the labor market. To summarize, differential game theory can be regarded as an optimal control process of the gaming interaction among relevant stakeholders. Therefore, this study regards opinion leaders and Internet users involved in social platforms as a false-information clarification system where false-information clarification issues after major emergencies could be studied based on differential game theory. We believe this work is innovative.

This study is based on optimal control theory and differential game theory, and it sets the post-major-emergency impact of multiple false information on the public involved in social platforms as its research object. First of all, three differential game models are constructed under decentralized decision-making, centralized decision-making, and subsidized decision-making between opinion leaders and Internet users; Second, the solution of three differential game models is obtained, and the optimal equilibrium strategies and the respective optimal benefit of opinion leaders and Internet users, the trajectory of the total volume of real information, and the steady-state value and the optimal benefit of the false-information clarification system are analyzed. Finally, a comparative analysis is performed on the three results, and MATLAB numerical simulation software is applied to all key parameters so that the validity of the equilibrium results could be determined. This study provides a vital theoretical basis and decision-making references.

2. Problem Description and Basic Assumption

2.1. Problem Description. The research objective is a false-information clarification system consisting of a single opinion leader (L) and a single Internet user (U), and the research is carried out under the differential game perspective. After a major emergency begins, many people pay attention to its relative progress, and due to information asymmetry, social platforms are flooded with false information. Therefore, when false information appears, taking self-interest into consideration, opinion leaders could attract Internet users' attention through investigation and evidence collection, so as to obtain more traffic and exposure. Internet users, on the other hand, could have a better sense of participation and the truth of the event through forwarding real information more frequently, so more people would be exposed to it. Benefits are therefore obtained by a sound information dissemination channel created by posting real information.

2.2. Model Assumption

Assumption 1. This study assumes that the effort cost for opinion leaders to release real information is a convex function of the level of their own effort, with diminishing marginal utility; the cost of effort for Internet users to forward real information is a convex function of the level of their own effort, with diminishing marginal utility. The effort cost for opinion leaders and Internet users at time t is denoted as $C_L(t)$ and $C_U(t)$, and the equations are as follows:

$$C_L(t) = \frac{1}{2}\mu_L E_L^2(t),$$
$$C_U(t) = \frac{1}{2}\mu_U E_U^2(t), \tag{1}$$

where μ_L and μ_U denote the effort cost coefficients of opinion leaders and Internet users, respectively, with both coefficients being greater than zero; and $E_L(t)$ and $E_U(t)$ denote the level of effort of opinion leaders and Internet users at time t, respectively.

Assumption 2. The total volume of real information released on social platforms changes dynamically with time and effort of opinion leaders and Internet users. It is noted that in the real world, some real information fails to reach its expected effect of clarifying false information due to a lack of dissemination. Therefore, it is presumed that the total volume of real information, $R(t)$, changes with time based on the following dynamic equation:

$$\begin{cases} \dot{R}(t) = \alpha_L E_L(t) + \alpha_U E_U(t) - \delta R(t), \\ R(0) = R_0 \geq 0, \end{cases} \tag{2}$$

where α_L and α_U denote the level of influence of effort by opinion leaders and Internet users on the volume of real information; and δ denotes real information's natural dissipation coefficient, with α, β, and δ being greater than zero.

Assumption 3. Opinion leaders and Internet users could benefit from traffic brought by real information dissemination, the amount of which is co-affected by the initial popularity level of social platforms and the efforts of opinion leaders and Internet users. A similar liner equation for the function of Internet traffic is as follows:

$$F(t) = f + \gamma\left[\lambda R(t) + \beta_L E_L(t) + \beta_U E_U(t)\right], \tag{3}$$

with f denoting the initial popularity level of social platforms, γ denoting the level of attention received by major emergencies, λ denoting the total volume of real information's influence coefficient on social platforms' traffic, β_L denoting the effort of opinion leaders' influence coefficient on social platforms' traffic, and β_U denoting the effort of Internet users' influence coefficient on social platforms' traffic, with $0 < \gamma \leq 1$ and β_L and β_U being greater than zero. Opinion leaders not only benefit from visitor traffic but also from Internet users directly.

Assumption 4. The discount rate, p, of opinion leaders and Internet users is the same and greater than zero. Behavior strategy selection of both opinion leaders and Internet users is on the basis of maximizing their own interest, with no time limit.

Based on Assumptions 1–4, the objective functions of opinion leaders and Internet users are as follows:

$$\begin{aligned} J_L &= \int_0^\infty e^{-\rho t}\left[\omega E_U(t) + \pi_L F(t) - C_L(t)\right]\mathrm{d}t, \\ J_U &= \int_0^\infty e^{-\rho t}\left[\pi_U F(t) - C_U(t)\right]\mathrm{d}t, \end{aligned} \tag{4}$$

where $\omega E_U(t)$ denotes benefits of opinion leaders obtained directly from Internet users, ω denotes direct benefit per unit gained by opinion leaders from the effort of Internet users, $\pi_L F(t)$ denotes benefits of opinion leaders obtained from the traffic of visitors on social platforms, π_L denotes benefits of marginal traffic of visitors obtained by opinion leaders, $\pi_U F(t)$ denotes benefits of Internet users obtained from traffic of visitors on social platforms, and π_U denotes marginal benefits of traffic obtained by Internet users.

All parameters of the models in this study are denoted by constants that do not vary with time, and the game behavior happens in any time period with no limitation. To simplify the writing process, time t will not be listed in the following paragraphs.

3. Model Construction and Solution

3.1. Decentralized Decision-Making of Opinion Leaders and Internet Users. Under decentralized decision-making, opinion leaders and Internet users need to make an independent decision based on the principle of maximizing their own benefits, and the post-game equilibrium strategy is called the Nash equilibrium strategy. Denoting N as a decentralized strategy, at this moment, the decision behavior of opinion leaders and Internet users is as follows:

$$\begin{aligned} \max_{E_L} J_L^N &= \int_0^\infty e^{-\rho t}\left\{\omega E_U + \pi_L f + \pi_L \gamma\left[\lambda R + \beta_L E_L + \beta_U E_U\right] - \frac{1}{2}\mu_L E_L^2\right\}\mathrm{d}t, \\ \max_{E_U} J_U^N &= \int_0^\infty e^{-\rho t}\left\{\pi_U f + \pi_U \gamma\left[\lambda R + \beta_L E_L + \beta_U E_U\right] - \frac{1}{2}\mu_U E_U^2\right\}\mathrm{d}t. \end{aligned} \tag{5}$$

Theorem 1. *Under the decentralized decision-making of opinion leaders and Internet users, the equilibrium results are as follows:*

(1) The optimal equilibrium strategy for opinion leaders is:

$$E_L^{N^*} = \frac{\gamma\pi_L\left[\lambda\alpha_L + (\delta+\rho)\beta_L\right]}{(\delta+\rho)\mu_L}. \tag{6}$$

(2) The optimal equilibrium strategy for Internet users is:

$$E_U^{N^*} = \frac{\gamma\pi_U\left[\lambda\alpha_U + (\delta+\rho)\beta_U\right]}{(\delta+\rho)\mu_U}. \tag{7}$$

(3) The optimal trajectory of the total volume of real information is:

$$\begin{cases} R^{N^*} = \left(R_0 - R_S^N\right)e^{-\delta t} + R_S^N, \\ R_S^N = \dfrac{\gamma\alpha_L\pi_L\left[\lambda\alpha_L + (\delta+\rho)\beta_L\right]}{\delta(\delta+\rho)\mu_L} + \dfrac{\gamma\alpha_U\pi_U\left[\lambda\alpha_U + (\delta+\rho)\beta_U\right]}{\delta(\delta+\rho)\mu_U}, \end{cases} \tag{8}$$

with R_S^n being the steady-state value of real information under decentralized decision-making.

(4) The optimal benefit for opinion leaders is:

$$V_L^{N^*}(R) = \frac{\lambda\pi_L\gamma}{\delta+\rho}R_S^N + \frac{\pi_L f}{\rho} + \frac{\pi_L\gamma^2\pi_U\left[\lambda\alpha_U + (\delta+\rho)\beta_U\right]^2}{\rho(\delta+\rho)^2\mu_U} + \frac{\gamma^2\pi_L^2\left[\lambda\alpha_L + (\delta+\rho)\beta_L\right]^2}{2\rho(\delta+\rho)^2\mu_L} + \frac{\gamma\pi_U\omega\left[\lambda\alpha_U + (\delta+\rho)\beta_U\right]}{\rho(\delta+\rho)\mu_U}. \tag{9}$$

(5) The optimal benefit for Internet users is:

$$V_U^{N^*}(R) = \frac{\lambda\pi_U\gamma}{\delta+\rho}R_S^N + \frac{\pi_U f}{\rho} + \frac{\pi_U^2\gamma^2\left(\lambda\alpha_U + (\delta+\rho)\beta_U\right)^2}{2\rho(\delta+\rho)^2\mu_U} + \frac{\pi_U\gamma^2\pi_L\left(\lambda\alpha_L + (\delta+\rho)\beta_L\right)^2}{\rho(\delta+\rho)^2\mu_L}. \tag{10}$$

(6) The optimal benefit for the system is:

$$\begin{cases} V^{N^*}(R) = V_L^{N^*}(R) + V_U^{N^*}(R) \\ V^{N^*}(R) = \dfrac{\lambda\gamma\left(\pi_L+\pi_U\right)}{\delta+\rho}R_S^N + \dfrac{f\left(\pi_L+\pi_U\right)}{\rho} \\ + \dfrac{\gamma^2\pi_U\left(\pi_U+2\pi_L\right)\left[\lambda\alpha_U + (\delta+\rho)\beta_U\right]^2}{2\rho(\delta+\rho)^2\mu_U} \\ + \dfrac{\gamma^2\pi_L\left(\pi_L+2\pi_U\right)\left[\lambda\alpha_L + (\delta+\rho)\beta_L\right]^2}{2\rho(\delta+\rho)^2\mu_L} \\ + \dfrac{\gamma\pi_U\omega\left[\lambda\alpha_U + (\delta+\rho)\beta_U\right]}{\rho(\delta+\rho)\mu_U}. \end{cases} \tag{11}$$

Verification 1. According to optimal control theory, if $R \geq 0$, then both $V_L^N(R)$ and $V_U^N(R)$ satisfy the Hamilton–Jacobi–Bellman (HJB) equation, and both have first and second derivatives, namely:

$$\rho V_L^N(R) = \max_{E_L}\left\{\begin{array}{l} \omega E_U + \pi_L f + \pi_L\gamma\left[\lambda R + \beta_L E_L + \beta_U E_U\right] \\ -\dfrac{1}{2}\mu_L E_L^2 + V_L^{N'}\left[\alpha_L E_L + \alpha_U E_U - \delta R\right] \end{array}\right\}, \tag{12}$$

$$\rho V_U^N(R) = \max_{E_U}\left\{\begin{array}{l} \pi_U f + \pi_U\gamma\left[\lambda R + \beta_L E_L + \beta_U E_U\right] \\ -\dfrac{1}{2}\mu_U E_U^2 + V_U^{N'}\left[\alpha_L E_L + \alpha_U E_U - \delta R\right] \end{array}\right\}. \tag{13}$$

To solve E_L, the first derivative of the function on the right side of equation (12) is taken and set equal to zero, which gives:

$$E_L^N = \frac{\pi_L\gamma\beta_L + \alpha_L V_L^{N'}}{\mu_L}. \tag{14}$$

To solve E_U, the first derivative of the function on the right of the equation (13) is taken and set equal to zero, which gives:

$$E_U^N = \frac{\pi_U\gamma\beta_U + \alpha_U V_U^{N'}}{\mu_U}. \tag{15}$$

After inputting equations (14) and (15) in to (12), it is concluded that:

$$\begin{aligned} \rho V_L^N(R) = {} & \left(\lambda\pi_L\gamma - \delta V_L^{N'}\right)R \\ & + V_L^{N'}\left[\frac{\alpha_L\left(\alpha_L V_L^{N'} + \beta_L\pi_L\gamma\right)}{\mu_L} + \frac{\alpha_U\left(\alpha_U V_U^{N'} + \beta_U\pi_U\gamma\right)}{\mu_U}\right] \\ & + \pi_L f - \frac{\left(\alpha_L V_L^{N'} + \beta_L\pi_L\gamma\right)^2}{2\mu_L} + \frac{\omega\left(\alpha_U V_U^{N'} + \beta_U\pi_U\gamma\right)}{\mu_U} \\ & + \pi_L\gamma\left[\frac{\beta_L\left(\alpha_L V_L^{N'} + \beta_L\pi_L\gamma\right)}{\mu_L} + \frac{\beta_U\left(\alpha_U V_U^{N'} + \beta_U\pi_U\gamma\right)}{\mu_U}\right]. \end{aligned} \tag{16}$$

Inputting equations (14) and (15) in to (13), it is concluded that:

$$\begin{aligned} \rho V_U^N(R) = {} & \left(\lambda\pi_U\gamma - \delta V_U^{N'}\right)R \\ & + V_U^{N'}\left[\frac{\alpha_L\left(\alpha_L V_L^{N'} + \beta_L\pi_L\gamma\right)}{\mu_L} + \frac{\alpha_U\left(\alpha_U V_U^{N'} + \beta_U\pi_U\gamma\right)}{\mu_U}\right] \\ & + \pi_U f - \frac{\left(\alpha_U V_U^{N'} + \beta_U\pi_U\gamma\right)^2}{2\mu_U} \\ & + \pi_U\gamma\left[\frac{\beta_L\left(\alpha_L V_L^{N'} + \beta_L\pi_L\gamma\right)}{\mu_L} + \frac{\beta_U\left(\alpha_U V_U^{N'} + \beta_U\pi_U\gamma\right)}{\mu_U}\right]. \end{aligned} \tag{17}$$

From the structural characteristics of equations (16) and (17), the linear optimal value function for R is the solution of the HJB equation. Therefore, it is assumed that the analytic equations of $V_L^N(R)$ and $V_U^N(R)$ for $R$are:

$$V_L^N(R) = a_1 R + a_2, \tag{18}$$

$$V_U^N(R) = b_1 R + b_2, \tag{19}$$

with a_1, a_2, b_1, and b_2 being undetermined coefficients. It is further concluded from equations (18) and (19) that:

$$V_L^{N'}(R) = a_1, \tag{20}$$

$$V_U^{N'}(R) = b_1. \tag{21}$$

Equations (18)–(21) are inputted into equations (16) and (17). Using the method of undetermined coefficients, the values of a_1, a_2, b_1, and b_2 could be obtained:

$$a_1 = \frac{\lambda \pi_L \gamma}{\delta + \rho}, \tag{22}$$

$$\begin{aligned} a_2 &= \frac{\pi_L f}{\rho} + \frac{\pi_L \gamma^2 \pi_U \left[\lambda \alpha_U + (\delta + \rho)\beta_U\right]^2}{\rho(\delta + \rho)^2 \mu_U} \\ &+ \frac{\gamma^2 \pi_L^2 \left[\lambda \alpha_L + (\delta + \rho)\beta_L\right]^2}{2\rho(\delta + \rho)^2 \mu_L} \\ &+ \frac{\gamma \pi_U \omega \left[\lambda \alpha_U + (\delta + \rho)\beta_U\right]}{\rho(\delta + \rho)\mu_U}, \end{aligned} \tag{23}$$

$$b_1 = \frac{\lambda \pi_U \gamma}{\delta + \rho}, \tag{24}$$

$$\begin{aligned} b_2 &= \frac{\pi_U f}{\rho} + \frac{\pi_U^2 \gamma^2 \left[\lambda \alpha_U + (\delta + \rho)\beta_U\right]^2}{2\rho(\delta + \rho)^2 \mu_U} \\ &+ \frac{\pi_U \gamma^2 \pi_L \left[\lambda \alpha_L + (\delta + \rho)\beta_L\right]^2}{\rho(\delta + \rho)^2 \mu_L}. \end{aligned} \tag{25}$$

Inputting equations (20) and (22) into equation (14), the optimal equilibrium strategy for opinion leaders is shown as equation (6); inputting equations (21) and (24) into equation (15), the optimal equilibrium strategy for Internet users is shown as equation (7); inputting equations (6) and (7) into equation (2), the optimal trajectory of the total volume of real information and the steady-state value are shown as equation (8); inputting equations (22) and (23) into equation (18), the optimal benefit for opinion leaders is shown as equation (9); inputting equations (24) and (25) into equation (19), the optimal benefit for Internet users is shown as equation (10); from equations (9) and (10), the optimal benefit for the whole false information clarification system is shown as equation (11). So far, theorem 1 has been verified.

Deduction 1. From Theorem 1, it is known that under the context of the decentralized decision, both Internet users and opinion leaders make their decision based on the maximum of their own benefit, and the decision behavior of both sides has no impact on the other. The optimal equilibrium of both sides (i.e., the level of their effort) is simultaneously affected by: the level of attention gained after major emergencies, each side's marginal traffic benefit, influential coefficients of the total volume of real information, and effort level of each side on social platform traffic, and effort level of each side's influential coefficient on the total volume of real information and each side's effort cost coefficient.

The total volume of real information is decided by the effort level of both opinion leaders and Internet users. The optimal benefit of opinion leaders, Internet users, and false information clarification systems increases with the growth of the total volume of real information. This means that the more effort opinion leaders and Internet users pay, the more benefit they will get. A detailed interrelated relationship is shown in Table 1.

3.2. Centralized Decision-Making of Opinion Leaders and Internet Users. Under the context of centralized decision-making, meaning cooperation, opinion leaders and Internet users, as a cooperative system who shares the same goal, aim to maximize system benefit while making decisions. The post-game equilibrium strategy is called the Nash equilibrium strategy. Denoting C as centralized decision-making, the decision behavior of the current system is:

$$\max_{E_L, E_U} J_S^C = \int_0^\infty e^{-\rho t} \left\{ \begin{array}{c} \omega E_U - \frac{1}{2}\mu_L E_L^2 - \frac{1}{2}\mu_U E_U^2 \\ + (\pi_L + \pi_U)\left[f + \gamma(\lambda R + \beta_L E_L + \beta_U E_U)\right] \end{array} \right\} \mathrm{d}t. \tag{26}$$

Theorem 2. *The equilibrium result under centralized decision-making of opinion leaders and Internet users is:*

(1) The optimal equilibrium strategy of opinion leaders is:

$$E_L^{C^*} = \frac{\gamma(\pi_L + \pi_U)\left[\lambda \alpha_L + (\delta + \rho)\beta_L\right]}{\mu_L(\delta + \rho)}. \tag{27}$$

(2) The optimal equilibrium strategy of Internet users is:

$$E_U^{C^*} = \frac{\omega(\delta + \rho) + \gamma(\pi_L + \pi_U)\left[\lambda \alpha_U + (\delta + \rho)\beta_U\right]}{\mu_U(\delta + \rho)}. \tag{28}$$

(3) The optimal trajectory of the total volume of real information is:

Table 1: Influence of different parameters on optimal equilibrium strategy of opinion leaders and internet users under decentralized decision strategy.

	γ	π_L	π_U	λ	α_L	α_U	β_L	β_U	μ_L	μ_U
E_L^N	↗	↗	—	↗	↗	—	↗	—	↘	—
E_U^N	↗	—	↗	↗	—	↗	—	↗	—	↘

Note. ↗ refers to positive influence, ↘ refers to negative influence, —refers to irrelevance.

$$\begin{cases} R^{C^*} = \left(R_0 - R_S^C\right)e^{-\delta t} + R_S^C \\ R_S^C = \dfrac{\gamma\alpha_L(\pi_L+\pi_U)[\lambda\alpha_L + (\delta+\rho)\beta_L]}{\delta\mu_L(\delta+\rho)} \\ + \dfrac{\omega\alpha_U(\delta+\rho) + \gamma\alpha_U(\pi_L+\pi_U)[\lambda\alpha_U + (\delta+\rho)\beta_U]}{\delta\mu_U(\delta+\rho)}. \end{cases} \tag{29}$$

with R_S^C being the steady-state value of real information under centralized decision-making.

(4) The optimal benefit of the system is:

$$\begin{aligned} V^{C^*}(R) = {} & \frac{\lambda\gamma(\pi_L+\pi_U)}{\delta+\rho}R_S^C + \frac{\omega\gamma(\pi_L+\pi_U)[\lambda\alpha_U + (\delta+\rho)\beta_U]}{\rho(\delta+\rho)\mu_U} \\ & + \frac{f(\pi_L+\pi_U)}{\rho} + \frac{\gamma^2(\pi_L+\pi_U)^2[\lambda\alpha_U + (\delta+\rho)\beta_U]^2}{2\rho(\delta+\rho)^2\mu_U} \\ & + \frac{\gamma^2(\pi_L+\pi_U)^2[\lambda\alpha_L + (\delta+\rho)\beta_L]^2}{2\rho(\delta+\rho)^2\mu_L} + \frac{\omega^2}{2\rho\mu_U} \end{aligned} \tag{30}$$

Verification 2. According to optimal control theory, if $R \geq 0$, then $V_S^C(R)$ satisfies the HJB equation, and $V_S^C(R)$ has first and second derivatives, namely:

$$\rho V_S^C(R) = \max_{E_L, E_U} \begin{cases} \omega E_U - \dfrac{1}{2}\mu_L E_L^2 - \dfrac{1}{2}\mu_U E_U^2 \\ + (\pi_L+\pi_U)[f + \gamma(\lambda R + \beta_L E_L + \beta_U E_U)] \\ + V_S^{C'}[\alpha_L E_L + \alpha_U E_U - \delta R] \end{cases}. \tag{31}$$

To solve E_L and E_U, the first derivatives of the function on the right side of the equations are taken and set equal to zero, which gives:

$$E_L^C = \frac{(\pi_L+\pi_U)\gamma\beta_L + \alpha_L V_S^{C'}}{\mu_L}, \tag{32}$$

$$E_U^C = \frac{\omega + (\pi_L+\pi_U)\gamma\beta_U + \alpha_U V_S^{C'}}{\mu_U}. \tag{33}$$

Inputting equations (32) and (33) into equation (31), it is concluded that:

$$\begin{aligned} \rho V_S^C(R) = {} & \left[\lambda\gamma(\pi_L+\pi_U) - \delta V_S^{C'}\right]R + \frac{\omega\left[\omega + \alpha_U V_S^{C'} + \beta_U\gamma(\pi_L+\pi_U)\right]}{\mu_U} \\ & + V_S^{C'}\left\{\frac{\alpha_L\left[\alpha_L V_S^{C'} + \beta_L\gamma(\pi_L+\pi_U)\right]}{\mu_L} + \frac{\alpha_U\left[\omega + \alpha_U V_S^{C'} + \beta_U\gamma(\pi_L+\pi_U)\right]}{\mu_U}\right\} \\ & + (\pi_L+\pi_U)\left\{f + \gamma\left[\frac{\beta_L\left[\alpha_L V_S^{C'} + \beta_L\gamma(\pi_L+\pi_U)\right]}{\mu_L} + \frac{\beta_U\left[\omega + \alpha_U V_S^{C'} + \beta_U\gamma(\pi_L+\pi_U)\right]}{\mu_U}\right]\right\} \\ & - \frac{\left[\omega + \alpha_U V_S^{C'} + \beta_U\gamma(\pi_L+\pi_U)\right]^2}{2\mu_U} - \frac{\left[\alpha_L V_S^{C'} + \beta_L\gamma(\pi_L+\pi_U)\right]^2}{2\mu_L}. \end{aligned} \tag{34}$$

From the structural characteristics of equation (34), it is assumed that the analytic equation of $V_S^C(R)$ for R is:

$$V_S^C(R) = c_1 R + c_2, \tag{35}$$

with c_1 and c_2 being undetermined coefficients. It is further obtained from equation (35) that:

$$V_S^{C'}(R) = c_1. \tag{36}$$

Equations (35) and (36) are inputted into equation (34). According to the method of undetermined coefficients, the values of c_1 and c_2 could be obtained:

$$c_1 = \frac{\lambda\gamma(\pi_L + \pi_U)}{\delta + \rho}, \tag{37}$$

$$\begin{aligned} c_2 = {} & \frac{\gamma^2(\pi_L + \pi_U)^2[\lambda\alpha_L + (\delta+\rho)\beta_L]^2}{2\rho(\delta+\rho)^2\mu_L} + \frac{\gamma^2(\pi_L + \pi_U)^2[\lambda\alpha_U + (\delta+\rho)\beta_U]^2}{2\rho(\delta+\rho)^2\mu_U} \\ & + \frac{f(\pi_L + \pi_U)}{\rho} + \frac{\omega^2}{2\rho\mu_U} + \frac{\omega\gamma(\pi_L + \pi_U)[\lambda\alpha_U + (\delta+\rho)\beta_U]}{\rho(\delta+\rho)\mu_U}. \end{aligned} \tag{38}$$

Inputting equations (36) and (37) into equation (32), the optimal equilibrium strategy for opinion leaders is shown as equation (27); inputting equations (36) and (37) into equation (33), the optimal equilibrium strategy for Internet users is shown as equation (28); inputting equations (27) and (28) into equation (2), the optimal trajectory of total volume of real information and the steady-state value are shown as equation (29); inputting equations (37) and (38) into equation (35), the optimal benefit for the whole false information clarification system is shown as equation (30). So far, theorem 2 has been verified.

Deduction 2. From Theorem 2, it is known that under the context of the centralized decision, both Internet users and opinion leaders make their decision based on the maximum of false information clarification system's benefit, and the decision behavior of both sides is interrelated. Compared with decentralized decision, the optimal equilibrium strategy of opinion leaders (i.e., effort level of themselves) is additionally affected by the marginal traffic benefit of Internet users; the optimal equilibrium strategy of Internet users (i.e., effort level of themselves) is additionally affected by opinion leaders' marginal traffic benefit and direct benefit per unit gained from Internet users' effort. The optimal trajectory of the total volume of real information is dependent on the effort paid by opinion leaders and Internet users, while the optimal benefit of the false information clarification system increases with the growth of the total volume of real information. This means that the more effort paid by opinion leaders and Internet users, the more benefit they will receive. A detailed interrelated relationship is shown in Table 2.

3.3. Cost-Subsidized Decision-Making of Opinion Leaders and Internet Users. In the real world, opinion leaders could attract Internet users' attention using the method of "Forwarding + Commenting, drawing a lottery." With rewards from opinion leaders, Internet users are more willing to forward and spread real information. This study refers to such reward behaviors of opinion leaders as a cost subsidy.

Under such a decision-making behavior, a Stackelberg subordinate game model is established, with opinion leaders being leaders and Internet users being followers. The whole decision-making process is divided into two phases: in the first phrase, opinion leaders confirm their own effort level as E_L^S and provide a cost subsidy for Internet users who forward and spread information. The proportion of the cost subsidy provided by opinion leaders to Internet users is $\varepsilon\,(0 \le \varepsilon \le 1)$; in the second phrase, based on the obtained cost subsidy and decision-making behavior of opinion leaders, Internet users confirm their own effort level as E_U^S. The post-game equilibrium strategy is called the Stackelberg equilibrium strategy. Denoting S as opinion leaders' cost-subsidy decision, the decision-making behavior of both opinion leaders and Internet users at this moment is:

$$\begin{aligned} \max_{E_L,\varepsilon} J_L^S &= \int_0^\infty e^{-\rho t}\left\{\omega E_U + \pi_L f + \pi_L\gamma[\lambda R + \beta_L E_L + \beta_U E_U] - \frac{1}{2}\mu_L E_L^2 - \frac{1}{2}\varepsilon\mu_U E_U^2\right\}\mathrm{d}t, \\ \max_{E_U} J_U^S &= \int_0^\infty e^{-\rho t}\left\{\pi_U f + \pi_U\gamma[\lambda R + \beta_L E_L + \beta_U E_U] - \frac{1}{2}(1-\varepsilon)\mu_U E_U^2\right\}\mathrm{d}t. \end{aligned} \tag{39}$$

Table 2: Influence of different parameters on optimal equilibrium strategy of opinion leaders and internet users under centralized decision strategy.

	γ	π_L	π_U	λ	α_L	α_U	β_L	β_U	μ_L	μ_U	ω
E_L^C	↗	↗	↗	↗	↗	—	↗	—	↘	—	—
E_U^C	↗	↗	↗	↗	—	↗	—	↗	—	↘	↗

Note. ↗ refers to positive influence, ↘ refers to negative influence, —refers to irrelevance.

Theorem 3. *The equilibrium results under the cost-subsidy decision of opinion leaders and Internet users are:*

(1) The cost-subsidy proportion of opinion leaders is:

$$\varepsilon^* = \begin{cases} \dfrac{2(\delta+\rho)\omega + \gamma(2\pi_L - \pi_U)[\lambda\alpha_U + (\delta+\rho)\beta_U]}{2(\delta+\rho)\omega + \gamma(2\pi_L + \pi_U)[\lambda\alpha_U + (\delta+\rho)\beta_U]}, D < 1, \\ 0, D \geq 1. \end{cases}$$

$$D = \frac{\gamma(\pi_U - 2\pi_L)[\lambda\alpha_U + (\delta+\rho)\beta_U]}{2(\delta+\rho)\omega}. \tag{40}$$

(2) The optimal equilibrium strategy of opinion leaders is:

$$E_L^{S^*} = \frac{\gamma\pi_L[\lambda\alpha_L + (\delta+\rho)\beta_L]}{(\delta+\rho)\mu_L}. \tag{41}$$

(3) The optimal equilibrium strategy of Internet users is:

$$\begin{aligned} E_U^{S^*} &= \frac{\gamma\pi_U[\lambda\alpha_U + (\delta+\rho)\beta_U]}{(1-\varepsilon)(\delta+\rho)\mu_U} \\ &= \frac{2(\delta+\rho)\omega + \gamma(2\pi_L + \pi_U)[\lambda\alpha_U + (\delta+\rho)\beta_U]}{2(\delta+\rho)\mu_U}. \end{aligned} \tag{42}$$

(4) The optimal trajectory of the total volume of real information is:

$$\begin{aligned} R^{S^*} &= (R_0 - R_S^S)e^{-\delta t} + R_S^S \\ R_S^S &= \frac{\gamma\alpha_L\pi_L[\lambda\alpha_L + (\delta+\rho)\beta_L]}{\delta(\delta+\rho)\mu_L} + \frac{\gamma\alpha_U\pi_U[\lambda\alpha_U + (\delta+\rho)\beta_U]}{\delta(1-\varepsilon)(\delta+\rho)\mu_U} \\ &= \frac{\gamma\alpha_L\pi_L[\lambda\alpha_L + (\delta+\rho)\beta_L]}{\delta(\delta+\rho)\mu_L} \\ &\quad + \frac{\alpha_U\{2(\delta+\rho)\omega + \gamma(2\pi_L + \pi_U)[\lambda\alpha_U + (\delta+\rho)\beta_U]\}}{2\delta(\delta+\rho)\mu_U}. \end{aligned} \tag{43}$$

with R_S^S being the steady-state value of the total volume of real information under the cost-subsidy decision.

(5) The optimal benefit of opinion leaders is:

$$\begin{aligned} V_L^{S^*}(R) &= \frac{\lambda\pi_L\gamma}{\delta+\rho}R_S^S + \frac{\pi_L\gamma^2\pi_U[\lambda\alpha_U + (\delta+\rho)\beta_U]^2}{\rho(1-\varepsilon)(\delta+\rho)^2\mu_U} + \frac{\gamma^2\pi_L^2[\lambda\alpha_L + (\delta+\rho)\beta_L]^2}{2\rho(\delta+\rho)^2\mu_L} \\ &\quad + \frac{\omega\gamma\pi_U[\lambda\alpha_U + (\delta+\rho)\beta_U]}{\rho(1-\varepsilon)(\delta+\rho)\mu_U} - \frac{\gamma^2\pi_U^2\varepsilon[\lambda\alpha_U + (\delta+\rho)\beta_U]^2}{2\rho(1-\varepsilon)^2(\delta+\rho)^2\mu_U} + \frac{\pi_L f}{\rho} \\ &= \frac{\lambda\pi_L\gamma}{\delta+\rho}R_S^S + \frac{\alpha_U^2\lambda^2\gamma^2(2\pi_L + \pi_U)^2}{8\rho(\delta+\rho)^2\mu_U} + \frac{[\alpha_L\lambda + \beta_L(\delta+\rho)]^2\pi_L^2\gamma^2}{2\rho(\delta+\rho)^2\mu_L} + \frac{\pi_L f}{\rho} \\ &\quad + \frac{\gamma\beta_U(2\pi_L + \pi_U)[\beta_U(2\pi_L + \pi_U)\gamma + 4\omega] + 4\omega^2}{8\rho\mu_U} \\ &\quad + \frac{\lambda\gamma\alpha_U(2\pi_L + \pi_U)[2\omega + \gamma\beta_U(2\pi_L + \pi_U)]}{4\rho(\delta+\rho)\mu_U}. \end{aligned} \tag{44}$$

(6) The optimal benefit of Internet users is:

$$\begin{aligned} V_U^{S^*}(R) &= \frac{\lambda\pi_U\gamma}{\delta+\rho}R_S^S + \frac{\pi_U\gamma^2\pi_L\left[\lambda\alpha_L+(\delta+\rho)\beta_L\right]^2}{\rho(\delta+\rho)^2\mu_L} \\ &+\frac{\pi_U f}{\rho} + \frac{\pi_U^2\gamma^2\left[\lambda\alpha_U+(\delta+\rho)\beta_U\right]^2}{2\rho(1-\varepsilon)(\delta+\rho)^2\mu_U} \\ &= \frac{\lambda\pi_U\gamma}{\delta+\rho}R_S^S + \frac{\pi_U\beta_U^2(2\pi_L+\pi_U)\gamma^2}{4\rho\mu_U} + \frac{\left[\alpha_L\lambda+\beta_L(\delta+\rho)\right]^2\pi_U\pi_L\gamma^2}{\rho(\delta+\rho)^2\mu_L} \\ &+\frac{\pi_U\alpha_U^2\lambda^2\gamma^2(2\pi_L+\pi_U)}{4\rho(\delta+\rho)^2\mu_U} + \frac{f\pi_U}{\rho} \\ &+\frac{\pi_U\gamma\{\alpha_U\lambda\omega+\beta_U[\alpha_U\lambda(2\pi_L+\pi_U)\gamma+(\delta+\rho)\omega]\}}{2\rho(\delta+\rho)\mu_U}. \end{aligned} \tag{45}$$

(7) The optimal benefit of the system is:

$$\begin{aligned} V^{S^*}(R) &= V_L^{S^*}(R) + V_U^{S^*}(R) \\ &= \frac{\lambda\gamma(\pi_L+\pi_U)}{\delta+\rho}R_S^S + \frac{\omega\gamma\pi_U[\lambda\alpha_U+(\delta+\rho)\beta_U]}{\rho(1-\varepsilon)(\delta+\rho)\mu_U} + \frac{f(\pi_L+\pi_U)}{\rho} \\ &+\frac{\gamma^2\pi_L[2\pi_U+\pi_L]\left[\lambda\alpha_L+(\delta+\rho)\beta_L\right]^2}{2\rho(\delta+\rho)^2\mu_L} - \frac{\gamma^2\pi_U^2\varepsilon\left[\lambda\alpha_U+(\delta+\rho)\beta_U\right]^2}{2\rho(1-\varepsilon)^2(\delta+\rho)^2\mu_U} \\ &+\frac{\gamma^2\pi_U[2\pi_L+\pi_U]\left[\lambda\alpha_U+(\delta+\rho)\beta_U\right]^2}{2\rho(1-\varepsilon)(\delta+\rho)^2\mu_U} \\ &= \frac{\lambda\gamma(\pi_L+\pi_U)}{\delta+\rho}R_S^S + \frac{f(\pi_L+\pi_U)}{\rho} + \frac{(2\pi_L+3\pi_U)(2\pi_L+\pi_U)\alpha_U^2\lambda^2\gamma^2}{8\rho(\delta+\rho)^2\mu_U} \\ &+\frac{4\omega^2+\gamma\beta_U(2\pi_L+\pi_U)\left[(2\pi_L+3\pi_U)\gamma\beta_U+4\omega\right]}{8\rho\mu_U} \\ &+\frac{(2\pi_U+\pi_L)\pi_L\gamma^2\left[\alpha_L\lambda+\beta_L(\delta+\rho)\right]^2}{2\rho(\delta+\rho)^2\mu_L} \\ &+\frac{\omega 2\pi_U\gamma\left[\alpha_U\lambda+\beta_U(\delta+\rho)\right]+\lambda\gamma\alpha_U(2\pi_L+\pi_U)\left[2\omega+(2\pi_L+3\pi_U)\gamma\beta_U\right]}{4\rho(\delta+\rho)\mu_U}. \end{aligned} \tag{46}$$

Verification 3. To obtain the equilibrium solution of the Stackelberg subordinate game, the optimal control issue of Internet users should be addressed first with the backward induction method. According to optimal control theory, if $R \geq 0$, then $V_U^S(R)$ satisfies the HJB equation, and $V_U^S(R)$ has first and second derivatives, namely:

$$\rho V_U^S(R) = \max_{E_U}\left\{\begin{array}{c} \pi_U f + \pi_U\gamma\left[\lambda R+\beta_L E_L+\beta_U E_U\right] \\ -\frac{1}{2}(1-\varepsilon)\mu_U E_U^2 + V_U^{S'}\left[\alpha_L E_L+\alpha_U E_U-\delta R\right] \end{array}\right\}. \tag{47}$$

To solve E_U, the first derivative of the function on the right side of the equation is taken and set equal to zero, which gives:

$$E_U^S = \frac{\pi_U \gamma \beta_U + \alpha_U V_U^{S'}}{\mu_U (1-\varepsilon)}. \tag{48}$$

To maximize their own interest, opinion leaders would predict the behavior strategy of Internet users so as to confirm their own effort level and cost-subsidy proportion. At this moment, the HJB equation for opinion leaders is:

$$\rho V_L^S(R) = \max_{E_L,\varepsilon} \left\{ \begin{array}{c} \omega E_U + \pi_L f + \pi_L \gamma [\lambda R + \beta_L E_L + \beta_U E_U] - \frac{1}{2}\mu_L E_L^2 \\ \\ -\frac{1}{2}\varepsilon \mu_U E_U^2 + V_L^S{}' [\alpha_L E_L + \alpha_U E_U - \delta R] \end{array} \right\}, \tag{49}$$

To solve E_L, the first derivative of the function on the right side of equation (49) is taken and set equal to zero, which gives:

$$E_L^S = \frac{\pi_L \gamma \beta_L + \alpha_L V_L^{S'}}{\mu_L}. \tag{50}$$

Inputting equation (48) into (49), it is concluded that:

$$\rho V_L^S(R) = \max_{E_L,\varepsilon} \left\{ \begin{array}{c} \dfrac{\omega\left(\pi_U \gamma \beta_U + \alpha_U V_U^{S'}\right)}{\mu_U (1-\varepsilon)} + \pi_L \gamma \left[\lambda R + \beta_L E_L + \dfrac{\beta_U\left(\pi_U \gamma \beta_U + \alpha_U V_U^{S'}\right)}{\mu_U (1-\varepsilon)}\right] \\ \\ -\dfrac{1}{2}\mu_L E_L^2 - \dfrac{1}{2}\varepsilon \mu_U \left[\dfrac{\pi_U \gamma \beta_U + \alpha_U V_U^{S'}}{\mu_U (1-\varepsilon)}\right]^2 + \pi_L f \\ \\ +V_L^S{}' \left[\alpha_L E_L + \dfrac{\alpha_U\left(\pi_U \gamma \beta_U + \alpha_U V_U^{S'}\right)}{\mu_U (1-\varepsilon)} - \delta R\right] \end{array} \right\}. \tag{51}$$

To solve ε, the first derivative of the function on the right of the formula (51) is taken and set equal to zero, which gives:

$$\varepsilon = \left\{ \begin{array}{l} \dfrac{2\left(\omega + \alpha_U V_L^{S'} + \gamma \beta_U \pi_L\right) - \left(\gamma \beta_U \pi_U + \alpha_U V_U^{S'}\right)}{2\left(\omega + \alpha_U V_L^{S'} + \gamma \beta_U \pi_L\right) + \left(\gamma \beta_U \pi_U + \alpha_U V_U^{S'}\right)}, B > C, \\ \\ 0, B < C, \end{array} \right. \tag{52}$$

With $B = 2(\omega + \alpha_U V_L^{S'} + \gamma \beta_U \pi_L), C = \gamma \beta_U \pi_U + \alpha_U V_U^{S'}$.

Inputting equations (48) and (50) into equation (47), it is concluded that:

$$\begin{aligned} \rho V_U^S(R) = {} & \left(\lambda \pi_U \gamma - \delta V_U^{S'}\right) R - \frac{\left(\alpha_U V_U^{S'} + \beta_U \pi_U \gamma\right)^2}{2\mu_U (1-\varepsilon)^2} + \pi_U f + \frac{\varepsilon\left(\alpha_U V_U^{S'} + \beta_U \pi_U \gamma\right)}{2\mu_U (1-\varepsilon)^2} \\ & + V_U^{S'} \left[\frac{\alpha_L\left(\alpha_L V_L^S{}' + \beta_L \pi_L \gamma\right)}{\mu_L} + \frac{\alpha_U\left(\alpha_U V_U^{S'} + \beta_U \pi_U \gamma\right)}{\mu_U (1-\varepsilon)}\right] \\ & + \pi_U \gamma \left[\frac{\beta_L\left(\alpha_L V_L^S{}' + \beta_L \pi_L \gamma\right)}{\mu_L} + \frac{\beta_U\left(\alpha_U V_U^{S'} + \beta_U \pi_U \gamma\right)}{\mu_U (1-\varepsilon)}\right] \end{aligned}. \tag{53}$$

Inputting equations (48) and (50) into equation (49), it is concluded that:

$$\rho V_L^S(R) = \left(\lambda\pi_L\gamma - \delta V_L^{S\prime}\right)R + \pi_L f - \frac{\left(\alpha_L V_U^{S'} + \beta_L\pi_L\gamma\right)^2}{2\mu_L} + V_L^{S\prime}\left[\frac{\alpha_L\left(\alpha_L V_U^{S'} + \beta_L\pi_L\gamma\right)}{\mu_L} + \frac{\alpha_U\left(\alpha_U V_U^{S'} + \beta_U\pi_U\gamma\right)}{\mu_U(1-\varepsilon)}\right] + \frac{\omega\left(\alpha_U V_U^{S'} + \beta_U\pi_U\gamma\right)}{\mu_U(1-\varepsilon)} - \frac{\varepsilon\left(\alpha_U V_U^{S'} + \beta_U\pi_U\gamma\right)^2}{2\mu_U(1-\varepsilon)^2} + \pi_L\gamma\left[\frac{\beta_L\left(\alpha_L V_U^{S'} + \beta_L\pi_L\gamma\right)}{\mu_L} + \frac{\beta_U\left(\alpha_U V_U^{S'} + \beta_U\pi_U\gamma\right)}{\mu_U(1-\varepsilon)}\right]. \tag{54}$$

From the structural characteristics of equations (53) and (54), the linear optimal value function for R is the solution to the HJB equation. Therefore, it is assumed that $V_L^S(R)$'s and $V_U^S(R)$'s linear analytic equations for R are:

$$V_L^S(R) = g_1 R + g_2, \tag{55}$$

$$V_U^S(R) = h_1 R + h_2. \tag{56}$$

With g_1, g_2, h_1, and h_2 being undetermined coefficients. From equations (55) and (56), it is further determined that:

$$V_U^{S'}(R) = g_1, \tag{57}$$

$$V_U^{S'}(R) = h_1. \tag{58}$$

Equations (55)–(58) are inputted into equations (53) and (54). With the undetermined coefficients method, the values of g_1, g_2, h_1, and h_2 could be obtained:

$$g_1 = \frac{\lambda\pi_L\gamma}{\delta+\rho}, \tag{59}$$

$$g_2 = \frac{\pi_L f}{\rho} + \frac{\pi_L\gamma^2\pi_U\left[\lambda\alpha_U + (\delta+\rho)\beta_U\right]^2}{\rho(1-\varepsilon)(\delta+\rho)^2\mu_U} + \frac{\gamma^2\pi_L^2\left[\lambda\alpha_L + (\delta+\rho)\beta_L\right]^2}{2\rho(\delta+\rho)^2\mu_L} + \frac{\omega\gamma\pi_U\left[\lambda\alpha_U + (\delta+\rho)\beta_U\right]}{\rho(1-\varepsilon)(\delta+\rho)\mu_U} - \frac{\gamma^2\pi_U^2\varepsilon\left[\lambda\alpha_U + (\delta+\rho)\beta_U\right]^2}{2\rho(1-\varepsilon)^2(\delta+\rho)^2\mu_U}, \tag{60}$$

$$h_1 = \frac{\lambda\pi_U\gamma}{\delta+\rho}, \tag{61}$$

$$h_2 = \frac{\pi_U f}{\rho} + \frac{\pi_U^2\gamma^2\left[\lambda\alpha_U + (\delta+\rho)\beta_U\right]^2}{2\rho(1-\varepsilon)(\delta+\rho)^2\mu_U} + \frac{\pi_U\gamma^2\pi_L\left[\lambda\alpha_L + (\delta+\rho)\beta_L\right]^2}{\rho(\delta+\rho)^2\mu_L}. \tag{62}$$

Inputting equations (57), (58), (59), and (61) into equation (52), can get the equation (40) of cost-subsidy proportion of opinion leaders.

Inputting equation (40) into equations (60) and (62), the values of g_2 and h_2 under $\gamma(\pi_U - 2\pi_L)[\lambda\alpha_U + (\delta+\rho)\beta_U] < 2(\delta+\rho)\omega$ could be obtained:

$$g_2 = \frac{\alpha_U^2\lambda^2\gamma^2(2\pi_L+\pi_U)^2}{8\rho(\delta+\rho)^2\mu_U} + \frac{\gamma\beta_U(2\pi_L+\pi_U)[\beta_U(2\pi_L+\pi_U)\gamma+4\omega]+4\omega^2}{8\rho\mu_U} + \frac{[\alpha_L\lambda+\beta_L(\delta+\rho)]^2\pi_L^2\gamma^2}{2\rho(\delta+\rho)^2\mu_L} + \frac{\pi_L f}{\rho} + \frac{\lambda\gamma\alpha_U(2\pi_L+\pi_U)[2\omega+\gamma\beta_U(2\pi_L+\pi_U)]}{4\rho(\delta+\rho)\mu_U}, \tag{63}$$

$$h_2 = \frac{\pi_U\beta_U^2(2\pi_L+\pi_U)\gamma^2}{4\rho\mu_U} + \frac{[\alpha_L\lambda+\beta_L(\delta+\rho)]^2\pi_U\pi_L\gamma^2}{\rho(\delta+\rho)^2\mu_L} + \frac{\pi_U\alpha_U^2\lambda^2\gamma^2(2\pi_L+\pi_U)}{4\rho(\delta+\rho)^2\mu_U} + \frac{\pi_U\gamma\{\alpha_U\lambda\omega+\beta_U[\alpha_U\lambda(2\pi_L+\pi_U)\gamma+(\delta+\rho)\omega]\}}{2\rho(\delta+\rho)\mu_U} + \frac{f\pi_U}{\rho}. \tag{64}$$

Inputting equations (57) and (59) into equation (50), the optimal equilibrium strategy for opinion leaders is shown as equation (41); inputting equations (40), (58), and (61) into equation (48), the optimal equilibrium strategy for Internet users is shown as equation (42); inputting equations (41) and (42) into equation (2), the optimal trajectory of total volume of real information and the steady-state value are shown as equation (43); inputting equations (59), (60), and (63) into equation (55), the optimal benefit of opinion leaders is shown as equation (44); inputting equations (61), (62), and (64) into equation (56), the optimal benefit of Internet users is shown as equation (45); from equations (44) and (45), the optimal benefit for the whole false information clarification system is shown as equation (46).

So far, Theorem 3 has been verified.

Deduction 3. From Theorem 3, it is known that opinion leaders would provide a cost subsidy to Internet users when $\gamma(\pi_U - 2\pi_L)[\lambda\alpha_U + (\delta+\rho)\beta_U]/2(\delta+\rho)\omega < 1$. In addition, the proportion of the cost subsidy provided by opinion leaders is affected simultaneously by the attention level of major emergencies, direct benefit per unit opinion leaders gained from effort paid by Internet users, marginal traffic benefit for opinion leaders and Internet users, the total volume of real information, and influential coefficients of the total volume of real information, and the effort level of Internet users on social platforms.

Under decentralized decision-making with a cost subsidy provided by opinion leaders, the optimal equilibrium strategy of opinion leaders (i.e., their effort level) is consistent with that under decentralized decision-making without a cost subsidy; the optimal equilibrium strategy (i.e., their effort level) is additionally affected by the cost-subsidy proportion of opinion leaders. The optimal trajectory of the total volume of real information is dependent on efforts paid by opinion leaders and Internet users, while the optimal benefit of the false information clarification system increases with the growth of the total volume of real information. This means that the more effort paid by opinion leaders and Internet users, the more benefit they will receive. Details of the interrelated relationship are shown in Table 3.

4. Model Analysis

4.1. Comparative Analysis. From equation (40), it is known that when $\gamma(\pi_U - 2\pi_L)[\lambda\alpha_U + (\delta+\rho)\beta_U] < 2(\delta+\rho)\omega$, opinion leaders will provide a cost subsidy for Internet users; when $\gamma(\pi_U - 2\pi_L)[\lambda\alpha_U + (\delta+\rho)\beta_U] \geq 2(\delta+\rho)\omega$, $\varepsilon = 0$, this means the cost-subsidy proportion is zero, so Internet users get zero cost subsidy, and the decision behavior at this time is the same as that under decentralized decision-making. Therefore, this study will do a comparative analysis under the circumstance of $\gamma(\pi_U - 2\pi_L)[\lambda\alpha_U + (\delta+\rho)\beta_U] < 2(\delta+\rho)\omega$ and determine the optimal equilibrium strategy for opinion leaders and Internet users, the steady-state value of the total volume of real information, and the optimal benefit for opinion leaders, Internet users, and the system under three decision behaviors (i.e., centralized decision-making, decentralized decision-making, and cost-subsidy decision-making). Deductions are as follows:

Deduction 4. The optimal strategy of opinion leaders under different decision behaviors: $E_L^{N^*} = E_L^{S^*} < E_L^{C^*}$

The optimal strategy of Internet users under different decision behaviors: $E_U^{N^*} < E_U^{S^*} < E_U^{C^*}$

Verification 4. Comparing equations (6), (27), and (41):

$$E_L^{N^*} - E_L^{S^*} = 0E_L^{C^*} - E_L^{S^*} = \frac{\gamma\pi_U[\lambda\alpha_L + (\delta+\rho)\beta_L]}{\mu_L(\delta+\rho)}, \tag{65}$$

Because all related parameters exceed zero, $E_L^{N^*} = E_L^{S^*} < E_L^{C^*}$ is met;

Comparing equations (7), (28), and (42):

$$E_U^{S^*} - E_U^{N^*} = \frac{2(\delta+\rho)\omega + \gamma(2\pi_L - \pi_U)[\lambda\alpha_U + (\delta+\rho)\beta_U]}{2(\delta+\rho)\mu_U}.$$

$$E_U^{C^*} - E_U^{S^*} = \frac{\gamma\pi_U[\lambda\alpha_U + (\delta+\rho)\beta_U]}{2\mu_U(\delta+\rho)} \tag{66}$$

Because all related parameters exceed zero, $E_U^{N^*} < E_U^{S^*} < E_U^{C^*}$ is met; So far,Deduction 4 has been verified.

Table 3: Influence of different parameters on optimal equilibrium strategy of opinion leaders and internet users and cost-subsidy proportion under decentralized decision with cost subsidy.

	γ	π_L	π_U	λ	α_L	α_U	β_L	β_U	μ_L	μ_U	ω
E_L^S	↗	↗	—	↗	↗	—	↗	—	↘	—	—
E_U^S	↗	↗	↗	↗	—	↗	—	↗	—	↘	↗
E	↗	↗	↘	↗	—	↗	—	↗	—	—	↗

Note. ↗ refers to positive influence, ↘ refers to negative influence, —refers to irrelevance.

From Deduction 4, it is known that whatever the value of parameters, the optimal effort level paid by opinion leaders and Internet users under centralized decision-making behavior is higher than that under the other two decision-making behaviors. Under decentralized decision-making and cost-subsidy decision-making, the optimal effort paid by opinion leaders is the same; only when a certain condition is met between the attention level of a major emergency and the direct benefit per unit opinion leaders gained from the effort paid by Internet users, marginal traffic benefit for opinion leaders and Internet users, total volume of real information, and the influential coefficients of effort level of Internet users on social platform traffic will the optimal effort level paid by Internet users under decentralized decision-making be lower than that under cost-subsidy decision-making. Otherwise, the results are the same.

Deduction 5. Steady-state value of the total volume of real information under different circumstances: $R_S^N < R_S^S < R_S^C$.

Verification 5. By comparing the steady-state value of the total volume of real information, it is known that:

$$R_S^C - R_S^S = \frac{\gamma\alpha_L\pi_U[\lambda\alpha_L + (\delta+\rho)\beta_L]}{\delta(\delta+\rho)\mu_L} + \frac{\gamma\alpha_U\pi_U[\lambda\alpha_U + (\delta+\rho)\beta_U]}{2\delta\mu_U(\delta+\rho)}$$

$$R_S^S - R_S^N = \frac{2\alpha_U(\delta+\rho)\omega + \gamma\alpha_U(2\pi_L - \pi_U)[\lambda\alpha_U + (\delta+\rho)\beta_U]}{2\delta(\delta+\rho)\mu_U} \tag{67}$$

Because all related parameters exceed zero and $\gamma(\pi_U - 2\pi_L)[\lambda\alpha_U + (\delta+\rho)\beta_U] < 2(\delta+\rho)\omega$, $R_S^N < R_S^S < R_S^C$ is met.

So far,Deduction 5 has been verified.

From Deduction 5, it is known that whatever the value of parameters, the steady-state value of the total volume of real information under centralized decision-making behavior is greater than that of under the other two decision-making behavior. Only when a certain condition is met between the attention level of a major emergency, the direct benefit per unit opinion leaders gained from effort paid by Internet users, marginal traffic benefit for opinion leaders and Internet users, the total volume of real information, and the influential coefficients of effort level of Internet users on social platform traffic will the steady-state value of the total volume of real information under decentralized decision-making behavior be smaller than that under cost-subsidy decision-making behavior. Otherwise, the results are the same.

Deduction 6. The optimal benefit for opinion leaders under different circumstances is: $V_L^{N^*}(R) < V_L^{S^*}(R)$.

The optimal benefit for Internet users under different circumstances is: $V_U^{N^*}(R) < V_U^{S^*}(R)$.

The optimal benefit for the system under different circumstances is: $V^{N^*}(R) < V^{S^*}(R) < V^{C^*}(R)$

Verification 6. Comparing (9) and (44):

$$V_L^{S^*}(R) - V_L^{N^*}(R) = \frac{\lambda\pi_L\gamma}{\delta+\rho}\left(R_S^S - R_S^N\right) + \frac{\{2(\delta+\rho)\omega + \gamma(2\pi_L - \pi_U)[\lambda\alpha_U + (\delta+\rho)\beta_U]\}^2}{8\rho(\delta+\rho)^2\mu_U}. \tag{68}$$

From Deduction 5 it is known that $R_S^N < R_S^S$, all related parameters exceed zero and $\gamma(\pi_U - 2\pi_L)[\lambda\alpha_U + (\delta+\rho)\beta_U] < 2(\delta+\rho)\omega$; therefore, $V_L^{N^*}(R) < V_L^{S^*}(R)$ is met.

Comparing (10) and (45):

$$V_U^{S^*}(R) - V_U^{N^*}(R) = \frac{\lambda\pi_U\gamma}{\delta+\rho}\left(R_S^S - R_S^N\right) + \frac{\varepsilon\pi_U^2\gamma^2[\lambda\alpha_U + (\delta+\rho)\beta_U]^2}{2\rho(1-\varepsilon)(\delta+\rho)^2\mu_U}. \tag{69}$$

From Deduction 5, it is known that $R_S^N < R_S^S$, all related parameters exceed zero, and $0 \le \varepsilon < 1$; therefore, $V_U^{N^*}(R) < V_U^{S^*}(R)$ is met.

Because $V^{N^*}(R) = V_L^{N^*}(R) + V_U^{N^*}(R), V^{S^*}(R) = V_L^{S^*}(R) + V_U^{S^*}(R)$ and $V_L^{N^*}(R) < V_L^{S^*}(R), V_U^{N^*}(R) < V_U^{S^*}(R)$, $V_L^{N^*}(R) < V_L^{S^*}(R), V_U^{N^*}(R) < V_U^{S^*}(R)$ must exist. Therefore, only comparing the value of $V^{C^*}(R)$ and $V^{S^*}(R)$ is needed. Comparing (30) and (46):

$$V^{C^*}(R) - V^{S^*}(R) = \frac{\lambda\gamma(\pi_L + \pi_U)}{\delta+\rho}\left(R_S^C - R_S^S\right) + \frac{\gamma^2\pi_U^2\left\{4[\lambda\alpha_L + (\delta+\rho)\beta_L]^2\mu_U + [\lambda\alpha_U + (\delta+\rho)\beta_U]^2\mu_L\right\}}{8\rho(\delta+\rho)^2\mu_U\mu_L}. \tag{70}$$

From Deduction 5, it is known that $R_S^S < R_S^C$, and all related parameters exceed zero; therefore, $V^{N^*}(R) < V^{S^*}(R) < V^{C^*}(R)$ is met.

So far, Deduction 6 has been verified.

From Deduction 6, it is known that the optimal benefit for both opinion leaders and Internet users under cost-subsidy decision-making is greater than that under decentralized decision-making. For the whole system, the optimal

benefit obtained under centralized decision-making, cost-subsidy decision-making, and decentralized decision-making diminishes.

4.2. Numerical Simulation Analysis. To further verify the above theoretical analysis, MATLAB 2017 has been applied to assign theoretical parameters under decentralized, centralized, and cost-subsidy decision-making of opinion leaders and Internet users, so as to explore the progressive evolution of the total volume of real information, the benefit of opinion leaders and Internet users, and the total benefit of false information clarification system over time in a more visual way. Because relevant parameters of opinion leaders and Internet users could not be obtained directly in the real world, this study will try its best to rationalize the above values according to the real situation. The assignment of relevant parameters is as follows:

$$\begin{cases} \mu_L = 6, \mu_U = 4.5, \alpha_L = 3, \alpha_U = 2, \delta = 1, \\ R_0 = 0, f = 1, \gamma = 0.7, \beta_L = 1.5, \beta_U = 1, \\ \rho = 0.2, \pi_L = 4, \pi_U = 2, \omega = 1.5, \lambda = 0.8. \end{cases} \tag{71}$$

Based on the above assignments, the equilibrium results of differential games under different decision-making behaviors are given in Table 4.

The equilibrium results in Table 4 prove that the theoretical analysis in Deduction 4–Deduction 6 is correct.

4.2.1. Simulation Analysis of Changing Trajectory of the Total Volume of Real Information. Keeping the values of other parameters unchanged, $R_0 = 5$ and $R_0 = 13$ are taken as the total volume of real information at the initial moment, and a numerical simulation analysis is applied to the optimal trajectory of the total volume of real information under three different decision-making types. The evolution trajectory of the total volume of real information over time is shown in Figure 1.

From Figure 1, it is found that the evolution trajectories of the total volume of real information under the three decision-making types are related to the initial value of the total volume of real information. When the initial value is relatively high, the total volume of real information diminishes over time; when the initial value is relatively low, the total volume of real information increases over time. Both converge to the same steady-state value. From the deductions above, it is known that the steady-state value of the total volume of real information is irrelevant to the initial value, but relevant only to different decision-making behaviors.

Because the cost-subsidy behavior of opinion leaders under subsidized decision-making behavior could reach Pareto improvement on the total volume of real information, the steady-state value of the total volume of real information under decentralized decision-making is the smallest, followed by that under cost-subsidy decision-making, and the value under centralized decision reaches Pareto optimality.

4.2.2. Simulation Analysis of Changing Trajectories of the Total Benefit of Opinion Leaders and Internet Users. A numerical simulation analysis is applied to the benefits of opinion leaders under decentralized and cost-subsidy decision-making, and the trajectories of opinion leaders' total benefit over time are shown in Figure 2. A numerical simulation analysis is also applied to the benefits of Internet users under decentralized and cost-subsidy decision-making, and the trajectories of Internet users' total benefits over time are shown in Figure 3.

Based on Figures 2 and 3, it is found that the total benefit of opinion leaders and Internet users increases slightly over time, and finally plateaus at a fixed value. After reaching the fixed value (the maximum), the total benefits of both parties will not change over time, and both parties' total benefits are higher under cost-subsidy decision-making than under decentralized decision. Although additional cost subsidy for Internet users is needed during cost-subsidy decision-making, the total benefits are significantly improved. This is because the total volume of real information achieves Pareto improvement; with the increase of the total volume of real information, the benefit for opinion leaders and Internet users increases.

4.2.3. Simulation Analysis of the Trajectory of the System's Total Benefit. A numerical simulation analysis is applied to the total benefit of the system under decentralized, centralized, and cost-subsidy decision-making, and the trajectories of the system's total benefit over time are shown in Figure 4.

Based on Figure 4, it is found that regardless of the decision-making behavior, the system's total benefit increased. Trajectories under the three decision-making behaviors plateaued at a fixed value over time, which means total benefit will not increase with time when it reaches the maximum. Under centralized decision-making, because both opinion leaders and Internet users set the maximum of the system's benefit as their goals, they fully cooperate with each other without changing their own behavior out of personal interest; therefore, the system's total benefit reaches Pareto optimality, higher than that under decentralized or cost-subsidy decision-making; under decentralized decision-making, because both opinion leaders and Internet users set the maximum of their own benefit as their goals, they will not change their behavior to improve the system's benefit, making the system's benefit the lowest among all three decision-making types; under cost-subsidy decision-making, which is an improvement to decentralized decision-making, opinion leaders provide a cost subsidy to Internet users so as to achieve Pareto improvement for the system's total benefit. Therefore, the system's total benefit under cost-subsidy decision-making is higher than that under decentralized decision-making but lower than that under centralized decision-making due to the failure to achieve Pareto optimality.

4.2.4. Analysis of Each Parameter's Sensibility to Equilibrium Results. Analyses of each important parameter's sensibility

Table 4: Equilibrium results of differential game under different decision behavior.

	Decentralized decision	Centralized decision	Cost-subsidy decision
Effort level of opinion leaders	1.6333	2.4500	1.6333
Effort level of internet users	0.7259	2.5111	2.1481
Cost-subsidy proportion	—	—	0.6621
Total volume of real information	6.3519	12.3722	9.1963
Total benefit of opinion leaders	101.0315	—	129.0967
Total benefit of internet users	61.8735	—	76.1431
Total benefit of the system	162.9049	225.6186	205.2398

Note. 4 digits after the decimal point kept.

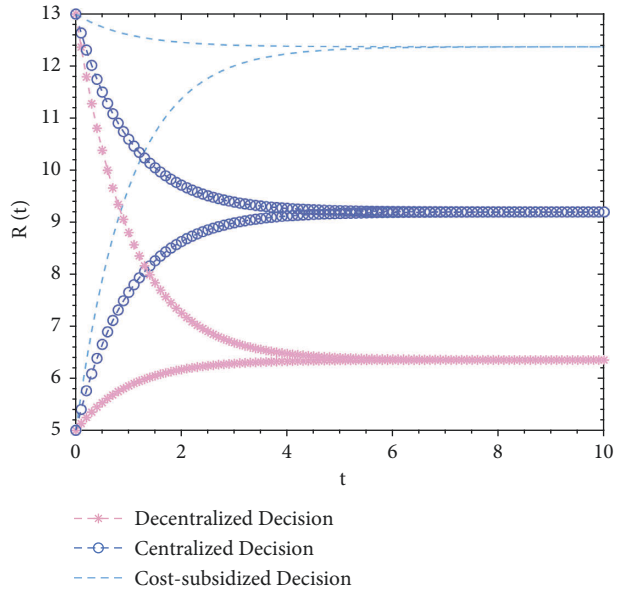

Figure 1: The evolution trajectory of the total volume of real information under three decisions.

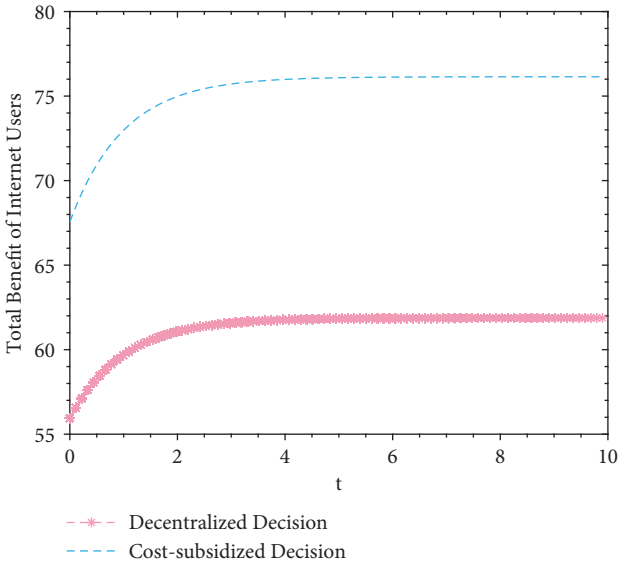

Figure 3: Trajectories of internet users' total benefit under decentralized and cost-subsidy decision.

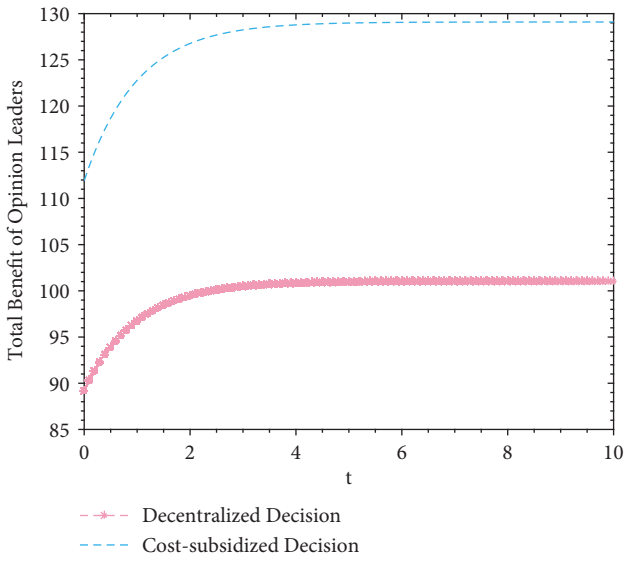

Figure 2: Trajectories of opinion leaders' total benefit under decentralized and cost-subsidy decision.

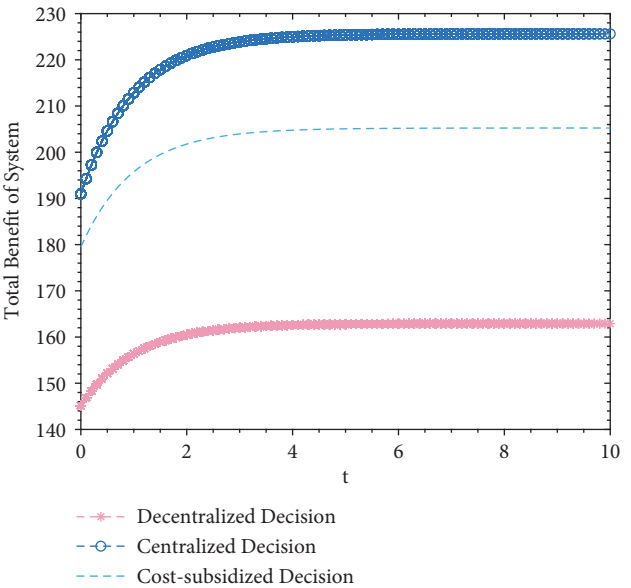

Figure 4: Trajectories of the system's total benefit over time under three decision behavior.

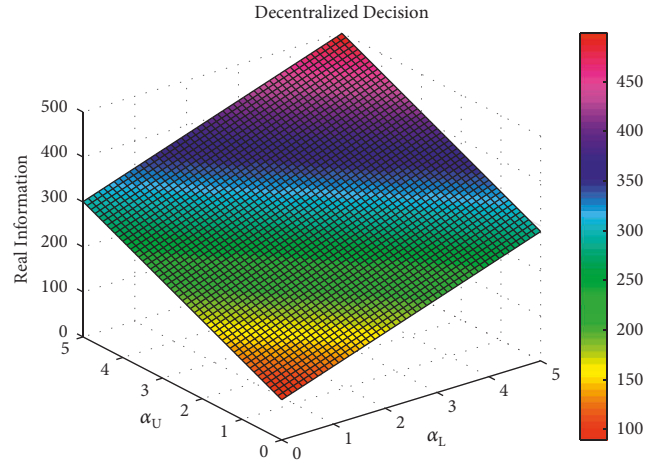

Figure 5: The influence of parameter α_L and α_U on the total volume of real information under decentralized decision.

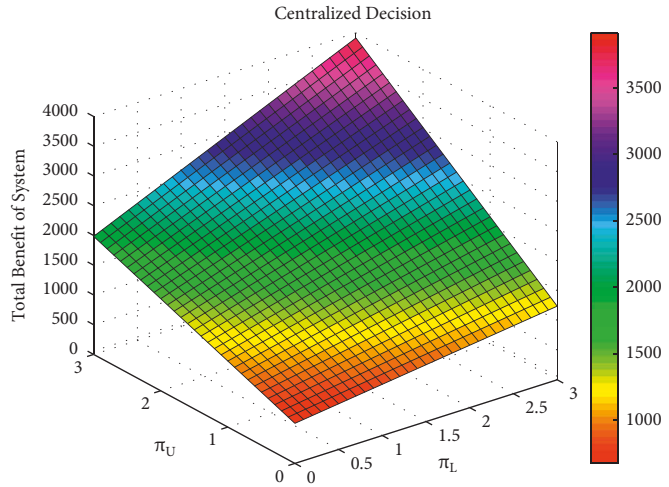

Figure 6: The influence of parameter π_L and π_U on the system's total benefit under centralized decision.

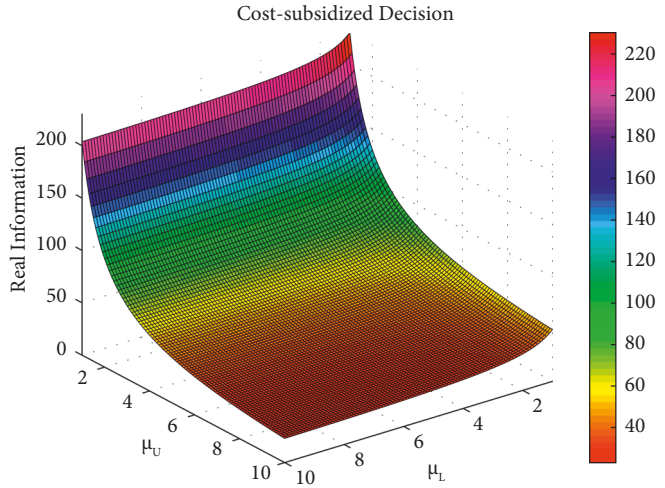

Figure 7: The influence of parameter μ_L and μ_U on the total volume of real information under cost-subsidy decision.

Table 5: Analysis of key parameters' sensitivity to differential game equilibrium results.

Key parameters	Decentralized decision		Centralized decision		Cost-subsidy decision	
	Total volume of real information	System's total benefit	Total volume of real information	System's total benefit	Total volume of real information	System's total benefit
$\lambda\uparrow$	↑	↑	↑	↑	↑	↑
$\omega\uparrow$	—	↑	↑	↑	↑	↑
$\gamma\uparrow$	↑	↑	↑	↑	↑	↑
f↑	—	↑	—	↑	—	↑
$\mu_L\uparrow$	↓	↓	↓	↓	↓	↓
$\mu_U\uparrow$	↓	↓	↓	↓	↓	↓
$\pi_L\uparrow$	↑	↑	↑	↑	↑	↑
$\pi_U\uparrow$	↑	↑	↑	↑	↑	↑
$\alpha_L\uparrow$	↑	↑	↑	↑	↑	↑
$\alpha_U\uparrow$	↑	↑	↑	↑	↑	↑
$\beta_L\uparrow$	↑	↑	↑	↑	↑	↑
$\beta_U\uparrow$	↑	↑	↑	↑	↑	↑
$\delta\uparrow$	↓	↓	↓	↓	↓	↓
$\rho\uparrow$	↓	↓	↓	↓	↓	↓

Note: ↗ refers to positive relevance, ↘ refers to negative relevance, —refers to irrelevance.

to equilibrium results under decentralized, centralized, and cost-subsidy decision-making are carried out. Limited by the length of this study, only several parameters' sensibility analysis figures are listed below, with the rest of the parameters' sensibilities analyzed based on −20%, −10%, +10%, and +20% of the previously mentioned (71) standard value. Details of the changes of equilibrium results with the increase of parameter value are given in Figure 5.

The influence of parameters α_L and α_U on the total volume of real information under decentralized decision-making, that of parameters π_L and π_U on the system's total benefit under centralized decision-making, and that parameters μ_L and μ_U on the total volume of real information under cost-subsidy decision-making are shown in Figures 5–7, respectively.

Based on Figure 5, the greater the influential coefficient of effort level of opinion leaders and Internet users on the total volume of real information under decentralized decision-making, the more real information on social platforms. Based on Figure 6, opinion leaders' and Internet users' marginal traffic under centralized decision-making is positively related to the system's total benefit, which means the greater the marginal traffic, the higher the system's total benefit. Based on Figure 7, opinion leaders' and Internet users' effort cost coefficient is negatively related to the total volume of real information under cost-subsidy decision-making, which means the greater the effort cost coefficient, the less real information on social platforms.

From the results in Table 5, it is found that:

(1) Regardless of decision behavior, opinion leaders and Internet users marginal traffic benefit π_L and π_U, effort level's influential coefficients α_L and α_U on the total volume of real information, effort level's influential coefficients β_L and β_U on the traffic of social platform, attention level γ received by major emergencies, and the total volume of real information's influential coefficient λ on the traffic of social platform are positively related to the total volume of real information and the system's total benefit.

(2) Regardless of decision behavior, the effort cost coefficients μ_L and μ_U of opinion leaders and Internet users, the natural dissipation coefficient of real information, and the discount rate ρ are negatively correlated with the total volume of real information and the system's total benefit.

(3) A social platform's initial traffic has no influence on the total volume of real information, but it is positively correlated with the system's total benefit. Under decentralized decision-making, the direct benefit per unit obtained by opinion leaders from the effort of Internet users ω has no influence on the total volume of real information, but it is positively correlated with the system's total benefit; under centralized and cost-subsidy decision-making, the direct benefit per unit obtained by opinion leaders from the effort of Internet users ω is positively correlated with the total volume of real information and the system's total benefit.

5. Conclusion

Under the background of false information on social platforms after major emergencies, this study explores the dynamic optimization of a clarification system consisting of false information released by opinion leaders and Internet users. Based on optimal control theory and differential game theory, differential game models under decentralized, centralized, and cost-subsidy decision-making are constructed, and opinion leaders' and Internet users' optimal equilibrium strategies and optimal benefit, optimal trajectory, and steady-state value of the total volume of real information, and the optimal benefit of the false information clarification system are obtained. The following conclusions can be

drawn after comparative analyses and numerical simulations:

(1) Compared with the other two decision behaviors, under centralized decision-making, opinion leaders' and Internet users' optimal equilibrium strategies and optimal benefit, the optimal trajectory and steady-state value of the total volume of real information, and the optimal benefit of false information clarification system reach their maxima; therefore, Pareto optimality is achieved. This means that centralized decision-making could, to the largest extent, reduce public panic caused by false information after major emergencies, and could be regarded as the optimal decision-making type for opinion leaders and Internet users.

(2) Cost-subsidy decision-making, as compared with centralized decision-making, fails to achieve Pareto optimality but efficiently improves decentralized behavior because opinion leaders provide a cost subsidy for Internet users. When the cost subsidy reaches a certain proportion, the optimal benefit of opinion leaders and Internet users, the optimal trajectory of the total volume of real information and its steady-state value, and the false information clarification system could achieve Pareto improvement. Although cost-subsidy decision-making fails to achieve Pareto optimality, as opinion leaders and Internet users could not be absolutely rational to reach centralized decision, cost-subsidy decision-making has its practical significance.

(3) Opinion leaders' and Internet users' effort cost coefficient, discount rate, and real information's natural dissipation rate are negatively correlated with the volume of real information. Therefore, in the real world, a certain extent of subsidy could be provided by social platforms or the relevant departments of the government to opinion leaders and Internet users, so as to increase the volume of real information and reduce public panic.

Data Availability

The authors confirm that the data supporting the findings of this study are included within the article.

Conflicts of Interest

The authors declare that the research was conducted in the absence of any commercial or financial relationships that could be construed as a potential conflict of interest.

Authors' Contributions

B.L. and H.L. conceptualized the study; B.L. developed the methodology; B.L. helped with software; B.L. and R.L. validated the study; B.L. wrote and prepared the original draft; H.L. and Q.S. wrote, reviewed, and edited the study; H.L. and Q.S. carried out funding acquisition. All authors have read and agreed to the published version of the manuscript.

Acknowledgments

This research was funded by the Natural Science Foundation of China (no. 71771112) and the Project of Liaoning Provincial Federation Social Science Circles of China (no. L20BGL047).

References

[1] B. Li, H. Li, Q. Sun, R. Lv, and J. Zhao, "Evolutionary game analysis of the dissemination of false information by multiple parties after major emergencies," *Complexity*, vol. 2022, Article ID 3527674, 14 pages, 2022.

[2] J. Kang, Y. Zeng, S. Chen, and Y. Wang, "E-commerce platform response to major public emergencies-Optimal strategies and benefits of e-commerce platform subsidies," *Systems Engineering-Theory & Practice*, vol. 42, no. 2, pp. 345–367, 2022.

[3] X. Wu, X. Liu, and J. Zhou, "Evolution model of NIMBY opinion based on public perception and governmental guidance," *Systems Engineering-Theory & Practice*, vol. 39, no. 11, pp. 2865–2879, 2019.

[4] J. Cao, X. Xu, and X. Chen, "Risk evolution model for large group emergency decision-making influenced by extreme preference," *Systems Engineering-Theory & Practice*, vol. 39, no. 3, pp. 596–614, 2019.

[5] A. U. Din, H. Han, A. Ariza-Montes, A. Vega-Munoz, A. Raposo, and S. Mohapatra, "The impact of COVID-19 on the food supply chain and the role of E-commerce for food purchasing," *Sustainability*, vol. 14, no. 5, 2022.

[6] T. Y. Akalu, K. A. Gelaye, M. A. Bishaw, S. Y. Tilahun, Y. Yeshaw, and T. Azale, "Depression, anxiety, and stress symptoms and its associated factors among residents of gondar town during the early stage of COVID-19 pandemic," *Risk Management and Healthcare Policy*, vol. 14, pp. 1073–1083, 2021.

[7] X. Hong, G. J. Zhang, D. J. Lu, H. Liu, L. Zhu, and M. L. Xu, "Personalized crowd emotional contagion coupling the virtual and physical cyberspace," *IEEE Transactions on Systems Man Cybernetics-Systems*, vol. 52, no. 3, pp. 1638–1652, 2022.

[8] H. Liu, "Official social media and its impact on public behavior during the first wave of COVID-19 in China," *BMC Public Health*, vol. 22, no. 1, 2022.

[9] E. McElroy, P. Patalay, B. Moltrecht, M. Shevlin, A. Shum, and C. Creswell, "Demographic and health factors associated with pandemic anxiety in the context of COVID-19," *British Journal of Health Psychology*, vol. 25, no. 4, pp. 934–944, 2020.

[10] H. P. Liao and J. L. Wang, "The impact of epidemic information on the public's worries and attitude toward epidemic prevention measures during the COVID-19 outbreak," *Current Psychology*, vol. 2021, no. 5, 2021.

[11] S. Hosseini and A. Zandvakili, "Information dissemination modeling based on rumor propagation in online social networks with fuzzy logic," *SOCIAL NETWORK ANALYSIS AND MINING*, vol. 12, no. 1, 2022.

[12] A. Pal and S. Banerjee, "Internet users beware, you follow online health rumors (more than counter-rumors) irrespective of risk propensity and prior endorsement," *Information Technology and People*, vol. 34, no. 7, pp. 1721–1739, 2021.

[13] P. Bordia, N. DiFonzo, R. Haines, and E. Chaseling, "Rumors denials as persuasive messages: effects of personal relevance, source, and message characteristics," *Journal of Applied Social Psychology*, vol. 35, no. 6, pp. 1301–1331, 2005.

[14] T. Buchanan and V. Benson, "Spreading disinformation on Facebook: do trust in message source, risk propensity, or personality affect the organic reach of fake news," *SOCIAL MEDIA + SOCIETY*, vol. 5, no. 4, 2019.

[15] A. Guess, J. Nagler, and J. Tucker, "Less than you think: prevalence and predictors of fake news dissemination on Facebook," *Science Advances*, vol. 5, no. 1, 2019.

[16] S. Vosoughi, D. Roy, and S. Aral, "The spread of true and false news online," *Science*, vol. 359, no. 6380, pp. 1146–+, 2018.

[17] P. Agarwal, R. Al Aziz, and J. Zhuang, "Interplay of rumor propagation and clarification on social media during crisis events-A game-theoretic approach," *European Journal of Operational Research*, vol. 298, no. 2, pp. 714–733, 2022.

[18] P. Ozturk, H. Y. Li, and Y. Sakamoto, "Combating rumor spread on social media: the effectiveness of refutation and warning," in *Proceedings of the 2015 48TH HAWAII INTERNATIONAL CONFERENCE ON SYSTEM SCIENCES (HICSS)*, pp. 2406–2414, Kauai, Hawaii, January, 2015.

[19] A. Perelman, T. Shima, and I. Rusnak, "Cooperative differential games strategies for active aircraft protection from a homing missile," *Journal of Guidance, Control, and Dynamics*, vol. 34, no. 3, pp. 761–773, 2011.

[20] H. G. Zhang, Q. L. Wei, and D. R. Liu, "An iterative adaptive dynamic programming method for solving a class of nonlinear zero-sum differential games," *Automatica*, vol. 47, no. 1, pp. 207–214, 2011.

[21] A. Prasad and S. P. Sethi, "Competitive advertising under uncertainty: a stochastic differential game approach," *Journal of Optimization Theory and Applications*, vol. 123, no. 1, pp. 163–185, 2004.

[22] G. Fibich, A. Gavious, and O. Lowengart, "Explicit solutions of optimization models and differential games with nonsmooth (asymmetric) reference-price effects," *Operations Research*, vol. 51, no. 5, pp. 721–734, 2003.

[23] K. A. Shchelchkov, "Estimate of the capture time and construction of the pursuer's strategy in a nonlinear two-person differential game," *Differential Equations*, vol. 58, no. 2, pp. 264–274, 2022.

[24] D. Machowska, A. Nowakowski, and A. Wiszniewska-Matyszkiel, "Closed-loop Nash equilibrium for a partial differential game with application to competitive personalized advertising," *Automatica*, vol. 140, 2022.

[25] M. Biancardi, G. Iannucci, and G. Villani, "Groundwater exploitation and illegal behaviors in a differential game," *Dynamic Games and Applications*, vol. 12, no. 3, pp. 996–1009, 2022.

[26] M. A. Garcia-Meza, "The cost of work discrimination: a market capture differential game model," *Mathematics*, vol. 9, no. 19, 2021.

Hindawi
Computational Intelligence and Neuroscience
Volume 2022, Article ID 2974960, 10 pages
https://doi.org/10.1155/2022/2974960

Research Article

A Fine-Grained Image Classification and Detection Method Based on Convolutional Neural Network Fused with Attention Mechanism

Yue Zhang

Centre for Modern Educational Technology, Henan College of Police, Zhengzhou 450000, Henan, China

Correspondence should be addressed to Yue Zhang; wlzx@hnp.edu.cn

Received 24 July 2022; Accepted 1 September 2022; Published 14 September 2022

Academic Editor: Zaoli Yang

Due to the existence of attention system, people pay attention to the distinguishable area of the image, rather than directly receiving and processing the information of the whole image. This natural advantage makes attention mechanism widely used in fine-grained image classification. The research goal of fine-grained image classification task often is to differentiate subclass objects belonging to the same basic category. The difficulty of classification is that there are only slight local differences between different categories, but there may be large feature differences within the same category. At the same time, complex background features also bring interference factors to image recognition. In order to further extract discriminant regional features, this paper proposes a fine-grained image classification method WSFF-BCNN based on weak supervision feature fusion from two aspects: the improvement of the loss function in the training process of convolution neural network and the refinement of fine-grained image feature extraction. It uses the mixed attention of channel domain and spatial domain to obtain the detailed description information in the feature to highlight the response of the corresponding channel and spatial location in the feature map and pay attention to the attention characteristics of different dimensions. The original images of different sizes are input into the improved bilinear model to obtain multi-scale features. The large-scale features can represent the spatial location information of key areas, and the small-scale features represent the low-level features of the image. The backbone network of bilinear network uses ResNet50 to extract features and sample and zoom and uses bilinear pooling to fuse features of different scales to obtain a rich image feature representation.

1. Introduction

Accurate classification of various types of visual objects is the basis of many advanced image understanding tasks. The research of fine-grained image classification has gradually become one of the hot research directions in the field of computer vision. It mainly includes two categories: fine-grained image classification based on strong supervision information and weak supervision information [1]. The former needs to introduce additional manual annotation, and the latter can locate the key areas of the image only under the supervision of label information. Fine-grained image classification is a research direction for fine-grained image classification [2]. Compared with the coarse-grained image classification task, the classification granularity of the category to which the fine-grained image belongs is more detailed. The characteristics of different subcategories often have only slight local differences but disturbed by uncertain factors such as light, occlusion, and shooting angle; the samples of the same subcategory may have large feature differences, making fine-grained image classification a challenging task [3].

As one of the important branches of machine learning, deep learning has developed rapidly in recent years and is widely used in computer vision, speech recognition, natural language processing, and other fields. The proposal of CNN meets the needs of automatic extraction of image features, greatly improves the operation speed and accuracy of image recognition, and saves unnecessary human consumption. Applying CNN to the field of fine-grained image

classification, with its powerful feature extraction ability, we can obtain more effective multi-dimensional abstract features, mine the subtle local feature information of fine-grained images, further improve the recognition efficiency and accuracy, and reduce the recognition cost. It is of great research significance to the application and development of fine-grained image recognition in various fields [4]. B-CNN (Bilinear CNN) model is an end-to-end fine-grained image classification algorithm based on feature coding. It can complete classification only by using image category tags, which belongs to the weak supervised learning method. However, the B-CNN model uses the image features extracted by two ResNet50 to complete the classification by feature fusion; the feature extractor does not capture the local regional features of the image comprehensively, and only considers the construction of a strong feature representation of the image [5, 6]. Therefore, this paper considers improving the B-CNN model from the aspect of capturing the local distinctive regional features of the image and adopts the improved ResNet50 as the backbone network of bilinear CNN, combine the proposed attention mechanism to automatically focus the space and channel, suppress the characteristics of background interference, integrate local localization into the bilinear deep learning framework, and carry out end-to-end training, so as to effectively improve the accuracy of fine-grained classification and further improve the classification performance of the model.

The main contribution of this paper is to propose a fine-grained classification scheme, which can learn useful regional features from many local features under the supervision of only label information and combine local features with semantic features to achieve effective classification. The model is composed of a target acquisition network and an image classification network. A bilinear convolution neural network based on attention mechanism is proposed. Two improved ResNet50 are used as feature extractors, which not only increase the depth of the network model but also reduce the amount of parameters. Then, an attention mechanism is proposed based on space and channel, which enables the network to automatically obtain the features of the image with distinguishing local areas and fuse the high-dimensional and low-dimensional features extracted by the two networks, respectively. With the help of the image category label, the image classification task is automatically completed, which improves the classification accuracy of the network and reduces the calculation cost.

2. Related Work

The fine-grained image classification method based on deep learning is divided into three ways: strong supervised learning, weak supervised learning, and unsupervised learning. The essential difference between these three ways is that the strong supervised learning method uses not only image-level labels but also bounding box and component annotation. The weak supervised learning method only uses image-level labels, while the unsupervised learning method does not use any labels for classification. When training the model, the fine-grained image classification algorithm based on strongly supervised learning needs to use the annotation box of image targets, the annotation information of target components, and image category labels [7, 8]. Extracting the component details of the target in the image is the key to the task of fine-grained image classification, so there are many algorithms using manually labeled component labels, but the labeled information needs to be made carefully and manually, and the cost is large, which hinders the application of the method relying on component label information in the actual scene under certain conditions.

Therefore, only using image category tags for classification and prediction is the research hotspot of fine-grained image classification. Attention mechanism plays an indispensable role in deep learning [9, 10]. Attention mechanism is a mode of resource allocation, which can focus on local information, invest more energy in dealing with important information, and ignore unimportant information. In recent years, the idea of attention mechanism has been widely used in various disciplines, especially in natural language processing and computer vision. Generally speaking, the attention mechanism is to get the parts that need to be mainly concerned from the image and then add a lot of attention resources to the parts that need to be mainly concerned, so as to obtain the information of the parts that need to be mainly concerned in the image [11]. At the same time, it also suppresses other irrelevant information in the image, so that we can accurately and quickly know what the main content of the painting is. From the differentiability of attention, attention can be divided into hard attention and soft attention. ResNet50 network adds attention modules to the convolution blocks of conv2 and conv3 and conv4 and conv5 of the two networks, respectively, to obtain richer and discriminative attention features [12]. Input the converged bilinear eigenvectors into the classification function to obtain the classification probability. Because the classification layer of Resnet50 network is set with 1000 categories of image classification tasks. Therefore, this paper is to remove the original classification layer and set a fixed number of neuron classification layer according to the actual needs of classification tasks [13].

Da P et al. [14] presented region-based, convolutional neural network for accurate and efficient TV logo classification. Maximally stable extremal region (MSER) was used as a method of generating candidate boxes per image. Zhang et al. [15] presented a novel method based on Random Forest classification with multi-type features to detect the logo regions on arbitrary images, and the detected logo regions were further recognized using the visual words with spatial correlated information. Druzhkov and Kustikova [16] consider such deep models as autoencoders, restricted Boltzmann machines, and convolutional neural networks. Existing software packages for deep learning problems are compared. Song et al. [17] proposed a synchronized deep autoencoder network for the simultaneous detection and classification of cells in bone marrow histology images. The proposed network used a single architecture to detect the positions of cells and classify the detected cells, in parallel. Liu and An [18] introduced the idea of sparse representation into the architecture of the deep learning network and

comprehensively utilized the sparse representation of well multi-dimensional data linear decomposition ability and the deep structural advantages of multilayer nonlinear mapping to complete the complex function approximation in the deep learning model. Liu et al. [19] proposed an active learning algorithm based on a weighted incremental dictionary learning. This algorithm trained a deep network efficiently by actively selecting training samples at each iteration. Chen et al. [20] proposed the idea of deep learning ensemble framework, which was loosely based on the integration of deep learning model and random subspace-based ensemble learning. Ma et al. [21] proposed a sparse representation classification method based on the optimized kernel function to replace the classifier in the deep learning model, thereby improving the image classification effect. [22] presented a vehicle logo recognition using a deep convolutional neural network (CNN) method and whitening transformation technique to remove the redundancy of adjacent image pixels.

Backpropagation algorithm with stochastic gradient descent optimization technique had been deployed to train and obtain weight filters of the networks. Li et al. [23] aimed to minimize the user variability in training CNN by automatically searching and optimizing the CNN architecture, particularly in the field of vehicle logo recognition system. Soon et al. [24] used deep learning methods that were based on data optimization for vehicle logo in complex scenes. They proposed three augmentation strategies for vehicle logo data: cross-sliding segmentation method, small frame method, and Gaussian distribution segmentation method. Bianco et al. [25] proposed a mapreduce-based CNN called MRCNN to train the networks. Furthermore, unlike the previous classical CNN starting from a random initialization, they proposed a novel genetic algorithm global optimization and Bayesian regularization approach called GABR in order to initialize the weights of classifier. Yousaf et al. [26] developed and applied an improved deep convolutional neural network model to perform the automatic classification of breast cancer using pathological images, in which data enhancement and migration learning methods were used to effectively avoid the overfitting problems with deep learning models when they are limited by the training image sample size. Soon et al. [27] proposed two multi-view learning approaches to tackle the insufficient data issue. On one hand, a multi-view ordinal classification with a multi-view max pooling (MVMP) approach was proposed. On the other hand, in order to account for the ordinal relation, they proposed a double-task learning on MVMP for classification and average pooling for regression. Ke and Du [28] proposed a deep multi-view learning method to deal with the small sample problem of HSI. Li and Hu [29] used an end-to-end Convolutional Long Short Term Memory (ConvLSTM) network to learn the deep mutual information of polarimetric coherent matrices in the rotation domain with different polarimetric orientation angles (POAs) for unsupervised PolSAR image classification.

The feature differences of objects in fine-grained images are only reflected in local nuances. The difficulties of classification are mainly manifested in two aspects: one is to accurately locate the key areas with discrimination in the image, and the other is to extract effective features from the detected key areas and classify them. Therefore, how to effectively detect the foreground objects in the image and mine the local details of fine-grained objects is the primary problem that fine-grained image classification algorithms need to solve. Most of the early fine-grained image classification algorithms follow this process: first, find the key feature areas of the foreground object, then extract features on these areas and process them appropriately, and finally complete the training or prediction of the model through the classifier. Most of these algorithms rely on artificial feature extraction, and the description of fine-grained image features is limited, which makes the classification accuracy difficult to meet the actual needs.

3. Convolutional Neural Network with Attention Mechanism

This paper studies a fine-grained image classification method with high classification accuracy without additional local information annotation, extracting distinguishing features and fusing global features to achieve effective classification.

3.1. Channel Domain Weighted Attention Network. Taking the features extracted from the convolution layer as the input features, the input features contain multiple different feature channels, and each channel may correspond to different feature information in the image. The information contained in these channel features is different, which leads to their different importance for fine-grained image classification. The desired result is to focus only on those channels with discriminative information and weaken the influence of features without discriminative information. Channel domain attention is simply to use a weight value coefficient to express the importance of each channel feature. For the two-dimensional feature map obtained by convolution, channel attention can be expressed as a $1*1$ dimensional eigenvector.

The bilinear convolution network used in this paper still adopts two branch networks. However, both branch networks use the improved ResNet50 as the feature extractor, mainly to enhance the representation ability of network feature extraction. In this paper, the attention module is added between conv2, conv3 and conv4, conv5 of the two branch networks, respectively. Then, the weighted feature map processed by the attention module adopts a bilinear pooling operation, and a full connection layer is connected at the end of the network as the classification function. The number of neurons in the classification layer should be consistent with the number of categories of the classification task. Input the bilinear feature vector into the classification function to get the final result of fine-grained image classification.

For the weighted features generated by the two branches through the attention module: $F_{sc} \in R^{w \times h \times c}$, the obtained weighted vectors are input to the next convolution block. Finally, the sum of the feature vectors obtained by network A and network B is bilinear fused

$$\varphi(I) = \sum_{I \in L} \left(F_A^T \bullet F_B\right). \tag{1}$$

Convert $\varphi(I) = R^{c \times c}$ into a one-dimensional vector and normalize the weighted bilinear vector into (2) and (3)

$$y = \text{sign}(\varphi)\sqrt{|\varphi|}, \tag{2}$$

$$z = \frac{y}{\|y\|_2}. \tag{3}$$

Finally, the obtained bilinear weighted vector is used as the input of the classification function to get the final classification result

$$s = \sigma(W_1 z + b), \tag{4}$$

where σ represents the Softmax classification function and b is the offset value of the current layer.

The bilinear convolution neural network based on the attention mechanism proposed in this paper, by adding the attention module, highlights the channels that can distinguish the local regional features, suppresses the useless information interference that has little impact on the classification results, improves the accuracy of local feature location, reduces the impact of background occlusion and object deformation on the classification results, and thus improves the classification accuracy of fine-grained images.

The calculation steps of the channel domain attention are as follows:

(1) Squeezing: the feature map generated by the residual network is used as the original input x of the attention model, and the global average pooling method is used to compress the features of all channels into a number, expressed in z, then:

$$z_c = \frac{1}{w \times h} \sum_{i=1}^{h} \sum_{j=1}^{w} x_c(i, j), x \in R^{w \times h \times c}, z \in R^c. \tag{5}$$

Among them, the dimension of x is $w * h * c$; c represents the channel of the feature, (i, j) represents the coordinate position on a certain channel, and after the extrusion calculation z is a vector of one dimension;

(2) Activation, input z to the full connection layer and calculate the relationship between channels;

$$s = \sigma(W_2 \text{ReLU}(W_1 z)). \tag{6}$$

The bottleneck structure is used in the two fully connected layers. An FC pair is used to reduce the dimension z. The dimension reduction ratio is $1/r$; $r$is the dimension reduction coefficient, and then activated it using Re L U, and an FC is used to increase the dimension. The parameters of the two fully connected layers are expressed by W_1 and W_2, respectively. s belongs to R^c. The dimension of s is equal to z. $\sigma(\bullet)$ indicates sigmoid activation;

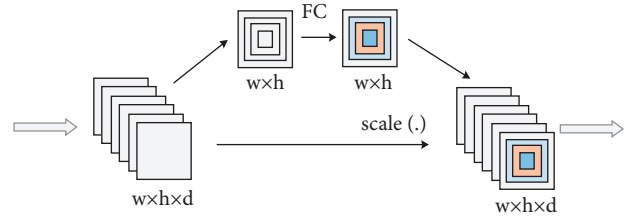

Figure 1: Channel domain attention network module.

(3) Sigmoid activation function normalizes the channel weight value to (0, 1) and multiplies the activated weight value with the original feature points to obtain the weighted feature map as $\overline{x} \in R^{w \times h \times c}$.

3.2. Spatial Domain Weighted Attention Network. Spatial attention pays more attention to the information on the spatial position of the discriminative region of the feature map. It can be said that spatial attention is a supplement to channel attention. The schematic diagram of the spatial attention module is shown in Figure 1 [30].

The pixel values of each spatial position in the feature map are taken out separately and combined into a one-dimensional feature vector. The spatial domain attention mechanism refers to learning a weighted real number for all one-dimensional features in these spatial positions to represent the importance of these features. For the entire three-dimensional feature map, the weight that spatial domain attention needs to learn is a two-dimensional weight matrix corresponding to the size. Through the learning of spatial attention, the feature response at the significant local spatial position in the feature map will continue to increase. The spatial attention module is added to the residual network. The specific process of feature extraction and fusion of attention module is as follows:

(1) The feature function extracts the feature map $F, F \in R^{w \times h \times c}$, where $w * h$ is the spatial dimension of the feature map, c indicating the number of channels.

(2) Global average pooling P_a and global maximum pooling P_m are used to reduce the dimension of the feature map F. The obtained two feature maps $w * h * 1$ are spliced by summing the corresponding elements, and useful information is extracted through a full connection layer.

(3) Using a 7×7 convolution kernel convolutes the characteristic image obtained in the previous step, and the size is compressed to $w * h * 1$. Then, use the sigmoid activation function to map and generate the spatial attention map $A_s, A_s \in R^{w \times h \times 1}$.

(4) The method of point multiplication by element is used to fuse the features of F and $A_s$to generate the final spatial attention feature map $F_s, F_s \in R^{w \times h \times c}$.

(5) Through global average pooling P_a and full connection layer learning of spatial attention feature mapF_s, the descriptors of all output feature maps are obtained, with the size of $1 \times c$.

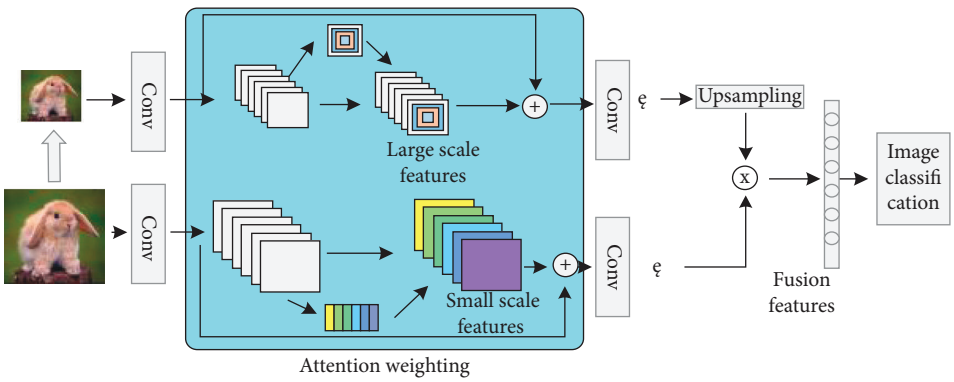

Figure 2: Overall network framework.

(6) Use the activation function ReLU to allocate the channel attention weight and generate the channel attention weight $A_c, A_c \in R^{1\times c}$.

(7) The feature fusion of F_s and A_c is carried out by the method of corresponding element point formation, and the key extraction of channel dimension is realized. Finally, a multi-dimensional attention feature map F_{sc} is generated, $F_{sc} \in R^{w\times h\times c}$.

Combining the two dimensions of attention, it has a stronger local feature extraction ability, so that the network can obtain more abundant features. Through multi-dimensional attention, we can avoid the loss of important information when extracting features from the network. Add the attention module, first obtain the local areas with discriminative information with spatial attention, and then distinguish the channels corresponding to the local features of different subcategories through the channel attention retention significant high response. The two promote each other. After weighting the feature map, it is input to the Softmax classification layer to get the category of the image and realize the classification task.

3.3. Fine-Grained Classification Based on Attention Mechanism and Multi-Scale Features. The difference between different subclasses of fine-grained images is small and difficult to detect; different individual images of the same subcategory have large intra-class differences due to the influence of posture, angle, background, and so on. In order to strengthen the attention to distinguishing local regional features, this paper designs a classification method that integrates attention mechanism and multi-scale features and improves it. ResNet50, a residual network with more layers of features and stronger expression ability, is used to extract global features and local features, respectively, and the upper and lower networks interact. By adding the attention mechanism of channel domain and spatial domain to the residual structure, filtering out the irrelevant channels in the feature map, and focusing on the local region of spatial response, we get rich multi-dimensional attention features. Automatically focus on key parts without using additional manual labels to improve the classification effect of the network.

3.3.1. Multiscale Feature Fusion. Through the multi-level feature combination to enrich the feature representation of the significant region, obtain the key part features while retaining the global features and get rich multi-level features. In the designed network model, it is also to improve the representation ability of features and fuse multi-scale features. The two inputs of the bilinear network correspond to the original graph. Multiscale feature fusion network model is shown in Figure 2.

The network convolutes the input images of different sizes with the scaled sample image of the original image to obtain the characteristic images of different sizes. Each position of the feature map output by the network corresponds to different sizes of regions in the original image, and the feature map of different scales can represent the features of different sizes in the image.

When the convolution kernel is in the same size, the large-scale features often correspond to the larger region in the original image, and the small-scale features correspond to the smaller region. They describe the global information and detailed information of the image, respectively. In the task of fine-grained image classification, large-scale features are used to represent the key parts, and small-scale features are used to represent the low-level information of these parts. By fusing the features of different scales, more expressive features can be combined, which is more conducive to fine-grained image classification.

Multi-scale features can be obtained by controlling the size of the input image. Before fusing different size features, the two feature images need to be unified into the same size. The bilinear interpolation method is used to sample the small-size feature map, enlarge it to the size of the large-size feature map, and make full use of the information in the two feature maps.

3.3.2. Attention Characteristics. This paper analyzes the fusion of channel attention and spatial attention features and uses ResNet50 as a feature extractor to add channel domain attention to the residual block of the upper network and spatial domain attention to the residual block of the lower network. Through the two kinds of attention, the salient parts of images with different sizes are detected, and the features are extracted, respectively, and finally combined

them. ResNet50 is composed of 50 convolution layers, which contain five stages, which are represented by stagel1-stage5, respectively. Each stage2-stage5 also contains three, four, six, and three residual blocks. If the size of the image input by ResNet50 is 224∗224∗3, the feature size of the convolution output of the last layer is 7∗7∗2048, the size of the feature image is reduced by half on each stage, and the number of channels is doubled.

After using the residual network to obtain the weighted feature maps in the channel domain and spatial domain, we can use bilinear interpolation to unify the size of these two different sized attention maps and then use bilinear pooling to fuse features. The channel attention characteristic map can be expressed as M_c, and the spatial attention characteristic map can be expressed as M_s, then:

$$M_f = (\varphi(M_c))^T M_s, \tag{7}$$

M_f represents the fusion result of the two feature maps, and $\varphi(\bullet)$ represents the bilinear interpolation operation. Adding multiple channel domain and spatial domain attention modules to the residual network can focus on the salient features from different dimensions.

4. Improved Loss Function

4.1. Improvement of Classification Function. The loss function of target detection task consists of classification loss and regression loss. The loss function is divided into the following four parts: confidence loss $\text{Loss}_{\text{conf}}$, category loss $\text{Loss}_{\text{class}}$, coordinate loss Loss_{xy} and width height loss Loss_{wh}. The formula is as follows:

$$\begin{aligned}
\text{Loss}(\text{object}) &= \text{Loss}_{xy} + \text{Loss}_{wh} + \text{Loss}_{\text{conf}} + \text{Loss}_{\text{class}} \\
&= \lambda \sum_{i=0}^{K*K} \sum_{j=0}^{M} I_{ij}^{\text{obj}} \left(2 - w_i \times h_j\right) \left[(x_i - \hat{x}_i)^2 + (y_i - \hat{y}_i)^2 \right] \\
&+ \lambda \sum_{i=0}^{K*K} \sum_{j=0}^{M} I_{ij}^{\text{obj}} \left(2 - w_i \times h_j\right) \left[(w_i - \hat{w}_i)^2 + \left(h_i - \hat{h}_i\right)^2 \right] \\
&- \sum_{i=0}^{K*K} \sum_{j=0}^{M} I_{ij}^{\text{obj}} \left[\hat{C}_i \log(C_i) + \left(1 - \hat{C}_i\right) \log\left(1 - \hat{C}_i\right) \right] \\
&- \beta \sum_{i=0}^{K*K} \sum_{j=0}^{M} I_{ij}^{\text{noobj}} \left[\hat{C}_i \log(C_i) + \left(1 - \hat{C}_i\right) \log\left(1 - \hat{C}_i\right) \right] \\
&- \sum_{i=0}^{K*K} I_{ij}^{\text{obj}} \sum_{c \in \text{class}} \left[\hat{p}_i \log\left(p_i(c)\right) + \left(1 - \hat{p}_i(c)\right) \log\left(1 - \hat{p}_i(c)\right) \right].
\end{aligned} \tag{8}$$

The loss function Loss_{xy} is expressed as (x_i, y_i) coordinate error, the second item Loss_{wh} is the width height coordinate error, WI, h_i is the length and width of the ith grid prediction frame, $k * k$ is the number of grids, M is the candidate boxes generated by the grid, and each candidate box will get the corresponding bounding box through the network, and finally get $k * k * m$ bounding boxes. The confidence error $\text{Loss}_{\text{conf}}$ is calculated using cross-entropy, using cross-entropy loss. However, the original cross-entropy loss function will reduce the recognition accuracy in the case of unbalanced samples, and there are more small targets and fewer targets in the target statistics of sample data. Therefore, the prominent challenge of target detection is the extreme imbalance between positive and negative samples and difficult samples. In order to solve the problem of sample imbalance, focal loss is introduced to replace the original cross-entropy classification loss function. The formula is as follows:

$$\text{Focal loss} = \begin{cases} -\alpha\left(1 - y'\right)^{\beta} \log y', & y = 1, \\ -(1 - \alpha) y'^{\beta} \bullet \log\left(1 - y'\right), & y = 0, \end{cases} \tag{9}$$

where $y \in \{\pm 1\}$is the real category, and the probability value between $y' \in \{0, 1\}$ is the model probability estimated by the activation function. In addition, focal loss introduces two hyperparametric sums α and β, in which the balance factor α represents the corresponding weights of different categories, which is equivalent to weighting the positive and negative samples, so as to balance the positive and negative samples; The attenuation coefficient $\beta > 0$, as the loss of samples, pays more attention to difficult samples. The larger the attenuation coefficient β is, the greater the attenuation degree of samples with the correct focus loss classification, which also makes its loss pay more attention to difficult and misclassified samples.

4.2. Improvement of Regression Function. The target detection task is to detect the position and category of the target in the image. The most commonly used evaluation index is average accuracy (MAP), and the index of accuracy between the prediction box and the real box is intersection union ratio (IOU). L2 regression loss function is the original regression loss function L1 norm loss function, also known as the minimum absolute deviation (LAD), which minimizes the sum of the absolute differences between the target value y and the estimated value. The L2 norm loss function, also known as least-squares error (LSE), minimizes the sum of squares of the differences between the target value and the estimated value. Formula:

$$\begin{aligned}
L_1(\hat{y}, y) &= \sum_{i=0}^{m} \left| y^{(i)} - \hat{y}^{(i)} \right|, \\
L_2(\hat{y}, y) &= \sum_{i=0}^{m} \left(y^{(i)} - \hat{y}^{(i)} \right)^2.
\end{aligned} \tag{10}$$

The original regression function uses the L2 loss function for bounding box regression, but this kind of loss function does not always reflect the positioning accuracy well. Therefore, in the process of target detection, IOU will be considered to measure the target positioning loss directly, and the IOU loss formula is expressed as

$$\text{IoU} = \frac{B^{pd} \cap B^{gt}}{B^{pd} \cup B^{gt}}, \tag{11}$$

where R_{CIOU} is the penalty term of the prediction box B_{pd} and target box B_{gt}. The original IOU-based loss function is defined as

$$L_{\mathrm{CIoU}} = 1 \bullet \mathrm{IoU}. \tag{12}$$

Although IOU loss solves the two major problems that smooth L1/L2 series variables are independent of each other and do not have scale invariance, IOU loss only works when the bounding boxes overlap and will not provide any moving gradient in the case of non-overlap. CIOU loss, based on IOU, introduces the minimum circumscribed rectangle of the prediction box and real box, which can solve the gradient optimization problem of a disjoint rectangular box, but there are still some limitations in training and convergence speed. In this paper, CIOU loss is added to replace the original regression function to achieve more accurate prediction box regression. The overall formula is expressed as

$$L_{\mathrm{CIoU}} = 1 \bullet \mathrm{IoU} + R_{\mathrm{CIoU}}\left(B_{pd}, B_{gt}\right). \tag{13}$$

The difference between $\mathrm{CIOU}_{\mathrm{Loss}}$ and IOU loss is that three geometric factors, including overlapping area, center point distance, and aspect ratio, are considered in the boundary box regression to solve the inconsistency between the measurement function and the boundary regression mechanism in the process of target detection. In $\mathrm{CIOU}_{\mathrm{Loss}}$, the specific settings are:

$$R_{\mathrm{CIoU}} = \frac{\varphi^2\left(b, b^{gt}\right)}{c^2} + \alpha v, \tag{14}$$

where b and b^{gt}, respectively, represent the distance between the center points of the prediction frame and the target frame, $\varphi(\cdot)$ represents the Euclidean distance between two points, and c represents the shortest distance of the diagonal between the two frames, while taking into account the overlapping area and the center point distance.

In addition, the parameters α and v take the aspect ratio between the two boxes into account, and the formula is as follows:

$$\begin{aligned} v &= \frac{4}{\pi^2}\left(\arctan\frac{w^{gt}}{h^{gt}} - \arctan\frac{w}{h}\right)^2, \\ \alpha &= \frac{v}{(1 - \mathrm{IoU}) + v}. \end{aligned} \tag{15}$$

The final regression function used for classification detection is

$$\begin{aligned} \mathrm{L}_{\mathrm{CIoU}} &= 1 - \mathrm{IoU} + \frac{\varphi^2\left(b, b^{gt}\right)}{c^2} \\ &\quad + \frac{v}{(1 - \mathrm{IoU}) + v} \bullet \frac{4}{\pi^2}\left(\arctan\frac{w^{gt}}{h^{gt}} - \arctan\frac{w}{h}\right)^2. \end{aligned} \tag{16}$$

5. Experimental Results and Performance Evaluation

The data sets used in the experiment are fine-grained public data sets: CUB-200-2011 data set. The CUB-200-2011 data set has 200 different bird categories, with a total of 11788 images. Each category covers different angles, different scenes, and different postures, including 5794 test pictures and 5994 training pictures. A comparison of the PR curve is shown in Figure 3.

The experimental process is divided into two stages: in the first stage, the data are input into two networks and the two networks work in parallel at the same time. All the convolution layer parameters in front of the attention module are fixed. The parameters of the attention module are initialized randomly, and then only the parameters of the attention module and the full connection layer are trained. Finally, the classification is completed and the parameters when the classification performance of the model is the best are saved. In the second stage, the whole model is initialized with the optimal parameters saved in the previous stage, and then the parameters of all layers in the network are fine-tuned to obtain the classification accuracy and model parameters of the final model. Since the full connection layer is used, it is necessary to set the size of the input data. In the experiment, the data input into the network is 448×448. The SGD optimizer with a momentum of 0.9 and a weight attenuation coefficient of 0.00001 was used in the experiment. Setting of learning rate: in the first stage, the initial learning rate of the full connection layer is 0.9, and the initial learning rate of the attention module is 0.09, and the initial learning rate of the second stage is 0.001.

It can be seen from Figure 3 that the number of categories gradually increases from 2000 to 4000 and 6000. Compared with BCNN, the WSFF-BCNN model achieves better performance than other benchmarks on data sets of different sizes. This paper further calculates the "precision" and "recall" of BCNN and WSFF-BCNN to illustrate the accuracy and missed detection rate of detection. The larger the area surrounded under the curve, the better the detection performance. It can be seen that WSFF-BCNN significantly improves the recall rate, which shows that this method alleviates the lack of small objects in target detection.

This paper evaluates the detection performance by changing different IOU thresholds from 0.6 to 0.9 at 0.05 intervals. As shown in Figure 4(a), when changing the IOU threshold, WSFF-BCNN (red curve) has a more stable performance improvement than BCNN (blue curve). This paper also sets different iteration times to compare the convergence and accuracy of the model. Figure 4(b) shows that with the increase of the number of iterations, the performance is gradually improved, and the accuracy is higher than that of BCNN.

Obviously, compared with the BCNN method, WSFF-BCNN can detect some targets that are not easy to detect, such as occluded, blurred, and small targets. The method proposed in this paper has great advantages in small area detection, which shows the effectiveness of multi-scale feature fusion.

The ROC curves of all methods are drawn in Figure 5 to show the stability of each method. The larger the area below the curve, the more stable its classification performance is, which shows that the performance of this method is the best. Compared with other methods, the classification difficulty increases with the increase of categories, and the prediction accuracy is still very high.

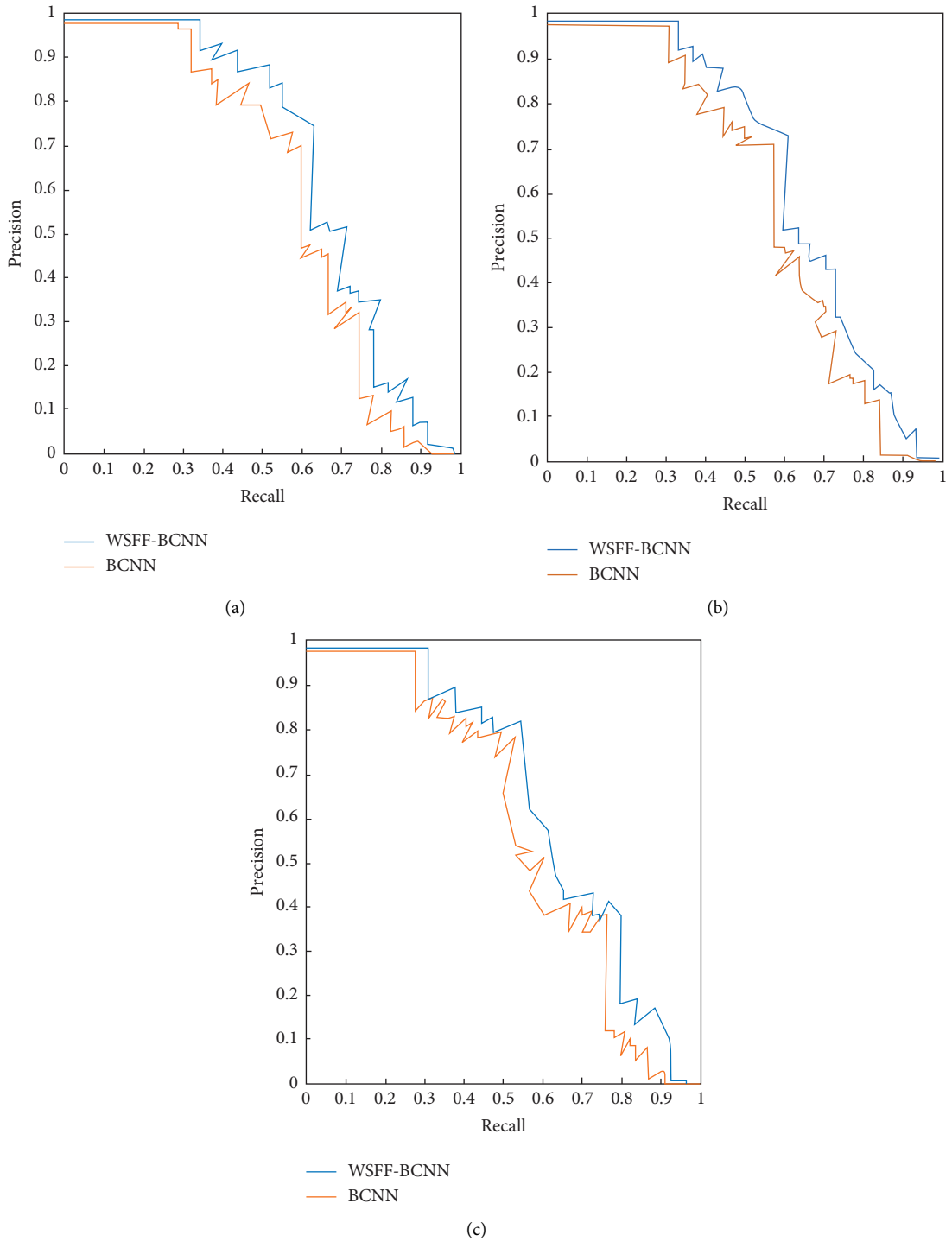

Figure 3: Comparison of PR curve (CUB-200-2011). (a) CUB-200-2011 2000, (b) CUB-200-2011 4000, and (c) CUB-200-2011 6000.

The improved model in this paper solves some limitations of the original B-CNN model. For the input image, the specific location of the target object is obtained through network to reduce the interference of background information. Compared with the network of the original model, the improved ResNet50 is used as the feature extractor to enhance the ability of feature representation, improve the training speed of the network, and reduce the phenomenon of overfitting. Adding the attention module to the residual network has a stronger ability of the local feature extraction and richer feature representation. The high-dimensional and low-dimensional features extracted by the two networks are fused with bilinear features, so that the proposed bilinear convolution neural network based on attention mechanism

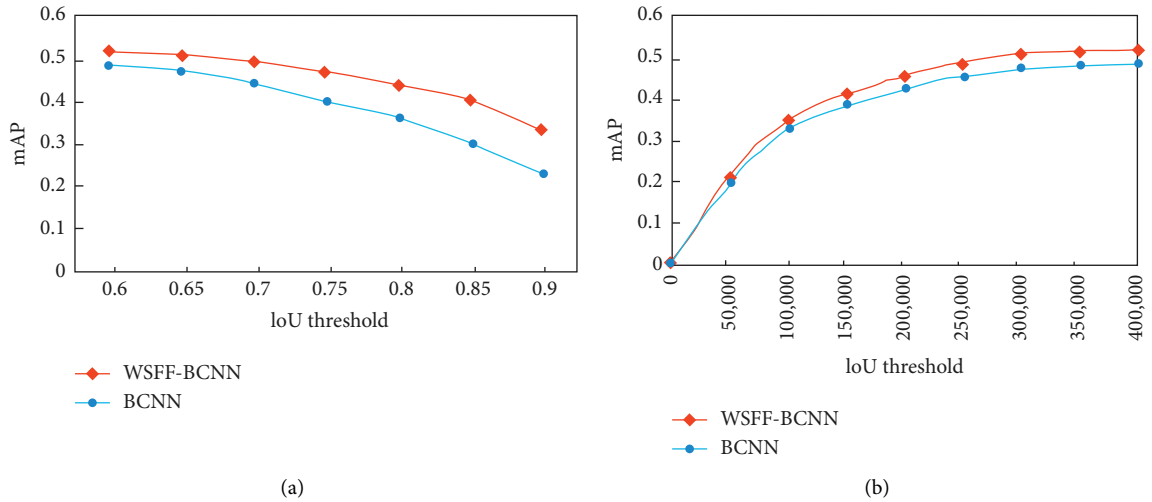

Figure 4: Sensitivity of parameters. (a) IoU threshold and (b) IoU threshold.

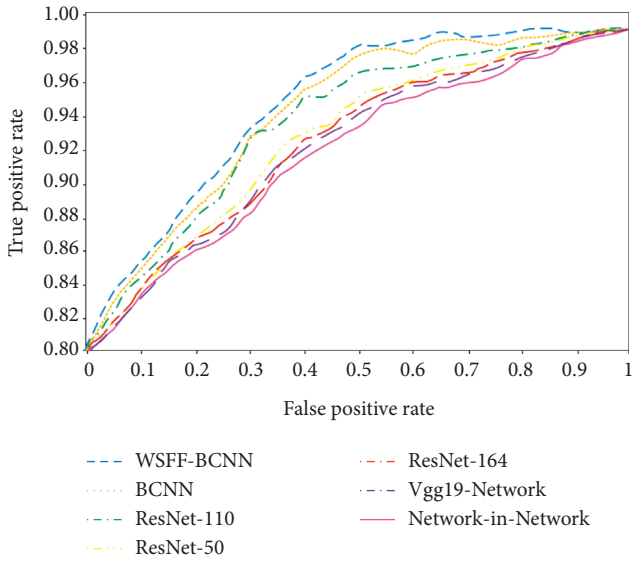

Figure 5: ROC classification curve.

pays more attention to the more discriminative local region features in learning and training and improves the classification accuracy of the whole network.

6. Conclusion and Future Work

There are many difficulties in fine-grained classification task, which leads to poor classification effect. There are only subtle feature differences among various types of fine-grained images. How to find and use these local area information is the problem that fine-grained image algorithm needs to solve. Based on the relevant research of CNN, this paper studies the fine-grained image feature extraction and thinning and the improvement of loss function in the training process of convolutional neural network. Firstly, the features extracted by the traditional CNN algorithm in the feature extraction stage cannot capture the location of the local region of the image, which makes the model unable to pay full attention to the local differentiated region of the target. This paper designs a WSFF-BCNN model based on the convolution attention module, which proves that the attention mechanism can capture the local area position of the image target, so as to improve the recognition ability of the model. Through relevant experiments on the open data set in the fine-grained field, it shows better advantages. Compared with other models, it proves the effectiveness of the WSFF-BCNN model proposed in this paper, the effect is better, and it is more suitable for the target detection task in the real scene.

In addition, although this paper solves the problems of large-scale classification, multi-scale detection, and effective feature extraction in images to a certain extent, due to the diversified development of various images, the algorithm should be further optimized. Although the training method proposed in this paper is an effective classification with label information, it is still a supervised method in essence. Therefore, the next step can focus on the unsupervised fine-grained classification. At the same time, in the detection task, we still face severe challenges such as multi-label and large-scale problems. Although the method proposed in this paper effectively improves the effect of target detection, it still needs further research on target classification and detection in the future.

Data Availability

The authors confirm that the data supporting the findings of this study are available within the article.

Conflicts of Interest

The authors declare that they have no conflicts of interest.

References

[1] Y. B. Hou, "Breast cancer pathological image classification based on deep learning," *Journal of X-Ray Science and Technology*, vol. 28, no. 4, pp. 727–738, 2020.

[2] C. Zhang, X. Xu, and C. Zhu, "Image ordinal classification with deep multi-view learning," *Electronics Letters*, vol. 54, no. 22, pp. 1280–1282, November 2018.

[3] B. Liu, A. Z. Yu, X. C. Yu, R. R. Wang, K. L. Gao, and W. Y. Guo, "Deep multiview learning for hyperspectral image classification," *IEEE Transactions on Geoscience and Remote Sensing*, vol. 59, no. 9, pp. 7758–7772, September 2021.

[4] Z. K. Li, X. Y. Tang, W. Li, C. Y. Wang, C. W. Liu, and J. R. He, "A two-stage deep domain adaptation method for hyperspectral image classification," *Remote Sensing*, vol. 12, no. 7, p. 1054, April 2020.

[5] L. Wang, X. Xu, R. Gui, R. Yang, and F. L. Pu, "Learning rotation domain deep mutual information using convolutional LSTM for unsupervised PolSAR image classification," *Remote Sensing*, vol. 12, no. 24, p. 4075, December 2020.

[6] P. J. Chang, J. S. Zhang, J. Y. Hu, and Z. J. Song, "A deep neural network based on ELM for semi-supervised learning of image classification," *Neural Processing Letters*, vol. 48, no. 1, pp. 375–388, August 2018.

[7] X. Y. Cao, J. Yao, Z. B. Xu, and D. Y. Meng, "Hyperspectral image classification with convolutional neural network and active learning," *IEEE Transactions on Geoscience and Remote Sensing*, vol. 58, no. 7, pp. 4604–4616, July 2020.

[8] X. Y. Zhao and Z. Y. Su, "Using deep learning in image hyper spectral segmentation, classification and detection," *Fourth Seminar on Novel Optoelectronic Detection Technology and Application*, vol. 10697, 2018.

[9] G. G. Song, X. L. Huang, G. Cao et al., "Enhanced deep feature representation for patent image classification," in *Proceedings of the Enth International Conference on Graphics and Image Processing (ICGIP 2018)*, vol. 11069, Chengdu China, December 2019.

[10] N. V. Kumar, Pratheek, V. V. Kantha, K. N. Govindaraju, and D. S. Guru, "Features fusion for classification of logos," *Procedia Computer Science*, vol. 85, pp. 370–379, 2016.

[11] X. R. Ma, J. Geng, and H. Y. Wang, "Hyperspectral image classification via contextual deep learning," *Eurasip Journal on Image and Video Processing*, vol. 20, no. 1, 2015.

[12] V. Singhal and A. Majumdar, "Row-sparse discriminative deep dictionary learning for hyperspectral image classification," *Ieee Journal of Selected Topics in Applied Earth Observations and Remote Sensing*, vol. 11, no. 12, pp. 5019–5028, December 2018.

[13] X. Hu, W. J. Yang, H. Wen, Y. Liu, and Y. X. Peng, "A lightweight 1-D convolution augmented transformer with metric learning for hyperspectral image classification," *Sensors*, vol. 21, no. 5, p. 1751, March 2021.

[14] P. Da, S. Ping, Z. H. Qiu, S. Yuan, Z. D. Xiu, and Z. S. Jing, "TV Logo Classification Based on Convolutional Neural Network," in *Proceedings of the IEEE International Conference on Information and Automation (ICIA)*, pp. 1793–1796, Ningbo, China, August 2016.

[15] Y. F. Zhang, M. M. Zhu, D. L. Wang, and S. Feng, "Logo detection and recognition based on classification," *Proceedings of the Web-Age Information Management, WAIM 2014*, vol. 8485, pp. 805–816, 2014.

[16] P. N. Druzhkov and V. D. Kustikova, "A survey of deep learning methods and software tools for image classification and object detection," *Pattern Recognition and Image Analysis*, vol. 26, no. 1, pp. 9–15, 2016.

[17] T. H. Song, V. Sanchez, H. Ei Daly, and N. M. Rajpoot, "Simultaneous cell detection and classification in bone marrow histology images," *IEEE Journal of Biomedical and Health Informatics*, vol. 23, no. 4, pp. 1469–1476, 2019.

[18] J. E. Liu and F. P. An, "Image Classification Algorithm Based on Deep Learning-Kernel Function," *Scientific Programming*, vol. 2020, Article ID 7607612, 14 pages, 2020.

[19] P. Liu, H. Zhang, and K. B. Eom, "Active deep learning for classification of hyperspectral images," *Ieee Journal of Selected Topics in Applied Earth Observations and Remote Sensing*, vol. 10, no. 2, pp. 712–724, February 2017.

[20] Y. S. Chen, Y. Wang, Y. F. Gu, X. He, P. Ghamisi, and X. P. Jia, "Deep learning ensemble for hyperspectral image classification," *Ieee Journal of Selected Topics in Applied Earth Observations and Remote Sensing*, vol. 12, no. 6, pp. 1882–1897, June 2019.

[21] M. A. Haq, G. Rahaman, P. Baral, and A. Ghosh, "Deep learning based supervised image classification using UAV images for forest areas classification," *Journal of the Indian Society of Remote Sensing*, vol. 49, no. 3, pp. 601–606, 2021.

[22] F. P. An, "Image classification algorithm based on stacked sparse coding deep learning model-optimized kernel function nonnegative sparse representation," *Soft Computing*, vol. 24, no. 22, pp. 16967–16981, 2020.

[23] J. J. Li, B. B. Xi, Q. Du, R. Song, Y. S. Li, and G. B. Ren, "Deep kernel extreme-learning machine for the spectral-spatial classification of hyperspectral imagery," *Remote Sensing*, vol. 10, no. 12, p. 2036, December 2018.

[24] F. C. Soon, H. Y. Khaw, J. H. Chuah, and J. Kanesan, "Vehicle logo recognition using whitening transformation and deep learning," *Signal Image and Video Processing*, vol. 13, no. 1, pp. 111–119, February 2019.

[25] S. Bianco, M. Buzzelli, D. Mazzini, and R. Schettini, "Deep learning for logo recognition," *Neurocomputing*, vol. 245, pp. 23–30, 2017.

[26] W. Yousaf, A. Umar, S. H. Shirazi, Z. Khan, I. Razzak, and M. Zaka, "Patch-CNN: deep learning for logo detection and brand recognition," *Journal of Intelligent and Fuzzy Systems*, vol. 40, no. 3, pp. 3849–3862, 2021.

[27] F. C. Soon, H. Y. Khaw, J. H. Chuah, and J. Kanesan, "Hyper-parameters optimisation of deep CNN architecture for vehicle logo recognition," *IET Intelligent Transport Systems*, vol. 12, no. 8, pp. 939–946, October 2018.

[28] X. Ke and P. Q. Du, "Vehicle logo recognition with small sample problem in complex scene based on data augmentation," *Mathematical Problems in Engineering*, vol. 2020, Article ID 6591873, 10 pages, 2020.

[29] B. Q. Li and X. H. Hu, "Effective vehicle logo recognition in real-world application using mapreduce based convolutional neural networks with a pre-training strategy," *Journal of Intelligent and Fuzzy Systems*, vol. 34, no. 3, pp. 1985–1994, 2018.

[30] S. W. Deng, *Research on Fine-Grained Image Classification Based on Weak Supervised Learning*, Guangdong University of technology, Guangdong, China, 2020.

Hindawi
Computational Intelligence and Neuroscience
Volume 2022, Article ID 3871129, 19 pages
https://doi.org/10.1155/2022/3871129

Research Article

A Closed-Loop Method for Multiperiod Intelligent Information Processing with Cost Constraints under the Fuzzy Environment

Ming Fu,[1] **Lifang Wang**,[2] **Xueneng Cao**,[1] **Bingyun Zheng**,[1] **Xianxian Zhou**,[1] **and Shishu Yin**[1]

[1]*School of Management Science and Engineering, Anhui University of Finance & Economics, Bengbu 233030, Anhui, China*
[2]*School of International Trade and Economics, Anhui University of Finance & Economics, Bengbu 233030, Anhui, China*

Correspondence should be addressed to Lifang Wang; wanglifang@aufe.edu.cn

Received 16 July 2022; Accepted 3 August 2022; Published 7 September 2022

Academic Editor: Zaoli Yang

From trivial matters in life to major scientific projects related to the fate of mankind, decision-making is everywhere. Whether high-quality decisions can be made often directly affects the development of affairs, especially when sudden disasters occur. As the basis of decision-making, data are crucial. The continuously probabilistic linguistic set, a data structure of the fuzzy mathematics, is selected in the paper to collect original data after careful comparisons, because this data structure can fully consider the hesitation of decision-makers and the fuzziness of complex problems. Although all alternatives are costly, the costs of different alternatives still vary greatly; obviously, the low-cost alternative is better than others when the same predetermined goal can be achieved, which is one of the research objectives and characteristics of this paper. Different from other researchers who only take the cost as one of the decision-making indicators, the algorithm proposed in the paper pays much more attention on the cost reduction. When dealing with an emergency, it is often difficult to solve the problem by taking measures only once; usually, multiple rounds of measures are needed. Each round of decision-making has both connections and differences, and the multiround decision-making model is proposed and built in the paper. Different from traditional linear structures, the model mainly adopts the closed-loop structure, which divides the whole process into multiple sub-decision-making points, the severities measured at the current time point will be compared with the values estimated at the latter time point, and then, the differences will be input into the system, the corresponding automatic adjustment modules will be activated immediately according to the values. The accuracy of the system can be verified and adjusted in time by the closed-loop control module. Finally, several experiments are carried out and the results show that the algorithm proposed in the paper is more effective and the cost is lower.

1. Introduction

People are always faced with all kinds of decision-making problems, how to make an appropriate decision in time is a scientific problem and has become one of research hotspots in the academic circle.

There are several different descriptions for the definition of decision-making. Simon believes that decision-making is essentially management [1]; Mikesell and Griffin, management professors, point out that decision-making is a process in which an appropriate alternative will be selected from multiple alternatives [2]; the American scholars Ebers and Maurer believe that decision-making should also include all activities, which must be carried out before making the final decision [3]. Generally speaking, decision-making is regarded as the process in which individuals or groups make appropriate decisions for specific goals.

Decision-making problems can be roughly divided into three categories from the perspective of known conditions: (1) the deterministic decision-making problem, such problems have clear alternatives and expected results; (2) the risky decision-making problem, the predetermined goal is clear; however, there are many paths to the goal, every path has certain risks and uncertainties, and fortunately, the probabilities can be roughly calculated; (3) the uncertain decision-making problem, it is similar to the risky decision-making problem; however, the probabilities can only be estimated, and even worse, there may be certain deviations

in the estimated values. The problem studied in this paper belongs to the third category, which has many uncertainties and is the most complex of the three categories.

Information collection is a basic and key step of the decision-making; however, most information provided by interviewees is uncertain, vague, and hard to be denoted mathematically, how to scientifically record uncertain information is the first problem to be solved. In 1965, the Professor Zadeh has put forward the concept of the fuzzy set, which provided a new idea for solving such problems [4], the main contribution is that the concept of the membership degree has been proposed; subsequently, the theory has been widely recognized and developed rapidly, and various forms have been expanded, such as the interval-valued fuzzy set [5], the n-type fuzzy set [6], the intuitionistic fuzzy set [7], the interval intuitionistic fuzzy set [8], the hesitant fuzzy set [9], and the probabilistic linguistic set [10]. The main features of these fuzzy sets can be briefly summarized as follows: the membership degrees are described by interval values in the interval-valued fuzzy set; the membership degrees are represented by sets in the n-type fuzzy set; both the membership degree and the nonmembership degree can be considered in the intuitionistic fuzzy set; beyond that, the hesitation degrees, which are denoted by interval values, are included in the interval intuitionistic fuzzy set. The hesitations of the decision-makers can be described in the hesitant fuzzy set; in addition, the structure is concise and efficient, and therefore, the theory of the hesitant fuzzy set has become one of research hotspots in recent years. The probabilistic linguistic set is developed on the basis of the hesitant fuzzy set, and it adds occurrence probabilities to membership degrees, so as to increase further descriptions for membership degrees.

Mathematics is recognized as one of the best analytical tools. In order to use mathematical tools to carry out researches, scholars have put forward several basic mathematical concepts for fuzzy sets. Xia and Xu first gave the mathematical definition of the hesitant fuzzy set [11], and Liao and Xu defined some special hesitant fuzzy sets from the perspective of solving practical problems [12], such as the empty set O^*, the complete set E^*, and the meaningless set Θ^*. Unfortunately, fuzzy sets cannot be added, subtracted, multiplied, and divided directly; for this reason, several basic operation methods for fuzzy sets are proposed by scholars. Torra defined the complement, union, and intersection operations for hesitant fuzzy elements [13]. Xu and Xia conducted further researches and proposed the addition, multiplication, number multiplication, and power operations for hesitant fuzzy elements [14]; on this basis, Liao and Xu proposed the definitions of subtraction and division [15].

In addition, fuzzy elements cannot be compared directly like real numbers. Therefore, Xia and Xu have put forward the concept of the score value, which provides a method for comparing different fuzzy elements; however, when the score values are equal, it needs to be further judged with the help of the variance values [16], which was proposed by Liao et al.

Unfortunately, the basic operation methods mentioned above can only meet simple aggregation requirements and would be unable to finish the calculation when a large number of fuzzy elements participate. Therefore, researchers proposed several effective fuzzy aggregation operators. Xia and Xu proposed the hesitant fuzzy-weighted averaging (HFWA) operator and the hesitant fuzzy hybrid averaging (HFHA) operator in the paper listed in the Reference [11] mentioned above, considering the importance of location and data simultaneously. Liao and Xu defined a series of new hesitant fuzzy mixed integration operators and studied their boundaries and relationships [17]. Zhu and Xu proposed the hesitant fuzzy Bonferroni average operator and the weighted hesitant fuzzy Bonferroni average operator from the perspective of logical relationships, and studied their monotonicity, commutativity, and boundedness [18].

In particular, due to its outstanding structure, the theory of the probabilistic hesitation fuzzy set has been developing rapidly. Zhang et al. studied the preference relationships, ranking methods, basic operation rules, and aggregation operators [19]. Hao et al. studied the basic properties of the probabilistic dual hesitant fuzzy sets and proposed the entropy measurement methods, the comparison methods, and the aggregation operators [20], such as the weighted average operator and the geometric average operator. On this basis, Garg and Kaur studied the distance measurement methods of probabilistic dual hesitant fuzzy sets [21]. Ye proposed the correlation coefficients of probabilistic hesitant fuzzy sets in discrete and continuous cases, respectively [22]. Li and Wang proposed the concept of the probability hesitation fuzzy likelihood [23]. These theories have built a solid foundation for the probabilistic hesitation fuzzy theory.

Scholars have also conducted in-depth discussions on decision-making methods. The main idea can be simply summarized as using operators to aggregate estimation data and then rank alternatives according to the score values. These methods can be roughly divided into two categories: (1) optimize the aggregation operators and (2) innovate decision-making methods. For the first category, Jiang and Ma proposed the probability hesitation fuzzy frank-weighted average operator and the probability hesitation fuzzy frank-weighted geometric operator, and then discussed the relationships between them [24]. Zhao et al. considered the psychological preferences of decision-makers and proposed the probabilistic hesitant fuzzy Einstein aggregation operator [25]. Shao et al. proposed the probabilistic hesitation fuzzy priority integration operator after considering the internal correlations of indicators [26]. Li et al. proposed a new probabilistic hesitant fuzzy priority aggregation operator, which can make full use of the priority relationships among indicators [27]. For the second category, on the one hand, several commonly used methods in the field of the decision-making have been extended to the probabilistic hesitation fuzzy environment, such as the TOPSIS method, the QUALIFLEX method, and the LINMAP method; on the other hand, other theories or methods are introduced into the probabilistic hesitation fuzzy environment and make the theory more diversified. Zhou and Xu introduced several financial concepts into fuzzy sets and

then applied the hybrid algorithm to the practice of the stock investment decision-making [28]. Tian et al. established a consensus process based on the probability hesitation fuzzy preference relationships and the prospect theory, and then applied it to financial venture investment [29]. Wu et al. introduced the GM (1,1) model of the grey theory and applied it to coal mine safety production [30]. Guo et al. introduced time series analysis and established a time series prediction model based on hesitation probability fuzzy sets [31]. For this article, we not only optimize the aggregation operators but also innovate decision-making methods; by comparison, the main work of the paper is to innovate the decision-making methods, and especially, the closed-loop control model is combined with the fuzzy decision-making algorithm.

2. The Basic Theories

This section will briefly introduce some important basic theories, which will be used in the following chapters, and it is helpful for other researchers to better understand the algorithm proposed in this paper.

2.1. The Continuously Probabilistic Linguistic Set. The continuously probabilistic linguistic set is an extended form of the probabilistic linguistic set, which overcomes the disadvantage of the limited number of possible values in the probabilistic linguistic set. The definition of the continuously probabilistic linguistic set (CPLS) can be mathematically described by the following equation:

$$L_{rs} = \left\{ \gamma_l \mid p_l \gamma_l \in [0,1], p_l \in [0,1], l = 1,2,\cdots,m, \sum_{l=1}^{m} p_l = 1 \right\}. \tag{1}$$

In the above definition, the evaluation value is recorded by the symbol γ_l and its corresponding probability is recorded by the symbol p_l; the restraint condition $\gamma_l \in [0,1]$ points out the range of evaluation values, and the greater the value of the γ_l, the higher the evaluation acquired from experts; similarly, the restraint condition $p_l \in [0,1]$ points out the range of probability values, and the greater the value of the p_l, the greater the occurrence probability of the corresponding evaluation value; the pair of the symbol $\gamma_l|p_l$ can be called the continuously probabilistic linguistic element (CPLE); the restraint condition $l = 1,2,\cdots,m$ indicates the value range of the l, and the symbol m indicates the total number of evaluation values in the CPLS; the restraint condition $\sum_{l=1}^{m} p_l = 1$ indicates that the sum of all the probability values in any CPLS must equal to 1.

Unlike real numbers, CPLSs cannot be directly compared with each other, how to compare CPLSs is a difficult problem in front of researchers. The score function, which is first proposed by Farhadinia, can handle this problem effectively [32], and the calculation results are real numbers; therefore, they are easy to compare with each other. The definition of the score function can be mathematically described as equation (2). Generally, the score value of the CPLS represents the final evaluation result.

$$S(L_{rs}) = \sum_{l=1}^{m} \gamma_l \cdot p_l. \tag{2}$$

It is also necessary to briefly introduce several other commonly used calculation formulas of CPLSs, which are listed as follows:

$$\begin{aligned}
(L_{rs})^{\lambda} &= \bigcup_{\gamma_l \in L_{rs}} \left\{ \gamma_l^{\lambda} | p_l l = 1,2,\cdots,m \right\}, \\
\lambda L_{rs} &= \bigcup_{\gamma_l \in L_{rs}} \left\{ 1 - (1-\gamma_l)^{\lambda} | p_l l = 1,2,\cdots,m \right\}, \\
L_{rs} \oplus L_{pq} &= \bigcup_{\gamma_{l_1} \in L_{rs}, \gamma_{l_2} \in L_{pq}, p_{l_1} \in L_{rs}, p_{l_2} \in L_{pq}} \left\{ \gamma_{l_1} + \gamma_{l_2} - \gamma_{l_1}\gamma_{l_2} | p_{l_1} p_{l_2} l_1 \right. \\
&\quad \left. = 1,2\cdots,m_1 l_2 = 1,2\cdots,m_2 \right\}, \\
L_{rs} \otimes L_{pq} &= \bigcup_{\gamma_{l_1} \in L_{rs}, \gamma_{l_2} \in L_{pq}, p_{l_1} \in L_{rs}, p_2 \in L_{pq}} \left\{ \gamma_{l_1}\gamma_{l_2} | p_{l_1} p_{1_2} l_1 = 1,2\cdots,m_1 l_2 \right. \\
&\quad \left. = 1,2\cdots,m_2 \right\}.
\end{aligned} \tag{3}$$

We can find that only one CPLS is involved in the first and the second calculation formulas; while there are two CPLSs involved in the third and the fourth calculation formulas, more calculation formulas can be obtained according to these four basic formulas.

2.2. The Collaborative Decision-Making Problem. The definition of the collaborative decision-making can be simply described as a process in which several experts try to find the most appropriate alternative from multiple alternatives according to values of key indicators [33]. The experts can be denoted as $E = \{E_1, E_2, \cdots, E_m\}$, and the alternatives can be denoted as $A = \{A_1, A_2, \cdots, A_n\}$ mathematically.

The emergency decision-making is an important branch of collaborative decision-making problems, and they have many similarities [34], while there are great differences in complexity between them. The main difference is that the emergency decision-making problem has strict restrictions on the time, and the information acquired by experts is limited; even worse, it is always difficult for experts to evaluate alternatives with single values, and they often hesitate among multiple values. Fortunately, the introduction of the continuously probabilistic linguistic set can handle this problem efficiently [35], and all the possible evaluation information for an alternative given by experts can be recorded, which avoids the loss of the original information.

A simple example is given to illustrate the above theory. Supposing dangerous chemicals suddenly leak on the highway and the emergency threatens the safety of people around and causes damage to the surrounding environment. Several experts are urgently summoned to find solutions for the incident, and then, they are asked to assess each solution within a limited time. It is assumed that there are three experts and four alternatives available to handle this incident, which can be denoted as

$A = \{A_1, A_2, A_3, A_4\}$ and $E = \{E_1, E_2, E_3\}$, respectively. The CPLSs mentioned above can be used to record all the original evaluation information. Supposing the evaluation information given by the third expert for the second alternative is denoted as $L_{23} = \{0.3|0.4, 0.36|0.42, 0.38|0.18\}$, the values in the set $\{0.3, 0.36, 0.38\}$ are evaluation values, and the values in the set $\{0.4, 0.42, 0.18\}$ are the corresponding probability information, the calculation process of the score value is $S_{23} = 0.3 \times 0.4 + 0.36 \times 0.42 + 0.38 \times 0.18 = 0.3396$.

The situation of emergencies always changes dynamically over time [36]; therefore, decisions need to be made according to the actual situations at different stages, and these problems will be discussed in detail in the next chapter of this paper.

2.3. The Information Aggregation Operators. The scattered information given by experts separately must be aggregated and obtained the final evaluation value for each alternative [37]. At present, there are several different aggregation methods [38], and the dynamic hesitant probability fuzzy weighted arithmetic (DHPFWA) operator is selected in this paper after comparisons because of its simple and intuitive characteristics.

Supposing a total of k experts have, respectively, given their evaluation information for the alternative A_r, which can be denoted mathematically as $L_r = \{L_{r1}, L_{r2}, \cdots, L_{rk}\}$, the weights of experts can be denoted as $\omega = (\omega_1, \omega_2, \cdots, \omega_k)$, which can be obtained according to their past experiences and authorities in this field; the greater the value is, the more important the evaluation information given by the expert is [39]; and the weights satisfy the constraints, which are $\omega_i \in (0, 1)$ and $\sum_{i=1}^{k} \omega_i = 1$. Equation (3) gives the specific calculation method of the DHPFWA operator.

$$DHPFWA(L_r) = \overset{k}{\underset{i=1}{\oplus}} (\omega_i L_{ri}) = \bigcup_{\gamma_{l_1} \in L_{r1}, \gamma_{l_2} \in L_{r2} \cdots \gamma_{l_k} \in L_{rk} p_{l_1} \in L_{r1}, p_{l_2} \in L_{r2} \cdots p_{l_k} \in L_{rk}} \left\{ 1 - \prod_{i=1}^{k} \left(1 - \gamma_{l_i}\right)^{\omega_i} | p_{l_1} p_{l_2} \cdots p_{l_k} \right\}, \quad (4)$$

where $l_1 = 1, 2 \cdots, m_1, l_2 = 1, 2 \cdots, m_2, l_k = 1, 2 \cdots, m_k$, and we must point out that the values of $m_1, m_2, \cdots, m_k$ are not necessarily equal to each other, which means that the total number of elements in different CPLSs can be completely unequal with each other. Let us give a simple example to illustrate the above theories, supposing the CPLSs $L_{r1} = \{034|036, 038|035, 040|029\}$, $L_{r2} = \{032|1\}$ and $L_{r3} = \{035|07, 039|03\}$ are the evaluation information for the alternative A_r given by three experts, respectively. We can find that a total number of elements in the three CPLSs are $m_1 = 3, m_2 = 1$, and $m_3 = 2$, respectively, and they are totally different from each other. Now further assume that the weights of the three experts are $\omega = (0.32, 0.27, 0.41)$, and the aggregated value of the three CPLSs can be calculated according to equation (3), which is shown as follows:

$$DHPFWA(L_r) = \overset{3}{\underset{i=1}{\oplus}} (\omega_i L_{ri}) = \begin{pmatrix} 0.338811|0.252, 0.351907|0.245 \\ 0.358672|0.203, 0.355806|0.108 \\ 0.368566|0.105, 0.375157|0.087 \end{pmatrix}. \quad (5)$$

We can find that the aggregated value is also in the form of CPLS and cannot be compared with other values directly [40], the score value can be further calculated according to equation (2) mentioned in Section 2.1, which is shown as follows:

$$S(L_r) = \sum_{l=1}^{m} \gamma_l \cdot p_l = 0.354173. \quad (6)$$

The form of the score value is very simple, and it is a real number, which is easy to be compared with other values and perform algebraic operations.

2.4. The Decision-Making Problem with Cost Constraints. Obviously, the cost is one of the most important constraints in the decision-making process, which cannot be ignored [41]. Although every alternative for dealing with emergencies is costly, while there are still wide gaps among different alternatives. The more rigorous the alternative is designed; usually, the better effect can be acquired, while the disadvantage is also obvious, which often have a great adverse impact on the local economy and increase burdens on the people and the government [42]. The costs include not only economic costs but also casualties, labour costs, environmental pollution, and expected income loss and so on; particularly, the casualties are the most important cost and must be seriously considered in the decision-making process [43].

Through the above analysis, we believe that the most appropriate alternative is not necessarily the one that just has the best effect, the cost and the effect must be considered comprehensively, which is more in line with the actual situation [44].

The main idea of dealing with the decision-making problem with cost constraints can be briefly described as follows: first, we reorder all the alternatives according to their costs, which can be denoted as $A = \{A_1, A_2, \cdots, A_n\}$; the estimated costs of these alternatives can be denoted as $\Delta\eta = \{\Delta\eta_{01}, \Delta\eta_{12}, \cdots, \Delta\eta_{k-1k}\}$, in which the symbol $\Delta\eta_{i-1i}$ indicates the estimated cost from the time point t_{i-1} to the time point t_i; the estimated effects acquired by implementing these alternatives can be denoted as $\Delta\tau = \{\Delta\tau_{01}, \Delta\tau_{12}, \cdots, \Delta\tau_{k-1k}\}$, and similarly, the symbol $\Delta\tau_{i-1i}$ indicates the estimated effect acquired from the time point t_{i-1} to the time point t_i. We give the definition of the effect per cost (EPC), which can be described as $\psi = \{\psi_{i-1i}, i = 1, 2, \cdots, k\}$, $\psi_{i-1i} = \Delta\tau_{i-1i}/\Delta\eta_{i-1i}$. The definition of the EPC firstly proposed in the paper can consider the cost and effect comprehensively, and we believe that the most appropriate alternative in the current time point is the one that has the lowest EPC.

2.5. The Closed-Loop Control System. The closed-loop control system is a concept of the automatic control theory in the engineering technology. Its principle can be briefly described as follows: part or all of the output signals will be sent back to the input of the system, the differential signals between the original input signals and the feedback signals will be calculated, and then, they will be input into the system to automatically adjust relevant parameters [45], which is helpful to avoid the system from deviating from the predetermined goal.

We find that there are always differences between the values estimated at the previous time point and the values measured currently, the closed-loop control system provides a way to solve this problem, and we try to construct a closed-loop control system in the decision-making field [46]. Specifically speaking, we calculate the differences of the values estimated at the previous time point and the values measured currently and then input the differences into the decision-making system; thus, the relevant parameters of the system will be automatically adjusted in time according to the differences, and this is helpful to improve the evaluation accuracy of the system [47]. This is also one of the important improvements between the algorithm proposed in the paper and other decision-making methods.

3. The Closed-Loop Method of Collaborative Decision-Making

In this section, we will introduce the algorithm proposed in this paper in detail and build the mathematical model.

3.1. Mathematicize the Decision-Making Problem. Usually, it is impossible to achieve the expected goal by taking measures only once for dealing with emergencies, we need to adjust measures in time with the development of the situation. First of all, we make the following assumptions: the initial time point is denoted as T_0, and the time point of achieving the expected goal is denoted as T_k, and all time points are recorded in the set $T = \{T_0, T_1, \cdots, T_k\}$. All the time intervals are recorded in the set $\Delta T = \{\Delta T_{01}, \Delta T_{12}, \cdots, \Delta T_{k-1k}\}$, and they can also be called periods. Generally, they are equal to each other, while, in some special cases, such as, when a major unexpected event occurs suddenly, a new time point must be inserted immediately.

The experts invited to deal with the emergency are denoted as $E = \{E_1, E_2, \cdots, E_m\}$, and their corresponding weights are denoted as $\omega = \{\omega_1, \omega_2, \cdots \omega_m\}$; the alternatives proposed by experts at the time point T_i are denoted as $A_i = \{A_i^1, A_i^2, \cdots, A_i^{n_i}\}$; the values of the parameter $i\,(i = 0, 1, \cdots k)$ indicate different time points; and the values of the $n_i\,(i = 1, 2, \cdots k)$ are not necessarily equal to each other. The experts will measure the current severity of the emergency according to the information acquired at each time point, these measurements will be denoted as $\tau = \{\tau_0, \tau_1, \cdots, \tau_k\}$, and each value τ_i in the set τ is in the form of CPLS.

3.2. The Subtraction between Any Two CPLSs. In order to build the feedback network, first of all, we need to calculate the differences between the estimated values made at the previous time point and the values measured at the current time point. Both data are in the form of CPLSs, and therefore, the subtraction between any two CPLSs must be required [48]; however, this theory is rarely mentioned by other researchers, and for this reason, the paper proposes a subtraction method between any two continuously probabilistic linguistic sets, which is shown as equation (4). We suppose the L_{rs} and the L_{pq} are two ordinary continuously probabilistic linguistic sets.

$$\begin{aligned} L_d &= L_{rs} - L_{pq}, \\ &= \bigcup_{\gamma_{l_1} \in L_{rs}, \gamma_{l_2} \in L_{pq}, p_{l_1} \in L_{rs}, p_{1_2} \in L_{pq}} \left\{ \gamma_{l_1} - \gamma_{l_2} | p_{l_1} p_{l_2} l_1 \right. \\ &\quad \left. = 1, 2 \cdots, m_1 l_2 = 1, 2 \cdots, m_2 \right\}. \end{aligned} \tag{7}$$

We find that the calculation result obtained by equation (4) is also a set, which can be called a special continuously probabilistic linguistic set. The main difference is that the values satisfy the constraint condition, which is $-1 \le \gamma_{l_1} - \gamma_{l_2} \le 1$ in the subtraction set, while the values satisfy the constraint condition, which is $0 \le \gamma_l \le 1$ in any ordinary continuously probabilistic linguistic set. It can be further illustrated by a simple example, supposing that there are two ordinary CPLSs, which are recorded as $L_{rs} = \{04|02, 041|08\}$ and $L_{pq} = \{0.38|0.3, 0.41|0.1, 0.43|0.6\}$, respectively, and the subtraction result can be calculated according to equation (4) and the result is as follows:

$$\begin{aligned} L_d &= L_{rs} - L_{pq} \\ &= \{0.02|0.06, -0.01|0.02, -0.03|0.12, 0.03|0.24, \\ &\quad 0|0.08, -0.02|0.48\}. \end{aligned} \tag{8}$$

We can find that some values are greater than zero, while other values are less than zero, which is different from the definition of the ordinary continuously probabilistic linguistic set. The sum of probabilities is also equal to one, which is the same with the ordinary continuously probabilistic linguistic set. However, the above result is still not intuitive enough to reflect the differences; therefore, the score value of the special continuously probabilistic linguistic set needs to be further calculated. We must point out that the method mentioned in equation (2) is still applicable to the calculation of the special continuously probabilistic linguistic set, and the result is called as the special score value. The only difference is that the value range is $0 \le S(L) \le 1$ for any ordinary CPLS, while the value range will be $-1 \le S(L_d) \le 1$ for the special CPLS. For example, the special score value of the above example can be calculated according to equation (2), and the result is as follows:

$$S(L_d) = \sum_{l=1}^{m} \gamma_l \cdot p_l = -0.0096. \tag{9}$$

When the score value is less than zero, it indicates that the value measured currently is better than the value estimated at the previous time point; when the score value is greater than zero, it indicates that the value measured currently is worse than the value estimated at the previous time point; when the score value is equal to zero, it indicates that the value measured currently is exactly equal to the value estimated at the previous time point; however, this ideal situation is almost impossible to happen.

3.3. The Method of Obtaining the Most Appropriate Alternative. Let us illustrate the algorithm proposed in the paper in the chronological order. At the initial time point T_0, the current severity of the emergency measured by experts is denoted as τ_0, the specific form can be denoted as $\tau_0 = \{\tau_0^1, \tau_0^2, \cdots, \tau_0^m\}$, each value τ_0^i given by the corresponding expert E_i is in the form of the continuously probabilistic linguistic set, and the specific form of the τ_0 is further described in Table 1. The alternatives proposed at the time point T_0 are denoted as $A_0 = \{A_0^1, A_0^2, \cdots, A_0^{n_0}\}$, and the estimated severities for the next time point T_1 are denoted as $\tau_1' = \left\{\tau_1^{1'}, \tau_1^{1'}, \cdots, \tau_1^{n_0'}\right\}$. When using different alternatives, each value $\tau_1^{i'}$ in the set τ_1' is also a set, which can be denoted as $\tau_1^{i'} = \left\{\tau_{10}^{i'}, \tau_{11}^{i'}, \cdots, \tau_{1m}^{i'}\right\}$; for example, the symbol $\tau_{1j}^{i'}$ indicates the severity that the expert E_j estimated at the time point T_1 by using the alternative A_i, and the specific form of the τ_1' is further described in Table 2. We must point out that all the elements in Table 2 are also in the form of the continuously probabilistic linguistic set. Each value $\tau_1^{i'}(i = 1, 2, \cdots, n_0)$ consists of the elements in the corresponding row of Table 2. For the sake of simplicity, the specific forms of the elements in Table 2 are not given and they are similar to the elements in Table 1.

All the scattered information provided by experts can be aggregated by the *DHPFWA* operator, and then, the score value can be further calculated, and these theories have already been introduced in Section 2.3. Equations (5) and (6) are specific expansion forms for this problem. The calculation result of the DHPFWA(τ_0) is in the form of the continuously probabilistic linguistic set, and the symbol m indicates the total number of elements in the DHPFWA(τ_0).

$$\begin{aligned}\mathrm{DHPFWA}(\tau_0) &= \overset{m}{\underset{i=1}{\oplus}}(\omega_i\tau_{0i}),\\ &= \bigcup_{\gamma_{l_1}\in\tau_{01},\gamma_{l_2}\in\tau_{02}\cdots\gamma_{l_k}\in\tau_{0m}p_{l_1}\in\tau_{01},p_{l_2}\in\tau_{02}\cdots p_{l_k}\in\tau_{0m}} \\ &\quad \left\{1-\prod_{i=1}^{m}\left(1-\gamma_{l_i}\right)^{\omega_i}|p_{l_1}p_{l_2}\cdots p_{l_k}\right\},\end{aligned} \tag{10}$$

$$S(T_0) = S(DHPFWA(\tau_0)) = \sum_{l=1}^{m'}\gamma_l\cdot p_l. \tag{11}$$

Similarly, the score values of the estimated severities at the time point T_1 can also be calculated, which can be denoted as $S'(T_1) = \left\{S(\tau_1^{1'}), S(\tau_1^{2'}), \cdots, S(\tau_1^{n_0'})\right\}$; then, all the estimated effects can be calculated according to equation (7).

Table 1: The current severity of the emergency at the initial time point.

Experts	E_1	E_2	$\cdots$	E_m
Measured values	$\tau_0^1 = \left\{\gamma_{l_0^1}\|p_{l_0^1}\right\}$	$\tau_0^2 = \left\{\gamma_{l_0^2}\|p_{l_0^2}\right\}$	$\cdots$	$\tau_0^m = \left\{\gamma_{l_0^m}\|p_{l_0^m}\right\}$

Table 2: The estimated severities at the time point T_1.

Experts estimated severities	E_1	E_2	$\cdots$	E_m
$\tau_1^{1'}$	$\tau_{11}^{1'}$	$\tau_{12}^{1'}$	$\cdots$	$\tau_{1m}^{1'}$
$\tau_1^{2'}$	$\tau_{11}^{2'}$	$\tau_{12}^{2'}$	$\cdots$	$\tau_{1m}^{2'}$
$\vdots$	$\vdots$	$\vdots$	$\vdots$	$\vdots$
$\tau_1^{n_0'}$	$\tau_{11}^{n_0'}$	$\tau_{12}^{n_0'}$	$\cdots$	$\tau_{1m}^{n_0'}$

$$\begin{aligned}\Delta\tau_{01} &= \left(\Delta\tau_{01}^{1'}, \Delta\tau_{01}^{2'}, \cdots, \Delta\tau_{01}^{n_0'}\right)\\ &= S'(T_1) - S(T_0)\\ &= \left\{S\left(\tau_1^{1'}\right) - S(T_0), S\left(\tau_1^{2'}\right) - S(T_0), \cdots, S\left(\tau_1^{n_0'}\right) - S(T_0)\right\}.\end{aligned} \tag{12}$$

Each value in the set $\Delta\tau_{01}$ satisfies the constraint, which is $-1 \le \Delta\tau_{01}^{i'} \le 1$; when the value is negative, it indicates that the emergency has become worse after using the corresponding alternative A_i; when the value is positive, it indicates that the emergency has been alleviated after using the corresponding alternative A_i; and when the value is zero, it indicates that the emergency has not changed after using the corresponding alternative A_i.

The cost of each period is recorded in the set $\Delta\eta = \{\Delta\eta_{01}, \Delta\eta_{12}, \cdots, \Delta\eta_{k-1k}\}$. The symbol $\Delta\eta_{ii+1}$ indicates the estimated cost from the time point T_i to the time point T_{i+1}, because different alternatives $A_i = \{A_i^1, A_i^2, \cdots, A_i^{n_i}\}$ for dealing with the emergency will produce different costs, and the $\Delta\eta_{ii+1}$ is also a set, which can be denoted as $\Delta\eta_{ii+1} = \{\Delta\eta_{ii+1}^1, \Delta\eta_{ii+1}^2, \cdots, \Delta\eta_{ii+1}^{n_i}\}$.

For the first period, the effect per cost ψ_{01} of using different alternatives can be calculated according to equation (8); obviously, the result is a set.

$$\psi_{01} = \left\{\psi_{01}^i|\psi_{01}^i = \frac{\Delta\tau_{01}^{i'}}{\Delta\eta_{01}^i}i = 1, 2, \cdots, n_0\right\}. \tag{13}$$

The most appropriate alternative at this time point is the one that has the lowest EPC, which is shown as follows:

$$\psi_{01}^{j*} = \min\left(\psi_{01}^i\right)_{i=1}^{n_0}. \tag{14}$$

Similarly, the most appropriate alternative at other time points can be obtained by this method.

3.4. The Construction of the Closed-Loop System. The most appropriate alternative A_j found in the previous step will be implemented immediately. The current severity of the emergency will be measured again at the time point T_1,

which can be denoted as τ_1. The τ_1 is a set that contains several values $\{\tau_1^1, \tau_1^2, \cdots, \tau_1^m\}$ given by different experts, respectively, according to the information acquired at the time point T_1, and the specific form of the τ_1 is further described in Table 3.

The differences between the values estimated at the initial time point T_0 and the values measured at the first time point T_1 will be calculated, and the calculation method is shown in equation (10), and its specific form is further described in Table 4.

$$\begin{aligned} d_1 &= \left\{d_1^1, d_1^2, \cdots, d_1^m\right\} \\ &= \left\{\tau_{11}^{j/} - \tau_1^1, \tau_{12}^{j/} - \tau_1^2, \cdots, \tau_{1m}^{j/} - \tau_1^m\right\}. \end{aligned} \tag{15}$$

We must point out that all the τ_1^i $(i = 1, 2, \cdots, m)$ and the $\tau_{1i}^{j/}$ $(i = 1, 2, \cdots, m)$ are in the form of CPLS; therefore, each calculation equation $d_1^i = \tau_{1i}^{j/} - \tau_1^i$ $(i = 1, 2, \cdots, m)$ is a subtraction between CPLSs, and they must be calculated according to equation (4) mentioned in Section 3.2. All the differences d_1^i $(i = 1, 2, \cdots, m)$ are also in the form of CPLS, and they will be aggregated according to equation (5) and equation (6) to obtain the total difference of the first period, which can be denoted as $S(d_1)$.

The flow chart of the closed-loop submodule is shown in Figure 1. At this time, the system will enter the automatic adjustment stage. Four parameters that are denoted as $\lambda_1, \lambda_2, \varepsilon$, and ς will be set in advance, and the inequalities $-1 \le \lambda_1 \le -\varepsilon \le 0 \le \varepsilon \le \lambda_2 \le 1$ and $0 \le \varsigma \le 1$ hold. The smaller the value of ε is set, the higher the system accuracy is required; the larger the value of λ_1 is set, the easier it is for the system to conduct conservative evaluation; the larger the value of λ_2 is set, the easier it is for the system to conduct optimistic evaluation; and the greater the value of ς is set, the easier the predetermined goal can be achieved. If the inequality $|S(d_1)| \le \varepsilon$ holds, it indicates that the system works well and no adjustment is required; if the inequalities $|S(d_1)| > \varepsilon$ and $\lambda_1 \le S(d_1) \le \lambda_2$ hold, it indicates that only minor adjustments are needed and the automatic adjustment method will be activated immediately; if the inequality $\lambda_2 < S(d_1) \le 1$ holds, it indicates that the system is too optimistic, experts are not fully aware of the severity and the development trend of the accident, and the system can be adjusted from two aspects: the first suggestion is that experts must propose more stringent alternatives, and the other suggestion is that experts should reduce the estimated values; if the inequality $-1 \le S(d_1) < \lambda_1$ holds, it indicates that the system is too pessimistic, the alternative used has achieved better results than expected. Similarly, the system can also be adjusted from two aspects: the first suggestion is that the experts can propose looser alternatives with lower costs, and the other suggestion is that the experts should appropriately raise the estimated values.

3.5. The Automatic Adjustment Algorithm. The symbol ε mentioned above is called the acceptable threshold. In this section, we propose an automatic adjustment algorithm for the estimated values and its specific steps are listed as follows:

Table 3: The current severity of the emergency at the first time point.

Experts	E_1	E_2	$\cdots$	E_m
Measured values	$\tau_1^1 = \left\{\gamma_{l_1^1} \middle\vert p_{l_1^1}\right\}$	$\tau_1^2 = \left\{\gamma_{l_1^2} \middle\vert p_{l_1^2}\right\}$	$\cdots$	$\tau_1^m = \left\{\gamma_{l_1^m} \middle\vert p_{l_1^m}\right\}$

Table 4: The differences between the estimated values and measured values.

Experts	E_1	E_2	$\cdots$	E_m
Differences	$d_1^1 = \tau_{11}^{j/} - \tau_1^1$	$d_1^2 = \tau_{12}^{j}{}' - \tau_1^2$	$\cdots$	$d_1^m = \tau_{1m}^{j/} - \tau_1^m$

Step 1. Appropriate values will be set for the system parameters λ_1, λ_2, and ε according to the actual situation of the emergency.

Step 2. Calculate the total differences of the current period $S(d) = \{S(d_i) | i = 1, 2, \cdots, k\}$ by using the method mentioned in Section 3.4.

Step 3. Let us take the first period as an example to illustrate the algorithm, suppose the inequality $\lambda_1 \le S(d_1) \le \lambda_2$ holds, and the inequality $|S(d_1)| \le \varepsilon$ does not hold.

Step 4. It can be divided into two categories according to the value of the $S(d_1)$. When the inequality $\lambda_1 \le S(d_1) < -\varepsilon$ holds, first of all, the maximum value must be found from all the estimated values, supposing the symbol γ_i represents the maximum value, then increase $m \times |S(d_1)|$ to the value, and the symbol m represents the total number of experts. On the other hand, when the inequality $\varepsilon < S(d_1) \le \lambda_2$ holds, similarly, the maximum value should decrease $m \times S(d_1)$. We can summarize that the adjustment method can be unified for both categories after the above analysis, which can be shown as follows:

$$\gamma_i = \gamma_i - m \times S(d_1). \tag{16}$$

Step 5. Similarly, the total difference $S'(d_1)$ can be calculated again according to the updated estimated values, and the step 3 and the step 4 will be repeated until the inequality $|S(d_1)| \le \varepsilon$ holds.

Step 6. The qualified estimated values will be obtained after several rounds of automatic adjustments.

The automatic adjustment algorithm has two advantages: the first advantage is that the algorithm is efficient and highly automated, and another advantage is that the original estimated information given by experts is minimally modified compared with other algorithms. The flow chart of the automatic adjustment submodule is shown in Figure 2.

3.6. The Brief Summary of the Algorithm Proposed in the Paper. The overall flow chart of the algorithm proposed in the paper is shown in Figure 3. The whole algorithm is divided into multiple time points, which are denoted as $\{T_0, T_1, \cdots, T_k\}$, and the time that spans any two adjacent time points can be called a period, such as $\Delta T_0 = [T_0, T_1]$.

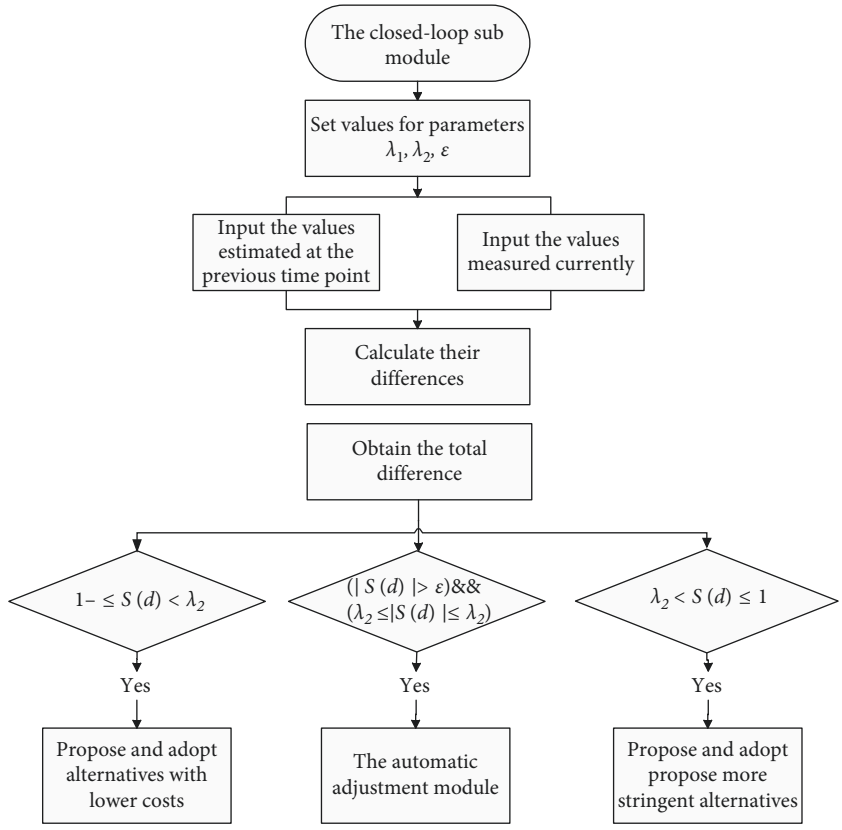

Figure 1: The flow chart of the closed-loop submodule.

At the time point T_0, the current severity of the emergency will be measured by experts, and the data can be called measured values for short; then, the algorithm will judge whether the predetermined goal has been achieved or not according to the measured values. If the goal has been achieved, the algorithm will be terminated immediately; if the goal has not been achieved, experts will estimate the severities at the next time point when using different alternatives and the data obtained can be called estimated values for short. The estimated effects of different alternatives can be calculated according to the measured values and the evaluated values, and the cost of each alternative can be estimated according to specific measures. After above preparation, the effect per cost of each alternative can be calculated. Finally, the most appropriate alternative that has the lowest EPC will be found and it will be implemented immediately.

Similarly, at the time point T_1, experts will measure the current severity of the emergency, and then, they will judge whether the predetermined goal has been achieved or not again. If the goal has been achieved, the algorithm will be terminated; if the goal has not been achieved, the total differences between the values estimated at the previous time point and the values measured currently will be calculated, and the corresponding automatic adjustment submodules will be activated according to the differences. The following processing methods are similar to the above steps, and the most appropriate alternative of this time point will be found and implemented.

From the time point T_2 to the time point T_{k-1}, the algorithm will repeat the above processes and the severity of the emergency will gradually decrease. The emergency will be effectively controlled after several rounds of treatment.

At the time point T_k, experts will measure the current severity of the emergency, and they find that the inequality $|1 - S(T_k)| \leq \varsigma$ holds, which indicates that the predetermined goal has been achieved, the algorithm will be terminated immediately. The parameter ς is called the completion threshold. The emergency has been handled effectively with the lowest cost.

4. A Case of the Closed-Loop Collaborative Decision-Making Algorithm

4.1. The General Description of the Emergency. The whole world is facing the severe challenge of the COVID-19 (corona virus disease 2019), and the latest prediction shows that the epidemic will lead to a global economic recession and large-scale unemployment. It has caused a large number of infections; even worse, various prevention and control methods are not mature enough to fundamentally eradicate the infectious disease.

At present, the COVID-19 has been basically controlled in China; however, we found that the epidemic is still breaking out occasionally in some areas of China and has the trend of further expansion, and it has added great resistance to the employment and the economic development of China. The Chinese government has taken various measures to deal with the epidemic for many years; however, the epidemic situation is changing continuously over time. Obviously, this problem belongs to the dynamic decision-making problem;

in addition, we can hardly hope to solve this problem through only a round of measures, and therefore, the multiround decision-making algorithm discussed in the paper is suitable to deal with this problem. The specific steps of the proposed algorithm will be introduced in this section according to the chronological order.

4.2. The Processing Methods at the Time Point T_0. Let us take one of universities in the high-risk areas as an example to illustrate the algorithm and the university is facing the threat of the epidemic. The appropriate alternatives must be found out at different time points to prevent and control the epidemic. Supposing that a total of three experts are summoned to deal with this emergency, and they have put forward four response alternatives, which can be denoted as $A_0 = \{A_0^1, A_0^2, A_0^3, A_0^4\}$ at the initial time point T_0. The predetermined goal is to minimize the adverse impact of the COVID-19 on normal teaching and student activities.

Table 5 lists the alternatives proposed by experts for handling the emergency at the initial time point (T_0). We can find that the measures in the table have gradually become more and more stringent from top to bottom, and we must admit that the latter alternative is indeed better than the former alternative in controlling the epidemic situation; however, the disadvantage is that the cost will be higher; once again, we point out that the most appropriate alternative is not necessarily the most stringent alternative.

The current severities of the emergency measured by experts separately according to the available information are listed in Table 6, and the weights of experts are also given. Obviously, the predetermined goal has not been achieved. The scattered information can be aggregated according to equations (5) and (6). The score value obtained ranges from 0 to 1, and the symbol "0" indicates that the situation is extremely bad, while the symbol "1" indicates that the situation is perfect. The current severity is 0.1554, and the specific calculation processes are shown as follows:

$$DHPFWA(t_0) = \overset{3}{\underset{k=1}{\oplus}}\left(\omega_k \tau_0^k\right) = \left\{\begin{array}{c} 0.117281|0.096, 0.136686|0.064, 0.144651 \\ |0.16, 0.130477|0.024 \\ 0.149592|0.016, 0.157438|0.04, 0.147927 \\ |0.144, 0.166659|0.096 \\ 0.174347|0.24, 0.160665|0.036, 0.179116 \\ |0.024, 0.18669|0.06 \end{array}\right\}, \tag{17}$$

$$S(T_0) = \sum_{l=1}^{m} \gamma_l \cdot p_l = 0.1554. \tag{18}$$

The values of the estimated severities at the time point T_1 when using different alternatives are listed in Table 7. Similarly, the score values are calculated and their specific calculation steps are shown as follows:

$$\begin{aligned}
&\tau_1^{1j} = \overset{3}{\underset{k=1}{\oplus}}\left(\omega_k \tau_{1k}^{1j}\right) = \left\{\begin{array}{c} 0.219122|0.144, 0.225504|0.072, 0.228737 \\ |0.024, 0.238284|0.096 \\ 0.244509|0.048, 0.247663|0.016, 0.225345 \\ |0.216, 0.231675|0.108 \\ 0.234882|0.036, 0.244354|0.144, 0.250529 \\ |0.072, 0.253658|0.024 \end{array}\right\}, \\
&S\left(\tau_1^{1j}\right) = \sum_{l=1}^{m} \gamma_l \cdot p_l = 0.2333, \\
&\tau_1^{2j} = \oplus_{k=1}^{3}\left(\omega_k \tau_{1k}^{2j}\right) = \left\{\begin{array}{c} 0.287015|0.045, 0.293015|0.075, 0.29606 \\ |0.03, 0.298616|0.105 \\ 0.304519|0.175, 0.307514|0.07, 0.293504 \\ |0.045, 0.29945|0.075 \\ 0.302467|0.03, 0.305|0.105, 0.310849 \\ |0.175, 0.313817|0.07 \end{array}\right\}, \\
&S\left(\tau_1^{2j}\right) = \sum_{l=1}^{m} \gamma_l \cdot p_l = 0.3031, \\
&\tau_1^{3j} = \oplus_{k=1}^{3}\left(\omega_k \tau_{1k}^{3j}\right) = \left\{\begin{array}{c} 0.345523|0.09, 0.352035|0.045, 0.35869 \\ |0.015, 0.356817|0.09 \\ 0.363217|0.045, 0.369757|0.015, 0.351727 \\ |0.21, 0.358178|0.105 \\ 0.364769|0.035, 0.362914|0.21, 0.369253 \\ |0.105, 0.375731|0.035 \end{array}\right\}, \\
&S\left(\tau_1^{3j}\right) = \sum_{l=1}^{m} \gamma_l \cdot p_l = 0.3587, \\
&\tau_1^{4j} = \oplus_{k=1}^{3}\left(\omega_k \tau_{1k}^{4j}\right) = \left\{\begin{array}{c} 0.373669|0.054, 0.376717|0.036, 0.3798 \\ |0.09, 0.385363|0.036 \\ 0.388354|0.024, 0.391379|0.06, 0.386471 \\ |0.126, 0.389457|0.084 \\ 0.392477|0.21, 0.397926|0.084, 0.400856 \\ |0.056, 0.40382|0.14 \end{array}\right\}, \\
&S\left(\tau_1^{4j}\right) = \sum_{l=1}^{m} \gamma_l \cdot p_l = 0.3908.
\end{aligned} \tag{19}$$

The score values of the estimated severities at the time point T_1 can be recorded as $S'(T_1) = \{0.2333, 0.3031, 0.3587, 0.3908\}$. Subsequently, the estimated effects at the period ΔT_{01} can be calculated according to equation (7), which are shown as follows:

$$\begin{aligned}
\Delta\tau_{01} &= \left\{\Delta\tau_{01}^{1}, \Delta\tau_{01}^{2}, \Delta\tau_{01}^{3}, \Delta\tau_{01}^{4}\right\} \\
&= \{0.0779, 0.1477, 0.2033, 0.2354\}.
\end{aligned} \tag{20}$$

The costs at the period ΔT_{01} can be denoted as $\Delta\eta_{01} = \{\Delta\eta_{01}^1, \Delta\eta_{01}^2, \Delta\eta_{01}^3, \Delta\eta_{01}^4\}$when using different alternatives. Supposing the cost of the alternative A_1 is normalized and is regarded as "1," other values will be standardized based on this value. The estimated costs of all alternatives are $\Delta\eta_{01} = (1, 1.2, 1.7, 2)$.

Obviously, the alternative A_4 has the best effect; however, its cost is also the highest, and therefore, the most appropriate alternative cannot be determined directly, and the effects per cost of all alternatives need to be further calculated according to equation (8), which are shown as follows:

$$\begin{aligned}
\psi_{01} &= |\left(\psi_{01}^i \psi_{01}^i = \frac{\Delta\tau_{01}^{i'}}{\Delta\eta_{01}^i} i = 1, 2, 3, 4\right) \\
&= \{0.0779, 0.123083, 0.119588, 0.1177\}.
\end{aligned} \tag{21}$$

The order of the alternatives can be denoted as $\psi_{01}^2 > \psi_{01}^3 > \psi_{01}^4 > \psi_{01}^1$ according to the values of EPCs; therefore, the alternative A_2 is the most appropriate alternative at the time point T_0, and it will be implemented immediately.

4.3. The Processing Methods at the Time Point T_1. Similarly, the experts will measure the severities again at the time point T_1 and their values are listed in Table 8.

Obviously, the predetermined goal has still not been achieved. In order to test and improve the accuracy of the system, the differences between the values estimated at the T_0 and the values measured at the T_1 will be calculated and their values are listed in Table 9.

$\lambda_1 < S(d_1) < \lambda_2$ holds; therefore, major adjustments are not required, and however, the inequality $-\varepsilon \le S(d_1) \le \varepsilon$ does not hold, which indicates minor adjustments are still required and the automatic adjustment module will be activated immediately. According to the algorithm, the maximum estimated value of the alternative A_0^2 in Table 7 can be found, the value 0.32 will increase to 0.3216081827 according to equation (11), and other values remain unchanged. The updated severities are shown in Table 10.

$$d_1 = \oplus_{k=1}^{3}\left(\omega_k d_1^k\right) = \left\{\begin{array}{c} -0.004481|0.0054, -0.010407|0.0126, 0.001529|0.0090, -0.004481|0.0210 \\ 0.004565|0.0036, -0.001487|0.0084, -0.017554|0.0081, -0.023557|0.0189 \\ -0.011467|0.0135, -0.017554|0.0315, -0.008391|0.0054, -0.014521|0.0126 \\ 0.002194|0.0054, -0.003693|0.0126, 0.008163|0.0090, 0.002194|0.0210 \\ 0.011179|0.0036, 0.005168|0.0084, -0.011062|0.0081, -0.017027|0.0189 \\ -0.005014|0.0135, -0.011062|0.0315, -0.001957|0.0054, -0.008048|0.0126 \\ 0.006739|0.0126, 0.000879|0.0294, 0.012681|0.0210, 0.006739|0.0490 \\ 0.015683|0.0084, 0.009700|0.0196, -0.006188|0.0189, -0.012125|0.0441 \\ -0.000169|0.0315, -0.006188|0.0735, 0.002873|0.0126, -0.003189|0.0294 \\ 0.013339|0.0126, 0.007518|0.0294, 0.019241|0.0210, 0.013339|0.0490 \\ 0.022224|0.0084, 0.016280|0.0196, 0.000231|0.0189, -0.005668|0.0441 \\ 0.006212|0.0315, 0.000231|0.0735, 0.009234|0.0126, 0.003211|0.0294 \end{array}\right\}, \tag{22}$$

$$S(d_1) = \sum_{l=1}^{m} \gamma_l \cdot p_l = -0.0005360609,$$

The system parameters are set as $\lambda_1 = -0.001, \lambda_2 = 0.001, \varepsilon = 00005$, and $\varsigma = 0.04$. We can find that the inequality

The total difference will be calculated again according to the data in Table 11, and the specific steps are shown as follows:

$$d_1' = \mathop{\oplus}_{k=1}^{3}\left(\omega_k d_1^{'k}\right) = \left\{\begin{array}{c} -0.004481|0.0054, -0.010407|0.0126, 0.001529|0.0090, -0.004481|0.0210 \\ 0.004565|0.0036, -0.001487|0.0084, -0.017554|0.0081, -0.023557|0.0189 \\ -0.011467|0.0135, -0.017554|0.0315, -0.008391|0.0054, -0.014521|0.0126 \\ 0.002194|0.0054, -0.003693|0.0126, 0.008163|0.0090, 0.002194|0.0210 \\ 0.011179|0.0036, 0.005168|0.0084, -0.011062|0.0081, -0.017027|0.0189 \\ -0.005014|0.0135, -0.011062|0.0315, -0.001957|0.0054, -0.008048|0.0126 \\ 0.007346|0.0126, 0.001490|0.0294, 0.013285|0.0210, 0.007346|0.0490 \\ 0.016285|0.0084, 0.010305|0.0196, -0.005573|0.0189, -0.011506|0.0441 \\ -0.000442|0.0315, -0.005573|0.0735, 0.003482|0.0126, -0.002576|0.0294 \\ 0.013942|0.0126, 0.008125|0.0294, 0.019841|0.0210, 0.013942|0.0490 \\ 0.022822|0.0084, 0.016881|0.0196, 0.000842|0.0189, -0.005053|0.0441 \\ 0.006819|0.0315, 0.000842|0.0735, 0.009840|0.0126, 0.003820|0.0294 \end{array}\right\}, \tag{23}$$

$$S'(d_1) = \sum_{l=1}^{m} \gamma_l \cdot p_l = -00001092876.$$

We can find that the inequality $-\varepsilon < S'(d_1) < \varepsilon$ holds at this time, which indicates that the automatic adjustment module works well. The updated values in Table 10 can provide references for experts in the next estimation.

Since the inequality $\lambda_1 < S(d_1) < \lambda_2$ holds, the most appropriate alternative at this time point is the same as the one at the previous time point; therefore, the alternative A_2 is still the most appropriate alternative at the time point T_1 and it will be implemented immediately. Table 12 lists the estimated severities at the time point T_2 when using different alternatives. Since all the alternatives proposed by experts have not changed, the costs remain unchanged.

4.4. The Processing Methods at the Time Point T_2. In the same way, the experts will measure the severities again at the time point T_2 and their values are listed in Table 13.

Obviously, the predetermined goal has not been achieved. The differences between the values estimated at the time point T_1 and the values measured at the time point T_2 will be calculated, which are shown in Table 14. The total difference will be aggregated according to the data in Table 14.

$$d_2 = \overset{3}{\underset{k=1}{\oplus}} \left(\omega_k d_1^k\right) = \left\{ \begin{array}{l} -0.17952|0.0105, -0.18553|0.0063, -0.19147|0.0042, -0.16727|0.0420 \\ -0.17343|0.0252, -0.17952|0.0168, -0.18265|0.0245, -0.18868|0.0147 \\ -0.19464|0.0098, -0.17038|0.0980, -0.17655|0.0588, -0.18265|0.0392 \\ -0.16356|0.0105, -0.16949|0.0063, -0.17536|0.0042, -0.15148|0.0420 \\ -0.15756|0.0252, -0.16356|0.0168, -0.16679|0.0245, -0.17274|0.0147 \\ -0.17862|0.0098, -0.15468|0.0980, -0.16077|0.0588, -0.16679|0.0392 \\ -0.17181|0.0045, -0.17779|0.0027, -0.18369|0.0018, -0.15965|0.0180 \\ -0.16577|0.0108, -0.17181|0.0072, -0.17493|0.0105, -0.18092|0.0063 \\ -0.18684|0.0042, -0.16273|0.0420, -0.16887|0.0252, -0.17493|0.0168 \\ -0.15596|0.0045, -0.16186|0.0027, -0.16768|0.0018, -0.14396|0.0180 \\ -0.15000|0.0108, -0.15596|0.0072, -0.15917|0.0105, -0.16508|0.0063 \\ -0.17092|0.0042, -0.14714|0.0420, -0.15319|0.0252, -0.15917|0.0168 \end{array} \right\}, \tag{24}$$

$$S(d_2) = \sum_{l=1}^{m} \gamma_l \cdot p_l = -01659861303.$$

We can find that the inequality $S(d_2) < \lambda_1$ holds, which indicates that the actual effects of the alternative are much better than the estimated effects and major adjustments must be required. Experts need to check the system carefully to find out whether any important information for decision-making is missing. The alternative with lower cost should be adopted, if the alternative adopted in the last round of decision-making is already the cheapest alternative, experts should propose a new and cheaper alternative. Since the inequality $\Delta\eta_{23}^1 < \Delta\eta_{23}^2$ holds in this case, which indicates that the alternative with lower cost exists, therefore, there is no need to propose a new alternative, and the alternative A_1 will be the most appropriate alternative at the time point T_2, and it will be implemented immediately.

Duo to the good effect of the alternative, the experts will give more optimistic estimated values in the next round of estimations, which are shown in Table 15.

4.5. Achieve the Predetermined Goal. The experts will measure the severities of the emergency again at the time point T_3, and their values are listed in Table 16, and then, the score value will be calculated.

$$S(T_3) = \sum_{l=1}^{m} \gamma_l \cdot p_l = 0968163. \tag{25}$$

We can find that the inequality $|1 - S(T_3)| \leq \varsigma$ holds, which indicates that the emergency has almost been eliminated, and only routine inspections are required and the algorithm will be terminated.

5. The Comparisons and Discussions

Many scholars have also proposed several outstanding algorithms in the field of decision-making from various perspectives, and these algorithms have their characteristics and suitable application scopes [49]. The comparisons between the algorithms proposed in the paper and others will be made in this section, which will be helpful for finding out the advantages and disadvantages of the algorithm proposed in this paper.

5.1. The Hesitant Fuzzy Set and Its Processing Methods. The hesitant fuzzy set, a classic data structure, is one of the important definitions in the fuzzy mathematics [50], and its information aggregation operators and comparison methods are also quite mature; particularly, many complex data structures are developed from it. Unfortunately, the probability information of the evaluation values cannot be recorded together in the hesitant fuzzy set. Table 17 lists the conversion values of Table 7 when the data are recorded in the form of hesitant fuzzy sets.

We find that only the evaluation values can be recorded, and all the corresponding probability information is missing. From the other point of view, it can be considered that all the

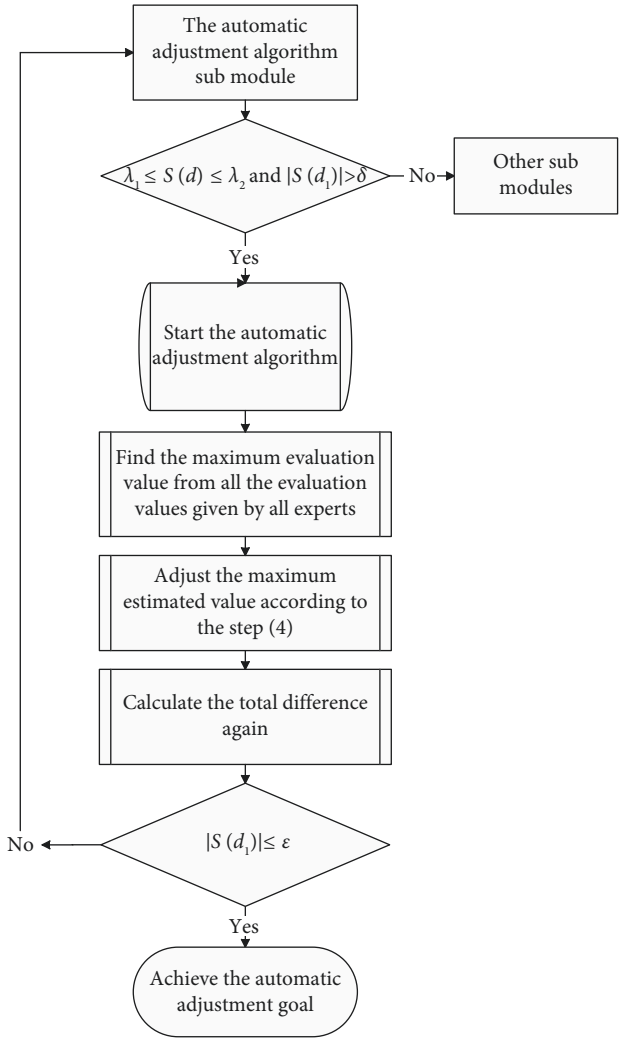

Figure 2: The flow chart of the automatic adjustment submodule.

probability values are equal to each other in any hesitant fuzzy set. Therefore, the hesitant fuzzy set is a special case of the continuously probabilistic linguistic set, and the continuously probabilistic linguistic set can record more detail information, which will make the algorithm more accurate fundamentally.

5.2. The Probabilistic Linguistic Set and Its Processing Methods. The probabilistic linguistic set (PLS) is also one of the efficient data structures, and it is widely used in the field of dealing with fuzzy problems, especially the collection and storage of the fuzzy data [51].

The total number of the possible evaluation values in the PLS is limited [52], and all the possible evaluation values are contained in the additive linguistic term set, which are denoted as $S = \{s_\alpha | \alpha = 0, 1, \cdots, 2\tau\}$, and the symbol τ indicates a positive integer. The definition of the probabilistic linguistic set can be described mathematically as follows:

$$L_p = \left\{ L_l(p_l) | L_l \in S, p_l \ge 0, l = 1, 2, \cdots, m, \sum_{l=1}^{m} p_l = 1 \right\}. \quad (26)$$

Obviously, the data structure CPLS proposed in the paper is developed from the probabilistic linguistic set and it not only inherits the advantages of the PLS but also overcomes its disadvantages, and it expands the number of possible evaluation values from limited to countless.

For the case mentioned above, the additive linguistic term set can be set as $S = \{s_\alpha | \alpha = 0, 1, 2, 3, 4\}$, the symbol s_0 indicates "terrible"; the symbol s_1 indicates "bad"; the symbol s_2 indicates "moderate"; the symbol s_3 indicates "good"; and the symbol s_4 indicates "perfect." Let us also take the data in Table 7 as an example to illustrate the data structure, and the estimated values cannot be directly converted to the additive linguistic term sets; therefore, first, we should establish the transformation rules, which can be described as follows: the values will be set as s_0 if the inequality $0 \le \tau^{1/\prime} < 0.2$ holds; the values will be set as s_1 if the inequality $0.2 \le \tau^{1/\prime} < 0.4$ holds; the values will be set as s_2 if the inequality $0.4 \le \tau^{1/\prime} < 0.6$ holds; the values will be set as s_3 if the inequality $0.6 \le \tau^{1\prime} < 0.8$ holds; and the values will be set as s_4 if the inequality $0.8 \le \tau^{1/\prime} \le 1$ holds. Table 18 lists the transformed values when the data are recorded in the form of the probabilistic hesitant fuzzy sets.

We find that the values in the A_1^1, A_1^2, A_1^3 are equal to each other and all the evaluation values given by different experts are s_1 and s_2; obviously, the discrimination ability of this method is poorer than the algorithm proposed in the paper.

5.3. The Decision-Making Algorithms without the Cost Limitation. The cost limitation in the decision-making process is one of the characteristics of the algorithm proposed in the paper. Although many other algorithms have considered costs, they only take the cost as one of decision-making indicators and do not list it separately [53]. In some cases, we found that the increase in cost does not improve any effect. For the case discussed in the paper, the most appropriate alternatives will be $A_4 \sim A_4 \sim A_4$ if only the effects are considered, the total cost will be $\eta = \Delta\eta_{01}^4 + \Delta\eta_{12}^4 + \Delta\eta_{23}^4 = 6$. The final result is $A_2 \sim A_2 \sim A_1$, which is obtained by the algorithm proposed in the paper, and the total cost is $\eta' = \Delta\eta_{01}^2 + \Delta\eta_{12}^2 + \Delta\eta_{23}^1 = 3.4$. We can find that the same goal has been achieved, but the cost is saved by 43.3%, which verifies the superiority of the algorithm proposed in the paper from the perspective of the cost.

5.4. The Open-Loop Decision-Making Algorithms. At present, most decision-making algorithms adopt the open-loop mode; in other words, they fail to establish a set of feedback mechanisms [54]. Now we will demonstrate the method without feedback mechanisms to solve the above case and point out the differences between the method and the algorithm proposed in the paper.

The alternative A_2 will still be the most appropriate alternative at the time point T_0. The estimated values cannot be compared with the measured values at the time point T_1; therefore, the accuracy of the system cannot be verified, the automatic adjustment module proposed in the paper cannot be activated, the system cannot be adjusted in time, and the error rate will be higher and higher with the increasing of

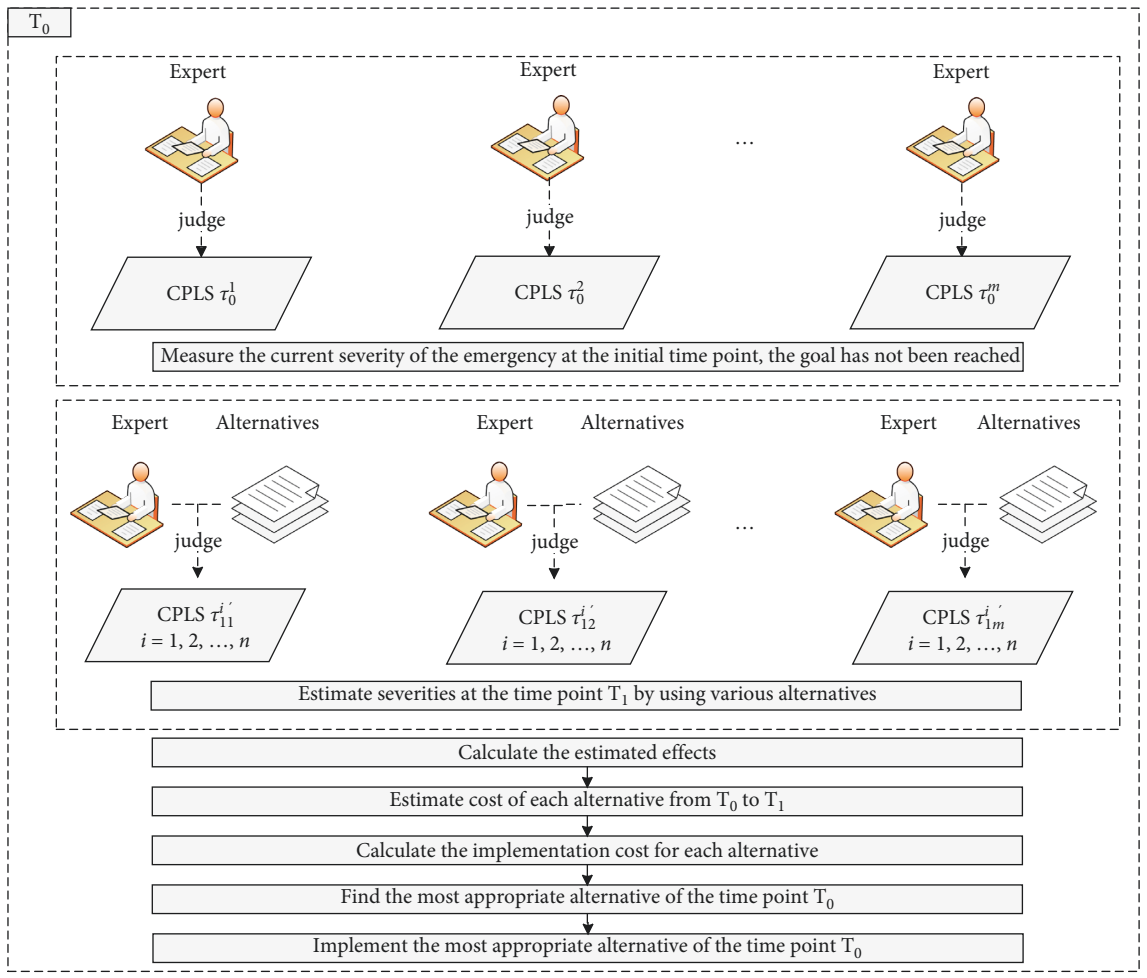

(a)

Figure 3: Continued.

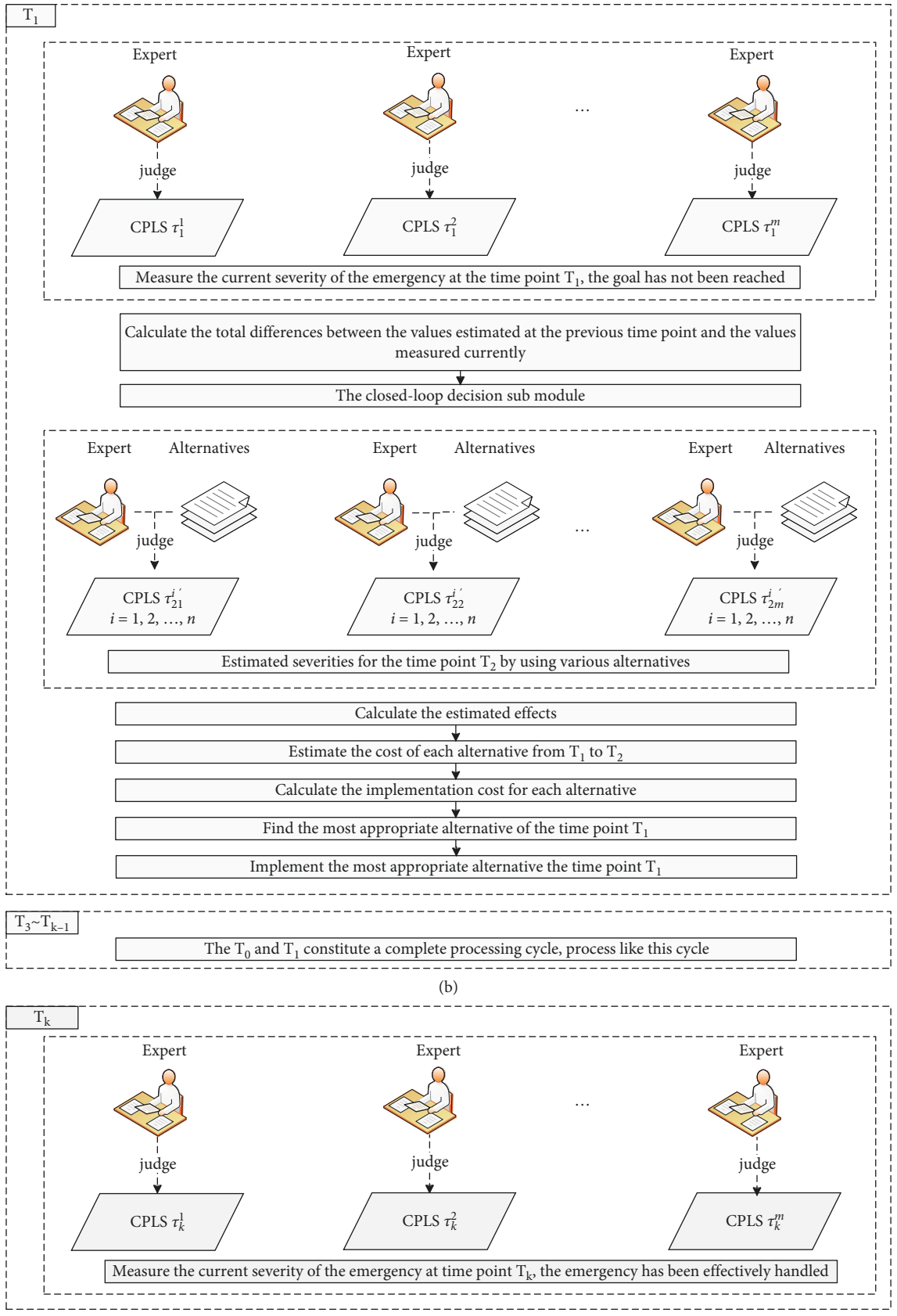

Figure 3: The overall flow chart of the algorithm proposed in the paper.

Table 5: The alternatives proposed by experts at the initial time point.

Alternatives	The specific measures
A_0^1	We isolate all close contacts and provide disinfection equipment for the dormitories and classrooms visited by close contacts
A_0^2	In addition to the A_0^1, we measure the temperature of all the students
A_0^3	In addition to the A_0^2, we suspend the courses held by the college of close contacts
A_0^4	In addition to the A_0^3, we suspend all the courses and cancel all unnecessary activities among students

Table 6: The current severities measured at the initial time point.

Experts	$E_1(\omega_1 = 0.3)$	$E_2(\omega_2 = 0.32)$	$E_3(\omega_3 = 0.38)$
Measured values	(0.1|0.4, 0.2|0.6)	(0.13|0.8, 0.17|0.2)	(0.12|0.3, 0.17|0.2, 0.19|0.5)

Table 7: The estimated severities at the time point T_1 when using different alternatives.

Experts alternatives	$E_1(\omega_1 = 0.3)$	$E_2(\omega_2 = 0.32)$	$E_3(\omega_3 = 0.38)$
A_1^1	(0.24|0.4, 0.26|0.6)	(0.21|0.6, 0.23|0.3, 0.24|0.1)	(0.21|0.6, 0.26|0.4)
A_1^2	(0.28|0.3, 0.30|0.5, 031|0.2)	(0.29|0.5, 0.31|0.5)	(0.29|0.3, 0.32|0.7)
A_1^3	(0.36|0.3, 0.38|0.7)	(0.35|0.6, 0.37|0.3, 0.39|0.1)	(0.33|0.5, 0.36|0.5)
A_1^4	(0.38|0.3, 0.39|0.2, 0.40|0.5)	(0.36|0.3, 0.40|0.7)	(0.38|0.6, 0.410.4|)

Table 8: The current severities measured at the time point T_1.

Experts	$E_1(\omega_1 = 0.3)$	$E_2(\omega_2 = 0.32)$	$E_3(\omega_3 = 0.38)$
Measured values	(0.29|0.3, 0.31|0.7)	(0.26|0.4, 0.3|0.6)	(0.32|1)

Table 9: The differences at the first period.

Experts	$E_1(\omega_1 = 0.3)$	$E_2(\omega_2 = 0.32)$	$E_3(\omega_3 = 0.38)$
Differences	$\begin{pmatrix} -0.0\|10.09, -0.03\|0.21 \\ 0.01\|0.15, -0.01\|0.35 \\ 0.02\|0.06, 0\|0.14 \end{pmatrix}$	$\begin{pmatrix} 0.030.2, -0.01\|\|0.3 \\ 0.05\|0.2, 0.01\|0.3 \end{pmatrix}$	(−0.03|0.3, 0|0.7)

Table 10: The updated estimated severities of the implemented alternative at the time point T_1.

Experts alternatives	$E_1(\omega_1 = 0.3)$	$E_2(\omega_2 = 0.32)$	$E_3(\omega_3 = 0.38)$
A'^2_0	(0.28|0.3, 0.30|0.5, 0.31|0.2)	(0.29|0.5, 0.31|0.5)	$\begin{pmatrix} 0.3216081827\|0.7 \\ 0.29\|0.3 \end{pmatrix}$

Table 11: The updated differences at the first period.

Experts	$E_1(\omega_1 = 0.3)$	$E_2(\omega_2 = 0.32)$	$E_3(\omega_3 = 0.38)$
Differences	$\begin{pmatrix} -0.01\|0.09, -0.03\|0.21 \\ 0.01\|0.15, -0.01\|0.35 \\ 0.02\|0.06, 0\|0.14 \end{pmatrix}$	$\begin{pmatrix} 0.03\|0.2, -0.01\|0.3 \\ 0.05\|0.2, 0.01\|0.3 \end{pmatrix}$	$\begin{pmatrix} 0.0016081827\|0.7 \\ -0.03\|0.3 \end{pmatrix}$

time. One of the noticed differences will occur at the time point T_2, the A_2 instead of the A_1 will be the most appropriate alternative if the feedback mechanism fails work, and the conclusion that only the alternative with lower cost is needed and the estimated values must be improved in the next estimation cannot be drawn, and this will directly lead to the increase of costs and processing cycles.

In short, the feedback mechanism is effective for timely verifying the correctness of the system, and it can save the

Table 12: The estimated severities at the time point T_2 when using different alternatives.

Experts alternatives	$E_1(\omega_1 = 0.3)$	$E_2(\omega_2 = 0.32)$	$E_3(\omega_3 = 0.38)$
A_2^1	(0.42|1)	(0.41|0.6, 0.44|0.4)	(0.39|0.3, 0.43|0.7)
A_2^2	(0.46|0.2, 0.5|0.8)	(0.47|0.5, 0.52|0.5)	(0.49|0.7, 0.51|0.3)
A_2^3	(0.55|0.8, 0.57|0.2)	(0.52|0.4, 0.56|0.6)	(0.54|1)
A_2^4	(0.58|0.4, 0.62|0.6)	(0.6|1)	(0.58|0.7|0.61|0.3)

Table 13: The current severities measured at the time point T_2.

Experts	$E_1(\omega_1 = 0.3)$	$E_2(\omega_2 = 0.32)$	$E_3(\omega_3 = 0.38)$
Measured values	(0.63|0.5, 0.65|0.3, 0.67|0.2)	(0.67|0.3, 0.68|0.7)	(0.66|1)

Table 14: The differences at the second period.

Experts	$E_1(\omega_1 = 0.3)$	$E_2(\omega_2 = 0.32)$	$E_3(\omega_3 = 0.38)$
Differences	$\begin{pmatrix} -0.17\|0.10, -0.19\|0.06 \\ -0.21\|0.04, -0.13\|0.40 \\ -0.15\|0.24, -0.17\|0.16 \end{pmatrix}$	$\begin{pmatrix} -0.20\|0.15, -0.21\|0.35 \\ -0.15\|0.15, -0.16\|0.35 \end{pmatrix}$	(−0.17|0.7, −0.15|0.3)

Table 15: The estimated severities at the time point T_3 when using different alternatives.

Experts alternatives	$E_1(\omega_1 = 0.3)$	$E_2(\omega_2 = 0.32)$	$E_3(\omega_3 = 0.38)$
A_3^1	(0.88|0.2, 0.92|0.2)	(0.91|0.6, 0.93|0.4)	(0.82|1)
A_3^2	(0.94|0.4, 0.96|0.6)	(0.95|1)	(0.93|0.7, 0.96|0.3)
A_3^3	(0.97|0.5, 0.98|0.5)	(0.95|0.4, 0.97|0.6)	(0.96|1)
A_3^4	(0.97|1)	(0.98|0.4, 0.99|0.6)	(0.94|0.7|0.96|0.3)

Table 16: The current severities measured at the time point T_3.

Experts	$E_1(\omega_1 = 0.3)$	$E_2(\omega_2 = 0.32)$	$E_3(\omega_3 = 0.38)$
Measured values	(0.95|0.4, 0.98|0.6)	(0.97|1)	(0.96|0.8, 0.98|0.2)

Table 17: The conversion values in the form of hesitant fuzzy sets.

Experts alternatives	$E_1(\omega_1 = 0.3)$	$E_2(\omega_2 = 0.32)$	$E_3(\omega_3 = 0.38)$
A_1^1	(0.24, 0.26)	(0.21, 0.23, 0.24)	(0.21, 0.26)
A_1^2	(0.28, 0.30, 0.31)	(0.29, 0.31)	(0.29, 0.32)
A_1^3	(0.36, 0.38)	(0.35, 0.37, 0.39)	(0.33, 0.36)
A_1^4	(0.38, 0.39, 0.40)	(0.36, 0.40)	(0.38, 0.41)

Table 18: The transformed values in the form of the probabilistic hesitant fuzzy sets.

Experts alternatives	$E_1(\omega_1 = 0.3)$	$E_2(\omega_2 = 0.32)$	$E_3(\omega_3 = 0.38)$
A_1^1	$(s_1(1))$	$(s_1(1))$	$(s_1(1))$
A_1^2	$(s_1(1))$	$(s_1(1))$	$(s_1(1))$
A_1^3	$(s_1(1))$	$(s_1(1))$	$(s_1(1))$
A_1^4	$(s_1(0.5), s_2(0.5))$	$(s_1(0.3), s_2(0.7))$	$(s_1(0.6), s_2(0.3))$

total cost and reduce time effectively [55], which verifies the superiority of the algorithm proposed in the paper from the perspective of the accuracy.

6. Conclusions

When faced with emergencies, especially disasters, it is crucial to make timely and appropriate decisions; however, it is not easy to achieve this goal because of the limited time for making decisions and the fuzzy information that can be acquired.

The accuracy of data can directly affect the quality of the final decision, while we find that it is hard to record data accurately and scientifically. How to improve the accuracy of the collected data is the first problem to be solved. The data structure, the continuously probabilistic linguistic set, is adopted to save original data after comparisons. This data structure allows multiple possible values can be stored together in a record; meanwhile, the probability information of each possible value can also be stored together, and these characteristics can overcome the uncertainty and fuzziness

in the process of data acquisition, which can improve the data quality to the greatest extent and lay a solid foundation for the later decision-making.

At present, most decision-making models adopt the linear structure and single-round mode, although these models have been elaborately designed, an important defect cannot be ignored; that is, it is impossible to verify the accuracy of the estimated results given by the system in time. In order to solve this problem, a new structure is proposed in the paper. The whole decision-making process is divided into multiple sub-decision-making stages, and each estimated result can be verified at the next decision-making time point. The estimated values and the current measured values are two different types of signals used in the system, the differences of the values estimated at the previous time point, and the values measured currently will be calculated by the fuzzy subtraction proposed in the paper. In general, there are certain differences between them, and the greater the difference, the lower the accuracy of the system. Due to time constraints, it is almost impossible for experts to reevaluate alternatives; fortunately, the paper proposes an automatic repair algorithm, which can solve this problem. The repair algorithm contains several submodules according to different situations, when the inequality $S(d) \leq |\varepsilon|$ holds, which indicates that the system works well and does not need any adjustment; when the inequalities $\lambda_1 \leq S(d) < -\varepsilon$ or $\varepsilon < S(d) \leq \lambda_2$ hold, which indicates that the system needs minor adjustments and the automatic adjustment algorithm will be activated immediately; when the inequality $\lambda_2 < S(d) \leq 1$ holds, which indicates that the system is too optimistic and the actual situation is more serious than estimated; and when the inequality $-1 \leq S(d) < \lambda_1$ holds, which indicates that the system is too prudent and the actual effect is much better than estimated. The closed-loop decision-making system can be constructed through the establishment of the feedback mechanisms, and the accuracy of the whole model will be improved effectively.

The cost is one of the most important factors in the decision-making process, and we must point out again that the cost mentioned in the paper refers to the generalized cost, not just the economic cost. The effectiveness of each alternative will be evaluated separately in each round of decision-making. Generally, the rigorous alternative can achieve better results, while it may also cause a lot of losses; thus, it is not necessarily the most appropriate alternative. Based on these considerations, the paper proposes the definition and calculation method of the effect per cost, when the predetermined goal can be achieved, we believe that the most appropriate alternative must be the one that has the lowest cost. The establishment of the above theory is also one of the innovations of this paper.

We have to point out some limitations of the paper. As one of the initial conditions, the estimated cost is essentially a fuzzy value, which is difficult to be accurately described by a simple value. Thus, the problem discussed in the paper is actually a double fuzzy problem and more fuzzy variables need to be considered. Further researches will be conducted by our team for this problem in the near future.

Data Availability

The data used to support the findings of this study are included within the article, and they are obtained through practical investigations.

Conflicts of Interest

The authors declare that there are no conflicts of interest.

Authors' Contributions

M.F. conceptualized the data; L.F.W. supervised the study; X.N.C. involved in project administration; B.Y.Z. validated the study; X.X.Z. investigated the study; and S.S.Y. wrote original draft preparation. All authors have read and agreed to the published version of the manuscript.

Acknowledgments

This research was funded by the Excellent Young Talents Fund Program of Higher Education Institutions of Anhui Province (no. gxyqZD2021110), the scientific research program of Anhui University of Finance and Economics (nos. ACKYB21014 and ACKYC19024), the humanities and social sciences research project of the Anhui Provincial Department of Education (no. SK2021A0250), and "the six outstanding and one top-notch" outstanding talent training innovation project of Anhui University of Finance and Economics, Anhui Province (nos. aclzy2020010 and 2020zyrc005).

References

[1] A. J. Simon, J. N. Schachtner, and C. L. Gallen, "Disentangling expectation from selective attention during perceptual decision making," *Journal of Neurophysiology*, vol. 121, no. 6, pp. 1977–1980, 2019.

[2] D. Mikesell and C. Griffin, "Optimal decision-making in an opportunistic sensing problem," *IEEE Transactions on Cybernetics*, vol. 46, no. 12, pp. 3285–3293, 2016.

[3] M. Ebers and I. Maurer, "To continue or not to continue? Drivers of recurrent partnering in temporary organizations," *Organization Studies*, vol. 37, no. 12, pp. 1861–1895, 2016.

[4] L. A. Zadeh, "Fuzzy sets," *Information and Control*, vol. 8, no. 3, pp. 338–353, 1965.

[5] I. B. Turksen, "Interval valued fuzzy sets based on normal forms," *Fuzzy Sets and Systems*, vol. 20, no. 2, pp. 191–210, 1986.

[6] Y. G. Shang, X. H. Yuan, and E. S. Lee, "The n-dimensional fuzzy sets and Zadeh fuzzy sets based on the finite valued fuzzy sets," *Computers & Mathematics with Applications*, vol. 60, pp. 442–463, 2010.

[7] K. T. Atanassov, "Intuitionistic fuzzy sets," *Fuzzy Sets and Systems*, vol. 20, no. 1, pp. 87–96, 1986.

[8] J. Ye, "Multicriteria fuzzy decision-making method using entropy weights-based correlation coefficients of interval-valued intuitionistic fuzzy sets," *Applied Mathematical Modelling*, vol. 34, no. 12, pp. 3864–3870, 2010.

[9] R. M. Rodriguez, L. Martinez, and F. Herrera, "Hesitant fuzzy linguistic term sets for decision making," *IEEE Transactions on Fuzzy Systems*, vol. 20, no. 1, pp. 109–119, 2012, [CrossRef].

[10] Z. S. Xu and W. Zhou, "Consensus building with a group of decision makers under the hesitant probabilistic fuzzy environment," *Fuzzy Optimization and Decision Making*, vol. 16, no. 4, pp. 481–503, 2017.

[11] M. M. Xia and Z. S. Xu, "Hesitant fuzzy information aggregation in decision making," *International Journal of Approximate Reasoning*, vol. 52, no. 3, pp. 395–407, 2011.

[12] H. C. Liao and Z. S. Xu, "Satisfaction degree based interactive decision making under hesitant fuzzy environment with incomplete weights," *International Journal of Uncertainty, Fuzziness and Knowledge-Based Systems*, vol. 22, no. 04, pp. 553–572, 2014.

[13] V. Torra, "Hesitant fuzzy sets," *International Journal of Intelligent Systems*, vol. 25, pp. 529–539, 2010.

[14] Z. S. Xu and M. M. Xia, "Distance and similarity measures for hesitant fuzzy sets," *Information Sciences*, vol. 181, no. 11, pp. 2128–2138, 2011.

[15] H. C. Liao and Z. S. Xu, "Subtraction and division operations over hesitant fuzzy sets," *Journal of Intelligent and Fuzzy Systems*, vol. 27, no. 1, pp. 65–72, 2014.

[16] H. C. Liao, Z. S. Xu, and M. M. Xia, "Multiplicative consistency of hesitant fuzzy preference relation and its application in group decision making," *International Journal of Information Technology and Decision Making*, vol. 13, no. 01, pp. 47–76, 2014.

[17] H. C. Liao and Z. S. Xu, "Some new hybrid weighted aggregation operators under hesitant fuzzy multi-criteria decision making environment," *Journal of Intelligent and Fuzzy Systems*, vol. 26, no. 4, pp. 1601–1617, 2014.

[18] B. Zhu and Z. S. Xu, "Hesitant fuzzy Bonferroni means for multi-criteria decision making," *Journal of the Operational Research Society*, vol. 64, no. 12, pp. 1831–1840, 2013.

[19] S. Zhang, Z. S. Xu, and Y. He, "Operations and integrations of probabilistic hesitant fuzzy information in decision making," *Information Fusion*, vol. 38, pp. 1–11, 2017.

[20] Z. N. Hao, Z. S. Xu, H. Zhao, and Z. Su, "Probabilistic dual hesitant fuzzy set and its application in risk evaluation," *Knowledge-Based Systems*, vol. 127, pp. 16–28, 2017.

[21] H. Garg and G. Kaur, "Algorithm for probabilistic dual hesitant fuzzy multi-criteria decision-making based on aggregation operators with new distance measures," *Mathematics*, vol. 6, no. 12, pp. 1–30, 2018.

[22] J. Ye, "Fuzzy decision-making method based on the weighted correlation coefficient under intuitionistic fuzzy environment," *European Journal of Operational Research*, vol. 205, no. 1, pp. 202–204, 2010, [CrossRef].

[23] J. Li and Z. X. Wang, "Multi-Attribute decision making based on prioritized operators under probabilistic hesitant fuzzy environments," *Soft Computing*, vol. 23, no. 11, pp. 3853–3868, 2019, [CrossRef].

[24] F. J. Jiang and Q. G. Ma, "Multi-Attribute group decision making under probabilistic hesitant fuzzy environment with application to evaluate the transformation efficiency," *Applied Intelligence*, vol. 48, no. 4, pp. 953–965, 2018, [CrossRef].

[25] X. F. Zhao, R. Lin, and G. W. Wei, "Hesitant triangular fuzzy information aggregation based on Einstein operations and their application to multiple attribute decision making," *Expert Systems with Applications*, vol. 41, no. 4, pp. 1086–1094, 2014, [CrossRef].

[26] S. T. Shao, X. H. Zhang, and Q. Zhao, "Multi-Attribute decision making based on probabilistic neutrosophic hesitant fuzzy choquet aggregation operators," *Symmetry*, vol. 11, no. 5, pp. 1–15, 2019, [CrossRef].

[27] C. Q. Li, H. Zhao, and Z. S. Xu, "Hesitant fuzzy psychological distance measure," *International Journal of Machine Learning and Cybernetics*, vol. 11, no. 9, pp. 2089–2100, 2020, [CrossRef].

[28] W. Zhou and Z. S. Xu, "Expected hesitant var for tail decision making under probabilistic hesitant fuzzy environment," *Applied Soft Computing*, vol. 60, pp. 297–311, 2017, [CrossRef].

[29] X. L. Tian, Z. S. Xu, and H. Fujita, "Sequential funding the venture project or not? A prospect consensus process with probabilistic hesitant fuzzy preference information," *Knowledge-Based Systems*, vol. 161, pp. 172–184, 2018, [CrossRef].

[30] J. Wu, X. D. Liu, Z. W. Wang, and S. T. Zhang, "Dynamic emergency decision-making method with probabilistic hesitant fuzzy information based on GM(1, 1) and TOPSIS," *IEEE Access*, vol. 7, pp. 7054–7066, 2019, [CrossRef].

[31] H. Y. Guo, W. Pedrycz, and X. D. Liu, "Fuzzy time series forecasting based on axiomatic fuzzy set theory," *Neural Computing & Applications*, vol. 31, no. 8, pp. 3921–3932, 2019, [CrossRef].

[32] B. Farhadinia, "A series of score functions for hesitant fuzzy sets," *Information Sciences*, vol. 277, pp. 102–110, 2014, [CrossRef].

[33] M. Fu, L. F. Wang, J. M. Zhu, and B. Y. Zheng, "Emergency optimization decision-making with incomplete probabilistic information under the background of COVID-19," *Complexity*, vol. 2021, pp. 1–16, [CrossRef].

[34] F. Ming, L. F. Wang, and J. Zhou, "The identification of poverty alleviation targets based on the multiple hybrid decision-making algorithms," *IEEE Access*, vol. 8, pp. 169585–169593, 2020, [CrossRef].

[35] M. Fu, L. F. Wang, B. Y. Zheng, and H. Y. Shao, "The optimal emergency decision-making method with incomplete probabilistic information," *Scientific Reports*, vol. 11, pp. 23400–23414, 2021, [CrossRef].

[36] X. J. Gou and Z. S. Xu, "Managing noncooperative behaviors in large-scale group decision-making with linguistic preference orderings: the application in Internet venture capital," *Information Fusion*, vol. 69, pp. 142–155, 2021, [CrossRef].

[37] M. W. Lin, X. M. Li, R. Q. Chen, H. Fujita, and J. Lin, "Picture fuzzy interactional partitioned Heronian mean aggregation operators: an application to MADM process," *Artificial Intelligence Review*, vol. 55, no. 2, pp. 1171–1208, 2021, [CrossRef].

[38] F. Y. Meng and S. M. Chen, "A framework for group decision making with multiplicative trapezoidal fuzzy preference relations," *Information Sciences*, vol. 577, pp. 722–747, 2021, [CrossRef].

[39] D. H. Peng, B. Peng, and T. D. Wang, "Reconfiguring IVHF-TOPSIS decision making method with parameterized reference solutions and a novel distance for corporate carbon performance evaluation," *Journal of Ambient Intelligence and Humanized Computing*, vol. 11, no. 9, pp. 3811–3832, 2020, [CrossRef].

[40] J. P. Liu, M. D. Fang, F. F. Jin, Z. F. Tao, H. Y. Chen, and P. C. Du, "Pythagorean fuzzy linguistic decision support model based on consistency-adjustment strategy and consensus reaching process," *Soft Computing*, vol. 25, no. 13, pp. 8205–8221, 2021, [CrossRef].

[41] L. G. Zhou, H. Fujita, H. Ding, and R. Ma, "Credit risk modeling on data with two timestamps in peer-to-peer lending by gradient boosting," *Applied Soft Computing*, p. 110, 2021 [CrossRef].

[42] S. Z. Zeng, S. M. Chen, and K. Y. Fan, "Interval-valued intuitionistic fuzzy multiple attribute decision making based on nonlinear programming methodology and TOPSIS method," *Information Sciences*, vol. 506, pp. 424–442, 2020, [CrossRef].

[43] Y. M. Song, G. X. Li, T. Li, and Y. H. Li, "A purchase decision support model considering consumer personalization about aspirations and risk attitudes," *Journal of Retailing and Consumer Services*, vol. 63, p. 102728, 2021 [CrossRef].

[44] J. D. Qin, M. X. Li, and Y. Y. Liang, "Minimum cost consensus model for CRP-driven preference optimization analysis in large-scale group decision making using Louvain algorithm," *Information Fusion*, vol. 80, pp. 121–136, 2022, [CrossRef].

[45] Q. Z. He, P. F. Xia, B. Li, and J. B. Liu, "Evaluating investors' recognition abilities for risk and profit in online loan markets using nonlinear models and financial big data," *J. Funct. Space.*, [CrossRef], 2021.

[46] Z. P. Fan, G. M. Li, and Y. Liu, "Processes and methods of information fusion for ranking products based on online reviews: an overview," *Information Fusion*, vol. 60, pp. 87–97, 2020, [CrossRef].

[47] Y. F. Ye and D. F. Li, "A direct approach to compute triangular fuzzy banzhaf values of cooperative games with coalitions' values represented by triangular fuzzy numbers," *IEEE Transactions on Fuzzy Systems*, vol. 29, no. 6, pp. 1567–1575, 2021, [CrossRef].

[48] J. M. Zhan, K. Zhang, and W. Z. Wu, "An investigation on Wu-Leung multi-scale information systems and multi-expert group decision-making," *Expert Systems with Applications*, p. 170, 2021 [CrossRef].

[49] H. Wang, D. J. Yu, and Z. S. Xu, "A novel process to determine consensus thresholds and its application in probabilistic linguistic group decision-making," *Expert Systems with Applications*, p. 168, 2021 [CrossRef].

[50] D. C. Liang, M. W. Wang, Z. S. Xu, and D. Liu, "Risk appetite dual hesitant fuzzy three-way decisions with TODIM," *Information Sciences*, vol. 507, pp. 585–605, 2020, [CrossRef].

[51] Z. W. Gong, W. W. Guo, and R. Slowinski, "Transaction and interaction behavior-based consensus model and its application to optimal carbon emission reduction," *Omega*, p. 102491, 2021 [CrossRef].

[52] S. P. Wan, W. C. Zou, J. Y. Dong, and L. Martinez, "A consensual method for multi-criteria group decision-making with linguistic intuitionistic information," *Information Sciences*, vol. 582, pp. 797–832, 2022, [CrossRef].

[53] Z. B. Wu and J. C. Tu, "Managing transitivity and consistency of preferences in AHP group decision making based on minimum modifications," *Information Fusion*, vol. 67, pp. 125–135, 2021, [CrossRef].

[54] W. Li and J. Ye, "Group decision-making problems based on mixed aggregation operations of interval-valued fuzzy and entropy elements in single- and interval-valued fuzzy environments," *Mathematics*, vol. 10, no. 7, p. 1077, 2022 [CrossRef].

[55] W. Yang and Y. Pang, "T-spherical fuzzy Bonferroni mean operators and their application in multiple attribute decision making," *Mathematics*, vol. 10, no. 6, p. 988, 2022 [CrossRef].

Hindawi
Computational Intelligence and Neuroscience
Volume 2023, Article ID 9790234, 1 page
https://doi.org/10.1155/2023/9790234

Retraction

Retracted: A Lightweight Semantic Segmentation Algorithm Based on Deep Convolutional Neural Networks

Computational Intelligence and Neuroscience

Received 10 October 2023; Accepted 10 October 2023; Published 11 October 2023

This article has been retracted by Hindawi following an investigation undertaken by the publisher [1]. This investigation has uncovered evidence of one or more of the following indicators of systematic manipulation of the publication process:

(1) Discrepancies in scope
(2) Discrepancies in the description of the research reported
(3) Discrepancies between the availability of data and the research described
(4) Inappropriate citations
(5) Incoherent, meaningless and/or irrelevant content included in the article
(6) Peer-review manipulation

The presence of these indicators undermines our confidence in the integrity of the article's content and we cannot, therefore, vouch for its reliability. Please note that this notice is intended solely to alert readers that the content of this article is unreliable. We have not investigated whether authors were aware of or involved in the systematic manipulation of the publication process.

Wiley and Hindawi regrets that the usual quality checks did not identify these issues before publication and have since put additional measures in place to safeguard research integrity.

We wish to credit our own Research Integrity and Research Publishing teams and anonymous and named external researchers and research integrity experts for contributing to this investigation.

The corresponding author, as the representative of all authors, has been given the opportunity to register their agreement or disagreement to this retraction. We have kept a record of any response received.

References

[1] C. Yang and H. Guo, "A Lightweight Semantic Segmentation Algorithm Based on Deep Convolutional Neural Networks," *Computational Intelligence and Neuroscience*, vol. 2022, Article ID 5339664, 9 pages, 2022.

Hindawi
Computational Intelligence and Neuroscience
Volume 2022, Article ID 5339664, 9 pages
https://doi.org/10.1155/2022/5339664

Research Article

A Lightweight Semantic Segmentation Algorithm Based on Deep Convolutional Neural Networks

Chengzhi Yang and Hongjun Guo

Laboratory of Intelligent Information Processing, Suzhou University, Suzhou 234000, Anhui, China

Correspondence should be addressed to Chengzhi Yang; szxyycz@ahszu.edu.cn

Received 27 July 2022; Accepted 20 August 2022; Published 6 September 2022

Academic Editor: Zaoli Yang

With the development of deep learning theory and the decrease of the cost of acquiring massive data, the image semantic segmentation algorithm based on Convolutional Neural Networks (CNNs) is gradually replacing the conventional segmentation algorithm by its high accuracy segmentation performance. By increasing the amount of training data and stacking more convolutional layers to form Deep Convolutional Neural Networks (DCNNs), a neural network model with higher segmentation accuracy can be obtained, but it faces the problems of serious memory consumption and long latency. For some special application scenarios, such as augmented reality and mobile interaction, real-time processing cannot be performed. To improve the speed of semantic segmentation while obtaining the most accurate segmentation results as possible, this paper proposes a semantic segmentation algorithm based on lightweight convolutional neural networks. Taking the computational complexity and segmentation accuracy into account, the algorithm starts from the perspective of extracting high-level semantic features and introduces a position-attention mechanism with richer contextual information to model the relationship between different pixels, avoiding the convolutional local perceptual field to be too small. To recover clearer target boundaries, a channel attention mechanism is introduced in the decoding part of the model to mine more useful feature channel information and effectively improve the fusion of low-level features with high-level features. By verifying the effectiveness of the above model on a publicly available dataset and comparing it with the more popular semantic segmentation methods, the model proposed in this paper has higher semantic segmentation accuracy and reflects certain advantages in objective evaluation.

1. Introduction

There are diverse targets in images, differences in sizes, and lighting conditions of the same object, and similar features among different objects, which increase the difficulty of semantic segmentation and are prone to confusion of organisms, so a broader range of feature information is needed to complete segmentation [1]. Convolutional neural networks have strong local perceptual abilities but are poor in acquiring global features. At the same time, the resolution of the feature map gradually decreases with the increasing number of network layers, and the extracted features change from figurative features such as texture and color to increasingly abstract feature information, so detail information is missing. The loss of detail information leads to coarser segmentation result, and there are also problems such as incomplete object contours [2].

In computer vision systems, image semantic segmentation is a difficult task. Among the deep learning methods, the techniques to implement the image semantic segmentation task are divided into two categories: one is the image semantic segmentation method based on region classification; the other is the image semantic segmentation method based on pixel classification. The region classification-based image semantic segmentation method is a method based on conventional methods combined with deep neural network structures. This method is to segment the input image into target candidate blocks according to certain rules, and then use deep neural networks to semantically classify the candidate blocks and label the classification to the original

image [3]. Since the semantic segmentation methods based on region classification have problems such as blurred segmentation boundaries and slow running speed, thus prompting researchers to invest a lot of effort in pixel-level-based image semantic segmentation methods. The current pixel-level-based methods are divided into two modes: a fully supervised mode; and a semisupervised mode. The semantic segmentation method in fully supervised mode means that manually labeled tags are required as the input samples, and the label data of each pixel in the image is first read after input, and then the label data are used to train the deep neural networks, and the trained neural networks are used for semantic segmentation [4]. The main methods for semantic segmentation of images in fully supervised mode are currently based on fully convolutional neural networks, methods based on optimized convolutional structures, methods based on codecs, methods based on probabilistic graphical models, methods based on feature fusion, methods based on convolutional neural networks, and methods based on adversarial generative networks. Due to the increasing width and depth of network layers, convolutional neural networks are getting deeper and deeper; however, deep convolutional neural networks require a lot of manual intervention, and it is very time-consuming to collect labeled data sets manually, so semantic segmentation of images in semisupervised or weakly supervised mode has become popular at present [5]. The current mainstream semisupervised or weakly supervised image semantic segmentation methods are classified into image-level labeling, multilevel labeling, and bounding box labeling methods. DeepLab network is a novel deep neural semantic segmentation network proposed after the fully convolutional semantic segmentation network, which has good advantages over the previously proposed semantic segmentation networks; recently the concept of attention mechanism has been proposed in academia, aiming to use the attention mechanism to simulate human vision and thus to provide an intuitive interpretation of the network model [6]. In problems involving language or vision, some parts of the input will be more helpful for decision-making than others. The DeepLab v2 network introduces three new ideas in the model based on the shortcomings and deficiencies of the FCN network: Atrous Convolution (also known as Dilated Convolution), Atrous Spatial Pyramid Pooling, and Full-connected Conditional Random Field (CRF) [7].

This paper focuses on proposing a new parallel multi-branching module for capturing contextual information to solve the problem of comparative dependence on square convolution and pooling operations, which lack the ability to perceive anisotropic contextual information. In order to better mine the channel information of the network output feature map, a channel attention module is introduced in the decoder of the network to ensure good performance and low computational complexity of the network.

2. Related Works

The success of AlexNet, VGG, GoogleNet, and ResNet's convolutional neural network for image classification and target detection has inspired researchers to explore the field of semantic segmentation with deep learning methods [8]. The key advantages of deep learning make it superior to conventional semantic segmentation methods. The pixel points of the images in the dataset are labeled one by one, and the results of semantic segmentation are obtained by end-to-end supervised training with CNNs, without the complicated processes of image processing, manual feature design, and feature extraction, so the successful semantic segmentation methods in recent years have been studied based on deep learning [9]. In recent years, the more successful semantic segmentation techniques are fully convolutional networks. This technique uses VGG as the network infrastructure and creatively replaces the fully connected layer at the end of the network with a fully convolutional layer, making the network directly output a segmentation result map with the same resolution as the original map. However, the segmentation map obtained by FCN is relatively coarse, so SegNet fills in the value of the maximum value and position of each pooling area before pooling by recording it and sets the value at that position and zero at other positions during up-sampling, but the obtained results are still not fine enough [10]. As the network structure deepens, the results of feature information extraction become more and more abstract, but at the same time, the obtained feature map resolution becomes smaller and smaller, and lacks a lot of spatial information. Most methods use direct recovery of the feature map to the resolution of the original map by bilinear interpolation, but the obtained results are mostly coarse. The convolutional operation of convolutional neural network extracts primary features such as texture and color in the shallow network and gets more abstract feature representation in the deep network, while the extracted information is based on local information features. The global information is necessary for segmentation, and the class to which the pixel belongs can be predicted more accurately by combining with the current environment [11, 12].

Compared with traditional image segmentation methods, the semantic segmentation algorithm based on CNN has great advantages in segmentation accuracy and visual performance. However, in some outdoor scenes, in the face of mutual occlusion of different objects, multi-scale changes of the same target and weather changes, the task of image semantic segmentation still faces great challenges. Zhao et al. [13] developed an image semantic segmentation algorithm that combined fully convolutional network (FCN) with Simple Linear Iterative Clustering (SLIC). They also mixed the FCN semantic segmentation results with the superpixel information and introduced the superpixel semantic annotation. Zhang et al. [14] presented a novel semantic segmentation algorithm with DeepLab v3+ and superpixel segmentation algorithm-quick shift, which can further refine the semantic segmentation results. Meng and Choi [15] designed a semantic segmentation algorithm for point clouds based on the PointNet architecture. Their approach also applied the PointSIFT module, which can encode polydirectional information and adapt to the proportions

of the shape being considered. Qiang et al. [16] proposed an object detection algorithm by jointing semantic segmentation (SSOD) for images. They constructed a feature extraction network that mixed the hourglass structure network with an attention mechanism layer to extract multiscale features and allowed the algorithm for multitask learning. Liu et al. [17] proposed an image semantic segmentation algorithm based on a deep neural network. Based on the Mask Scoring R-CNN, this algorithm used a symmetrical feature pyramid network and added a multiple-threshold architecture to improve the sample screening precision. Jiang and Li [18] proposed an improved semantic segmentation method for remote sensing images based on neural network. Based on residual network, it changed the dilated convolution kernels before extracting the correlations between geophysical objects, thus improving the segmentation accuracy and used a pixel-level method to achieve semantic segmentation. Girisha et al. [19] proposed an enhanced encoder–decoder based CNN architecture (UVid-Net) for unmanned aerial vehicle (UAV) video semantic segmentation. This advanced algorithm greatly enhanced the accuracy of the localization. Gharghabi et al. [20] presented a multidimensional algorithm, which was domain agnostic, had only one, easily determined parameter, and could handle data streaming at a high rate. Jiang et al. [21] designed Random-Walk-SegNet (RWSNet), a semantic segmentation network based on SegNet combined with random walk. It took SegNet as the basic architecture and adopted the sliding window strategy, realizing high-performance semantic segmentation of remote-sensing images. Yi et al. [22] trained the semantic segmentation neural network in different scenarios to obtain the models with the same number of scene categories, and experiments showed that the results of scene-aware semantic segmentation were much better than semantic segmentation without considering categories. Yang and Yu [23] introduced the progression of object detection and semantic segmentation in medical imaging study. They also discussed how to accurately define the location and boundary of diseases. Tan et al. [24] proposed a novel framework called joint 3D semantic-instance segmentation via multiscale semantic association and salient point clustering optimization, and designed a Multi-scale Semantic Association (MSA) module to explore the constructive effect of the context information for semantic segmentation. Jiang et al. [25] proposed a contouraware network for semantic segmentation via adaptive depth. They also constructed an adaptive deep model that could adaptively determine feedback from neural network and forward processes. Su and Wang [26] proposed a novel and practical convolutional neural network for effective semantic segmentation. It was comprised of three modules, namely broadening the residual convolutional neural network module, refining the residual feature pyramid module, and rolling the guidance edge retention layer module. Wu et al. [27] proposed a special semantic segmentation network by simulating the ventral and dorsal pathways of the brain visual cortex, which greatly enhanced the extraction of semantic information, and effectively improved the problem of spatial information loss during segmentation. Some classical image segmentation methods, such as FCN, SegNet, in order to pursue high segmentation accuracy, lead to complex models and high requirements for computing resources, which are not conducive to the use of semantic segmentation algorithms on resource constrained embedded devices. Because of its simplified model structure, lightweight semantic segmentation algorithm has the advantages of small amount of computation and fast segmentation speed, and can run in devices with limited computing resources. Therefore, the lightweight semantic segmentation method not only has practical application prospects but also promotes the improvement of segmentation algorithm.

3. Improvement of Image Semantic Segmentation Algorithm for DeepLabV3+

3.1. DeepLabV3+ Algorithm. The DeepLab algorithm is a model that focuses on semantic segmentation and introduces multiscale features, designs convolution and pooling operations with different parameters to obtain feature maps of different sizes, and efficiently fuses the obtained feature maps in the network model to improve the training performance of the whole network model. DeepLabV3+ algorithm is one of the more popular network model structures for the field of image semantic segmentation. The general construction of the DeepLabV3+ algorithm is shown in Figure 1 [28].

DeepLabV3+ is based on the structure of DeepLabV3, with a simple and efficient decoding module to refine the feature information and improve the segmentation effect. In the encoder part, the improved Xception model is used as the backbone network to extract different feature information in the image through the depth-separable convolution operation of different channels in the Xception model, and then the $1 * 1$ convolution and 3 parallel $3 * 3$ null convolutions with void rates of 6, 12 and 18, respectively, in the spatial pyramid pooling module and the global average pooling operation are used. After processing, and channel compression by $1 * 1$ convolution, the high-level semantic information is obtained. In the decoder part, the feature maps extracted from the input layer of the backbone network are first downscaled using $1 * 1$ convolution, after which they are fused with the high-level features obtained after encoder up-sampling, and then the spatial information in the feature maps is recovered using several $3 * 3$ convolutions and the target boundaries are refined using bilinear up-sampling to obtain the final segmentation result maps.

In the implementation of the DeepLabV3+ algorithm, the depth-separable convolution layer is proposed to replace the original maximum pooling layer, and the depth-separable convolution replaces the empty convolution operation in the Xception network model and decoder module, respectively, which can effectively by combining the ideas of depthwise conv and pointwise conv instead of null convolution, the computational complexity of the model in the

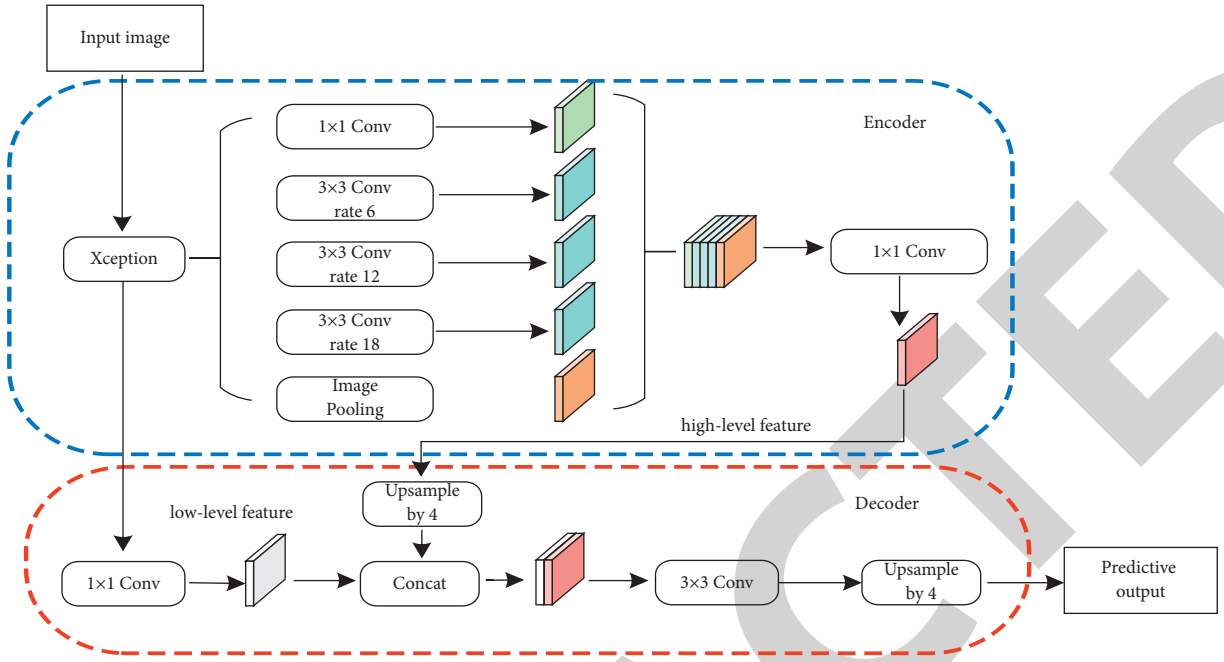

Figure 1: DeepLabV3+ algorithm structure diagram.

training process can be effectively reduced to achieve a faster and stronger coder–decoder network.

3.2. Improvement of DeepLabV3+ Image Semantic Segmentation Algorithm. In order to improve the quality of feature map and solve the problems ignored in Deeplabv3+ algorithm, such as the different importance of features displayed in different feature maps, the loss of a large amount of detail information, and the impact on the final segmentation effect, this paper proposes an image semantic segmentation method based on improved Deeplabv3+. According to different levels of feature map and different attention mechanism modules, the image semantic segmentation algorithm adopts encoding–decoding structure, the backbone network still adopts Xception model. The attention mechanism module is divided into channel attention (CA) module and spatial attention (SA) module. Channel attention is added to the encoder and spatial attention is added to the decoder.

The input image is first extracted by the depth-separable convolutional layer of different channels in the Xception model; second, the feature map obtained from the output layer is processed in parallel by the atrous spatial pyramid pooling module and the channel attention module, and the specific implementation process is as follows: (1) the 1×1 convolution, the 3×3 null convolution with 3 null rates of 6, 12 and 18, respectively, and the global average pooling are used in the atrous spatial pyramid pooling module. After processing, stitching and fusion are performed, and then 1 pair of convolution is used for dimensionality reduction. (2) The feature map obtained through the network model is first reduced to 256 by 1×1 convolution, and then the channel attention module is used for weighting; finally, the feature map processed by ca and the feature map reduced by atrous spatial pyramid pooling module are summed for feature fusion to extract the rich contextual information to obtain effective high-level features.

Because the encoder part obtains high-level features through the parallel way of channel attention module and spatial pyramid pooling module, in order to obtain more efficient segmentation effect, this paper adopts the way of connecting channel attention module and spatial pyramid pooling module in series. In the encoder, the input image goes through the depth-separable convolution layer of different channels in the Xception model for feature extraction, and the feature map output from the output layer is processed by the atrous spatial pyramid pooling module and the channel attention module. Firstly, using the 1×1 convolution in the atrous spatial pyramid pooling module, the void rate of 6, 12, and 18, respectively, and global average pooling operation, respectively, and then perform feature fusion operation on them, and reduce the number of feature map channels from 2048 to 256 by 1×1 convolution of the obtained feature map again, and second, fuse the feature map obtained in atrous spatial pyramid pooling module using the channel attention module and perform weighting operation on them to obtain effective high-level features.

3.3. DeepLab Network Model Based on Attention Mechanism Module. The formula according to the SE attention module is

$$f_{\{w_1,w_2\}}(y) = W_2 \mathrm{Relu}(W_1 y), \tag{1}$$

W_1 and W_2 are the fully connected parameter matrices, y is the output weight of the feature map after global average

pooling, Relu is the activation function. The use of fully connected layers W_1 and W_2 reduces the complexity of the model and consequently the dimensionality; this indirect approach also destroys the direct correspondence between channels and weights.

This paper proposes the module which aims to ensure the multidimensional relationship between channels and weights as well as not to increase the complexity of the whole module computation. The formula for the module is the following:

$$\omega = \sigma(Wy), \tag{2}$$

y is still the output weight after global average pooling, $\sigma(\bullet)$ is the activation function. W is the vector matrix used to calculate the channel attention. Its form is

$$\begin{bmatrix} W^{1,1} & \cdots & W^{1,k} & 0 & 0 & \cdots & \cdots & 0 \\ \cdots & W^{2,2} & 0 & W^{2,k+1} & 0 & \cdots & \cdots & 0 \\ \cdots & \cdots & \cdots & \cdots & \cdots & \cdots & \cdots & \cdots \\ 0 & \cdots & 0 & 0 & \cdots & W^{C,C-K+1} & \cdots & W^{C,C} \end{bmatrix}. \tag{3}$$

The matrix W involves $K \times C$ parameters, and the matrix avoids the complete independence of the different group categories in the SE module. For the weight y, in order to simplify the calculation and avoid dimensionality reduction, only the information interaction between it and its k neighboring elements is considered here and calculated as follows:

$$\omega_i = \sigma\left(\sum_{j=1}^{k} w_i^j y_i^j\right), y_i^j \in \Omega_i^k. \tag{4}$$

To further improve performance, let all channels share weight information, that is,

$$\omega_i = \sigma\left(\sum_{j=1}^{k} w^j y_i^j\right), y_i^j \in \Omega_i^k. \tag{5}$$

Therefore, if all channels share the weight information, then the information sharing and interaction between channels can be achieved by one-dimensional convolution with a convolution kernel of size k:

$$\omega_i = \sigma(\mathrm{Convld}_k(y)), \tag{6}$$

Convld means the one-dimensional convolution operation, which involves only k parameter information, and when $k = 3$, the module can achieve the same effect as the SE module but with a lower model complexity. This approach of capturing cross-channel information interactions without downscaling ensures performance results and low complexity of the module.

Since the module aims to properly capture the local cross-channel information interaction sharing, it is necessary to determine the approximate region k (the size of the convolutional kernel in a 1D convolution) of the channel interaction. Although manual optimization can be performed for different convolutional blocks with different number of channels in different convolutional neural network architectures to achieve the optimal solution for information interaction, cross-validation tuning can be resource-intensive if performed manually and manually. Grouped convolution methods are known to have been successfully used to improve deep convolutional network architectures: for a fixed number of groups, high-dimensional (low-dimensional) channels are proportional to long-distance (short-distance) convolutions. Similarly, it follows that the coverage k of cross-channel information interactions should also be proportional to the number of channel dimensions C. That is, there may be a mapping relationship φ between region C and channel C:

$$C = \varphi(k). \tag{7}$$

The simplest mapping method is the linear mapping relationship. Due to the limitations of linear functions in deep neural networks for some features and the fact that the channel depth is generally an exponential multiple of 2, an exponent with a base of 2 is used to represent the nonlinear mapping relationship:

$$C = \varphi(k) = 2^{(\gamma \times k - b)}. \tag{8}$$

In this way, given the channel dimension C, the one-dimensional convolutional kernel size k can be derived from the following equation:

$$k = \psi(C) = \left|\frac{\log_2(C)}{\gamma} + \frac{b}{\gamma}\right|_{\mathrm{odd}}, \tag{9}$$

$|t|_{\mathrm{odd}}$ is the nearest odd number to t. γ and b are hyperparameters that need to be set, which are related to the structure of the network being joined. In the DeepLab network to be optimized, it is set to $\gamma = 2, b = 1$.

At the same time, since the module only introduces a one-dimensional convolutional kernel size k as a parameter, it does not introduce a large number of parameters when the attention mechanism module is introduced into the network, and only one one-dimensional convolutional computation and dimensional expansion operations are calculated in terms of computation.

After performing a null convolution, after global average pooling (GAP) without dimensionality reduction, a one-dimensional convolution of convolution kernel size is used to extract cross-channel interaction information of neighboring elements between channels, where the k-value indicates the coverage of local cross-channel interactions, that is, how many neighboring elements are involved in the attention prediction of that channel. The tensor of the one-dimensional convolution output is passed through the activation function q, which has different weight shares of the attention prediction attributes; the tensor is matrixed with the original null convolution channel to obtain an output with the same dimensions as the original input and with channel attention prediction. It is proved that this method ensures the learning efficiency and computational results of the model.

In order to compare the effect before and after the improvement, the DeepLab network model based on the module is constructed in this paper. In order to avoid the easy overfitting problem caused by the unavailability of the pretrained network model after the module is added to the backbone network, the module is added to the structure of the decoder part of the DeepLab network, and this is embedded in the feature pyramid after the convolution of the voids, and then multiscale feature fusion is performed after the attention mechanism prediction, as shown in Figure 2. In addition to using different backbone networks VGG-16 network and Res-50 network in the experiments with and without the addition of module, the Res-101 network with deeper structure is also added. Since these three networks have more layers, in order to achieve better classification results on the SBD and ADE20K datasets, the input image size was preset to 321×321 when conducting the computer simulation experiments, and then the images were fed into the network for learning training and validating the predictions.

In this paper, the proposed algorithm combines the advantages of depth-separable convolution with the attention mechanism and uses different attention modules to effectively fuse the low-level and high-level features for different levels of important features in the input image. In the process of implementation, all the empty convolution operations in the attention mechanism are replaced by the deep separable convolution operations, and as the number of features to be extracted gradually increases, the deep separable convolution can save more parameters and improve the computational speed of the training model compared with the empty convolution.

4. Experimental Results and Analysis

4.1. Data Sources and Evaluation Indicators

4.1.1. Data Sources. The SBD dataset is an enhanced version of the VOC 2011 dataset, which contains the annotation of 11355 images from the Pascal VOC 2011 data set. The 11355 images in the SBD are completely selected from the pictures in the VOC 2011 dataset, and more of them are annotated. The category is also the same as VOC 2011 (21 categories). ADE20k is composed of 27000 images from the sun and places data sets. ADE20k consists of more than 3000 object categories, many of which comprise the categories of parts and components of objects, as well as the categories of parts and components of parts and components, such as auto parts, door parts, and windows. The ID of the instance is also marked in ADE20k, which can be used for instance segmentation.

4.1.2. Evaluation Indicators. In this paper, we use mean Intersection over Union (mIoU) to evaluate the network performance, which is a standard measure of semantic segmentation accuracy. mIoU is larger, which means better segmentation. In semantic segmentation, the two sets in IoU represent the predicted segmentation and the true value (GT) of the segmentation. The IoU of each category is calculated first, which is the intersection of the two sets of the predicted and true values of the model segmentation and the overlap ratio of its concurrent set, and then averaged to obtain mIoU. The expression is shown as

$$\text{mIoU} = \frac{1}{k+1} \sum_{t=0}^{k} \frac{TP}{TP + FP + FN}. \tag{10}$$

TP denotes positive samples predicted to be positive, FN denotes positive samples predicted to be negative, FP denotes negative samples predicted to be positive, and TN denotes negative samples predicted to be negative.

4.2. Model Parameter Tuning. Before starting to train the model, the weights of the network are initialized, and the weights of the remaining convolutional layers of the network to be learned are initialized to obey a Gaussian distribution with mean 0 and standard deviation 0.01, and the bias is set to 0. During the training process, the weights are updated iteratively according to the chain rule, and this fine-tuning scheme greatly reduces the convergence time during the training of the semantic segmentation model.

In the process of model design, the ReLU function is used in the activation layer and the Softmax function is used in the loss layer. During the training of the semantic segmentation model, the input is the predicted value of the network with the real label map. To prevent overfitting, the weight decay rate decay = 0.0001. The function is the cross-entropy loss function:

$$\text{loss} = -\sum_{t}^{N} y_i \log\left(\frac{e^{z_i}}{\sum_{j=1}^{n} e^{z_j}}\right). \tag{11}$$

The optimizer uses the Stochastic Gradient Descent (SGD) and Momentum method (Momentum = 0.9) with the following equation for the optimization function:

$$w_t = w_{t-1} + \text{momentum} \times v - lr \times \Delta w. \tag{12}$$

In (12), lr denotes the learning rate, Δw denotes the first-order derivative of the loss function with respect to the weights, denotes the update rate, and w_{t-1} and w_t denote the weights of the previous iteration and the updated weights values, respectively. In the process of gradient update, the momentum term can be increased for dimensions with the same direction out at the gradient point, while the momentum term is reduced for dimensions that change direction at the gradient point. Therefore, the optimization method of SGD and momentum helps to reduce the training time.

In the later stages of training, the decay of the learning rate lr contributes to the stability of convergence, and the learning strategy in this paper is as follows:

$$lr = \text{base}_{lr} \times \left(1 - \frac{\text{iter}}{\text{maxiter}}\right)^{\text{power}}. \tag{13}$$

In (13), power is 0.95, base_lr is 0.007, maximum iterations is 40 k, set the output step to 15, and batch size to 10. The following shows the training results with different

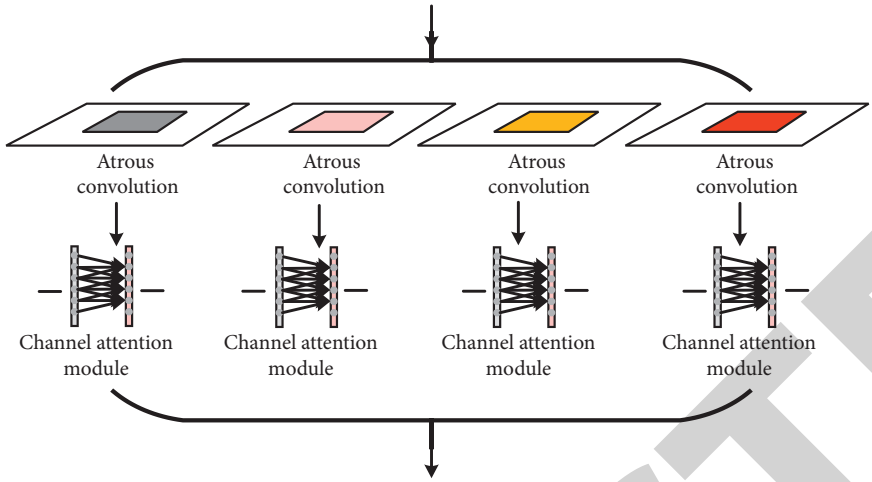

Figure 2: DeepLab network decoder model based on channel attention module.

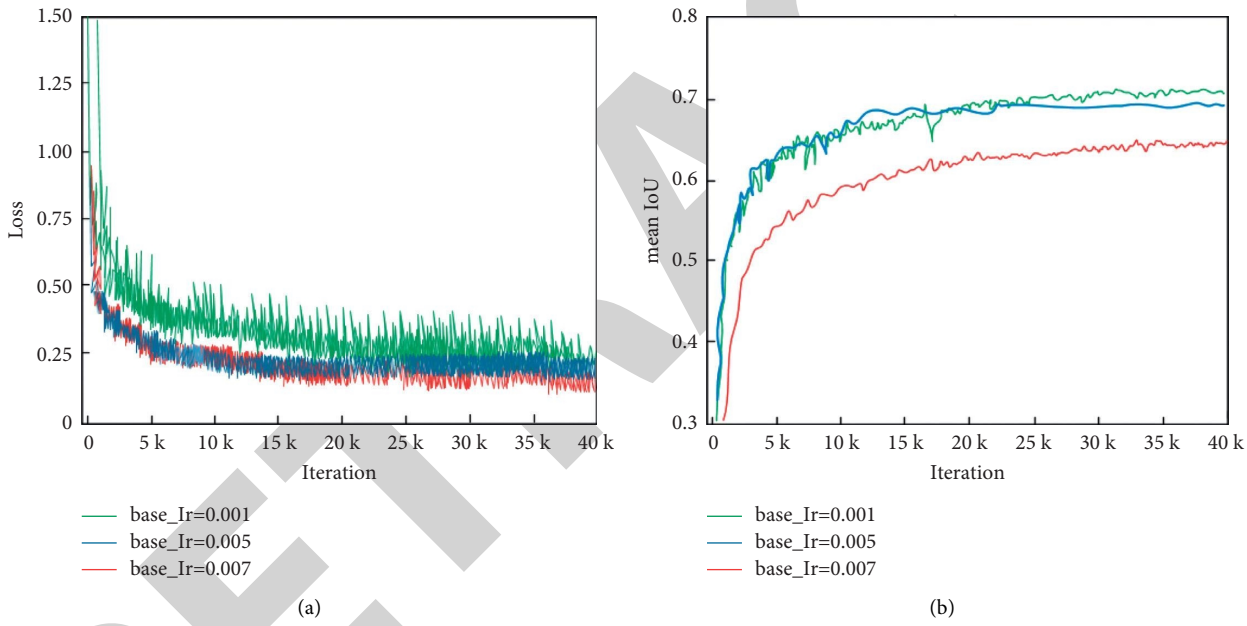

Figure 3: Training of the model proposed in this paper on the SBD dataset: (a) loss curve and (b) accuracy curve.

parameter settings. Figures 3(a) and 3(b) show the loss curve (Loss) and accuracy curve (mIoU) obtained from the model training under different experimental schemes, respectively, on SBD dataset.

From Figure 3 we can see that the model converges basically after 30 k iterations, and the loss value converges to a smaller value when the initial learning rate base_lr is 0.007; the initial learning rate is set too small at the beginning, which leads to the slow convergence of SGD + momentum method, and the final accuracy is poor.

4.3. Comparative Experimental Results and Analysis. Under the experimental conditions, semantic segmentation models of different backbone networks, including FCN-8s, DeepLabV3, and DeepLabV3+, were trained under the same configuration using the same data enhancement (flipping and multiscale), and the methods in this paper were compared with these semantic segmentation methods. Table 1 shows the results of the comparison experiments on the SBD dataset.

Table 1: Comparison results of each model on the SBD dataset.

Segmentation method	Backbone network	mIoU (%)
FCN-8s	VGG16	63.72
DeepLabV3	MobileNetV1	73.56
DeepLabV3+	ResNet50	76.18
This model	MobileNetV2	79.03

As seen from Table 1, the method in this paper takes good care of the number of parameters, computation and performance of the network, and achieves a good balance

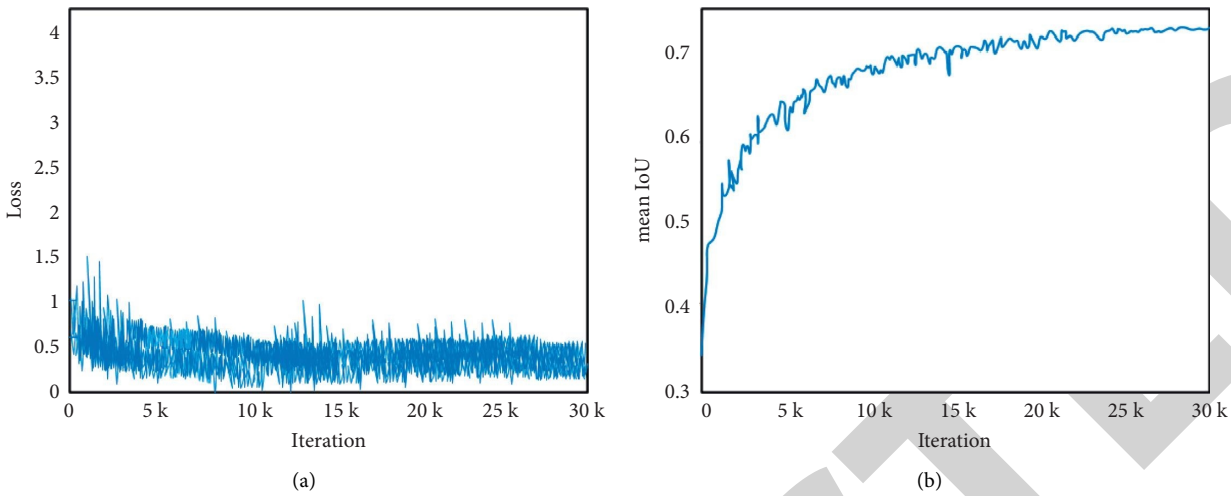

Figure 4: Training of the model proposed in this paper on the ADE20k dataset (a) loss curve (b) accuracy curve.

between segmentation accuracy and efficiency. In terms of segmentation accuracy, this method has different degrees of advantages over FCN-8s (VGG16), DeepLabV3 (MobileNetV1), and DeepLabV3+ (ResNet50) in Table 1.

When training this paper's model on the ADE20k dataset, the images were cropped to 768×768, the batch size is 10 and the maximum iterations is 30 k for the maximum number of iterations, and the rest of the hyperparameters were set as above. The loss (Loss) curve as well as the accuracy curve (mIoU) plots during model training is shown in Figure 4. The final mIoU of the method in this paper on the ADE20k is up to 72.8%.

5. Conclusion and Future Work

In this paper, we study the backbone network, atrous spatial pyramid pooling module and decoder in DeepLabV3+, analyze the limitations of each part, introduce the channel attention module, and propose an image semantic segmentation algorithm based on spatial attention mechanism to address the problem of insufficient segmentation accuracy of existing algorithms. The proposed algorithm uses channel attention to weight the feature maps obtained from the backbone network, and then fuses them with the feature maps processed by the atrous spatial pyramid pooling module to obtain rich contextual information and get high-level features; spatial attention is used to fuse the two low-level features with the high-level features processed by convolution, respectively, to filter a large amount of background information and highlight feature points. In addition, the feature map is linearly transformed using the feature transformation principle to reduce unnecessary convolution operations. In addition, the shallow feature map information is reused in the decoder section using a shortcut connection to enrich the image details. The experimental results verify the effectiveness of the proposed algorithm in this paper, which has obvious advantages in terms of computational complexity and segmentation accuracy compared with similar algorithms.

The efficient semantic segmentation method based on DCNN is also based on the convolutional and pooling layers of CNN, and the network architecture is optimized. However, the activation layer is also an important part of the deep network design. Therefore, the impact of the activation function on the model performance will be further investigated in the subsequent study. Since the great success of transformer in natural language processing tasks has been explored in the field of computer vision, using transformer for semantic segmentation vision tasks to reduce the complexity of the structure and explore scalability and training efficiency will also be a direction for future research.

Data Availability

The data supporting the findings of this study are included within the article.

Conflicts of Interest

The authors declare that they have no conflicts of interest.

References

[1] S. J. Hao, Y. Zhou, Y. M. Zhang, and Y. R. Guo, "Contextual attention refinement network for real-time semantic segmentation," *IEEE Access*, vol. 8, pp. 55230–55240, 2020.

[2] Y. Ouyang, "Strong-structural convolution neural network for semantic segmentation," *Pattern Recognition and Image Analysis*, vol. 29, no. 4, pp. 716–729, 2019.

[3] G. S. Chen, C. Li, W. Wei et al., "Fully convolutional neural network with augmented atrous spatial pyramid pool and fully connected fusion path for high resolution remote sensing image segmentation," *Applied Sciences*, vol. 9, no. 9, p. 1816, MAY 1 2019.

[4] X. Liang and S. Kamata, "Hybrid connection network for semantic segmentation," *Tenth International Conference on Digital Image Processing*, vol. 10806, 2018.

[5] Q. Zhou, W. B. Yang, G. W. Gao et al., "Multi-scale deep context convolutional neural networks for semantic